STUDIES OF FACTORS RELATING TO THE OPERATION AND DESIGN OF ELECTRIC FURNACES FOR MATTE SMELTING WITH PARTICULAR REFERENCE TO SLAG CHARACTERISTICS.

---

by

Andras A. Hejja

A dissertation presented to the Faculty of Engineering University of the Witwatersrand, in fulfilment of the requirements for the degree of Doctor of Philosophy

This work was carried out in the Department of Metallurgy of the University of the Witwatersrand under the supervision of Professor D.D. Howat, B.Sc.(Glas), Ph.D., F.I.M, F.R.I.C.

Johannesburg
September, 1975

...RTAKING

I hereby cer'.fy that this is my own work and that it has no' been submitted for the degree of Doctor of Philosophy at any other University.

A.A. Hejja

ACKNOWLEDGEMENT.

I wish to record my sincerest thanks to Professor D.D. Howat B.Sc.(Glas), Ph.D., F.I.M. (Fellow), Head of the Department of Metallurgy at the University of Witwatersrand, supervisor of this work for his continuous interest, kind encouragement and many useful suggestions.

My thanks are due also to the Staff and Personnel of the Rustenburg Platinum Mines Limited, both at the Rustenburg and Mortimer Smelters, whose understanding and willing support greatly facilitated the accomplishment of the practical task involved in this project.

The generous financial support of the Johannesburg Consolidated Investment Company Limited in the form of a bursary is gratefully acknowledged.

C O N T E N T S.

SECTION III./...

SECTION 1.

PREVIEW.

The Bushveld Igneous Complex, the source of ore processed for copper-nickel recovery lies in the Transvaal province of the Republic of South Africa. The chief constituent of the vast orebody is magnetite associated with titanium dioxide and in some parts with vanadium oxide. In the Lydenburg and Rustenburg areas it contains also rich deposits of platinum group metals accompanied by copper, nickel, silver and gold. In these deposits the major gangue minerals are in the form of pyroxene, feldspar and biotite, while the base metal sulphide minerals occur as chalchopyrite, pentlandite and pyrrhotite. The platinum group metals can be associated either with the base metal sulphides or occur in the form of various minerals, like braggite, cooperite, laurite or ferro - platinum (1). Similar association between copper-nickel sulphides and PGM (platinum group minerals) is found in the Sudbury district of Canada and the Noril'sk-Talnakh area of the USSR.

There are a number of large mining companies engaged in the processing of the platinum group minerals in the Republic, the byproducts, though very valuable assets to the economy of the operation being copper and nickel. The ore is treated by gravity and flotation process and the concentrate is smelted to matte mostly in electric furnaces.

Electrothermal vs. reverberatory smelting of concentrate containing copper and nickel.

As for an example to the trend of developments in smelting of the ore in the Republic of South Africa one of the mining companies, The Rustenburg Platinum Mines Ltd. in its early stage of operation treated the concentrates solely in blast furnaces (2). It became apparent that the blast furnace smelting, apart from being labour-intensive, required also large amounts of coke the price of which has increased rapidly in recent years. Antipollution laws introduced by the Government added further to the problems of blast furnace operation producing excessive volume of gases of low sulphur dioxide content. In an intensive expansion programme, initiated by the worldwide increased demand for platinum metal and also for copper and nickel, the Company decided to introduce electric smelting. The main reasons behind this choice, which may be regarded as probably fairly typical also to the motivation of other companies

active in the/...

active in the same line in this country were obviated by two facts: a.) the high magnesium oxide content of the concentrates leading to relatively high operating temperatures and b.) the favourably low power costs in the Republic of South Africa, at present about R 0,045 to 0,05 (0,07 - 0,077 $/) per kwh.

As an alternative to the electric furnace, the treatment of the concentrate could also be carried out in reverberatory furnaces. However, the disadvantage referred to above in connection with blast furnace gases, namely their large quantity and low SO_2 content, applies also to the gaseous products of reverberatory smelting. The SO_2 content on an average is 1 to 2 per cent, a rather low value for any kind of economic considerations. The electric furnace gases, on the other hand, may contain as high as 3,5 to 4,0 per cent SO_2 which can be regarded already as economically attractive for example for sulphuric acid production.

Furthermore, the temperature of the combustion gases in a reverberatory furnace is high, around 1000 - 1200°C and the lucrative operation of the unit necessitates the recovery of sensible heat in the form of steam in waste heat boilers. These boilers produce about 4 tons of steam per ton of coal, or in case of oil firing, 5 tons steam per ton of oil. With electric furnaces the waste heat recovery does not constitute any particular problem since the temperature of gases seldom exceeds 500°C and under normal circumstances it is rather below this figure. The lower temperature and smaller quantity of the furnace gases permits effective cleaning with Cottrell electrostatic precipitators and also the recovery of valuable flue dust usually high in PGM.

Next point to the advantage of electric smelting above its reverberatory counterpart is the intrinsic versatility. Witness to this is the worldwide spectacular extension of matte smelting furnaces to the reduction of nickel and copper oxide bearing ores and the recovery of copper values from slags. Equally important is the versatility of the furnace operation proper. Adjustment of current to changes in material flow rates may be effected more rapidly and the response of the unit to these changes (the action of the electrodes may be likened to that of a submerged burner) is considerably faster than the response of the reverberatory to alterations made to its fuel burners. Due chiefly to these reasons the prospect of control and automation of an electric furnace is considerably enhanced.

Obviously, in comparing furnace operational characteristics and

suitability of the/...

Table I - 1. Typical composition of concentrates and furnace products at Rustenburg Platinum Mines Ltd.

Material	PGM g/ton	Ni	Cu	Fe	S	B	FeO	CaO	MgO	Al_2O_3	SiO_2
		Percent				$\frac{CaO+MgO}{SiO_2}$	Percent				
Concentrate (pellets)	110-150	3,5-4,0	2,0-2,3	15,0	8,5-10			3	11	6	3,9
Furnace matte	500-800	16-18	9-11	38-42	26-28						
Converter matte	1800-2000	47-48	27-28	1-2	20-21						
Furnace slag	0,54	0,10	0,06-0,08		0,27	0,74	20	15	15	6	41
Furnace slag	Western Platinum Mines (Ref.3.)					0,55	23	8	18	3	47

Table I - 2. Heat balance of reverberatory and electric furnaces smelting copper-nickel concentrates.

		Reverberatory furnace (4)		Electric furnace. E-I (Ref.5.)		E-II (Ref.2.)
			%		%	%
I. Heat supplied						
	From combustion of coal	(Q_c)	94,6	Electrical energy (Q_E)	73,7	87
	Heat in roasted ore	(Q_o)	5,4	Combustion of electrode (Q_{CO})	3,2	3
				Converter return slag ($Q_{c.sl}$)	6,1	10
				Exothermic reactions ($Q_{ex.r}$)	17,4	
		$\sum Q_{suppl}$	100,0	$\sum Q_{suppl.}$	100,0	100
II. Heat absorbed	Heat in slag	(Q_{sl})	17,4	Water vaporisation (Q_v)	5,3	
	Heat in matte	(Q_m)	5,0	Endothermic reactions ($Q_{en.r}$)	8,8	18
	Endothermic reactions (decomposition of limestone)	($Q_{en.r}$)	5,0	Heat in slag (Q_{sl})	29,8	49
	Heat in flue gases	(Q_g)	47,9	Heat in matte (Q_m)	14,1	7
	Heat lost by radiation	(Q_r)	24,7	Heat in waste gas (Q_g)	25,4	10
				Radiation loss (Q_r)	11,4	16
				Electrical losses (Q_e)	5,2	
		$\sum Q$	100,0	$\sum Q$	100,0	100
III. Thermal efficiency	$\eta_{th} = \frac{Q_{en.r} + Q_m + Q_{sl}}{\sum Q_{suppl.}}$		25,8		58,0	67,0
	with 43% waste heat recovery		45,3			
	$(Q_g \times 0,43 + Q_{en.r} + Q_m + Q_{sl}) / \sum Q_{suppl}$					

suitability of the type to be used in a given process, the character of the raw material and the purpose of the operation proper are equally important factors and should therefore be considered together. In the process of ore concentration for the recovery of platinum group minerals the ore has to be stripped of every conceivable metal value in order to have the maximum recovery of the PGM values ensured. Consequently, the concentrate will have a completely different composition from that characteristic of the products of conventional ore dressing aiming purely at the production of copper and nickel. With the recovery of PGM as a main objective a lean concentrate is obtained the gangue material content of which is high, greater than 60 per cent. As a result, the grade of the electric furnace matte will be low. Table I - 1 based on Ref.2 illustrates these points.

Smelting a concentrate with such a large amount of gangue material results in slag compositions also vastly different from those encountered in smelting operations pursued for copper-nickel recovery only. With the slag composition shown in the table a considerable increase in slag-matte ratio can be anticipated which in practice is in the range of 4,0-4,5 to 1 as compared with the average ratio 1,0-1,5 to 1 obtaining in reverberatory furnaces. Therefore in electrothermic smelting the slag bed will be much deeper. The deep bed is advantageous for an effective slag-matte separation and it is easy to realise that with the type of concentrate handled the lower slag-matte ratio of the reverberatory would cause the slag to flow at about twice as high velocity as in the electric furnace. As a result the anticipated matte losses at the same rate of production would also be almost doubled.

An essential difference between the two processes is the source of heat and the way it is transferred in the melt. In a fuel-heated reverb furnace the heat transfer from the impinging flame is via the charge, slag and matte, that is from the top to the bottom zones. In the electric furnace where the heat is generated by the electric current through the resistivity of the slag, the heat is produced under the electrode in the path of the current. Therefore the preferred, though not necessarily exclusive direction of heat flow is from the bottom zone to the top. In an electric furnace there are no combustion gases; those produced originate only from chemical reactions including the oxidation of the electrodes by the charge. The heat balance in the two types of furnace differs considerably. Based on available literature data this aspect is exemplified in Table I - 2. Heat recovery in the waste heat boiler of reverberatory furnaces for the case of dry concentrate is

around 40 per cent/...

Figure I - 1. .rode geometry in the electric furnace.

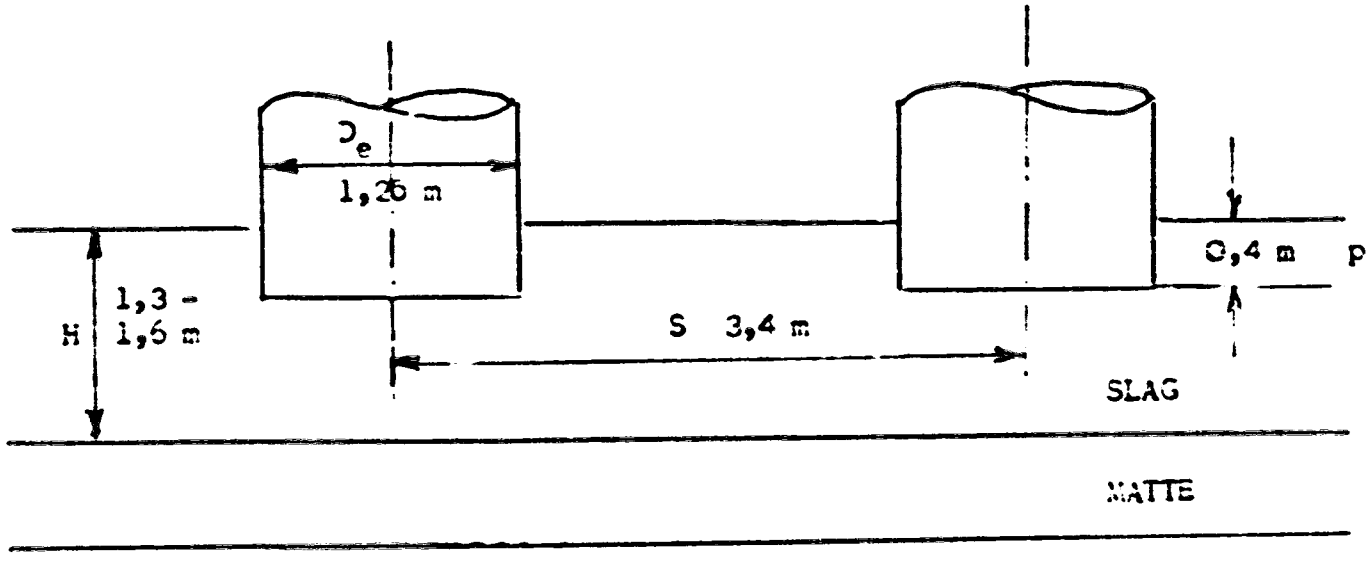

Table I -3. Furnace characteristics and operating data.

Size of furnace inside brick work, lengthxwidthxheight, m			26x7x4,5
Diameter of electrodes, m			1,25
Electrode distance centre to centre, m			3,4
Transformer: three single phase, rating of each MVA			6,5
Secondary voltage: variable by on-load tap changers, V			17[illegible] to 350
Maximum power MW			19,5
Maximum electrode current, kA			32,4
Total bed depth m			2,1-2,3
Slag depth m			1,3-1,6
Matte depth m			0,7-1,0
Taphole location, meter, from bottom of furnace			1,56, 1,76, 196
Slag tapping : continuous, temperature ^{o}C			132o)-1380
Matte tapping: intermittent, temperature ^{o}C			1100 -1200
Typical operating data			
Power MW			18,5
Current kA			175-18,5
cos φ			0,98
Materials:	concentrate (pellets)	t/h	18
	total charge	t/h	23
	converter return slag	t/d	90-110
	furnace slag	t/h	21
	furnace matte	t/h	4,5
Temperature :	slag out	^{o}C	1350
	matte out	"	1180
Ratios :	slag:matte		4,6:1
	slag:concentrate		1,1:1

around 40 per cent of the heating value of the fuel burned. When operating with direct smelting of wet concentrates, the recovery is higher, amounting to something of the order of 51 per cent of the fuel's heating value. For the case of the pellets charged into the electric furnaces concerned, a figure of 42 to 43 per cent is a realistic value and was used in the calculation of thermal efficiencies. By the indication of the results even with waste heat recovery the thermal efficiency of the reverberatory furnace is much lower than that of the electric furnaces.

Scope of the present work.

The electric furnaces installed at Rustenburg Platinum Mines Ltd were chosen as "model" or "reference furnaces" and as such served for basis of the investigations. Their detailed description is given in the literature. (2). The main furnace characteristics and operating data relevant to this study are compiled in Table I - 3 while figure I-1.) illustrates the electrode geometry of the units. In a brief summary the smelting operation treats a flotation concentrate which is a low-grade base metal concentrate of high MgO content. The concentrate is dried then pelletised on disc pelletizers. The semi-dried pellets, containing about 2 per cent moisture are blended with fluxes (consisting of lime stone and occasionally iron ore) and are choke-fed along the side-walls of the furnace. The feeding to each electrode is carried out by manual control. The furnace is rectangular with 6-in-line electrodes connected in pairs, each pair supplied by a separate transformer from a single-phase of a three-phase system. In the process of smelting the concentrate separates into two phases, slag and matte, The slag is tapped continuously, the matte intermittently. This is cast into moulds for further processing while the slag is granulated with water and discarded. The converter slag obtained from the blowing of the furnace matte is returned to the electric furnace for the removal of entrapped matte. By virtue of its FeO and SiO_2 content it also serves as a conditioning agent for the electric furnace slag.

Thus the role of the electric furnace is 1.) to melt the concentrate, 2.) to recover most of the matte entrapped in the converter slag by way of physical and chemical interaction with the furnace slag and 3.) to separate the produced matte, containing the valuable metallics, from the slag. In a true sense it is by no means a submerged arc furnace since, apart from micro-arcs, no real arcing takes place in the units. Consequently, the matte smelting furnace operates at substantially lower temperatures than those

obtaining around the/...

obtaining around the tips of the electrode in a true submerged-arc furnace. As for a basic difference between the operation of the two the position of the electrode in case of the matte smelting furnaces is always well-defined in the slag bed, while the exact electrode-slag relationship in the submerged arc furnace is not known. The heat in the furnace is generated by the current passing through the slag according to the I^2R formula, thus the resistivity of the slag is of prime importance in the overall efficiency of the operation. As a control parameter it stipulates the distance between the electrode and matte surface and, consequently, it serves also as a design parameter in the electrode geometry. To this effect the position of the electrode in the melt determines the mode of heat dissipation which, on the other hand, gives the smelting area, in other words the depth (as well as width) of the bed proper. As regards the electrical efficiency, a deeper slag layer is advantageous in that it permits the use of higher voltage, lower amperage and, thereby a higher power factor can be attained. Since the depth of the molten slag layer is decisive also in settling of the matte particles separated from the concentrate, the electrode position set by the resistivity of the slag has an important bearing in the whole economy of the furnace operation.

From the smelting efficiency point of view the viscosity of the slag is an equally important factor both in reverberatory and in electric furnace operation. It affects the flow quality of the melt and, as such, also the settling of the matte through the molten bed of slag. Unfortunately the action of these two most important slag properties is opposing, i.e. increasing conductivities are associated with decreasing viscosities. Thus while the decrease in conductivity (i.e. increasing resistivity) would be beneficial for the heating of the slag, the simultaneous increase in viscosity, due to its detrimental implications in matte settling, tends to diminish the gain that would ensue from the increase of the resistivity.

The third factor in the line of equal importance is the liquidus temperature of the slag. From the standpoint of process economy this should be as low as possible to diminish radiation losses. The significance of low liquidus temperatures is even greater in that they decrease lining wear and could bring about rather important savings in costly refractories.

In every electric smelting process there is a slag of a given composition range which is best suited for optimum operation efficiency by virtue of its physical characteristics. The previous line of thought amply

illustrates the/...

illustrates the significance of the knowledge of these important parameters. There is no way of predicting theoretically these properties from the com - position of the slag a fact, which will also exclude, or at least strongly diminish, the possibility of making predictions as to the economic feasibility of an electric smelting process with the use of a slag of given composition but with rather vaguely defined physical characteristics. Therefore the purpose of an investigation of this kind should be to establish, at least within a limited range, the trend of change in slag behaviour that can be expected when the slag composition will be subject to alterations.

The present work was undertaken with an objective to investigate the change of various slag properties with the change of slag composition relevant to the smelting (copper-nickel concentrates when the operation is carried out with the main purpose to recover the PGM values in rectangular furnaces having six-in-line electrode arrangement. The topics selected for study were: viscosity, electrical conductivity and liquidus temperatures of composite slags having compositions which are likely to occur with the change of the type of ore from one deposit to an other; the same properties of current plant slags; solubility of matte in the slag and the degree of slag-matte separation with the change of slag composition; size distribution of matte particles in the slag bed. - The data obtained were used to determine the effect of slag composition upon furnace operating characteristics such as voltage, current, power, furnace resistance (hearth resistance). Viscosity data were correlated with matte settling in order to define settler dimensions required for optimum matte, i.e. metal values recovery. The possibility of slag optimisation in the light of the measured viscosities and electrical conductivities was examined. Finally, in the possession of the available results the investigations were extended on the basis of similarity principles and heat transfer considerations toward scale-up and in general, to furnace symmetries in the frame of the special rectangular furnace design. Some thought was also given to symmetry relationships with electrodes being arranged in 6-in-line and 3-in-equi - lateral-triangle configuration.

Basically this study is an attempt to analyse the operation of an existing unit in the light of the slag characteristics concerned. That is how various physical and physico-chemical properties as determined in labor- atory testwork may be applied to predicting the operating conditions of a working unit and how they could be used as basic criteria in furnace design. While considerable work has been done on this line pertinent to three- electrode circular furnaces used for the production of ferro-alloys, pig iron

and electric steel/...

Table I - 4. Comparison of electric furnaces used for smelting copper-nickel concentrates, with and without PGM content.

Particulars			Furnace I Rustenburg Platinum Mines Rep. S. Africa	Furnace II Thompson Smelter Sudbury (6) Canada
Furnace data :	inside width	m	7	6
	inside length	m	26	25,5
	electrode diameter	m	1,25	1,22
	electrode spacing cl to cl	m	3,4	3,4
	power	MW	19,5	18
	current	kA	17-19	18
	voltage	V	170-350	160-300
Concentrate treted			with PGM	without PGM
Slag.	Composition per cent	FeO	20	35 - 40
		CaO	15	2 - 3
		MgO	15	1 - 2
		Al_2O_3	6	4 - 6
		SiO_2	41	34 - 38
		$B = (CaO+MgO)/SiO_2$	0,73	
Matte	Composition per cent	Cu + Ni	25 - 29	16 - 17
		Fe	38 - 42	45 - 50
		S	26 - 28	25 - 27
Production:		Slag t/hr	21	30 - 45
		Matte "	4,5-5	15 - 20
Tapping temperatures	°C	slag	1350	1290
		matte	1180	1120

and electric steel, the data available in the literature concerning non-ferrous applications with particular reference to the treatment of copper-nickel concentartes are far from being abundant. The difficulty as well as shortcomings involved in an analysis of this kind is that it has to be restricted to a fairly narrow range of slag composition in order to obtain comparable results. Otherwise the comparison can easily be misleading or even meaningless. Let the point be illustrated by the example of two furnaces of virtually identical size treating copper-nickel concentrates and producing slags of entirely different character. Relevant data are shown in Table 1-4. In addition to the composition quoted the Thompson slag contains some 3 to 4 per cent alkalies with 1 - 2 per cent sulphur. With the exception of Al_2O_3 and to a certain degree of SiO_2 there is virtually nothing common between the two slags and by practical considerations and also by the results of the present investigations not much succes, if any, could be expected with the Thompson slag under the operating conditions of the Rustenburg furnaces. Yet the slag is perfectly suitable for the purpose of the Thompson furnace, the symmetry relationships and electrical data of which are almost identical with those of the RPM units.

From this comparison the importance of the character of the feed material becomes immediately evident. The indication is that materials of vastly different properties can be successfully processed in the same unit provided the operating parameters and electrode geometries, that is for a given electrode diameter the depth of the slag and matte beds and the depth of electrode penetration, are set according to optimum operation efficiency. For the particular characteristics of the ores originating from the Bushveld Igneous Complex the mode of furnace operation adapted for the recovery of PGM, copper and nickel in the plants proved to be the most economical. Since the general approach of the present study rests on this particular raw material and mode of processing, the results and conclusions arrived at will have to be viewed and judged primarily in this conte.

References.

1./ Cabri L.J.: The mineralogy of platinum group elements. Minerals Science Engineering, 4, No-3, 1973, 3-29

2./ Mostert J.C.-Roberts P.N/...

2./ Mostert J.C. & Roberts P.N.: Electric smelting at Rustenburg Platinum Mines Ltd of nickel-copper concentrates containing platinum group metals. J. S. Afr. Inst. Min. Met. Apr. 1973, 290-299

3./ Newmann S.C.: Platinum. Trans. I.M.M. 82, 797, 1973, A52-A68

4./ Schumann R.: Metallurgical Engineering. Vol.1. Addison-Wesley, 1952.

5./ Barth O.: Electrical smelting of sulphide ores in "Extractive Metallurgy of Copper, Nickel and Cobalt. Ed. P. Queneau. Interscience Publishers, N.Y. 1961.

6./ McConnel J.B. - Klassen I.P. - Berkovich S.A.: Roasting and smelting practice at the Thompson plant of the International Nickel Co of Canada Ltd. Canad, Min. Met. Bull. Aug. 1963, 615-24

McConnel J.B.:- Maddison H.A.: The Thompson Smelter. Ibid. 1964, Nov, 1173 - 1180

SECTION II

MEASUREMENT OF ELECTRICAL CONDUCTIVITY AND VISCOSITY OF SLAGS.

1./ The range of slag composition selected for the measurement of electrical conductivity and viscosity.

The selection of the range of slag composition was borne out by practical considerations pertinent to the operation of electric furnaces already in use for the smelting of copper-nickel containing ores in which platinum group metals are accompanying elements. It can be anticipated with reasonable certainty that from these type of ores from the Merensky Reef deposits having comparable composition and similar metal values, the process of beneficiation will yield concentrates also of similar composition and metal contents. Obviously, the conditions of their processing in electric furnaces should also bear close resemblance both with regard to the quality and quantity of flux to be used and the physical characteristics and composition of the slag, as the important heating media, to be produced in the most economic way of furnace operation.

Since the composition of the ore, therefore also that of the con - centrate varies from location to location, it is of considerable advantage to be in the position of predicting the smelting behaviour and thus the economy of the furnace on the basis of expected changes in the composition of the slag. Because the resistivity stipulates the heating characteristics and the viscosity the matte-settling ability of the slag, in the knowledge of the effect of slag composition upon these parameters it will be possible to predict the necessary adjustments that will have to be made to the operation of the furnace with the change of one or more of the slag-forming constituents. Thus for example if the FeO or MgO content of the slag originating from the smelting of ore from a new orebody is anticipated to increase noticeably above that contained in a slag which can be termed as economically sound for electric furnace processing, the knowledge of the response of variations in conductivity and viscosity facilitates the adjustment of flux addition, the estimation of the quantity of new ore that can be processed on a monthly or yearly bases, etc. Therefore to obtain results of immediate practical importance, the range of composition of the slags to be investigated was selected partly so as to follow closely those of the electric smelting furnaces, called hierafter reference or model

furnaces in operation/...

Table II-1. Composition of slags selected for the tests work.

A. Synthetic slags

Group No	Slag No	Chemical composition per cent					Basicity ratio $\frac{CaO+MgO}{SiO_2}$	Ratio $\frac{CaO}{MgO}$
		FeO	CaO	MgO	SiO_2	Al_2O_3		
I	1	20	13	16	46	5	0,63	0,8
	2	20	16	16	43	5	0,74	1,0
	3	20	19	16	40	5	0,85	1,2
II	4	20	16	13	46	5	0,63	0,8
	5	20	16	19	40	5	0,85	1,2
III	6	20	14	15	46	5	0,63	0,95
	7	20	16	17	42	5	0,78	0,95
	8	20	18	19	38	5	0,97	0,95
IV	9	14	19	16	46	5	0,76	1,2
	10	26	14	16	39	5	0,77	0,9
V	11	14	16	19	46	5	0,76	0,8
	12	26	16	14	39	5	0,77	0,9
		$\frac{FeO}{}$	$\frac{Fe_2O_3}{}$					
	13	85	15	16	17	42	5	0,77	0,95
	14	40	60	16	17	42	5	0,77	0,95

B. Slag samples obtained from the plant.

Composite Monthly								
Oct. 1972	1	20,9	17,7	13,7	40,4	4,8	0,78	1,29
Nov. 1972	2	21,2	15,9	14,4	41,6	4,9	0,73	1,10
Daily Sample								
4/12/72	3	20,0	16,1	12,8	40,3	4,5	0,72	1,26
5/12/72	4	19,2	16,6	14,1	40,2	4,4	0,77	1,18
7/12/72	5	18,3	16,6	13,6	40,1	5,1	0,76	1,23
9/12/72	6	15,7	18,1	14,8	41,9	5,1	0,76	1,23
12/12/72	7	19,0	15,6	13,2	40,9	4,6	0,71	1,21

Table II-2. Correlation between electrical conductivity of slag and selected parameters of composition.

Slags in group	Correlatin with	Components kept at constant values	Components Varied	Slag numbers with correlation in each group
1	Basicity ratio	FeO, MgO	CaO, SiO_2	1, 2, 3
2	Basicity ratio	FeO, CaO	MgO, SiO_2	2, 4, 5
3	Basicity ratio	FeO, CaO/MgO	CaO, MgO	6, 7, 8
4	Total iron content of slag	Basicity ratio, MgO	CaO, SiO_2	2, 9 10
5	Total iron content of slag	Basicity ratio, CaO	MgO, SiO_2	2, 11, 12
6	Fe^{2+}/Fe^{3+} ratio	CaO, MgO, SiO_2 CaO/MgO, Total Fe Basicity ratio	F^{2+}/Fe^{3+}	7, 13, 14

furnaces in operation at RTM. In this context, for a start, these slags were regarded as standard slags for further considerations. A study was made of the slag composition reported at the plant, embracing a two months period in 1972. The composition fell within the following ranges:

Chemical composition, per cent					Basicity ratio $\frac{CaO+MgO}{SiO_2}$	Ratio CaO/MgO
FeO	CaO	MgO	SiO_2	Al_2O_3		
14 -24	13 - 18	13-17	35 - 44	4 - 6	0,65-0,80	0,9 - 1,0

Because of considerations involving plant extensions with new units operating on raw materials from new orebodies with an anticipated increase in the FeO and MgO contents of the slags, the ranges of the components quoted in the table had to be extended.

The proposed slag compositions were based on grouping the FeO contents in the ranges of 14, 20 and 26 per cent respectively. The other oxides have been varied within a smaller range, the ratios being maintained in accord with those experienced in the reported range of slag composition for the plant as shown in Table II - 1.

It was considered desirable to fix certain constituents of the slag in such a way that the electrical conductivity and the viscosity of the slag may be correlated with one other parameter, e.g. basicity ratio. For example in slags 1 to 3 in Group I the FeO and MgO contents have been kept constant so that the value of the physical properties of the slag may be plotted against the basicity ratio. A similar correlation may be obtained by keeping the CaO content constant or by maintaining a constant value for the ratio CaO/MgO.

In the same manner the physical properties of the slag may be correlated with the iron oxide content by maintaining a constant value for the basicity and either a constant value for MgO or CaO. Table II-2. indicates the correlation which should be possible between the physical properties of slags and the selected parameters of composition.

Experimental./

Figure II-1 SKETCH OF LABORATORY FURNACE USED IN VISCOSITY – ELECTRICAL CONDUCTIVITY TESTS.

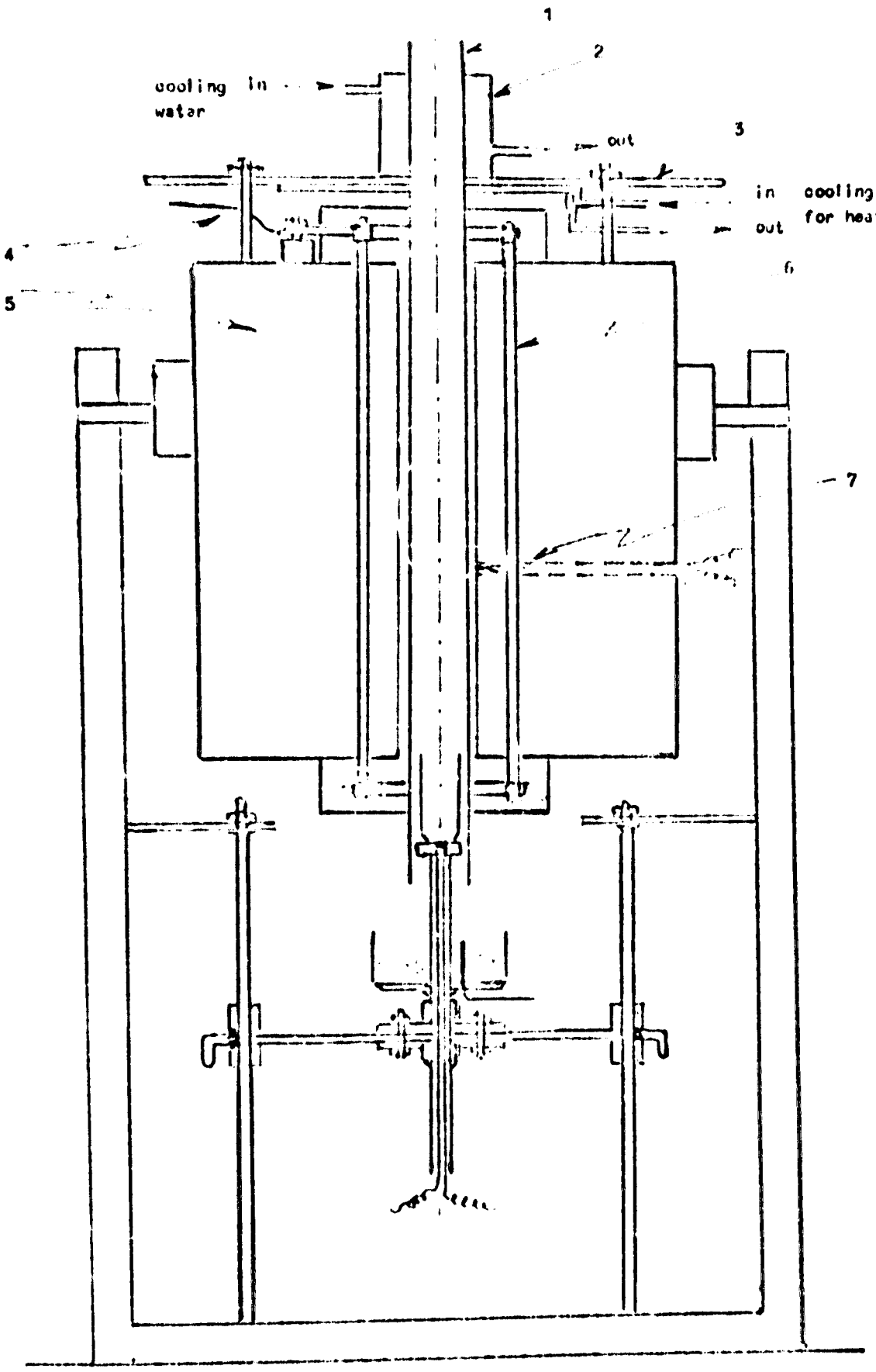

1 Sintered alumina furnace tube
2 Water-cooled muffle
3 Heat shield
4 Electric leads
5 Furnace body
6 SiC heating elements
7 Thermocouple for control of furnace temperature

Key to Figures II-2 and II-3.

Figure II-2

1. Rubber stopper
2. Asbestos cement heat shield
3. Mullite furnace tube (5,1 cm o.d.)
4. Platinum crucible
5. Pt-Rh thermocouple
6. Alumina cement crucible support
7. Mullite tube holder for crucible support
8. Sand seal box
9. Flanged holder for mullite tube
10. Movable base attached to furnace supporting bars
11. Holder for thermocouple sheath
12. Thermocouple sheath
13. Pipe for gas inlet at the top of the furnace
14. Pipe for gas inlet at the bottom of the furnace

Figure II-3

1. U-tube manometers
2. Gas drier and mixer tube
3. 3-way stop cock
4. Line for gas inlet to the top of furnace
5. Line for gas inlet to the bottom of furnace
6. Variac for power supply to furnace
7. Furnace
8. Silicon carbide heating elements
9. Thermocouple for power supply control
10. Electrode holder
11. Platinum electrodes
12. Constant resistance
13. Oscilloscope
14. Variable resitance box
15. High frequency power generator
16. Variable capacitors
17. Temperature recorder

Figure 11-2 PLATINUM CRUCIBLE SUPPORTING MECHANISM AND FURNACE TUBE.

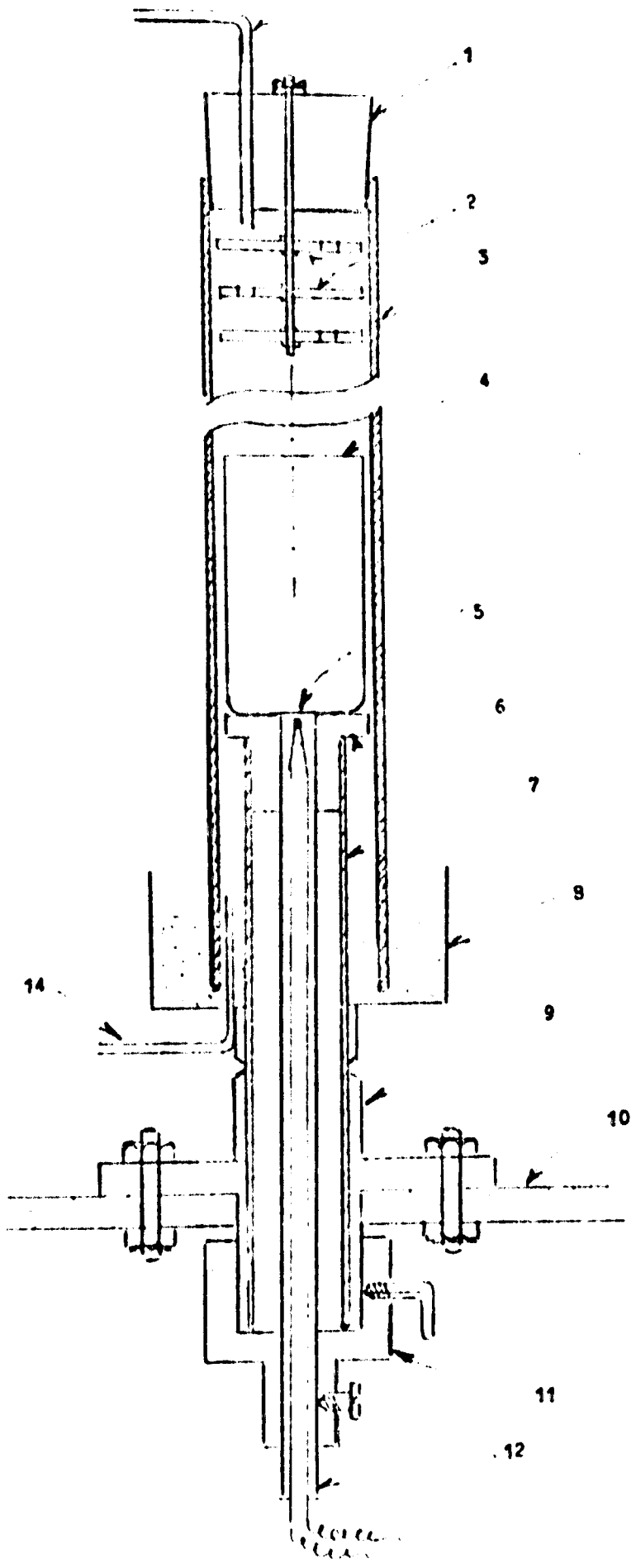

2./ Experimental.

2.1. Raw materials for composite slags.

In these series of investigations in order to simulate conditions closely to those obtaining in practical furnace operation, the iron oxide had to be present predominantly as divalent oxide, Fe^{2+}. The ferrous oxide was produced by the thermal decomposition of ferrous oxalate, $Fe(COO)_2 \cdot 2H_2O$, by heating slowly to 700°C in an atmosphere of nitrogen, keeping it at this temperature for 10-15 minutes, then raising the temperature to 950-1000°C. The high temperature caused the oxide to sinter slightly which effectively reduced the surface reactivity toward air after cooling.. The samples were held at 1000°C for about 15 minutes then cooled rapidly to a temperature below 500°C. The fast cooling was necessary to prevent the material from being transformed into magnetite. The average divalent oxide content of the compound that could be attained by this method varied between 89 and 95 per cent.

The other oxide constituents of the slag were calcined at 1100°C prior to making up the slag composition. The oxide mixtures were then compressed into discs and melted down under reducing conditions in the furnace in platinum crucibles. 150 g of melts were used in each test which secured adequate depth for electrode immersion.

2.2. Equipment. A./ Furnace.

The furnace was of circular cross-section housing six silicon - carbide heating elements connected in series from an automatic control panel and capable in this way of operating at temperatures up to 1600°C. A schematic representation is given in Figure II-1.

The ancillary equipment had to facilitate investigations to be performed under controlled atmosphere. This involved the installation and calibration of various U-tube manometers for measuring the flow rates of N_2, H_2, CO and CO_2. For the purpose of introducing gases on the top of the furnace tube, a heat shield constructed of asbestos cement discs was attached to the rubber plug closing the tube. It was also necessary to ensure a complete air seal for the bottom of the tube and also for the thermocouple sheath. The arrangement is shown in Figure II-2.

During preliminary runs it became evident that the rates of heating

and cooling were/...

and cooling were of considerable importance in securing truly comparable conditions for the various runs. For the recording and controlling of the heating and cooling rates a"Riko Denki" two-point temperature recorder was used.

The platinum crucibles, 75 mm high by 35 mm wide with 0,4 mm wall thickness were seated on a sintered alumina or alternately, firebrick holder supported by a mullite tube containing the thermocouple sheath. The tube was mounted on a base that could be raised or lowered and thereby the required position of the crucible in the hot zone of the furnace tube attained.

2.3./ Electrical conductivity.

The electrical conductivity was measured by a modified Wheatstone bridge technique. The modifications included a variable capacitance opposite the conductivity cell in order to balance out any inductance effect. No provisions were made to minimise the effect of furnace frequency and the mains frequency by the application of say a combined system of shunt capacitors and low frequency filters. As it became evident in the course of the calibration of the equipment, even the variable capacitors that were supposed to counteract induction effects proved to be superfluous and could be dispensed with.

The electrical measuring system consisted thus of a bridge circuit containing the two constant resistances, the measuring cell containing the slag, and variable capacitors connected in parallel with the cell. High - frequency alternating current was fed to the bridge by a transistor R.C. oscillator Type TG 150 BM, while for null-instrument an oscilloscope, Type 561 was used. The temperature of the slag was measured by a 6-Rh-Pt/30-Rh-Pt thermocouple inserted from the bottom through the mullite tube supporting the platinum crucible. The point weld of the thermocouple was carefully adjusted in each test to a distance of 1 mm from the crucible bottom. Thermocouple EMF was determined with the aid of a Cambridge potentiometer. In order to attain maximum sensitivity in the circuit, the constant resistances were selected so as to be close to the resistivity of the slag, being thus of 5 ohm value.

The electrodes were made of 2 mm diameter platinum wires spaced parallel to eachother 10 mm apart between centres. The electrodes could be lowered or raised by a rack-and-pinion device to which a vernier caliper

was attached./...

Figure 11-3 DIAGRAM OF EXPERIMENTAL INSTALLATION FOR ELECTRICAL CONDUCTIVITY MEASUREMENTS

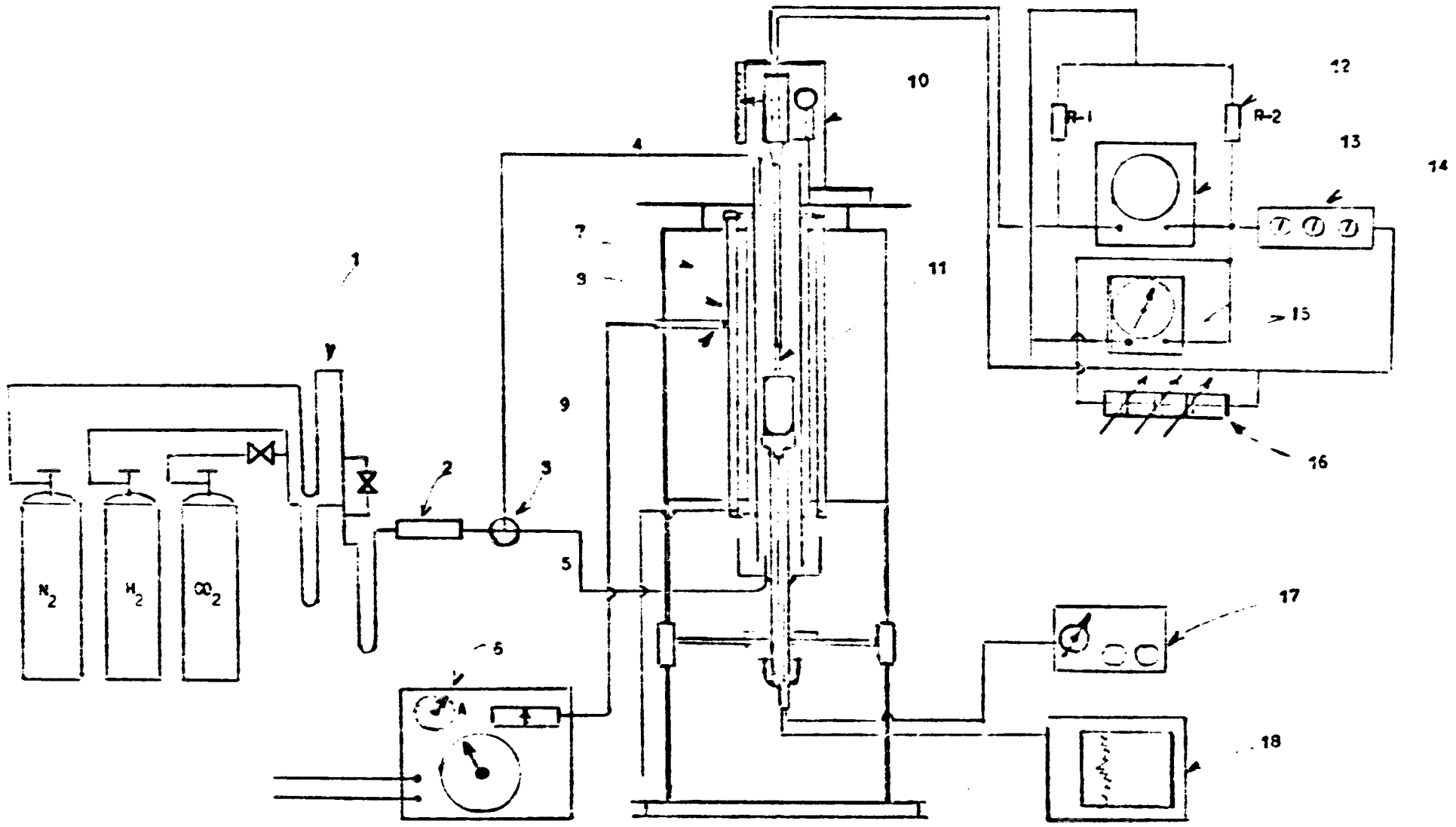

was attached; in this way their depth of immersion could be easily adjusted within ± 0,1 mm both for calibration and high temperature measurements. A diagram of the complete installation is given in figure II-3.

Calibration for conductivity. From the works of various investigators it would appear that a frequency of 10 kHz is the most sensitive range for Wheatstone bridge technique. A series of tests were carried out using 15 kHz and 150 kHz frequencies with aqueous solutions of various concentrations. No difference whatsoever in the sensitivity of the system was noticed, but the absolute resistivity values were considerably different. Since the industrial furnaces operate at low frequencies (50-60 Hz), this fact may leave some doubt as to the absolute value of resistivities measured in the laboratory when they are to be interpreted for large - scale operating furnaces. However, a reasonable assumption that can be made for the present purpose is that the relative resistance of different slags at say 10 kHz corresponds with the relative resistance of slags at 50 Hz. The measurement of resistivity at this low frequency would, in any case, involve considerable difficulties, say by the use of direct (i.e. voltage/current) measurements leading to impedance rather than resistance values.

The calibration of the cell containing the electrodes was performed using 0,1, 0,5, 1,0, 2,0, 3,0, n. NaCl and KCl solutions with the analytical-grade reagent dissolved in de-ionised water. A brass crucible, identical in size to the platinum crucibles of the high temperature tests was used in the calibration. It was kept in a thermostat the temperature of which was controlled at 20°C. The depth of immersion of the electrodes was adjusted to a constant 10 mm, this being measured from the point at which the electrodes first became in contact, i.e. bridged by the electrolyte. The cell resistance varies greatly with the depth of immersion in such a way that the smaller the depth the greater is the resistance, indicated by a hyperbolic plot. The gradient of the curve increases as the depth of immersion decreases; thus the error in positioning the electrodes increases. A 10 mm depth of im - mersion appeared to be a suitable compromise.

On the other hand it was found that in aqueous solution the separation of the electrodes does not alter substantially the cell resistance. For the sake of comparison the calibration was carried out with electrodes being respectively 9 and 10 mm apart (centre line to centre line).

The depth of the liquids was kept constant at 50 mm in the crucible

for all solution/...

Figure II-4 CALIBRATION CURVES FOR CELL CONSTANT DETERMINATION

Legend 1 electrode distance 9 mm
2 " " 10 mm
NaCl solutions
KCl solutions

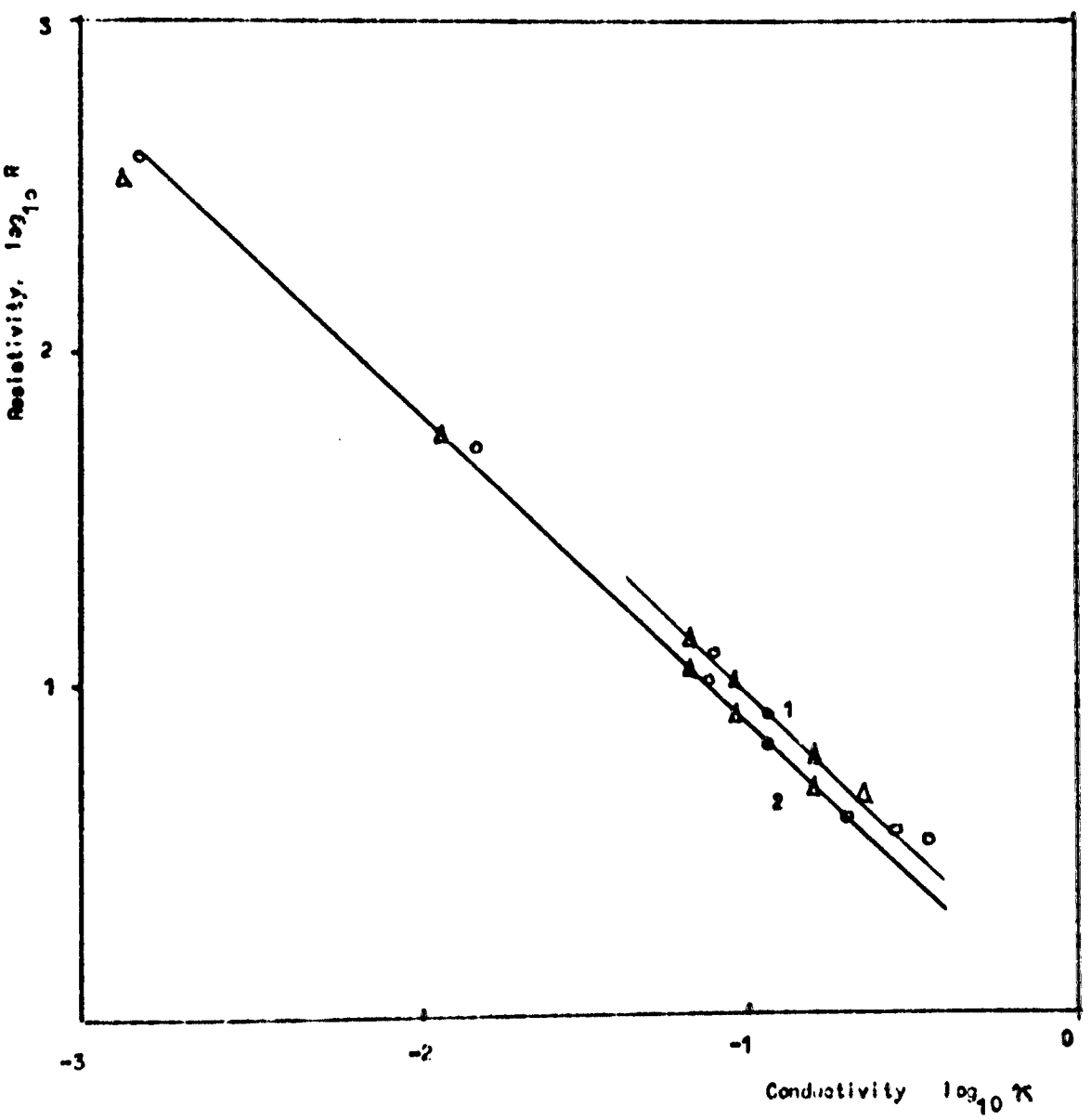

Table II-3. Results of cell calibration at 15 kHz and 150 kHz frequencies.

Concentration of calibrating solution	n, C	0,1	0,5	1,0	2,0
	log C	-1,0	-0,302	0	0,302
KCl solution					
150 kHz, resist. Ohm	R	45,3	11,8	6,25	3,85
	log R	1,655	1,071	0,795	0,584
15 kHz resist. Ohm	R	-	13,6	7,50	4,60
	log R	-	1,133	0,874	0,662
NaCl solution					
150 kHz resist. Ohm	R	49,5	13,4	7,83	5,0
	log R	1,694	1,127	0,893	0,698
15 kHz resist. Ohm	R	52,0	16,3	9,2	6,0
	log R	1,715	1,212	0,962	0,778

for all solution concentrations, although Riebling has found (1) that the cell constant at fixed depth of immersion and frequency of current was independent of liquid levels between 25 and 40 mm.

The resistivity of the slag is inversely proportional to the conductivity according to the relationship

$$R = \frac{1}{\kappa} G \qquad 1./$$

where R = resistivity of slag in the cell
κ = conductivity of the slag (specific resistivity)
G = cell constant.

The constant G is a term dependent on cell geometry

$$G = l/A$$

in a cell of length l and uniform cross-section A. By taking logarithms, from equ 1./ we get

$$\log R = -\log\kappa + \log G \qquad 2./$$

Thus a plot of $\log_{10} R$ vs $\log_{10}\kappa$ should be a straight line as indicated in figure II-4. from which

$$\log_{10} G = 1{,}815 + (-2)$$

and

$$G = 0{,}655 \text{ ohm.cm}^{-1} = 65{,}5 \text{ Sm}^{-1}$$

Figure II-4. incorporates the relationship for both 9 mm and 10 mm electrode distances showing good agreement between the two graphs. As will be obvious, the points obtained with solution concentrations of 0,5 to 3,0 n show very slight scatter from the straight line, but the value given by the 0,1 normal solution is off the trend. In an attempt to improve the results various capacitors (0,01 to 1,0 μF) were added to the circuit by inserting these capacitors in parallel with the variable resistance. Even the smallest addition of capacitors to the circuit could not bring about balanced conditions. The same type of circuit in which no capacitors were used was employed in tests carried out both in aqueous solutions and in the molten slags. The results of calibrations obtained with various standard solutions at frequencies of 150 kHz and 15 kHz are compiled in Table II-3.

Fortunately, the deviation from linearity was found to be greatest for the least concentrated solution of high resistivity, much above the resistivity of the slags under investigation. Thus for practical considerations the non-linearity in this region does not constitute any problem in the present work. The deviation from linearity could be attributed to

polarisation of the/...

Figure 11-5 TEMPERATURE GRADIENT OF FURNACE

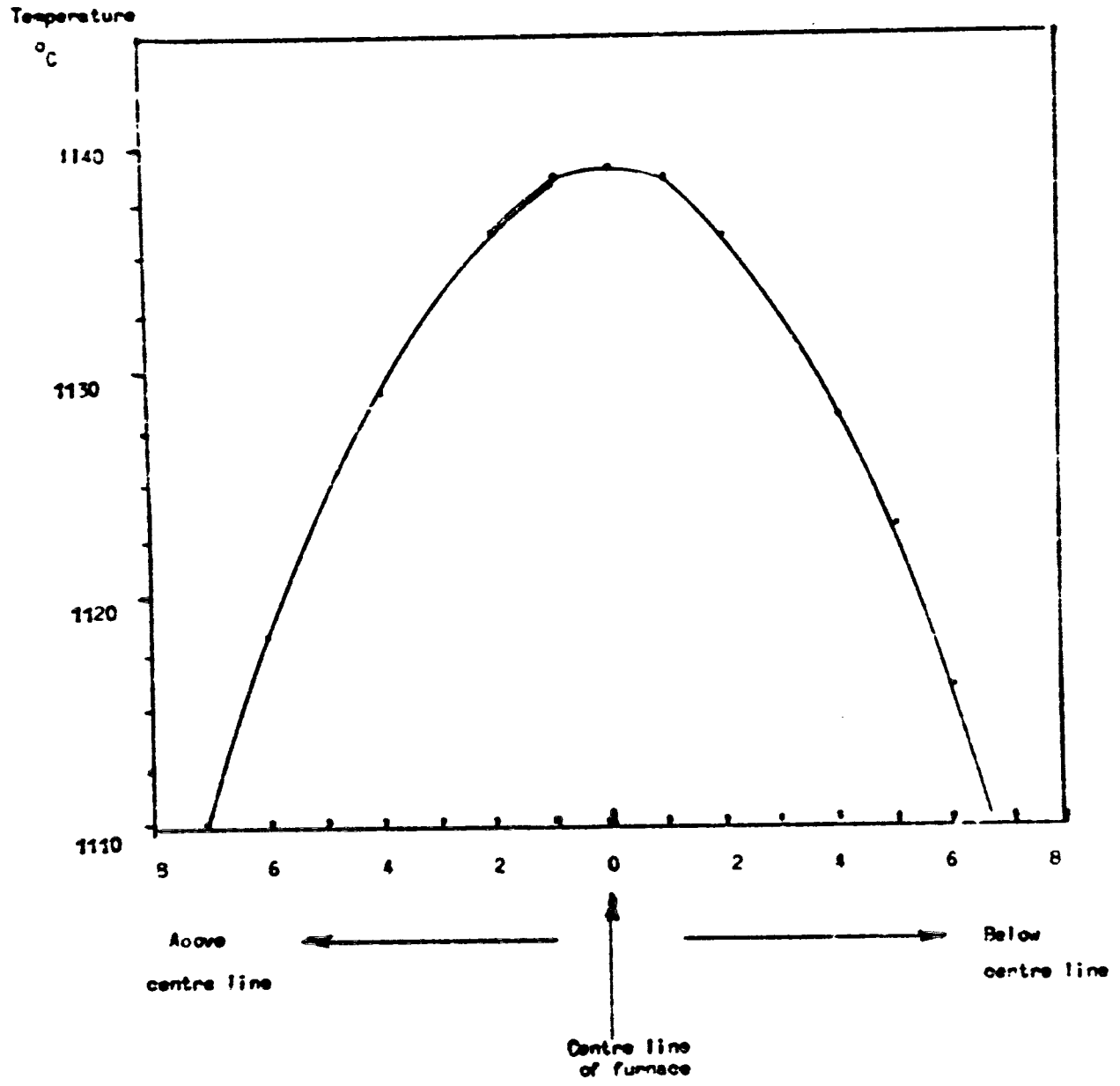

polarisation of the electrodes by ions in the solution. According to Riebling and Logel (1) the capacitance effects appeared for the more concentrated solutions of KCl, which is contrary to the present findings. They obtained reactance-free impedance by extrapolating the measured impedance to infinite frequency. When using Wheatstone or Kelvin Bridge methods, the frequency dependence of resistivity is about 5% over the range of 500 - 10.000 Hz according to

$$R_{\nu(m)} = R_{\nu(\infty)} + K/\nu^{\frac{1}{2}} \qquad 2a./$$

Here $R_{\nu(m)}$ =measured resitance at frequency ν and $R_{\nu(\infty)}$ = polarisation-free resistance at infinite frequency respectively. K is a constant depending on the character of the aqueous solution, molten slag or salt sample. Now a plot of $R_{\nu(m)}$ vs. $1/\nu^{\frac{1}{2}}$ can be used to find $R_{\nu(\infty)}$ by extrapolating the plot. However in the present study the same procedure was of little help in improving the results, the points continued to deviate from the straight line relationship.

The measured resistivities had to be corrected for the resistivity of the leads and platinum electrodes. This was determined by shortcircuiting the electrodes in mercury giving a result of 0,88 ohm. The resistivity had to be corrected also for temperature, the effect of which was found to be 0,02 ohm between 1[illegible]° and 15[illegible]°C. - A check was made on the performance of the wheatstone bridge by substituting a variable resistance box for the cell. Deviations between the actual (cell) resistance and the resistance measured although present, were found to be of no significance for practical considerations.

Mode of operation. After melting down the pelletised material the molten slag was maintained for approximately 1 hr in the furnace whereafter the resistivity measurements commenced. The highest temperature zone in the furnace had been determined previously by positioning the thermocouple along the length of the furnace tube and plotting the length vs. temperature readings. Figure II-5. indicates that within 4 centimeters around the centre line there is very little change in furnace temperature. Therefore all slags were kept in this range whereby temperature fluctuations of not more than $\pm$ 5°; could be secured.

During melting-down the protective gas was introduced from the top of the tube. At the start of the resistivity measurements the flow was then

reversed with the/...

Table II-4.

Liquidus temperatures and resistivities of synthetic slags.

Group No	Slag Number	Determined Liquidus Temperatures °C	Resistance measurements L.T.+30°C (Ohm)	L.T.+50°C (Ohm)	L.T.+100°C (Ohm)
I	1	1320	3,95	3,55	2,90
	2	1320	3,35	3,10	2,60
	3	1315	3,60	3,25	2,35
II	4	1305	4,40	4,00	3,00
	5	1355	2,36	2,20	1,97
III	6	1310	4,00	3,60	3,00
	7	1350	3,00	2,80	2,45
	8	1380	2,85	2,35	1,80
IV	9	1330	4,50	3,95	3,10
	10	1325	2,20	2,10	1,80
V	11	1330	4,30	3,70	2,60
	12	>2	2,30	2,17	1,95
VI	13	1375	2,77	2,58	-
	14	1330	2,87	2,68	2,20
	15	1275	2,15	1,90	1,80

Table II-5.

Liquidus temperatures and resistances of plant slags.

Date of Sampling	Slag Number	Determi Liquidus Temperatures °C	Resistance Measurements L.T.+30°C (Ohm)	L.T.+50°C	L.T.+100°C
Composite Monthly Sample					
October 1972	1	13138	3,30	3,00	2,60
November 1972	2	1328	3,36	3,24	2,85
Composite Day Sample					
4/12/72	3	1330	3,39	3,10	2,60
5/12/72	4	1335	3,10	2,65	2,35
7/12/72	5	1340	3,22	2,99	2,50
9/12/72	6	1340	3,31	3,08	2,45
12/12/72	7	1325	3,28	3,04	2,50

Figure 11-6 MEASURED RESISTANCE - TEMPERATURE RELATIONSHIP

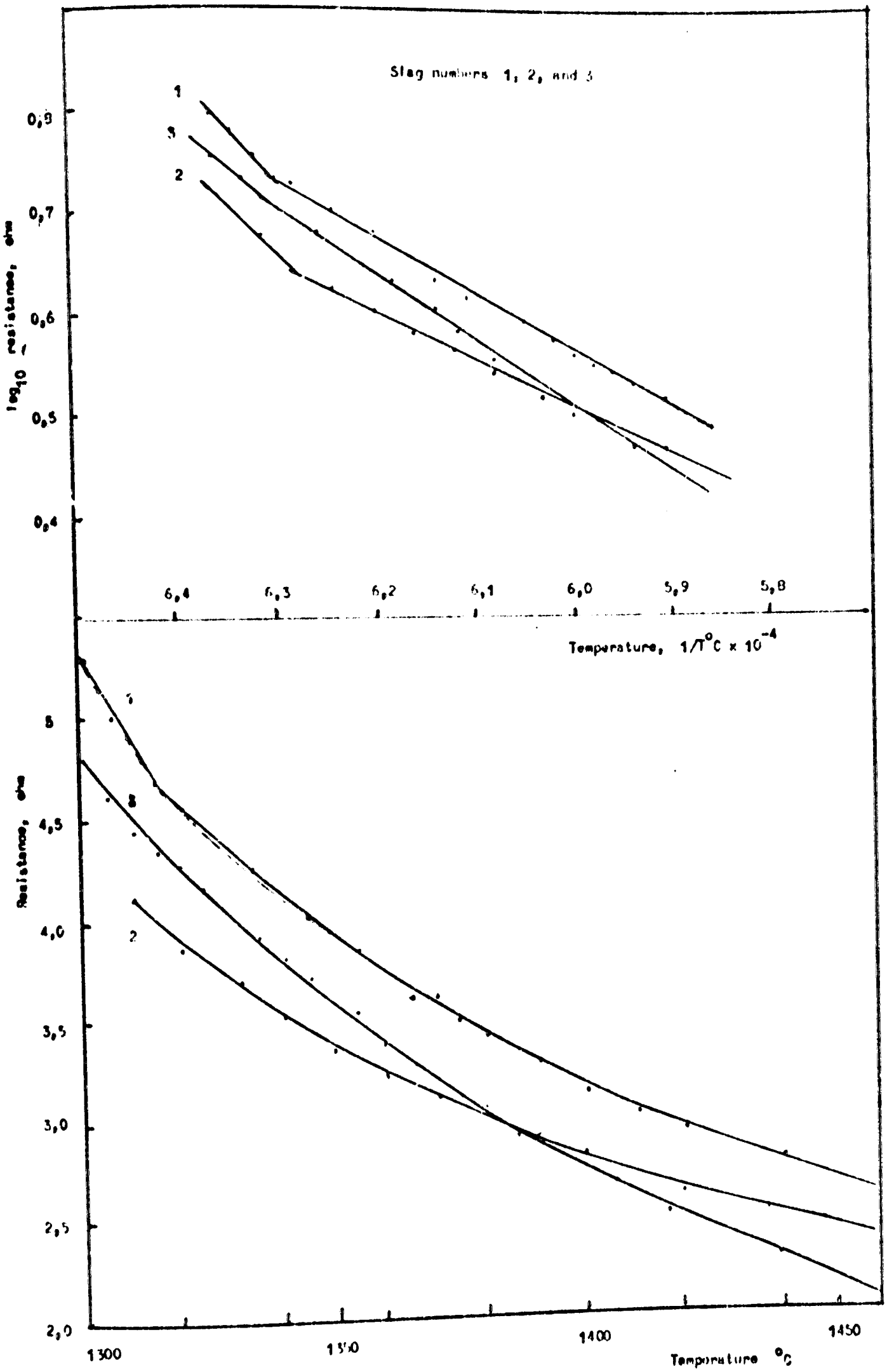

Figure 11-7 MEASURED RESISTANCE - TEMPERATURE RELATIONSHIP

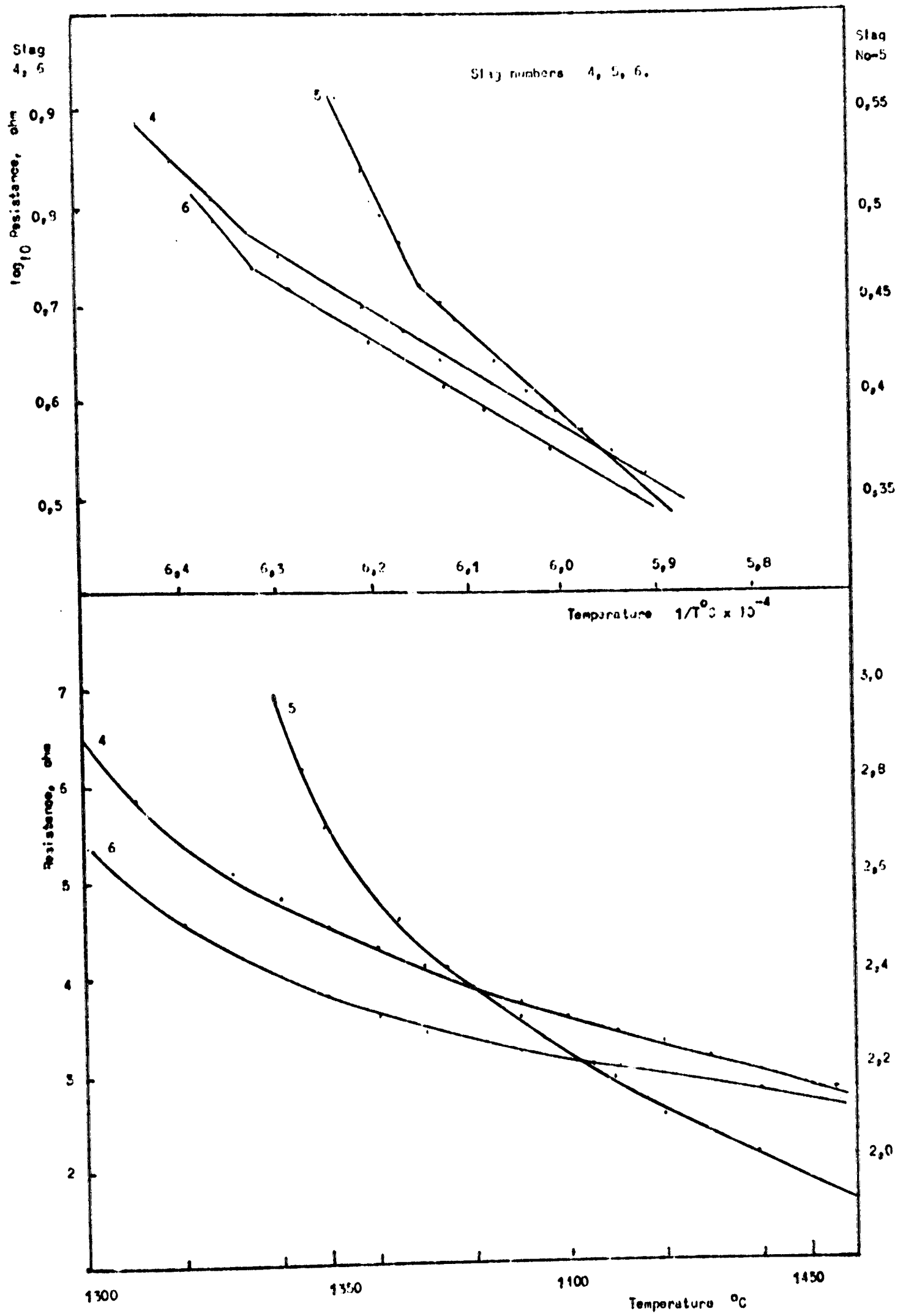

Figure II-8. MEASURED RESISTANCE - TEMPERATURE RELATIONSHIP

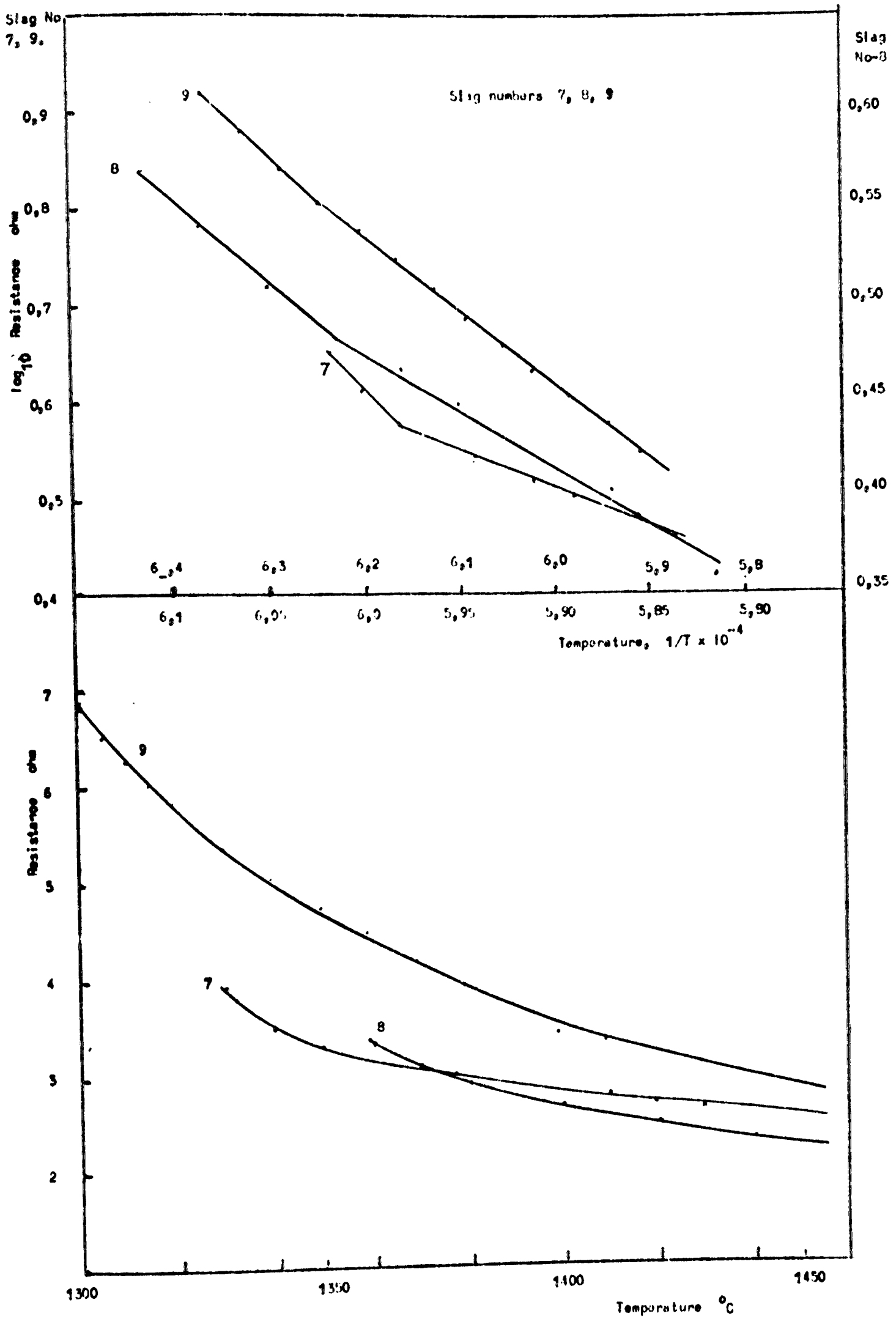

Figure 11-9 MEA[illegible] RESISTANCE & TEMPERATURE RELATIONSHIP

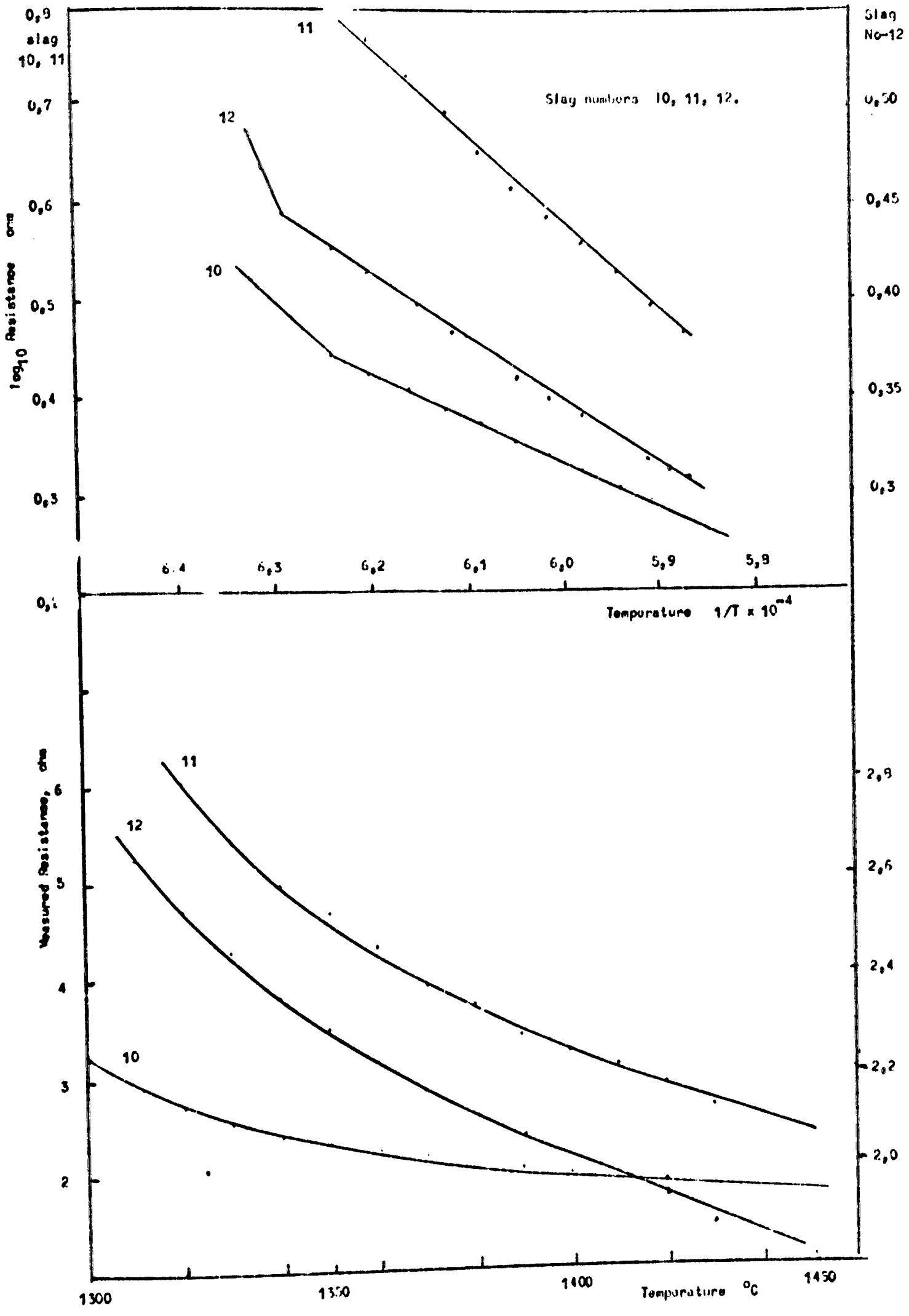

Figure 11-10 MEASURED RESISTANCE - TEMPERATURE RELATIONSHIP

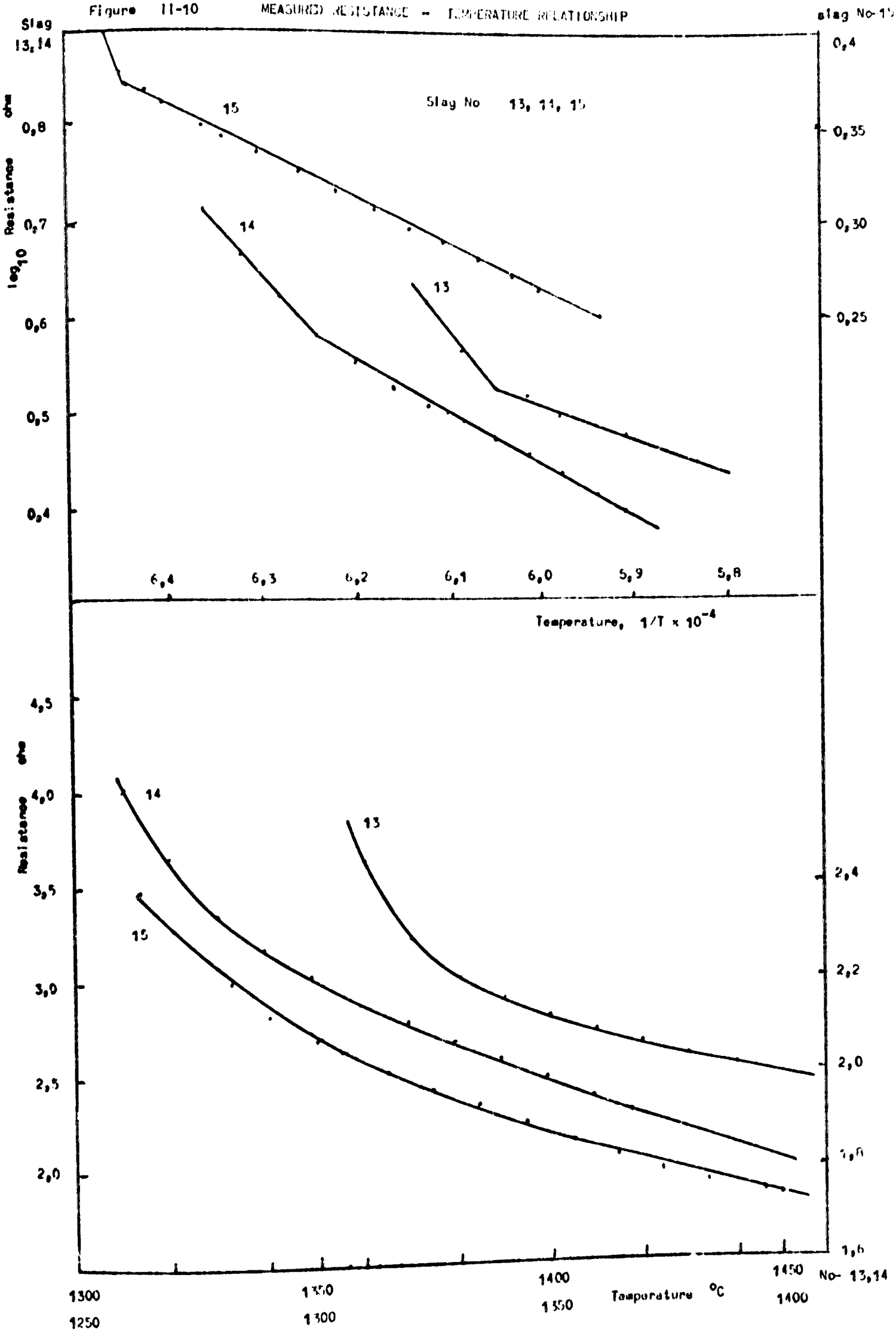

reversed with the aid of the 3-way cock shown in figure II-2./, and the gas was blown into the tube from the bottom. The gas mixture, composed of N_2 and H_2 (in a few trial tests with CO instead of H_2) was adjusted generally so as to give a flow rate of 1,2 to 1,5 l/min N_2 and 20 cc/min H_2 measured by the calibrated U-tube manometers. This maintained appropriate reducing conditions in the furnace and kept the FeO from being oxidised by the at - mosphere while the Fe^{2+}/Fe^{3+} equilibrium was fixed solely by the composition of the slag.

With the aid of a mirror system the electrodes were carefully aligned in the centre of the crucible and lowered into the melt when the temperature of this reached about 1315-1320°C. The contact with the melt surface was indicated by the collapse of the wide oscilloscope band, then the depth of immersion was adjusted exactly to 10 mm on the vernier scale.

Some of the slags, especially those with high FeO and SiO_2 contents exhibited a tendency to boiling. Due to this tendency it was difficult to carry out conductivity measurements with these slags on both rising and falling temperatures. The best mode of operation had to be found out during the test.

As mentioned already, the heating and cooling rates were found to have a significant effect on the measured resistivity. For the sake of uniformity of the operation with the aid of the temperature recorder the rates were kept at 1,5 to 2°C/min, from above the liquidus temperature. - On the completion of the test the slag was quickly cooled in controlled atmosphere and from the cold slag a sample was taken for FeO determination.

Results and discussion. The results of the conductivity measurements at three different temperatures above liquidus to - gether with the liquidus temperatures of the slags are given in Table II-4. In addition to the synthetic slags further tests were carried out on seven plant slags originating from one of the furnaces in the smelting plant. The results of tests carried out on these slags are contained in Table II-5. Figures II-6 to 10 give the changes in resistance with temperature. The results are plotted as ohms vs. temperature and log of resistance versus the reciprocal of temperature. Therefore these graphs give the actually measured net resistance (R) in ohms, as read from the dial settings of the resistance box, between two electrodes spaced at a distance

of 10 mm/...

Figure 11-11 RELATIONSHIP BETWEEN MEASURED RESISTANCE AND SPECIFIC RESISTIVITY (ρ) (determined with the use of the cell constant)

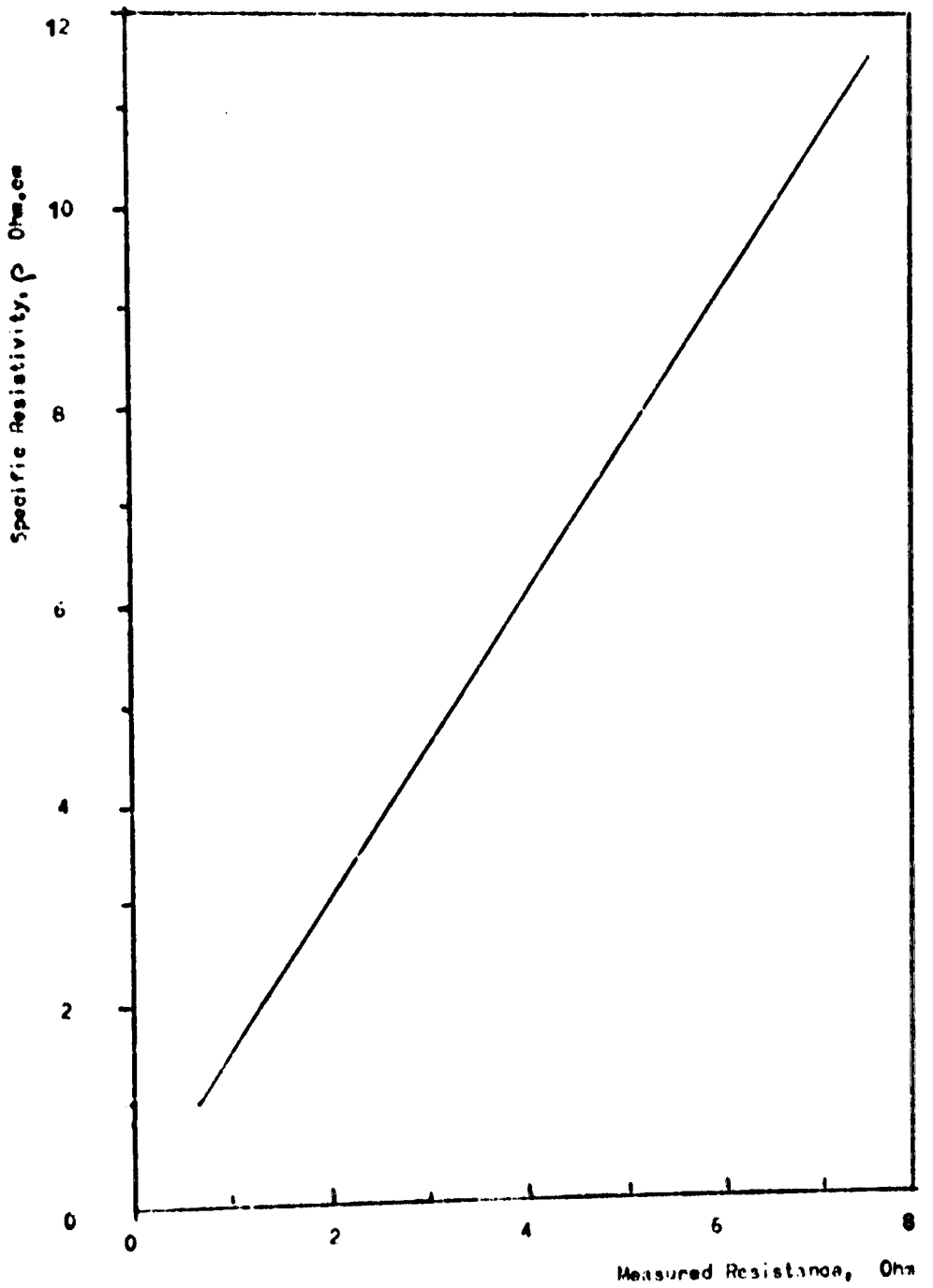

Figure 11-12 ELECTRICAL CONDUCTIVITY - TEMPERATURE RELATIONSHIP

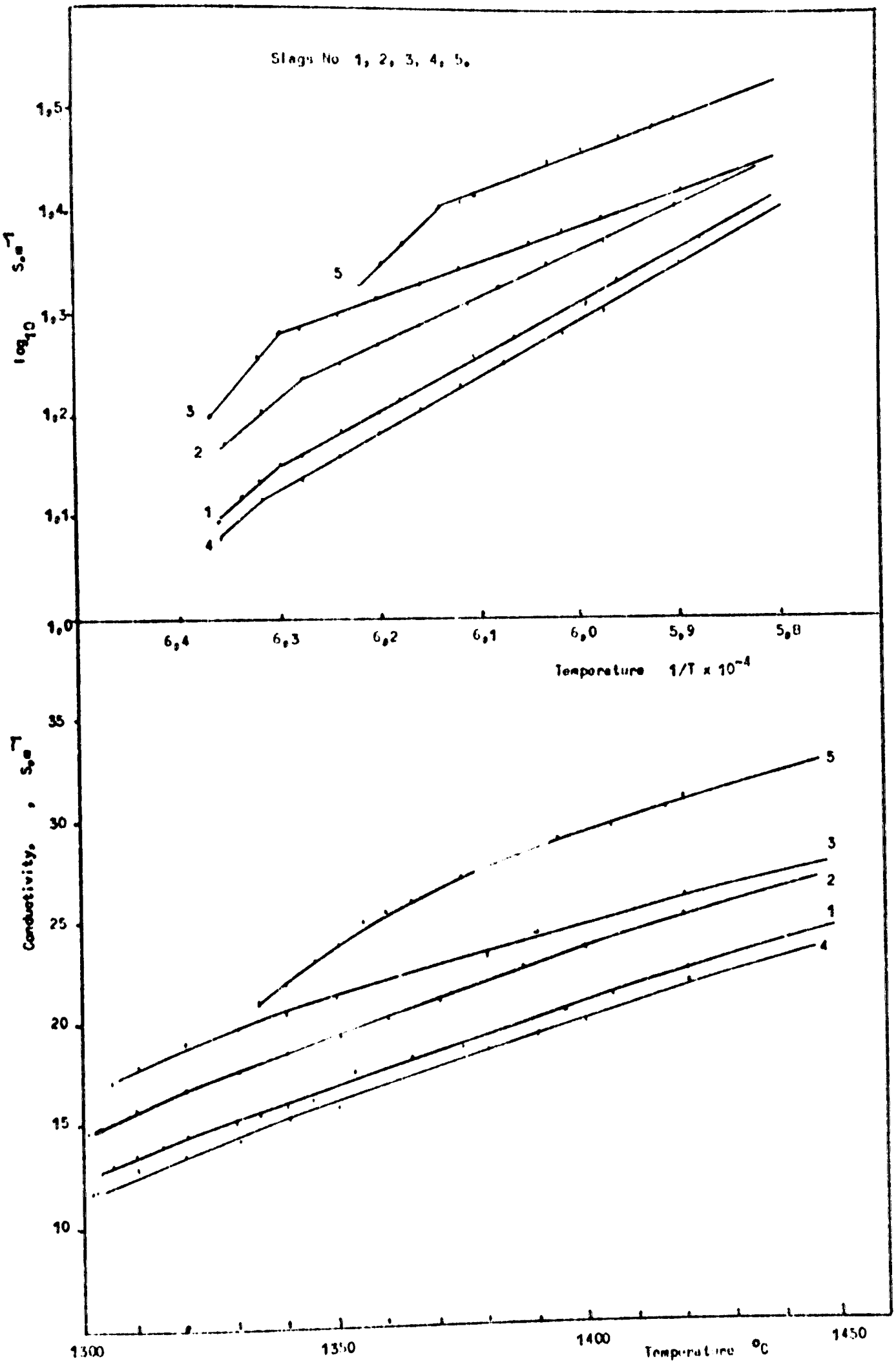

Figure 11 - 13. ELECTRICAL CONDUCTIVITY - TEMPERATURE RELATIONSHIP

Slags No 6 to 15

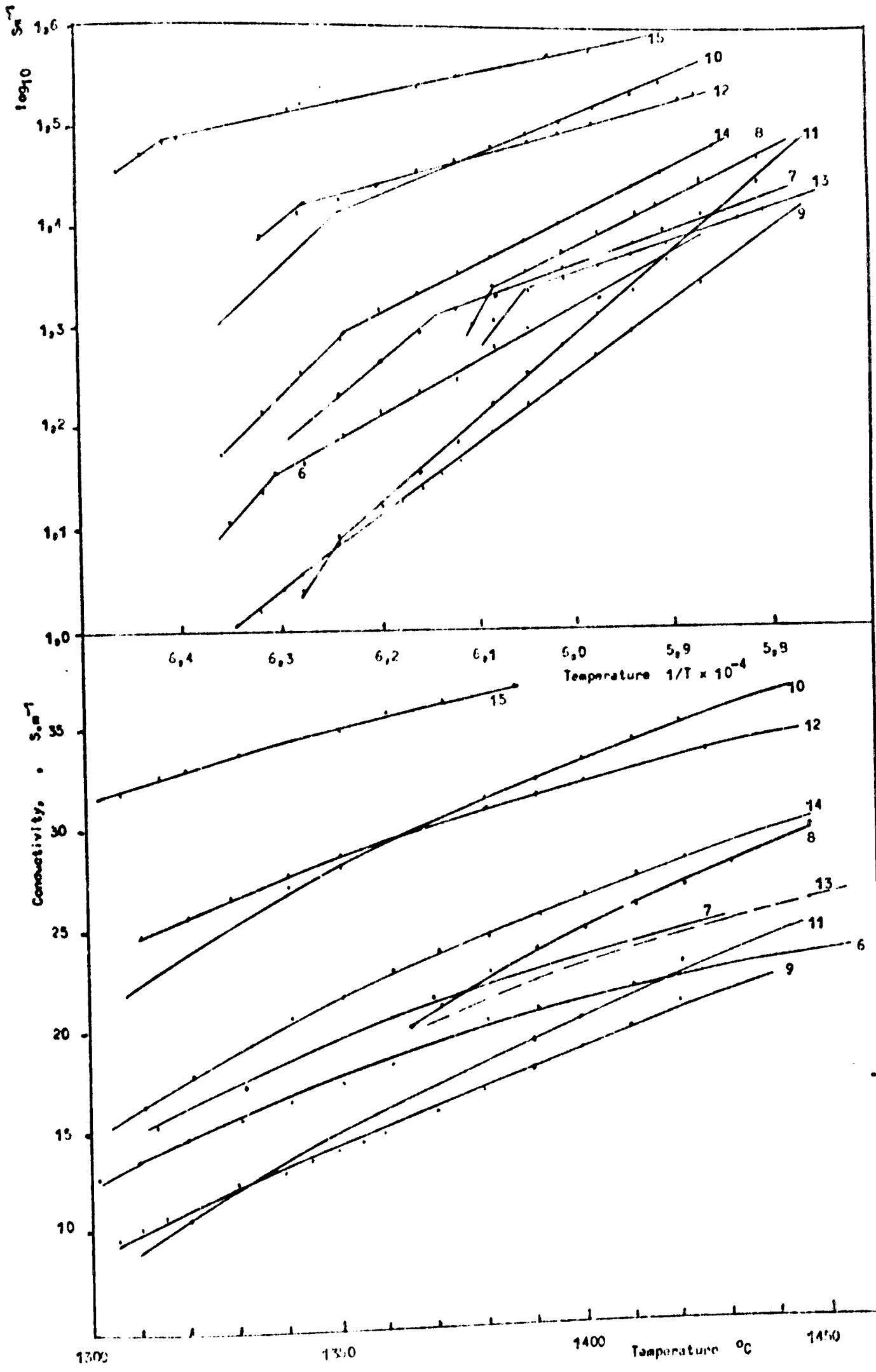

Figure 11-14 RESISTIVITY - TEMPERATURE RELATIONSHIP. PLANT SLAGS

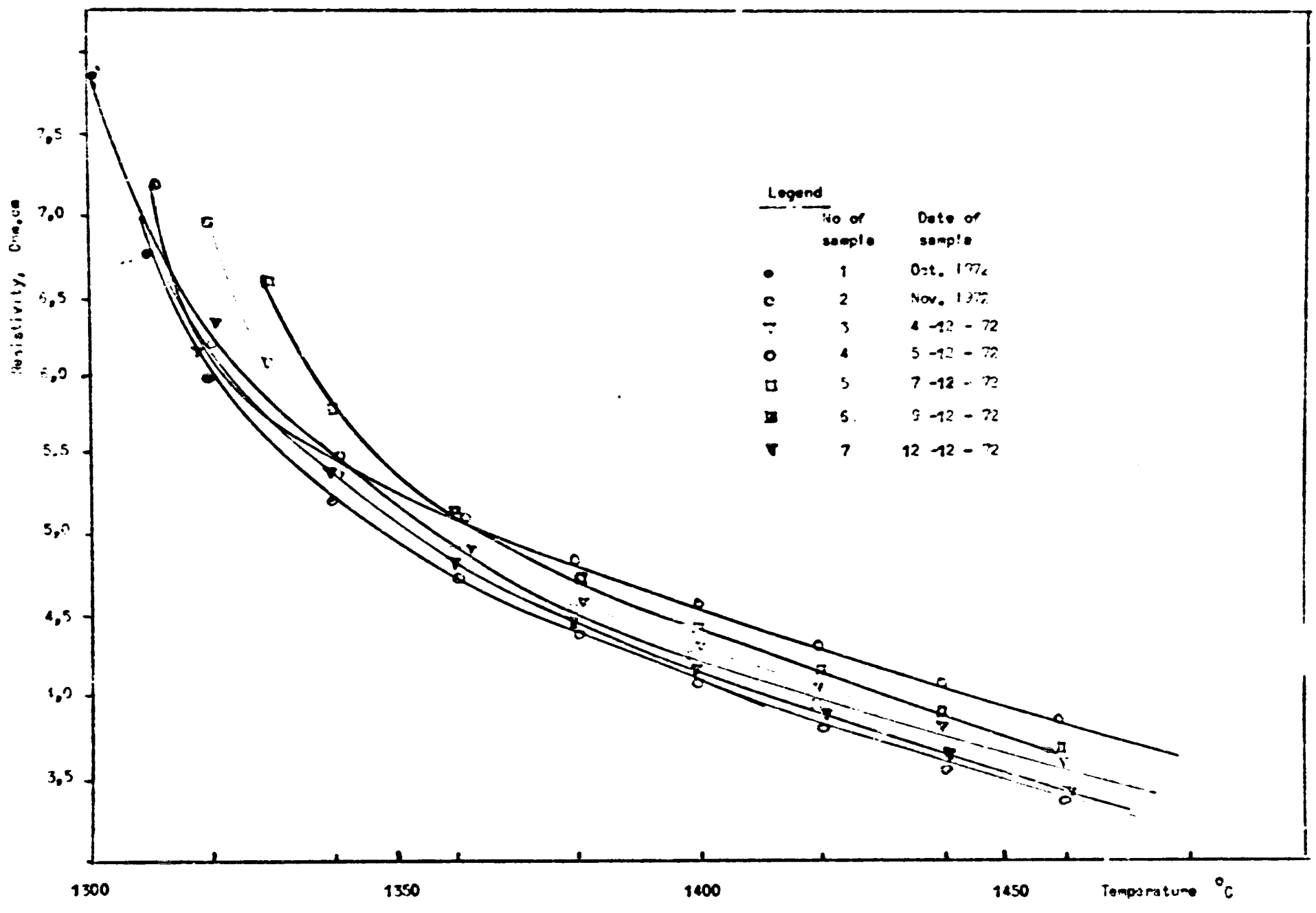

Figure 11 – 15. Log_{10} RESISTIVITY & RECIPROCAL OF TEMPERATURE RELATIONSHIP

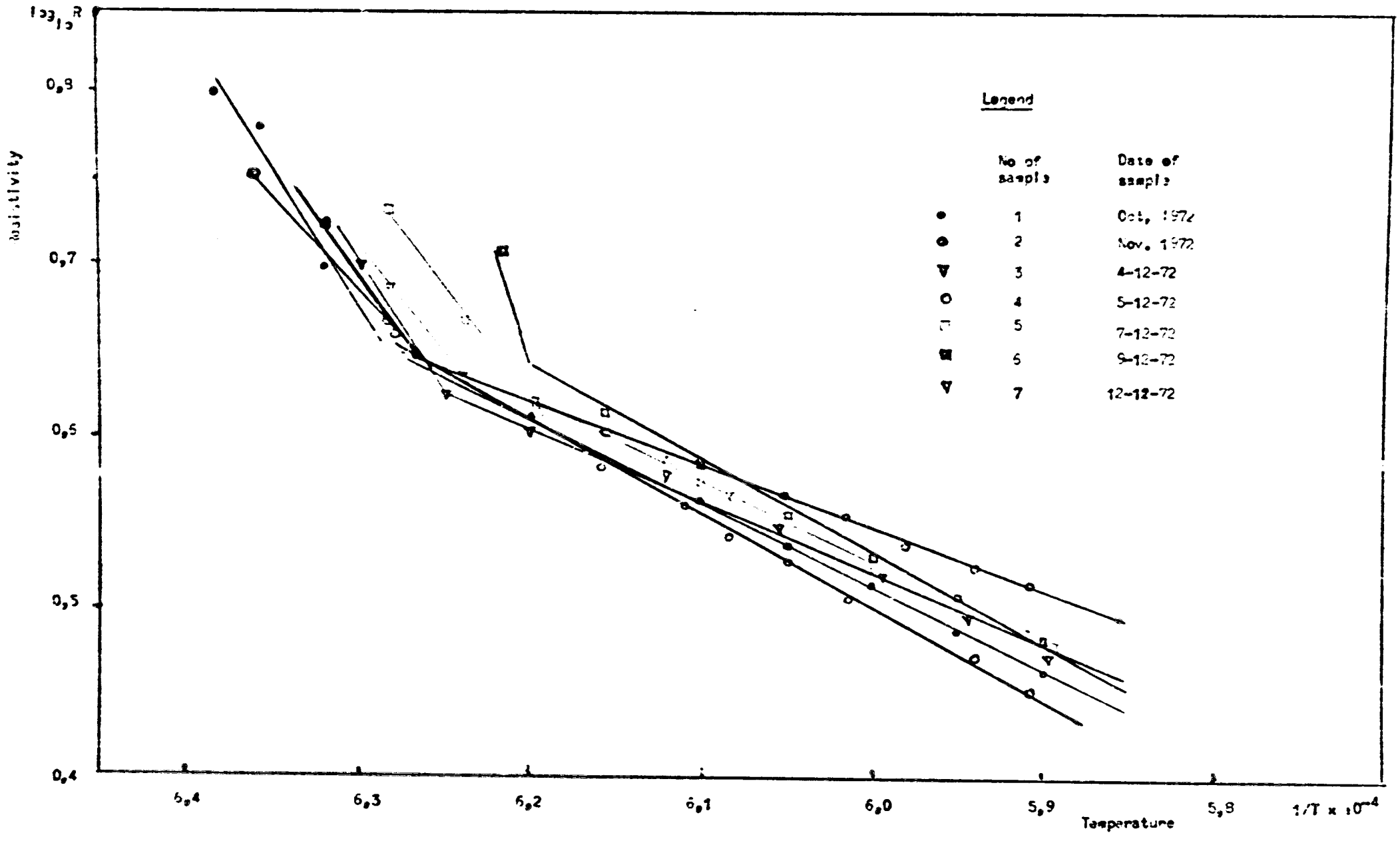

of 10 mm. To convert the data either to conductivity κ ($ohm^{-1}.cm^{-1}$ (or Sm^{-1}) or to specific resistivity, ρ ohm.cm, the cell constant must be taken into consideration. As indicated already, from from the plot of $\log_{10} K$ vs $\log_{10} R$ in figure 4. the cell constant was calculated as 65,5 Sm^{-1} or 0,655 $ohm^{-1} cm^{-1}$. Since

$$\kappa = \frac{G}{R_n} \qquad 4./$$

the conductivity values can be obtained by divivding the cell constant by the measured resistance values to get κ in Sm^{-1}. Actually the results will represent

$$\kappa = \frac{G_{r_1 r_2}}{R - r_\ell} \qquad \text{when} \quad R_n = R - r_\ell \qquad 5./$$

Where $G_{r_1 r_2}$ is the cell constant for the given depth of melt (r_1) and depth of immersion of electrode, (r_2), R is the apparent resistance and r_ℓ is the resistance of the leads. The lead resistance had already been accounted for and r_1 and r_2 were kept constant throughout the tests. The specific resistivity in ohm.cm is then given by

$$\rho = \frac{100}{65,5} \times R_n \qquad 6./$$

The conversion between ρ and R is indicated in figure 11.) The calculated conductivities together with the $\log_{10}$ values are plotted in graphs 12.) and 13.). The relevant data relating to the plant slags are shown in figures 14.) and 15.)

The cell constant is an important parameter in determining the relationship between cell geometry and slag resistivity as from equ.1./

$$R = \frac{1}{\kappa} \frac{1}{A} \qquad 7./$$

Since the electrical conduction takes place between cylindrical conductors, by theoretical considerations based on the concept of equally charged cylindrical infinite wires as proposed by Attwood (2) (further on this point see next section), the above expression relating to the cell constant can be formulated so as to involve electrode geometry, i.e. size, spacing and depth of immersion into the electrolyte and slag melt respectively. In the cell arrangement used for conductivity measurements the expression will relate to the capacitance between two electrodes these being regarded as equally charged, parallel, cylindrical infinite wires l units in length (immersed into the slag) and of radius r spaced at a distance S between centre to centre. Thus

G = /...

Figure 11-16 RESISTANCE OF ELECTRIC FURNACE SLAG AS A FUNCTION OF TEMPERATURE

RPM Plant slag. Data : October, 1972 (monthly composit)

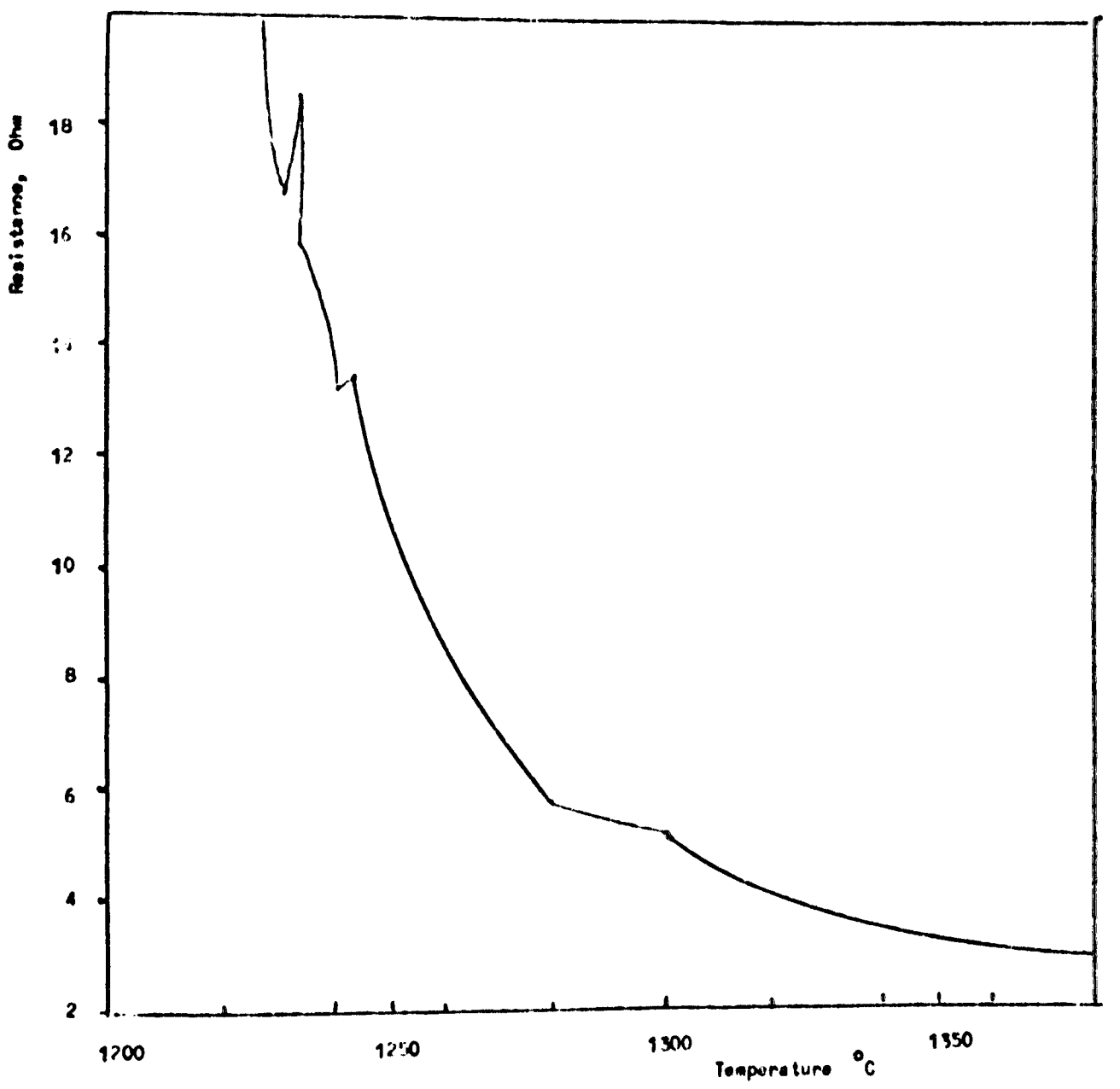

$$G = \frac{\ln\left[\frac{S}{2r} + \sqrt{\left(\frac{S}{2r}\right)^2 - 1}\right]}{W.l} \qquad 8./$$

giving in fact the capacitance in the region between two electrodes. The basic principle of this formulation is that by virtue of the relationship between capacitance and conductance

$$C = \frac{\epsilon}{\sigma} G \qquad 9./$$

(ϵ = dielectric constant of the medium and σ = charge density per unit area of conductor) formulas related to capacitance can be applied to the cal - culation of conductance. For the cell system used in the conductivity tests where the diameter of the electrode was 2 mm and the depth of immersion 10 mm, the cell constant will be

$$G = \frac{\ln\left[\frac{12}{2} + \sqrt{\left(\frac{12}{2}\right)^2 - 1}\right] \times 10^2}{3,14 \times 10} = 78,9\ Sm^{-1}$$

The difference between the higher theoretical and the previously quoted measured values of G is most likely to be due to what is known as the crucible effect in which the proximity of the crucible side walls and base offer additional path of conduction and hence contribute to the decrease in cell constant. With the incorporation of the cell constant and figures 14. and 15. the range of the electrical characteristics of the plant slags would be as follows:

	1400°C	1450°C
Conductivity Sm^{-1}	23,8 - 21,5	28,5 - 21,2
Specific resistivity ohm.cm	4,67 - 4,21	3,98 - 3,52

Results obtained with synthetic slags.

The liquidus temperatures were determined from the graphs showing log of resistance vs. reciprocal of temperature. There is a distinct change in the slope of the lines at the onset of the solidification of the slag and this point was taken as the liquidus temperature. It should be mentioned, however, that the value obtained in this way is not necessarily in complete agreement with the liquidus temperatures measured by the viscosity method. The electrical system for determining resistance, depending on the character of the slag, might pick up at an earlier stage than does the viscometer, changes brought about a./ by crystal formation in the liquid slag, or b./ changes in the composition of the liquid phase consequent upon crystallisation of the primary phase. The temperature - resistivity relationship for plant slag No - 1 is shown in figure 16 for a wide range down to the temperature

at which/...

Figure 11-17

RESISTIVITY - BASICITY RELATION

CaO, SiO_2 varied

FeO, MgO constant

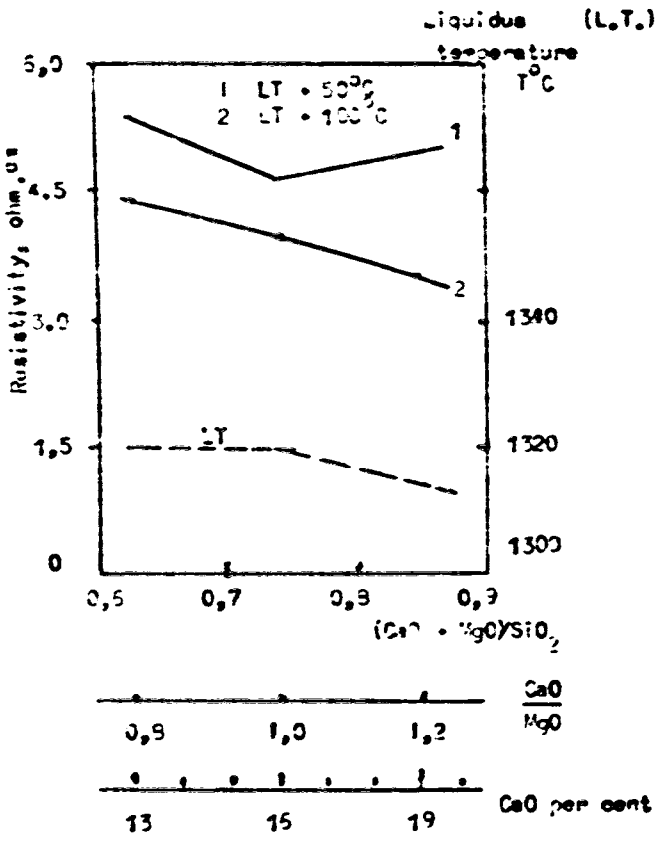

Figure 11-18

RESISTIVITY - BASICITY RELATION

MgO, SiO_2 varied

FeO, CaO constant

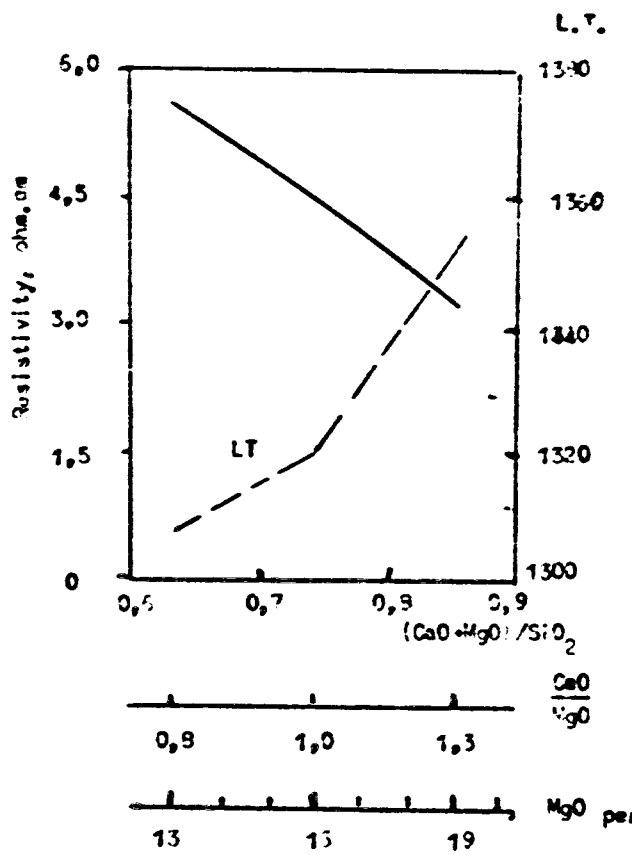

Figure 11-19

RESISTIVITY - BASICITY RELATION

CaO, MgO varied

FeO, CaO/MgO constant

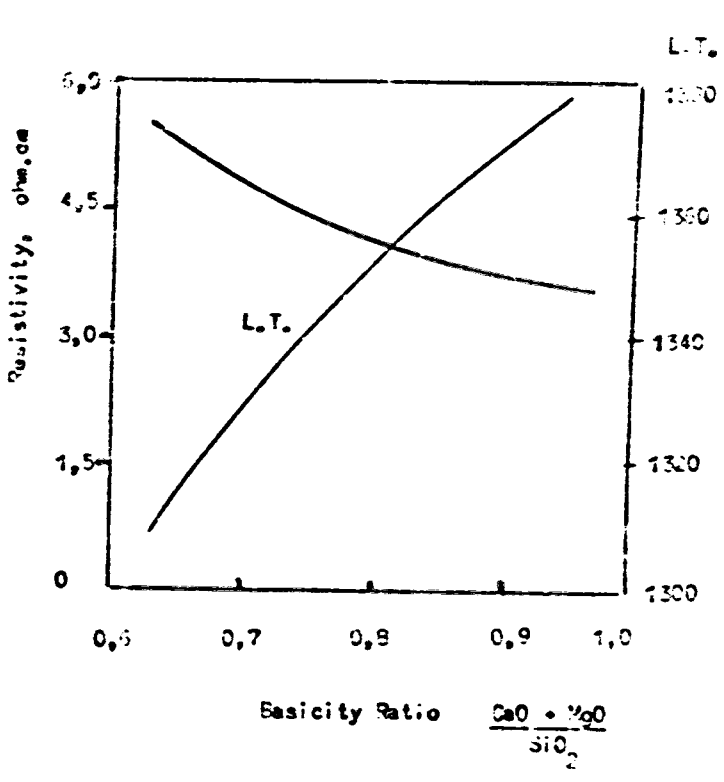

Figure 11-20

EFFECT OF TOTAL IRON ON THE RESISTIVITY

CaO, SiO_2 varied
Basicity, MgO constant

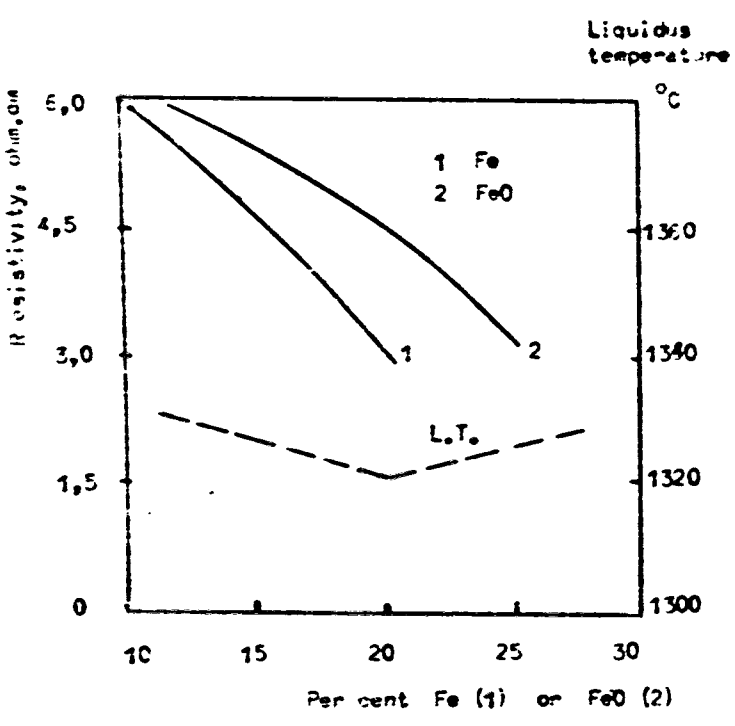

Figure 11-21

EFFECT OF TOTAL IRON ON RESISTIVITY

MgO, SiO_2 varied
Basicity, CaO constant

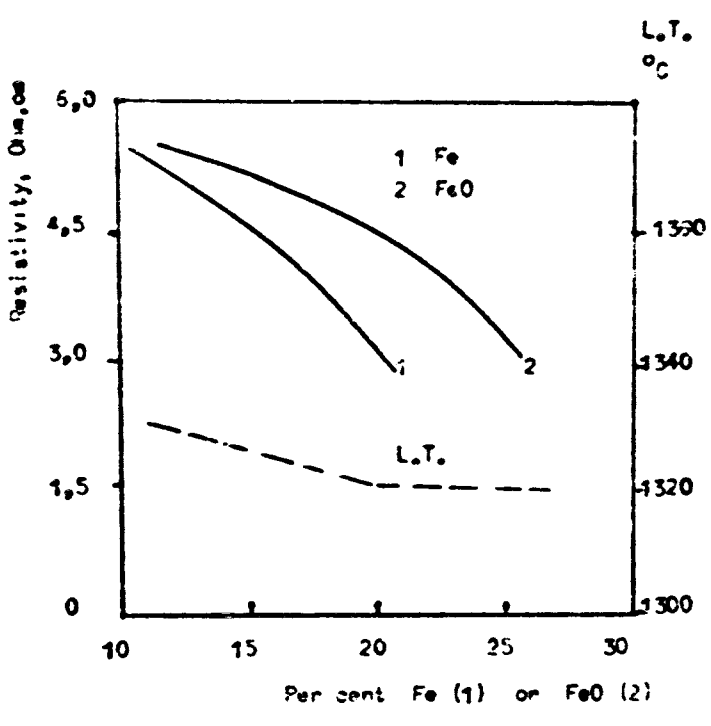

Figure 11-22

RELATIONSHIP BETWEEN RESISTIVITY AND THE Fe^{2+}/Fe^{3+} RATIO IN THE SLAG

Total iron = 15,4 per cent

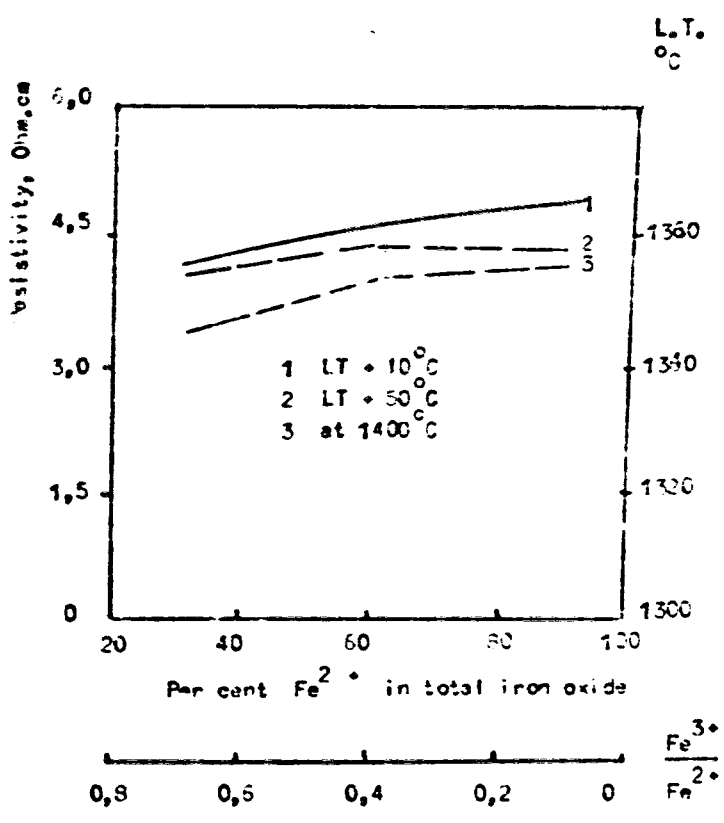

at which there is a predominance of crystalline material. According to the graph the first indication of the liquidus is around 1320°C. From resistivity measurements the former was taken for liquidus temperature.

The discussion of results using the grouping of slags as outlined in Table II-2 can be summed up as follows: (the given resistivities if not indicated otherwise, represent values obtained 50°C above liquidus temp.)

Group I. Relation between resistivity and basicity ratio at constant MgO, FeO and varying CaO, SiO_2 contents.

As indicated in fig. II-17. the resistivity decreases slightly with the increase in the CaO content and in basicity ratio. The slight increase at 50°C above liquidus is probably due to incomplete equilibrium in the slag, plus experimental error. The small decrease in liquidus temperature cannot be regarded as significant.

Group II. Relationship between resistivity and basicity ratio with constant CaO and FeO but with increasing MgO content in the slag.

Figure 18. shows that the effect of the change in MgO content is far more pronounced than that of CaO. Increasing the MgO content from 13 to 19 per cent will decrease the resistivity by 30 per cent while the liquidus temperature will rise from 1308 to 1350°C.

Group III. Relationship between resistivity and basicity ratio with increased CaO and MgO contents but at constant FeO content.

The change in resistivity as shown in figure 19. is very similar to that of the previous case, but as could be expected, the rise in liquidus temperature is more pronounced.

Groups IV and V. Relationship between resistivity and total iron content with variation in CaO, MgO and SiO_2 contents.

As shown in figures 20 and 21. changes in resistivity are very similar in the two groups. An increase in the total iron from 10,7 to 19,7 per cent (corresponding to 12,7 to 25,4 per cent FeO) results in a marked decrease of 4 to 45 % in the resistivity of the slag.

The liquidus temperature decreases with decreasing CaO and MgO content, but the effect is not significant.

Group VI. Relationship between resistivity and oxidation potential of the slag.

Figure 22 indicates the effect of the Fe^{2+}/Fe^{3+} ratio on the resistivity at 10°, 30° and 50°C above the liquidus temperature of the slag. As will be obvious, the change in Fe^{2+} content from 40 to about 90 per cent has very limited effect on the resistivity at temperatures

30° above liquidus/...

30^{o}C above liquidus or higher. On the other hand, the effect of the oxidation potential becomes slightly more significant when slags are tested at constant temperature. Even in this case the change in resistivity becomes negligible with divalent iron contents above 60 per cent.

Pertaining to the effect of Fe^{2+}/Fe^{3+} ratio on the electrical conductivity Engell and Vygen (3) have carried out detailed investigation on the system $CaO-FeO-Fe_2O_3-SiO_2$ using a fixed CaO/SiO_2 ratio of 0,79 and total iron content varying from N_{Fe}=0,034 to 0,44. With the condition $B=n_{CaO}/n_{SiO_2}$= 0,79 the oxidation state of the slag as characterised by the relative amount of trivalent iron content $x = n_{Fe^{3+}}/(n_{Fe^{3+}} + n_{Fe^{2+}})$ within the range of the chosen slag composition depends only on the partial pressure of oxygen. At other values of B the relationships become more complicated. (see for example Larson H. - Chipman J.: Trans Met. Soc. AIME, 197, 1953, 1089). The electrical conductivity tests were performed at 1600°C and the Fe^{3+}/Fe^{2+} ratio was varied by the adjustment of the gas phase above the melt, between 0,25 and 0,77. The conductivity could be expressed by the following equation

$$\kappa = \kappa_o - ax + bx(1 - x) \qquad 10./$$

where $x = n_{Fe^{3+}}/(n_{Fe^{3+}} + n_{Fe^{2+}})$

and κ_o, a and b were given in ohm^{-1},cm^{-1}. For N_{Fe} = 0,55, that is the range of the iron content of the model furnace slags (average iron content), between 40 and 90 per cent Fe^{2+} they found a much greater change in resistivity than was evident in this study. The change in resistivity with the change of the Fe^{2+}/Fe^{3+} ratio was found by Engell and Vygen to be more pronounced the higher the iron content became. With the increase of the trivalent-divalent iron ratio the conductivity increased and reached a flat maximum, then it decreased again. A similar trend was evident with the electrical conductivity of glasses containing phosphorus and iron with ratios of Fe^{3+}/Fe^{2+} varying between 0,5 and 0,8. In the composition range of slags investigated for the effect of the oxidation state upon the electrical conductivity, the iron oxide content in the present study corresponded to N_{FeO} = 0,267 = N_{Fe} = 0,192. It is interesting to note that the change in resistivity at this iron content, as referred to the absolute value of κ, was similar to that obtained by Engell and Vygen for their system at N_{Fe} = 0,063.

In equ. 10. the term κ_o-ax represents ionic conduction and its variation with the oxidation state of the slag, while the quadratic term, bx(1 - x), represents electronic conduction this being attributable to charge transfer between Fe^{2+} and Fe^{3+}. Thus in slags containing divalen iron(ferrous oxide), there is always electronic conduction present the extent of which will

depend on the/...

Figure 11-23

RANGE OF RESISTIVITY OF COMPOSITE SLAGS AND PLANT SLAGS

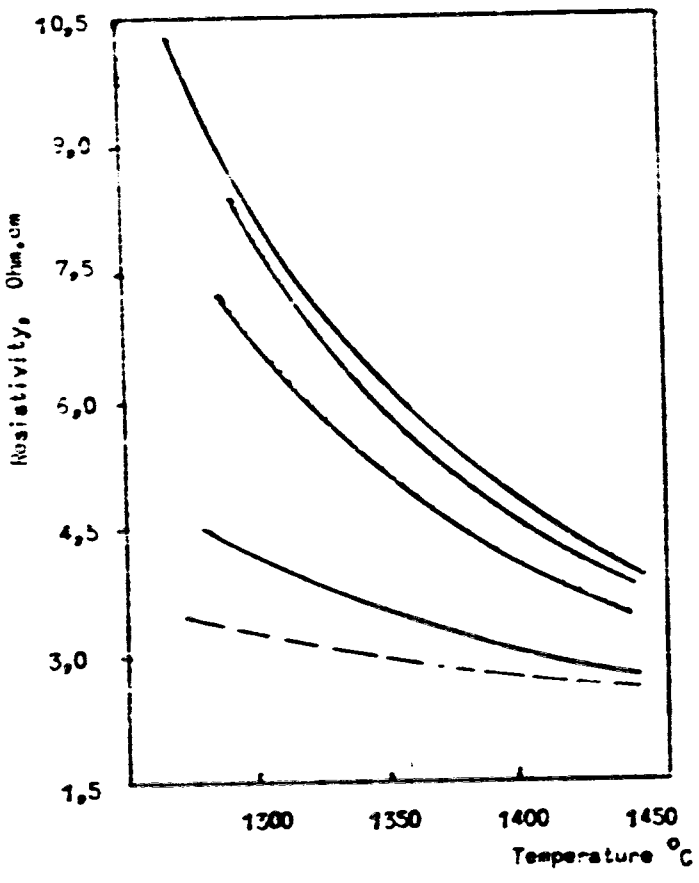

Figure 11-24

COMPARISON BETWEEN THE RESISTIVITIES OF A PLANT SLAG AND A COMPOSITE SLAG

1 Composite slag No-1
2 Plant slag No-7

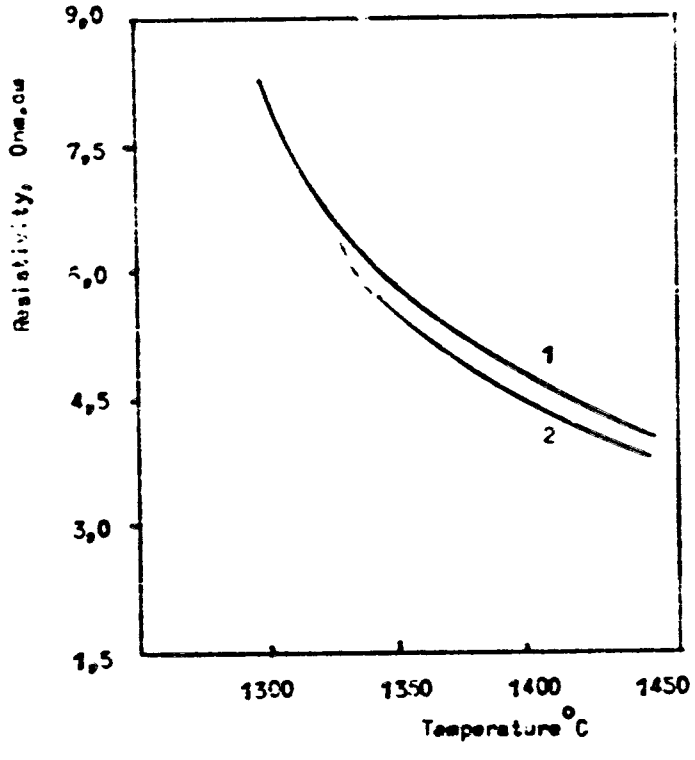

Figure 11-25

EFFECT OF THE INCREASE OF THE SiO_2 CONTENT ON THE RESISTIVITY OF SLAG

SiO_2 increased in composite slag

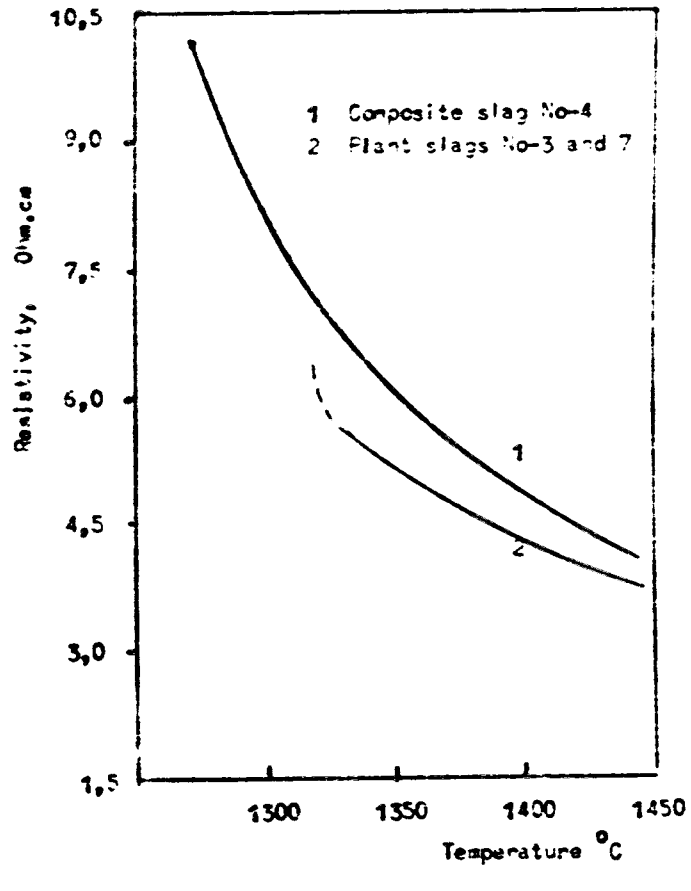

depend on the divalent iron content. With N_{Fe} = 0,063 the absolute value of K, as noted above was similar to that of the present study at N_{Fe} = 0,192. For the low iron content the values of the constants a and b of equation 10. were given as a=0,25 and b= $8x10^{-2}$ with κ_o = 0,57. This would indicate that at the quoted iron content of the slag (i.e. N_{Fe} = 0,063) the ionic conduction was predominat in the system under study and the influence, exerted upon it by the increase of the Fe^{2+} content from 40 to 90 per cent was negligible.

Pertaining to the influence of the partial pressure of oxygen upon the electrical conductivity Russian investigators have found that in quaternary $CaO-Al_2O_3-SiO_2-Fe_xO_y$ melts an appreciable change of γ with the change of oxygen partial pressure occured when the iron content exceeded 10 per cent. Until this concentration was reached the conductivity of the melts appeared to be practically only of ionic type. (4)

The behaviour of plant slags. The resistivity versus temperature relationships for the plant slags are shown in figures 14. and 15. As will be obvious from the graphs the trend is virtually the same for all slags with a narrow range of resistivity between the extreme values that varies from 0,25 to 0,40 ohm.cm. depending on the temperature. In considering the limited variations in their composition this is understandable.

Figure 23. indicates the resistivity range of the plant slags (shaded area) in that of the composite slags. The dotted line at the bottom represents extreme slag composition. (Slag No-15). As shown by the graph the resistivity range of the plant slags is in the upper area of the range of the composite slags which is in accord with the differences in composition of the two slag groups.

Figure 24. shows a comparison between a plant slag(No-7) and a composite slag (No-1) of very similar composition in regard to the change of resistivity with temperature. The agreement between the measured resistivities is good and the minior differences could partly be attributable to experimental error. However, the difference in liquidus temperatures is noteworthy, a fact, that might possibly be explained on the basis of the different oxidation potential of the two slags.

On keeping the concentration of the other components by and large the same and increasing the silica content in the composite slag, that is decreasing the basicity ratio, increases the resistivity (see figures 17 and 18). In plant-

slag composite slag/...

Figure 11-26

EFFECT OF THE TOTAL IRON CONTENT ON THE RESISTIVITY OF THE SLAG

Plant slag - composite slag relationship. FeO content increased in composite slag.

1 Composite slag No-12
2 Plant slag No-5

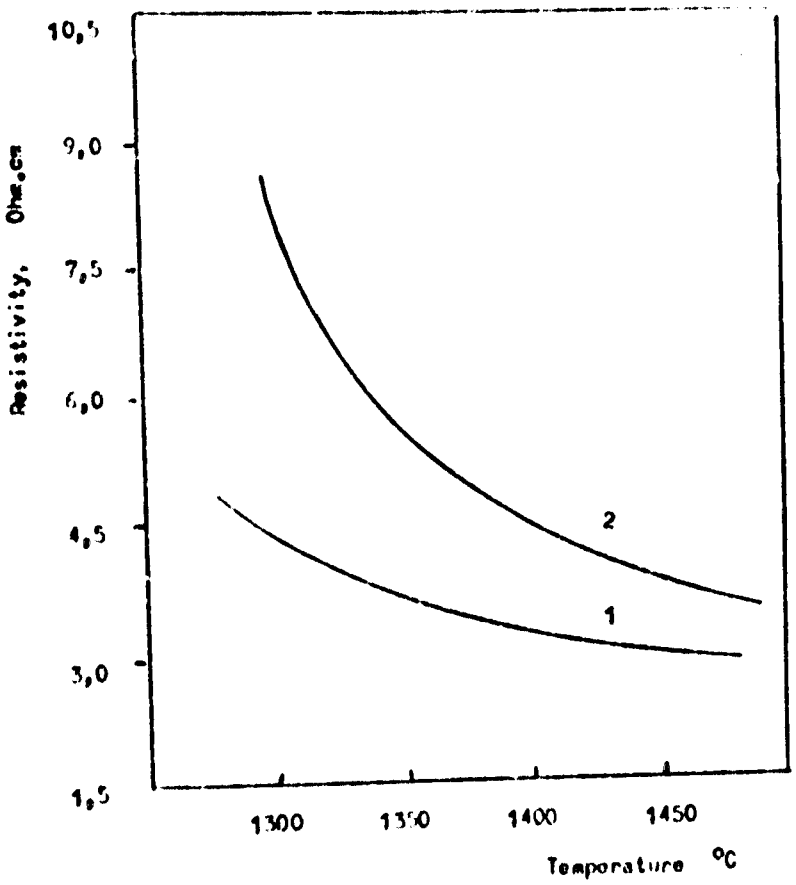

slag - composite slag relationship this is depicted in figure 25 with composite slag No-4 and plant slags No-3 and No-7.

The increase of the total iron content, as it was found with the composite slags considerably decreases the resistivity. The same could be established in plant slag (No-5)and composite slag (No-12) relationship as shown in fig. 26.

Generally, no distinct relationship could be found between resistivity and other variables for the plant slags. This was undoubtedly due to the narrow composition range and also to the random pattern of the change of the slag composition. One important fact that emerges in this context is the reduced significance of the change in both total iron and MgO contents, which, on the basis of the finding for composite slags, would be of rather important consequence. As compared with the composite slags it should be noted that the change in the FeO content in the range of 15,7 to 21,2 per cent, according to figures 14 and 15 would result in a change of only 0,5 ohm.cm in a total of about 4,6 ohm corresponding roughly to 11 per cent.

2.4./ Viscosity.

Mode of slag preparation. The mode of pre-treatment of the slag-forming constituents and the preparation of slags was identical with that described for the conductivity tests with the composition range of the slags being also the same.

Equipment. a. Viscometer. A commercially available viscometer of the concentric cylinder type using a rotating inner cylinder is the Brookfield which was selected for use for viscosity measurements. This equipment gives reasonably precise results for viscosity much more rapidly than any other measuring device. In principle a platinum spindle forms the inner cylinder rotating in the molten slag and the shear force or viscous drag exerted by the slag causes the inner cylinder to lag behind the main drive shaft and the coupling to which the spindle is attached. In equilibrium the restoring force from the spring equals the force produced by the viscous drag on the inner cylinder. A pointer attached to the spring gives an indication of the magnitude of the viscous force absorbed by the spring and this can be read from the position of the pointer against a graduated scale.

The inner cylinder/...

Table II-6. Calibration of viscometer

Type of oil used	Temperature °C	BVN Number	Viscosity poise
C - 600	20,0	100,0	21,10
	25,0	76,5 - 77,0	13,00
	37,8	34,0 - 34,5	5,24
	50,0	10,0	2,39
S - 60	20,0	1.46	8,50

Figure 11-27 VISCOMETER CALIBRATION CHART

Revolution of spindle : 12 rpm

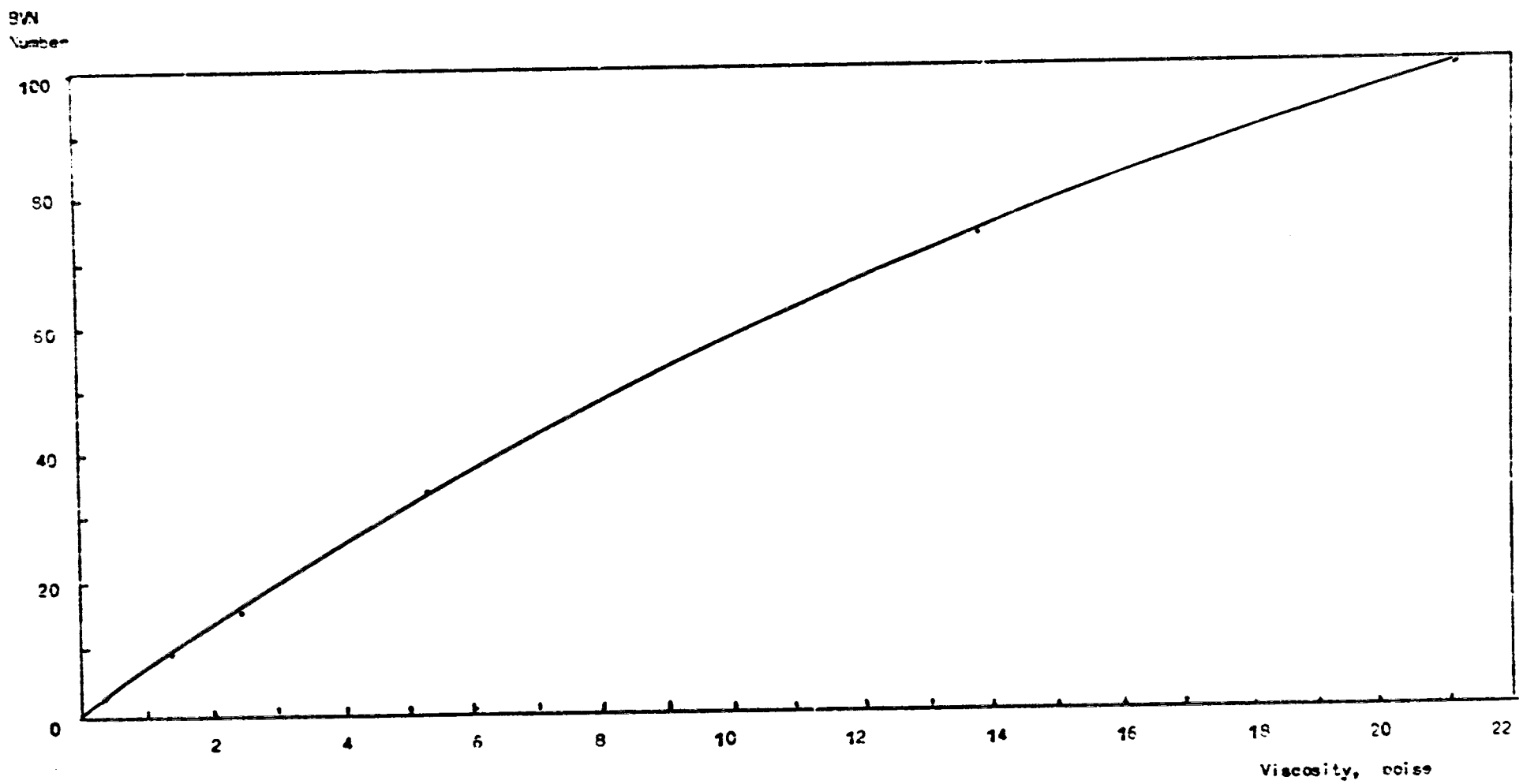

The inner cylinder attached to the spindle of the viscometer was constructed of platinum being 25 mm length by 16 mm diameter and wall thickness 1,3 mm. Part of the shaft exposed to the high temperature was made also of platinum and the remainder of inconel alloy.

The outer cylinder was a platinum crucible of identical dimensions as that described earlier for use in the conductivity tests. Similarly, it was supported by a cast alumina or firebrick base seated on the top of a mullite tube which could be raised or lowered into the hot zone of the furnace.

b./ Furnace. The furnace and ancillary equipment used for the viscosity tests was the same as that applied in the measurement of electrical conductivities.

Calibration of viscometer. Because of the narrow range of slag comosition the calibration was performed at a constant speed of 12 rpm of the viscometer shaft using the following calibration oils : S - 600 Type and S - 60 Type ASTM oil standards (Cannon Instrument Co, USA). The calibration was carried out at various temperatures in a thermostatic - controlled water bath using a brass crucible of identical dimensions to that of the platinum crucible of the high temperature tests. Details of the calibration are given in Table II-6 and the corresponding chart is shown in figure 27.

Mode of measurement. Considerable bubbling was experienced with some of the slags during the melting-down period. The evolution of the bubbles occurred irrespective of the composition of the gas atmosphere above the melt generally represented by a flow of 25 to 30 cc/min hydrogen and 1200 to 1500 cc/min nitrogen of spectrographic purity. The bubbling phenomenon, to which further reference will be made later, did not permit readings to be taken in both the heating and cooling cycles of the individual tests. For sake of uniformity of the operation all slags were heated to a maximum temperature (about 120°C above liquidus) and the viscosity values were recorded only while the slag was cooling. During the cooling cycle the formation of bubbles appeared to be far less pronounced or even have ceased.

The reproducibility of the measurements was ensured by positioning the top of the spindle in all tests 10 mm below the surface of the molten slag in the platinum crucible. All viscosity tests were carried out at 12 rpm of the spindle which gave BVN readings sufficiently high even at the low

viscosities/...

Table II-7. Viscosities of synthetic slags.

Slag number	Viscosity, (poise) 1400°C	1450°C
1	3,70	2,70
2	2,70	1,90
3	2,50	1,75
4	4,20	3,00
5	2,50	1,40
6	3,85	2,50
7	2,50	1,50
8	2,00	1,40
9	4,30	3,00
10	2,20	1,80
11	4,00	3,70
12	1,75	1,45
13	2,75	1,75
14	3,30	2,55

Table II-8. Viscosities of plant slags.

Slag number	Viscosity, (poise) 1400°C	1450°C	Date of sample
1	3,42	2,90	Oct. 1972
2	3,32	3,02	Nov. 1972
3	3,32	2,75	4/12/72
4	3,20	2,57	5/12/72
5	3,35	2,69	7/12/72
6	3,48	3,10	9/12/72
7	3,25	2,65	12/12/72

Figure II-28. VISCOSITY - TEMPERATURE RELATIONSHIP.

Slag numbers 1, 2, 3.

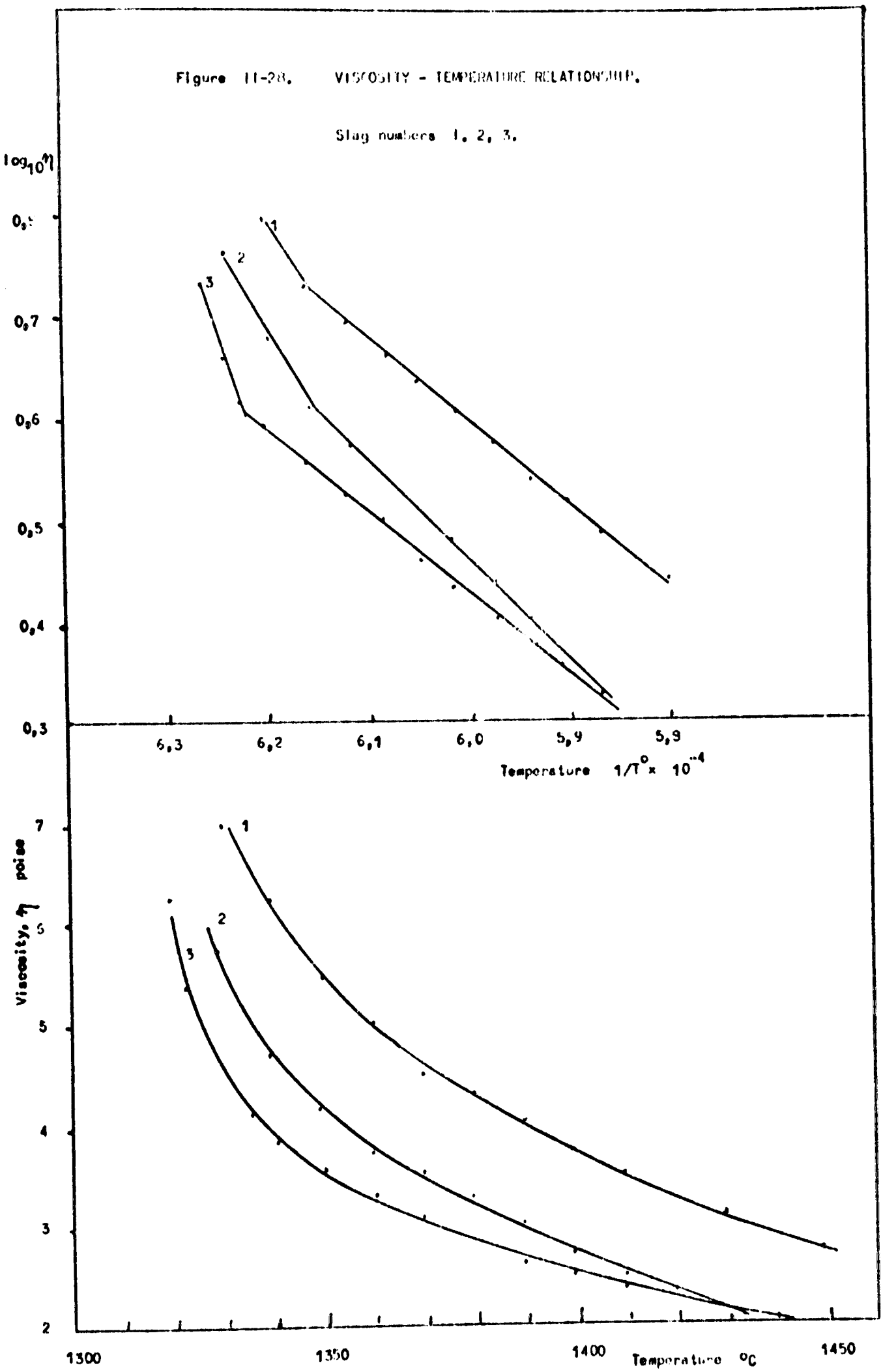

Figure II-29. VISCOSITY - TEMPERATURE RELATIONSHIP

Slag numbers 4, 5.

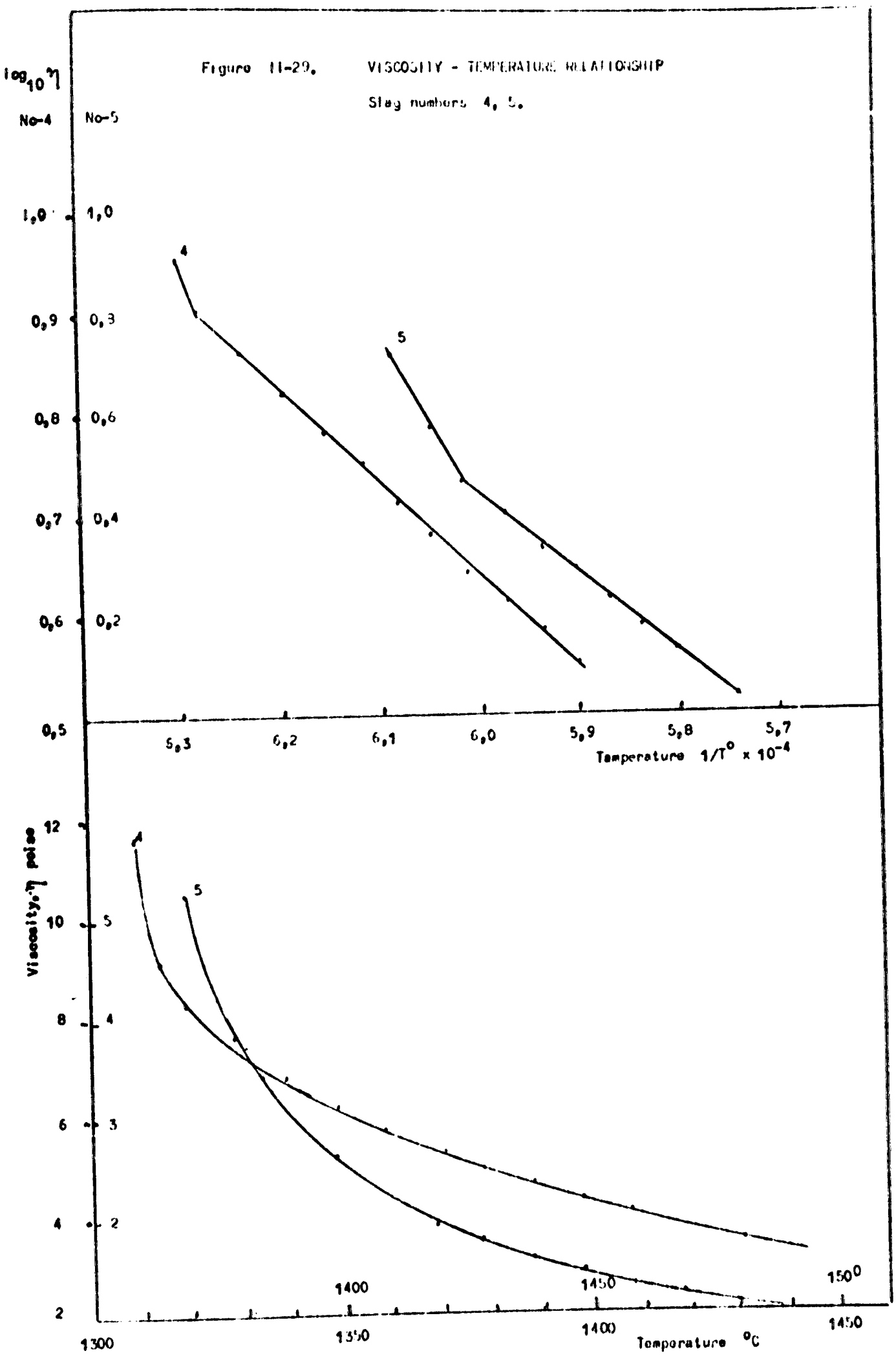

Figure 11-30. VISCOSITY - TEMPERATURE RELATIONSHIP.

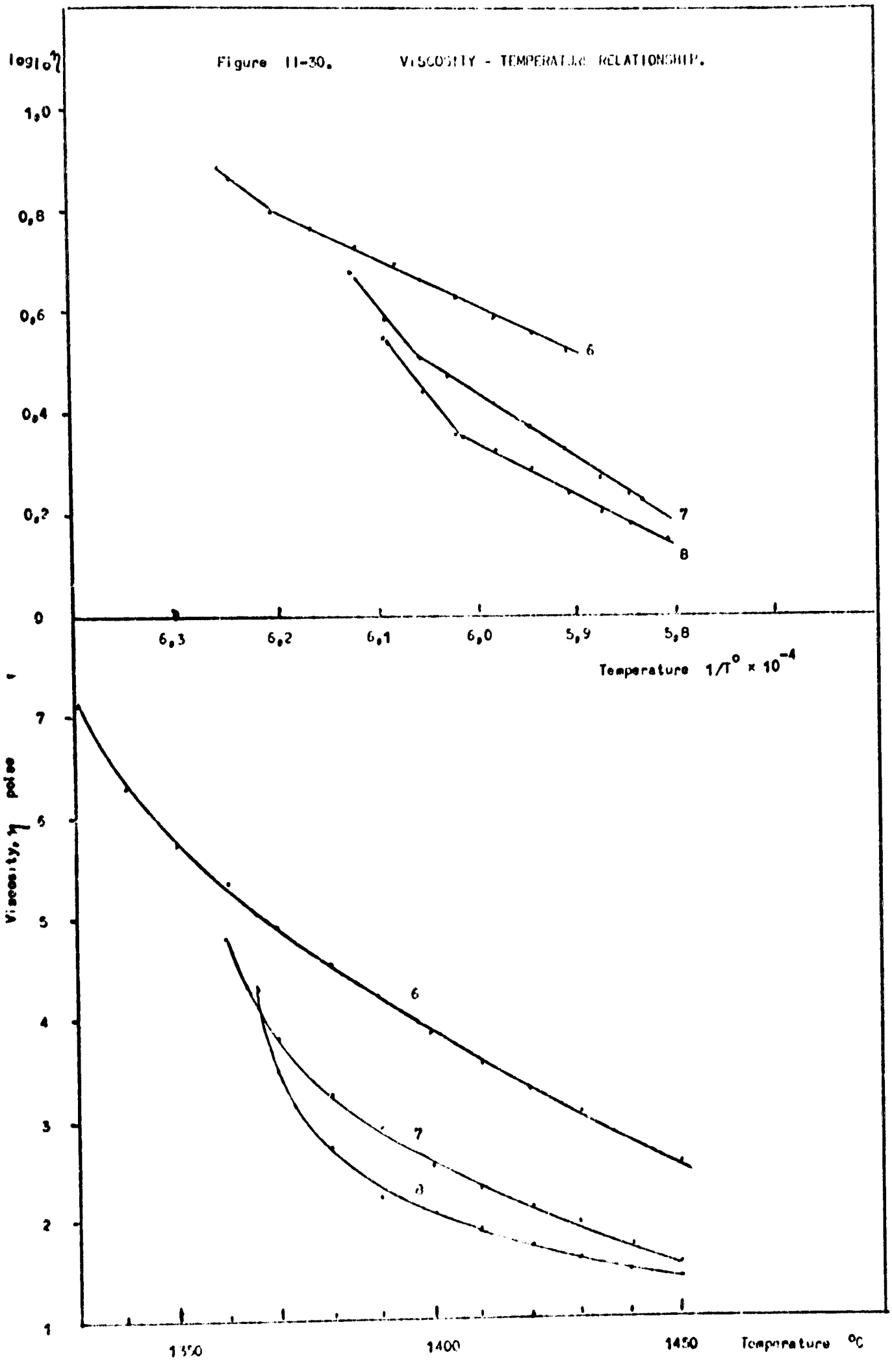

Fibure 11-31. VISCOSITY - TEMPERATURE RELATIONSHIP.

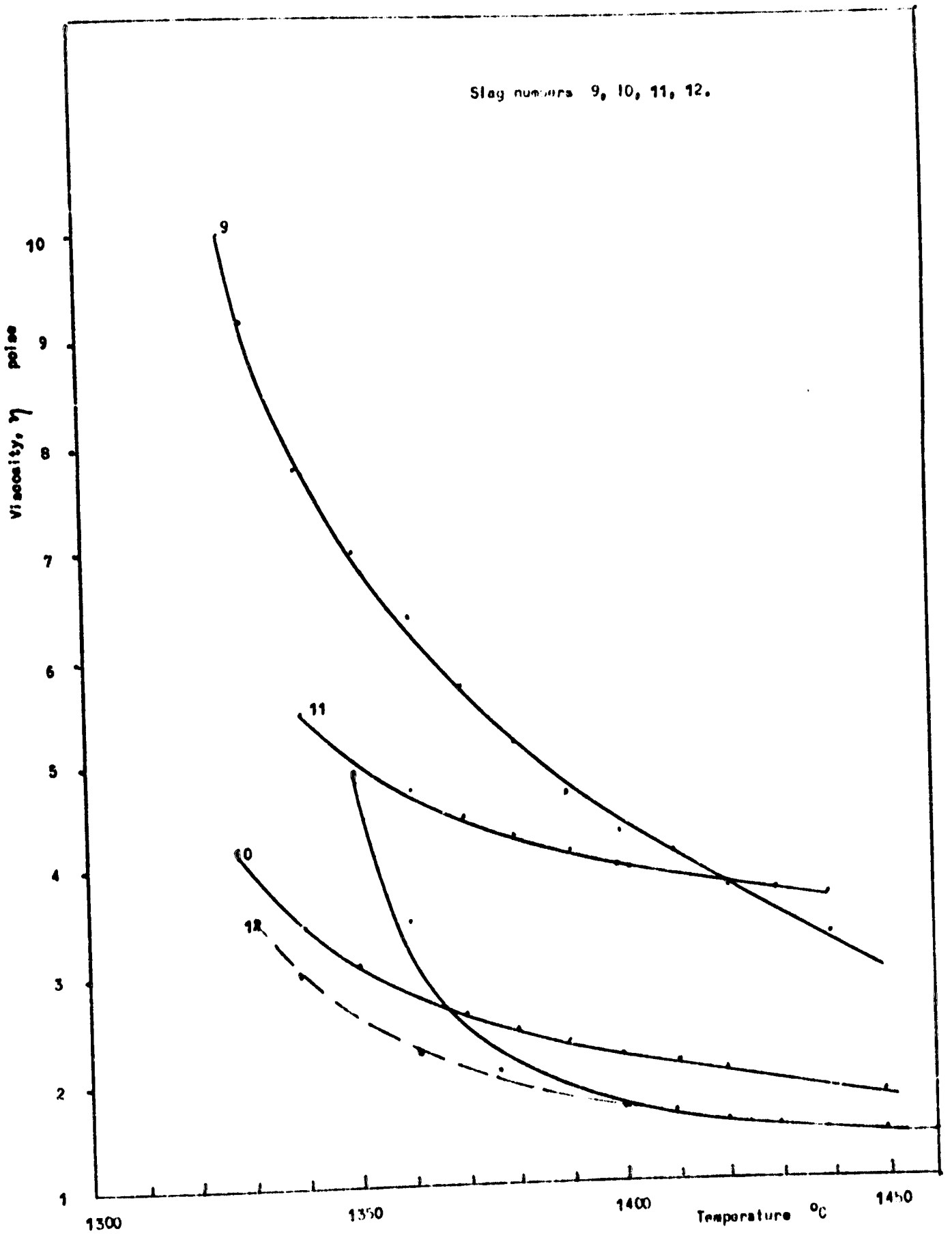

Figure 11-32. VISCOSITY - TEMPERATURE RELATIONSHIP.

Slag numbers 9, 10, 11, 12.

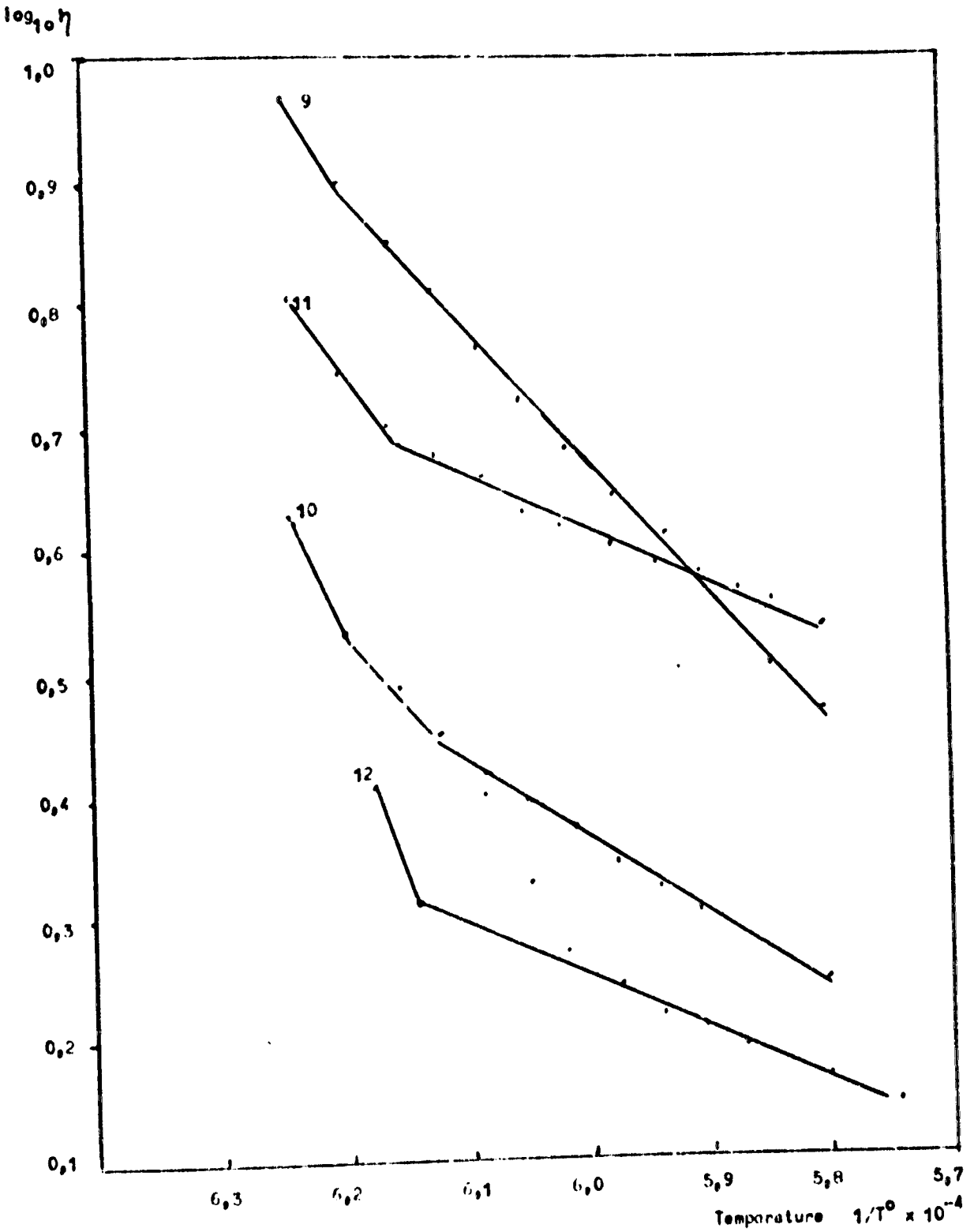

Figure 11 - 33. VISCOSITY - TEMPERATURE RELATIONSHIP.

Slag numbers 13, 14.

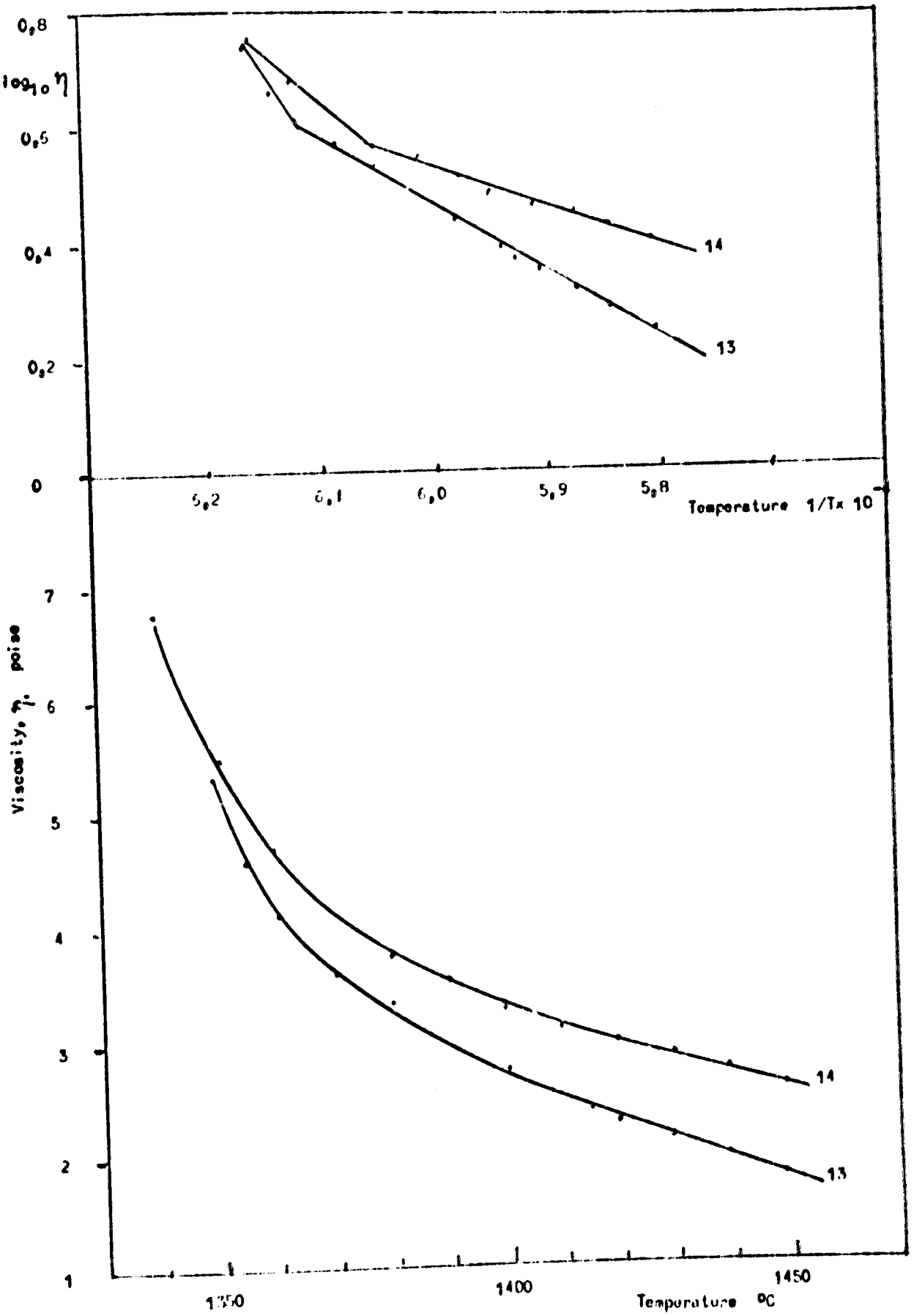

Figure 11-34. VISCOSITY - TEMPERATURE RELATIONSHIP

PLANT GLASS

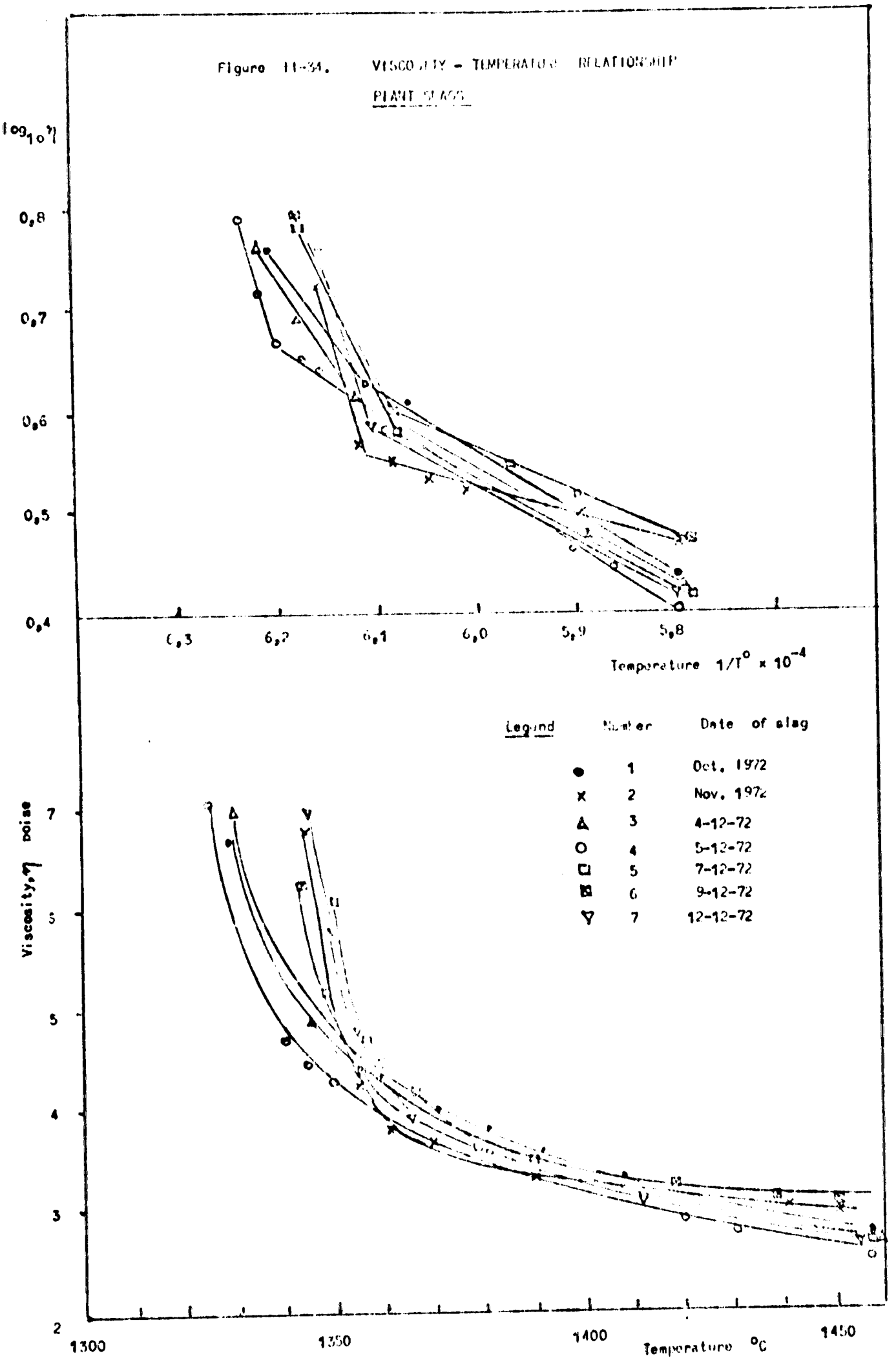

Figure II-35.

VISCOSITY-BASICITY RELATIONSHIP

SLAG GROUP I

1 1400°C
2 1450°C

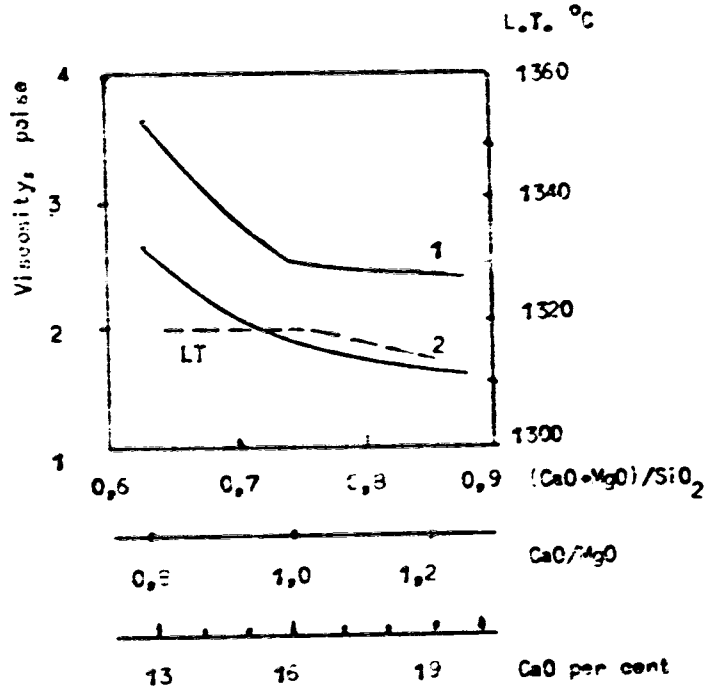

Figure II-36.

VISCOSITY-BASICITY RELATIONSHIP

SLAG GROUP II

1 1400°C
2 1450°C

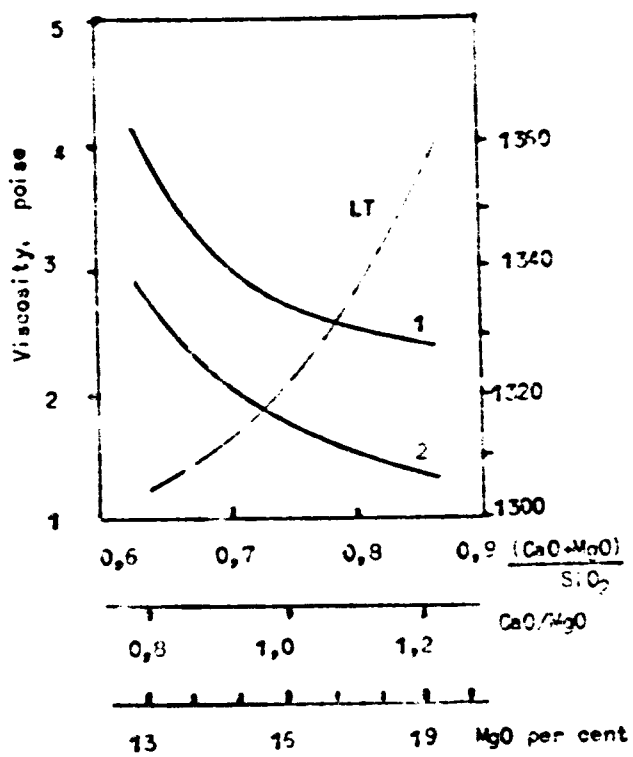

Figure II-37.

VISCOSITY-BASICITY RELATIONSHIP

SLAG GROUP III

1 1400°C
2 1450°C

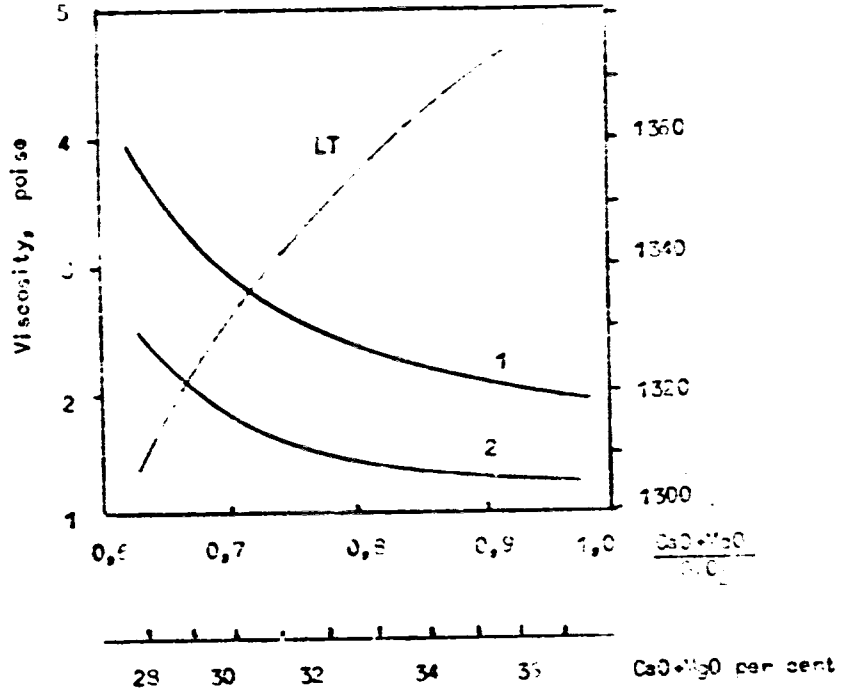

viscosities associated with the relatively small changes (1,5 to 10 poise) in viscosity ensuing from the limited changes of slag composition investigated.

Results and discussion.

The results given for viscosity values obtained at 1400°C and 1450°C are compiled in Table II-7. Figures 28 to 33 show changes in viscosity in poise versus temperature and log of viscosity versus reciprocal of temperature. The relation for plant slags of composition identical with those used in the conductivity tests are plotted in figure 34, the relevant data being compiled in Table II-8. For sake of easier comparison the discussion of the results of the viscosity tests will follow the same pattern with slag groupings identical with those given in the description of the conductivity studies.

a./ Results obtained with synthetic slags.

For the sake of convenience the viscosity values are given at fixed temperatures (1400°C and 1450°C) instead of at specified temperatures, say 50°or 100°C above the liquidus.

Group I. Relation between viscosity and basicity ratio at constant MgO and FeO and varying CaO and SiO_2 contents.

Figure 35. indicates that the viscosity decreases with the increase in the CaO content and in the basicity ratio. The decrease is significant up to about 16 per cent CaO corresponding with an approximate 30 per cent change in viscosity, but with CaO contents between 16 and 19 per cent CaO it levels out and drops to a low change of 5 per cent, as referred to the starting viscosity. The liquidus temperature determinations based on viscosity measurements show the same change as that obtained from conductivity tests.

Group II. Relationship between viscosity and basicity ratio with constant CaO and FeO but varying MgO in the slag.

This relationship is shown in figure 36. As with the resistivities, the effect of the change in MgO content on the viscosities is more pronounced than that of CaO. Increasing the MgO content from 13 to 19 per cent will decrease the viscosity by about 40 per cent at 1400°C and by more than 53 per cent at 1450°C. Both viscosity and conductivity measurements indicate a rise in the liquidus temperature of the slag.

Group III. Relationship between viscosity and basicity ratio with increasing CaO and MgO contents but at constant FeO content.

This group with the simultaneous and proportionate changes in the CaO and MgO contents might indicate what could be expected if either the lime or MgO additions were replaced by a dolomite addition to the electric furnace.

As will be obvious/...

Figure 11-38.

EFFECT OF TOTAL IRON CONTENT
OF SLAG ON VISCOSITY

SLAG GROUP IV

Temperature of slag 1400°C

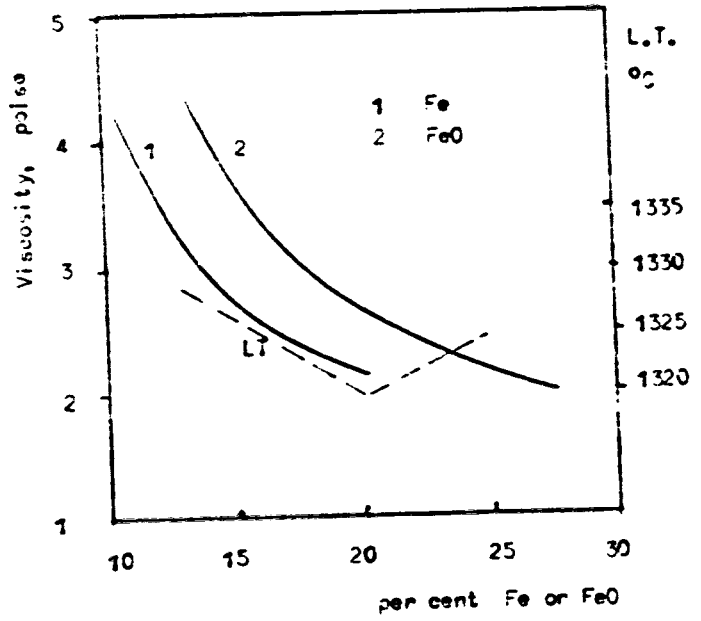

Figure 11-39.

EFFECT OF THE TOTAL IRON CONTENT
OF SLAG ON VISCOSITY

SLAG GROUP V

Temperature of slag 1400°C

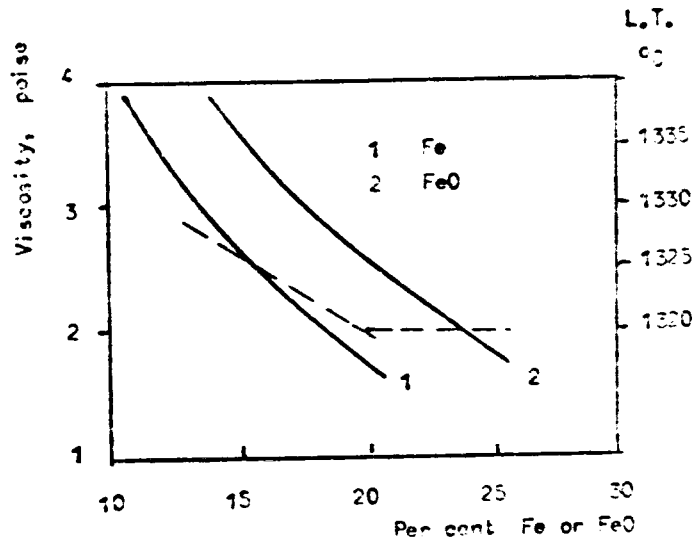

Figure 11-40. ELECTRICAL CONDUCTIVITIES (Sm^{-1}) at 1400°C and 1450°C in the PSEUDO-TERNARY SYSTEM FeO - (CaO • MgO) - SiO_2 CONTAINING 5 PER CENT Al_2O_3

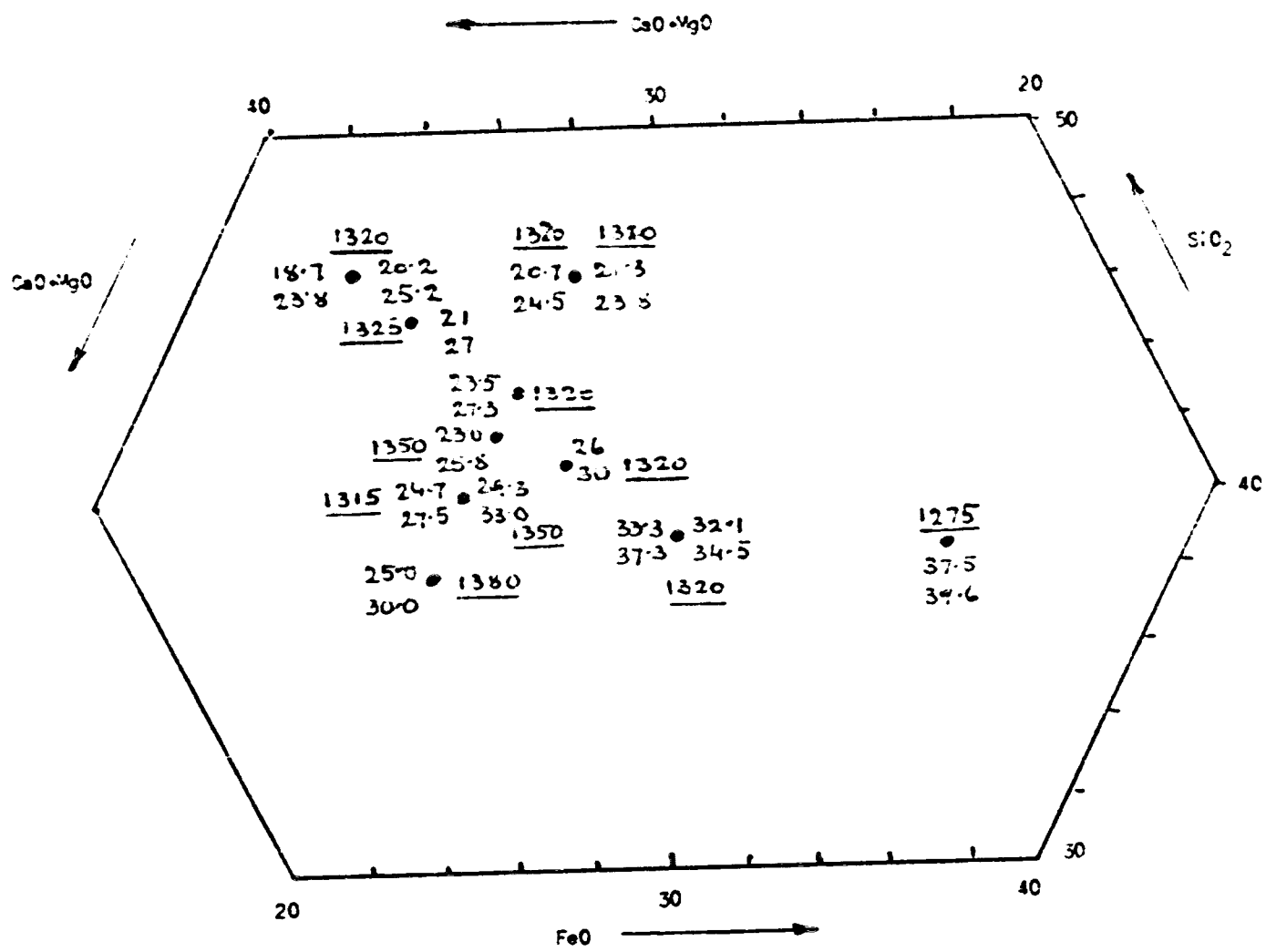

Fugure 11-41. VISCOSITIES AT 1400°C and 1450°C in the FeO - (CaO • MgO) - SiO_2 SYSTEM CONTAINING 5 PER CENT Al_2O_3

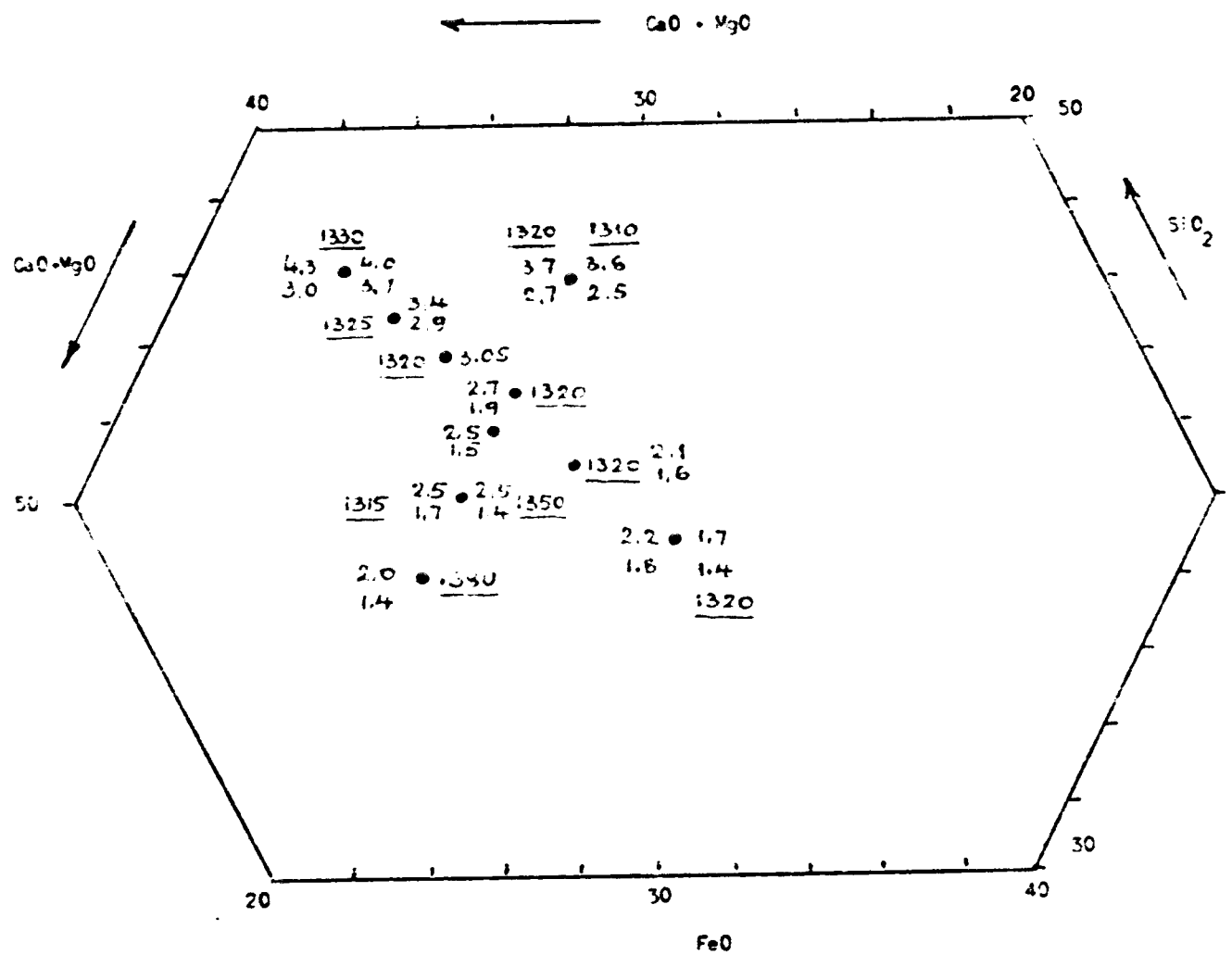

Figure 11 - 42. EFFECT OF THE OXIDATION STATE OF THE SLAG ON VISCOSITY

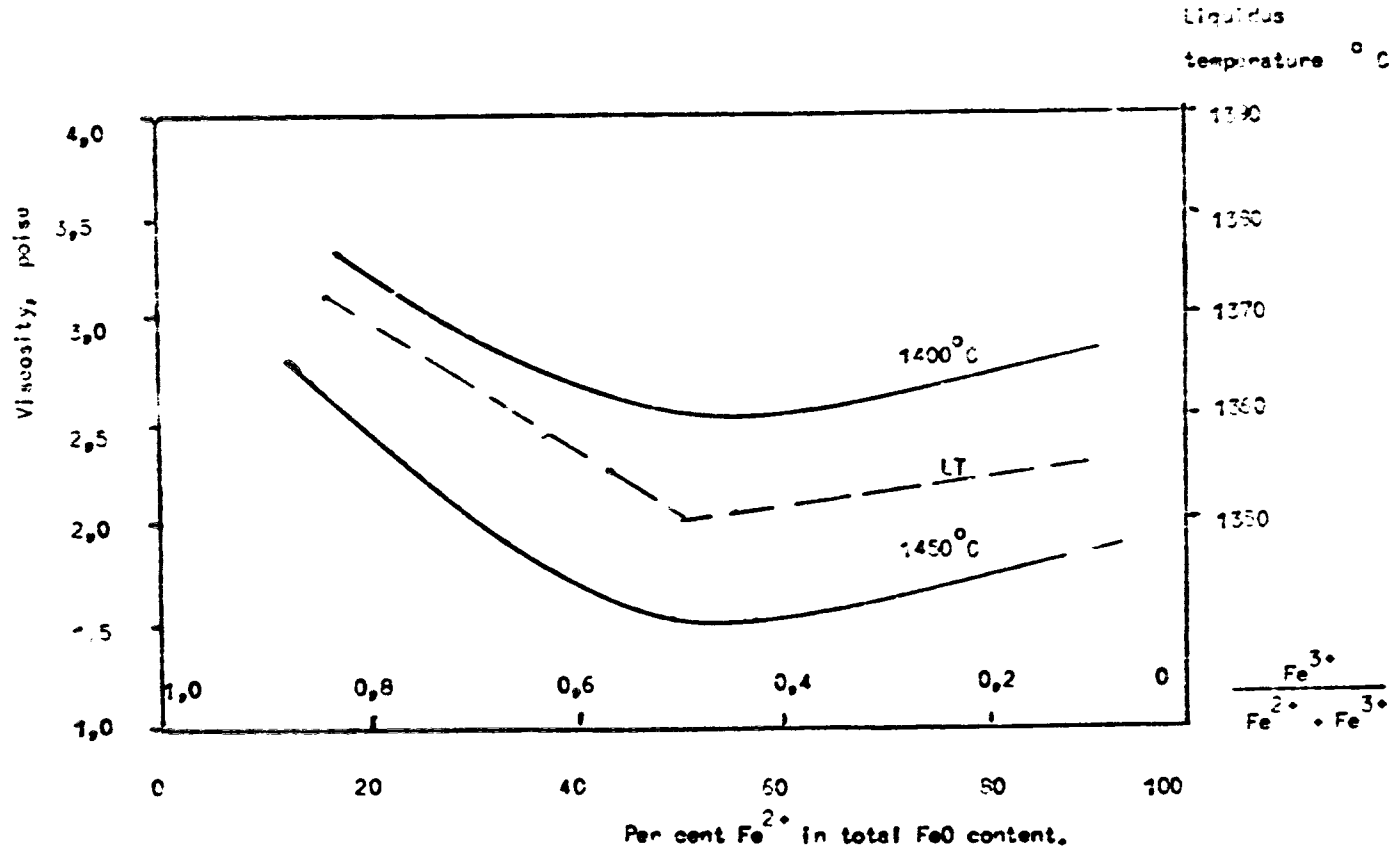

As will be obvious from graph 37., the change in viscosity is very similar to that of the previous group , but the rise in liquidus temperature is much more pronounced.

Groups IV and V. Relationship between viscosity and total iron content with variations in CaO, MgO and SiO_2 contents.

According to graphs 38 and 39 the changes in viscosity are very similar in the two groups. Nevertheless, by comparison with the previous three groups it would appear that the variation in the FeO content has an even more significant impact on the viscosity and also on the electrical resistivity of the slag than either the CaO or MgO component. An increase of the total iron content from 10,7 to 19,7 per cent (corresponding with 13,7 - 25,4 per cent FeO) will bring about a very substantial decrease of the viscosity (approximately 55 per cent) at a temperature of 1400°C.

The liquidus temperature as determined by the conductivity tests is lowered slightly while on the basis of viscosity measurements it remains virtually constant throughout the composition range.

Further to the illustration of the behaviour of slags in the various groups the data points presented in figures 35 - 39 have been re - plotted in a quasi-ternary FeO-(CaO+MgO)-SiO_2 phase diagram as shown in figure 40 and 41, for viscosities and electrical conductivities. The graphs incorporate also the relevant liquidus temperature values based on conductivity measurements. Numbers on the left of the data points represent conditions at constant MgO with varying CaO contents, while those on the right of the plots indicate the opposite condition. These graphs clearly show the trend of change in viscosity and conductivity with slag composition, With CaO and MgO contents increasing from 13 to 19 per cent the viscosity decreases while the conductivity follows the opposite trend. With increasing FeO contents the viscosity again decreases followed by a slight decrease in liquidus temperature which, later, up to 26 per cent, remains unchanged. In the previous case it has risen from 1310°C to 1380°C. The results of the conductivity tests show an approximate 15 per cent increase in the value when the FeO content increased from 26 to 33 per cent. The liquidus temperature on the other hand was lowered from 1350° to 1275°C,

Group VI. Relation between viscosity and oxidation potential of slag.

The effect of the oxidation potential of the slag corresponds reasonably well with its effect upon the resistivity. From figure 42 the viscosity increases only to a very limited degree with the

change of the/...

Figure II-43. COMPARISON BETWEEN THE VISCOSITY RANGE OF PLANT SLAGS AND SYNTHETIC SLAGS

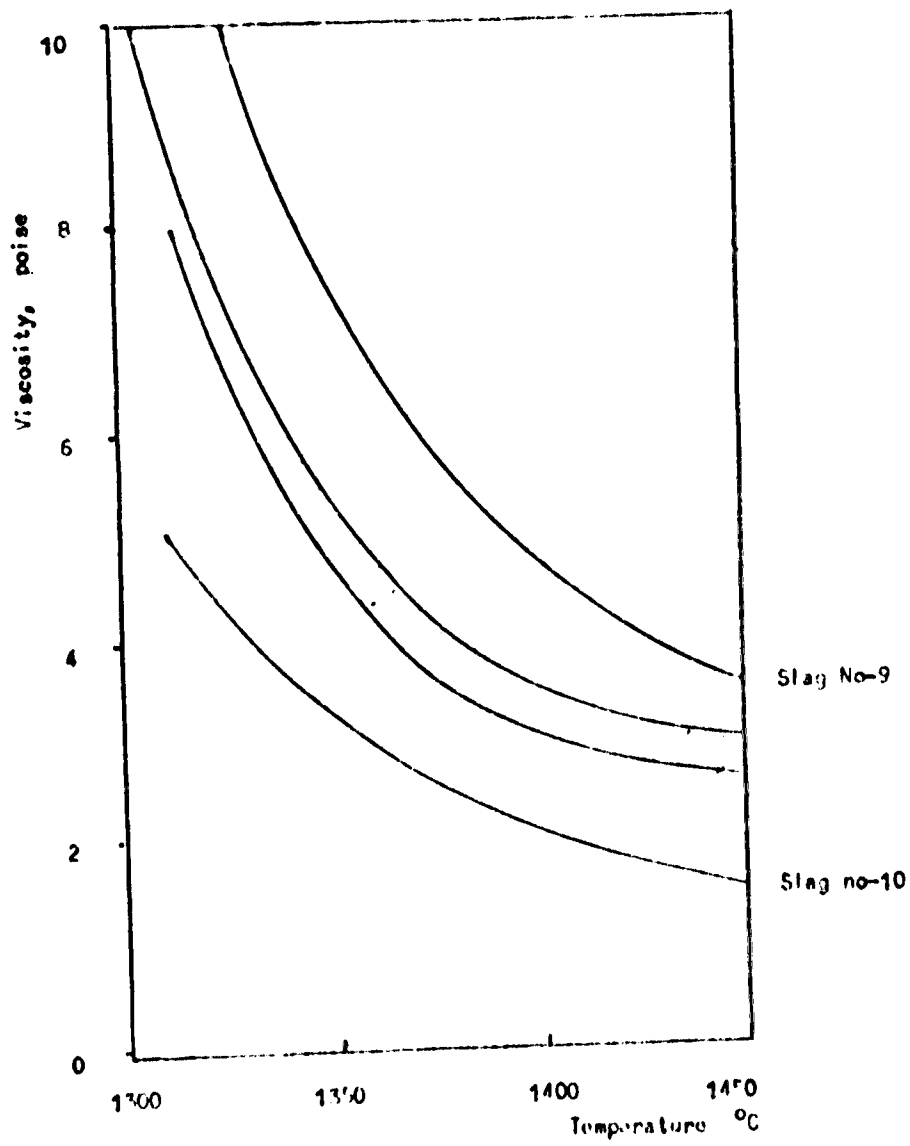

Figure 11-44

COMPARISON BETWEEN THE VISCOSITIES OF PLANT SLAG AND SYNTHETIC SLAG OF THE SAME COMPOSITION

1 Synthetic slag No-1
2 Plant slag No-7

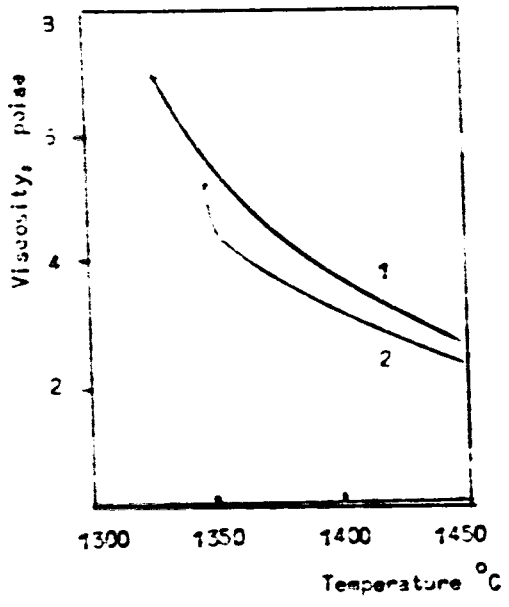

Figure 11-45.

EFFECT OF THE INCREASE OF THE SiO_2 CONTENT ON THE VISCOSITY OF SLAG

SiO_2 increased in synthetic slag

1 Synthetic slag No-4
2 Plant slag No-3

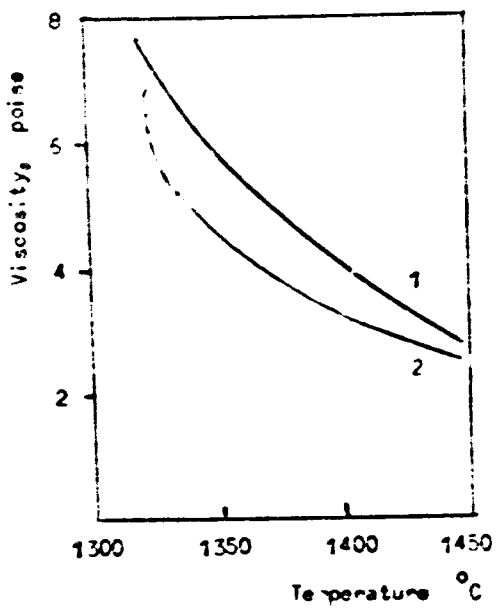

Figure 11-45

EFFECT OF THE TOTAL IRON CONTENT ON THE VISCOSITY

Total iron increased in synthetic slag

1 Synthetic slag No-12
2 Plant slag No-5

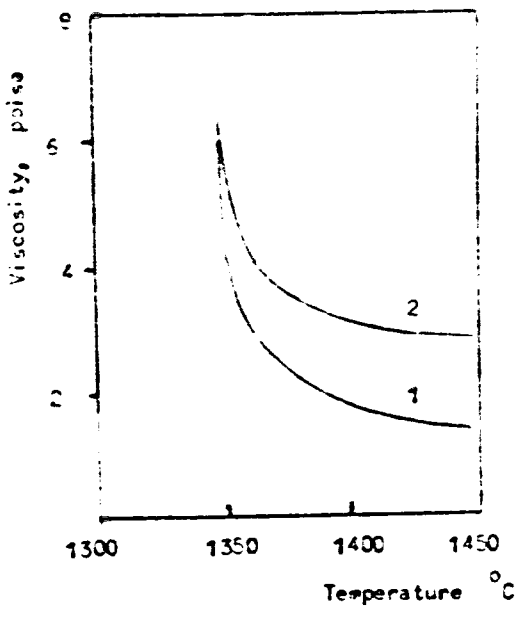

change of the divalent iron content (from 90 to about 50 per cent) while in case of electrical conductivity this change in Fe^{2+}/Fe^{3+} ratio had virtually no effect. However, a further decrease in the Fe^{2+} content brings about a noticeable increase in viscosity both at 1400°C and 1450°C in accord with the decrease of the resistivity as it was shown in Fig. 25. The liquidus tem - perature based on conductivity measurements dropped from 1385°C to 1355°C with the decrease of the oxidation state of the slag i.e. increase of the Fe^{2+} content from [illegible] to 9[illegible]% of the total iron oxide present. An increase of the Fe^{2+} above 50% brought about a very slight change in liquidus tem - perature which is probably within the limit of experimental error. The decrease of L.T. with the decrease of the oxidation potential of the slag is in accord with phase diagram considerations pertinent to the quaternary $FeO-Fe_2O_3-FeS-SiO_2$ system. (5).

b./ <u>The behaviour of plant slags.</u>

The viscosity-temperature relationship for seven plant slags is shown in figure 34. The trend is rather similar to that of the electrical resistivities with a somewhat greater scatter in the conductivity values. This is due mainly to the previously noted boiling phenomenon which in the case of plant slags became more pronounced. Only after extended periods of careful equilibration was it possible to measure the conductivity and viscosity values. Figure 43. illustrates the viscosity range of the plant slags (shaded area) as compared with the synthetic slags. It is well within the range of the two extreme values of the latter.

A comparison between the viscosities of plant slag (date:12/12/72) and synthetic slag No-1 of very similar composition is shown in figure 44. Considering the difficulties of measurement with semi-quiescent slags the agreement between the measured values is reasonably good.

With the synthetic slags increasing the silica content while keeping the other components relatively constant (decreasing basicity ratio) increased the viscosity readings (see figs. 35 and 36 for slag groups I and II). The same relationship is shown in figure 45 for synthetic slag No-4 and plant slag dated 4/12/[illegible]. Similarly, the viscosity-decreasing effect of the increase of the slag FeO content in a plant slag-synthetic slag relation is illustrated in figure 46.

No relationship could be established between viscosity and other variables in the case of plant slags, most probably because of the narrow compositinn/...

Table II-9.

Comparison between the results obtained on two slags of similar composition by V.P. Bonfil (fully oxidised slags) and the present investigator (reduced slags)

Case	Slag Number	Composition of slag per cent					Liquidus Temperature	Viscosities (poise)		
		MgO	CaO	SiO_2	FeO	Al_2O_3	°C	L.T.+20°C	L.T.+50°C	L.T.+100°C
Case A										
V.P. Bonfil	15	19	16	39	21	4	1400	2,45	2,04	1.58
Present Author	5	19	17	40	20	5	1385	-	1,55	1.00
Case B										
V.P. Bonfil	18	15	14,5	40,5	28	2	1345	2,83	2,42	1.97
Present Author	10	15	14	39	26	5	1325	2,20	1,90	1,70
					Difference - per cent			22	22	11

narrow composition range. Likewise, as indicated earlier, there was no relationship for resistivities on account of the random pattern in change of the slag components. In this respect the limited significance of the variations in both total iron and MgO contents is particularly noteworthy. Judged by their effect on synthetic slags the role of there two compounds would be expected to be more important in the plant slags. Later in the discussion of optimisation this aspect will be dealt with in more detail. Numerically the change of FeO content in the range of 15,7 to 21,2 per cent (i.e. the range of FeO in plant slags investigated) according to figures 38 and 39 would be equivalent to a viscosity change of 1 poise, that is a 29 per cent change at 1400°C. In comparison, the extreme values represented by slags dated Nov. 1972 and 9/12/72 show a difference of only 0,1 poise (see fig. 34.) at the same temperature. Further it is noteworthy that the maximum difference in viscosity values at 1400°C in the case of plant slags is not more than 0,3 poise from a total of 3,5 poise, that is less than 9%, despite the sizeable variation in slag composition.

The foaming of slags, characteristic of the synthetic but particularly noticeable in plant slags, is a well-known and by no means an isolated phenomenon. Although there are conflicting reports in the literature, it is generally agreed that a high silica content or basicity less than 2 is favourable to foaming, the SiO_2 acting as a stabiliser in foam formation. The effect of FeO is in its ability toincrease the oxidising power of the slag resulting in a greater gas evolution. Thus its role is probably more in influencing the volume of gas and the rate at which it is produced. (6). Charges containing chromium appear particularly troublesome in causing foaming which may be due to increased viscosity. As the fundamental investigations of Cooper and Kitchener indicated (7) the foam life increased greatly with increase of bulk viscosity whether this was brought about by fall of tem - perature or by decrease in the CaO/SiO_2 ratio.

Comparison of results with earlier work.

Viscosity tests carried out by V.P. Ponfil (8) were conducted on fully oxidised slags having a much wider composition range than those discussed in the present work. However, two of the slags agree fairly well in composition and the results obtained with these slags may be used for the purpose of comparing the two separate methods used in the investigation. The comparison is shown in Table II-9.

Table II-9/....

As shown in the Table, at 50°C above liquidus temperature, i.e. at a point where the rate of change in viscosity with change of temperature is becoming less significant, the difference in viscosities is 22 per cent and 24 per cent respectively. At 25°C above liquidus temperature in Case A no reasonable values could be measured in the present investigation, while in Case B the difference is again 22 per cent. At 100°C above liquidus tem - perature in Case A the difference is 27 per cent while in Case B, probably due to some oxidation effects, only 11 per cent was found. Although the number of slags is very limited to draw a general conclusion from the values given in the table, the indication is that a probable average difference of 22 to 27 per cent might exist between the viscosities determined by the two separate methods, the higher value being represented by the fully oxidised slag samples. Indeed, reverting back to figure 42, it would appear that the decrease of the Fe^{2+} content of the slag from 90 per cent to about 18 per cent would be equivalent to an increase in viscosity from 2,75 poise to 3,20 poise at 1400°C, i.e. 17 per cent, and from 1,75 poise to 2,25 poise at 1450°C , i.e. 31 per cent.

As to the general trend of the effect of the various slag con - stituents upon the viscosities the finding;outlined by V.P. Bonfil seem to be in full accord with the present investigation irrespective of the differences in the oxidation potentials of the slags investigated. Summarising briefly:

a./ Increase of both CaO and MgO contents decreases the viscosity and increases the liquidus temperature, the latter being more noticeable with the increase of the MgO content.

b./ Additions of FeO markedly lower the viscosity but up to 26 % FeO content of the slag affe slightly the liquidus tem- perature which tends to be l. further as the FeO content is rained to a maximum of 33 per cent in the present range of slag compositions.

c./ A simultaneous increase of the CaO and Mg contents from 28 to 37 per cent, i.e. the condition of using dolomite as flux, de- creases the viscosity but brings about a 70°C rise in the liquidus temperature, that is the refractory character of the slag will be increased.

Comparison with data found in the literature.

A direct comparison of the results with literature data is made difficult by the fact/...

by the fact that work on the complex quinnary $FeO-CaO-MgO-SiO_2-Al_2O_3$ system is rather scarce and even that available relates mostly to reverberatory furnace slags of considerably different composition from the slags of the reference furnaces.

Higgins and Jones (9, 10) carried out comprehensive investigations on the viscosities of Rhodesian copper smelting slags involving the above five components. In spite of the great difference in composition range their findings are relevant to the present study. Thus they noted that the addition of MgO up to 16 per cent causes a continuous reduction in viscosity and also, the addition of ferrous oxide decreases viscosity markedly throughout the whole temperature range of investigation. Furthermore, the replacement of CaO by MgO at first reduces the viscosity and lowers the liquidus, but with increasing replacement both viscosity and liquidus temperature are increased. Pertaining to the effect of ferric oxide it was found that, in accord with the present study, the increase of this compound increased the viscosity.

The work of P. Bills (11) on the same quinnary system is particularly interesting with regard to the effect of the FeO which was added up to about 27 per cent by weight to the slag. A regular decrease in viscosity of slags containing up to about 15 per cent ferrous oxide was found and up to approx. 8 per cent FeO content the ferrous oxide could replace magnesia on a molar basis without affecting the viscous properties indicating that no structural changes of the slag were involved. At higher ferrous oxide contents the effect of the addition of more FeO appeared to be no longer equivalent to the addition of MgO. The log. viscosity values (poise) given for slags containing 6,5-7,1 per cent MgO, 6,5-7,0 per cent Al_2O_3, 16,8-18,2 per cent CaO, 43,3-47,0 SiO_2 and 20,5-26,8 FeO were reported as follows: at 1400°C 0,618 - 0,799; at 1450°C 0,492 - 0,581, that is considerably higher than those obtained in the present study.

Irchanov and Sushkov (12) studied the viscosities and electrical conductivities of slags recommended for the electric smelting of copper concentrates. However, the concentration range of their slags was very different from that of the slags investigated in the present study, with much higher FeO (25 to 44 per cent) and lower CaO (2 to 10 per cent) contents. The SiO_2 varied between 40 to 50 per cent, the alumina content around 10 per cent and no MgO was used as a slag component. As was expected, and in agreement with this study, the replacement of FeO by CaO increased the viscosity and decreased the electrical conductivity. The viscosity values given by these authors were very high, 12 to 90 poise, as were the conductivities, reaching 0,74 $ohm^{-1}.cm^{-1}$ values. The most suitable slag

composition for the/...

composition for the electrical smelting of copper concentrate was found to be: - SiO_2 40 to 50, Al_2O_3 10, FeO 30,to 45, CaO 4 to 6 percent, the alumina content around 10 per cent, rather hard to envisage for effective usage in the reference furnaces.

While the direct comparison with data published in the literature is somewhat doubtful on a numerical or absolute value basis, the trend imparted by the effect of the various slag constituents upon viscosity or electrical conductivity can be judged with sufficient clarity. This is the more important point since the magnitude of numerical values is often the matter of the experimental technique employed by the various investigators and in no case could it be regarded as absolute.

2.5. Energy of activation.

In the assessment of physico-chemical behaviour of slags the knowledge of the energy of activation might be of some importance. In electrical conduction it refers to one mole of conducting entity. According to Bockris et al.(13) a cation M^{2+} can be regarded as existing in an"energy well" in the interstices of the silicate structure of the slag, the height of the energy well being E. The probability of the cation escaping from the energy well is proportional to $\exp(-E_\kappa/RT)$ and E_κ will be reduced by the application of an applied potential. Eyring assumes a lattice-like liquid structure such that each molecule is encaged by its neighbours. Thus the fundamental rate process of molecular transport is that of movement of an atom to a vacant neighbouring site. The intermediate activated state of energy maximum or high point is represented by E while the frequency of jumps is described by the probability term A. In any case in a general form the specific conductivity is given by

$$\kappa = Ae^{-E_\kappa/RT} \qquad 11./$$

where A is the frequency factor and E_κ the energy of activation. 'A' contains also ion mobility and concentration terms. Taking logarithms equ. 11 becomes

$$\ln \kappa = \frac{-E}{R} \quad \text{const.} \qquad 12./$$

assuming here that A is constant and almost independent of temperature for a given reaction. Equation 11./ empirically deduced for electric conduction by Rasch and Hinrichsen (14) is appropriately called the Rasch-Hinrichsen Law since it is often confused with the Arrhenius relationship.

The flow of liquid/...

Table II-10

Energies of activation and temperature coefficients of viscous flow and electrical conductivity

Slag Number	Energy of activation kcal/mole		Temperature coefficient	
	Viscosity	Conductivity	Viscosity	Conductivity
1	37,5	24,4	6,45	3,57
2	45,6	20,5	9,00	2,67
3	34,1	16,1	5,36	2,40
4	42,4	25,2	6,10	4,78
5	47,4	17,1	10,80	2,60
6	42,1	24,6	8,45	1,77
7	52,5	17,1	9,41	1,79
8	45,6	22,8	5,92	3,97
9	48,0	32,6	8,57	4,74
10	29,4	16,6	4,44	2,34
11	31,2	38,0	2,19	4,57
12	16,3	13,0	4,55	2,34
13	39,6	14,2	8,50	3,09
14	31,7	22,8	5,25	3,34
15	n.d.	10,0	-	1,17
Plant slags				
Date of Sample				
Oct. 1972	28,7	29,6	4,53	
Nov. 1972	15,2	42,5	2,20	
4/12/72	22,8	32,7	4,30	
5/12/72	28,0	29,1	5,08	
7/12/72	18,6	31,2	4,30	
9/12/72	25,5	35,4	2,56	
12/12/72	23,0	32,2	4,61	

The flow of liquid is a rate process and the expression formulated for its activation energy is analogous to that used in connection with reaction rates. The counterpart of the activation energy of a chemical reaction is the energy maximum encountered by a molecule as it is forced past its nearest neighbours. If this activation energy is denoted by ΔE_η (may also be termed as the height of energy barrier for viscous flow), then the fraction of the molecules having energy in excess of this amount and being therefore capable of moving past the surrounding molecules is given by a Boltzmann-type of expression

$$\eta = B\, e^{\Delta E_\eta / RkT}$$

$$\text{or} \qquad \ln \eta = \ln B + \Delta E_\eta / RkT \qquad 13./$$

Hence the plot of $\log_{10}\eta$ versus $1/T$ has actually the slope of $\frac{E_\eta}{2{,}303\ Rk}$

Obviously, the lower E_κ or E_η, the easier the electrical conduction or viscous flow will come about. With the use of the log κ or log η plots against $1/T$ the values of E_κ or E_η can be calculated. Thus at two different temperatures T_1 and T_2

$$\frac{\kappa_1}{\kappa_2} = \exp \frac{E_\kappa}{R} \left(\frac{1}{T_2} - \frac{1}{T_1} \right) \qquad 14./$$

$$E = R \frac{\log (\kappa_2 - \kappa_1) \times 2{,}303}{\left(\frac{1}{T_2} - \frac{1}{T_1}\right) \times 10^{-4}} \qquad 15./$$

and with the incorporation of the cell constant

$$\kappa = \frac{G}{\varrho} = \frac{G}{\varrho_o \exp \frac{E_\kappa}{RT}} = \kappa_o \exp(-E_\kappa / RT) \qquad 16./$$

Relevant values of activation energies calculated from these expressions are compiled in Table II-10, which contains also the temperature coefficients of viscosity and specific electrical resistivity in the temperature interval 1390 to 1450°C expressed by the following equations:

$$\lambda_\eta = \frac{\eta_1 - \eta_2}{(T_1 - T_2)\, \eta_{avg}} \qquad 17./$$

$$\lambda_\varrho = \frac{\varrho_1 - \varrho_2}{(T_1 - T_2)\, \varrho_{avg}} \qquad 18./$$

where η_{avg} and ϱ_{avg} represent the average viscosities and specific

electrical resistivities/...

Figure 11-47

RELATION BETWEEN VISCOSITY AND ACTIVATION ENERGY OF VISCOUS FLOW at 1400°C

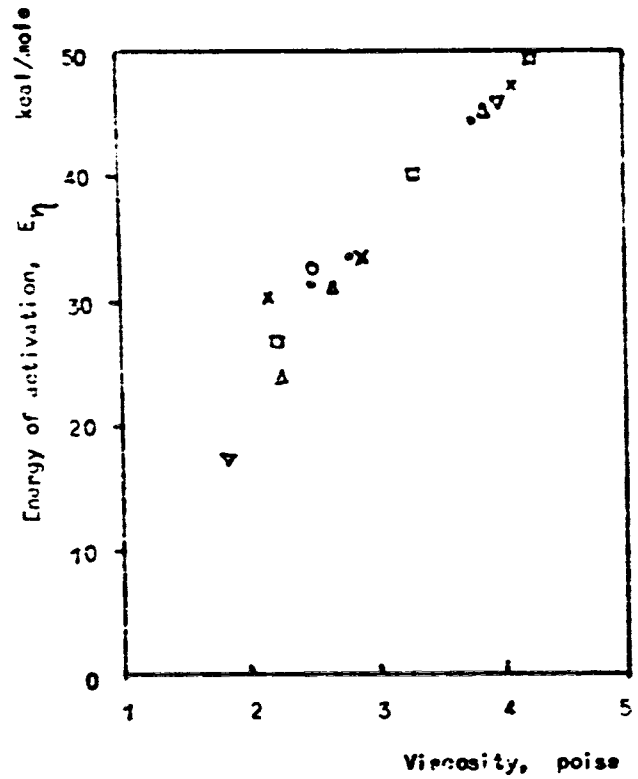

Figure 11-48

RELATION BETWEEN RESISTIVITY AND ACTIVATION ENERGY OF ELECTRICAL CONDUCTION at 1400°C

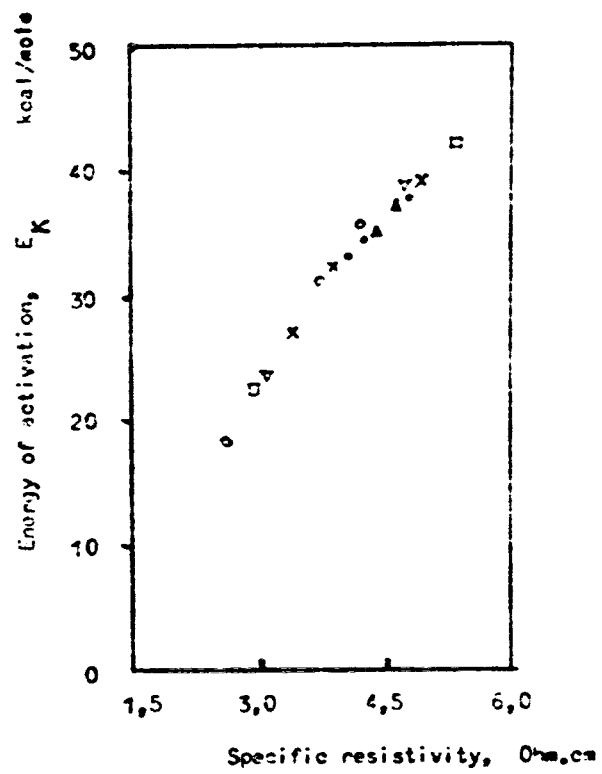

electrical resistivities in the quoted temperature range. The viscosity versus activation energy and electrical resistivity vs. activation energy relationships are shown in figures 47 and 48. (strictly for 1400°C !)

According to the data of Table II-10 the energy of activation calculated from conductivity measurements decreases with increasing CaO, MgO and FeO contents and decreasing Fe^{2+}/Fe^{3+} ration. The value of E_κ in the composition range of the slags is between 19 and 38 kcal/mole.

The results based on viscosity measurements show certain discrepancies and in the effect of changes in composition the trends of the activation energy remain uncertain. Apart from slag No-12 with higher FeO and MgO content the range of the energy of activation of viscous flow is between 30 and 45 kcal/mole. Bills (11) quoted an average figure of 45 kcal/mole for slags of similar type.

Since the change of the viscosity and conductivity curves with temperature can be regarded as asymptotic to the x-axis (temperature axis), the value of the energy of activation will depend to a certain extent on whether the lower reference temperature for the y = ax + b relationship was chosen, close to the liquidus temperature, or far above. In other words, a different result would arise if the range were chosen from say 1385°C to 1450°C or 1450°C to 1550°C. As viscosities appear to be more temperature sensitive than conductivities, this difference will report in the energy of activation values and might lead to anomalous data.

The temperature coefficient of viscosities and electrical conductivities is important in judging the behaviour of any given slag upon the change of temperature. From a practical point of view it would be advantageous to have slags with temperature coefficients as low as possible. This would facilitate an easier removal of the slag from the furnace and would also have less effect on the electrical operating parameters of the furnace if substantial variations in temperature were to be expected.

2.6. Comparison between plant slags and synthetic slags pertaining to the effect of change of slag composition upon viscosity and electrical conductivity.

From the point of view of practical application it is iportant to see how far the results obtained from laboratory investigations on the effect

of slag composition/...

Table II - 11.

Comparison between the changes of viscosities and electrical conductivities in synthetic slags and plant slags upon the effect of equal variations in slag composition.

Reference temperature : 1400°C

Slag group number	Variation in plant slag composition				Slag constituent upon which comparison is based	Variations in viscosity and electrical conductivity in plant and synthetic slags of equivalent composition	
	CaO	MgO	SiO_2	Fe_{total}		Viscosity poise	Conductivity $ohm^{-1}.cm^{-1}$
	per cent						
II	const. 16,0	12,8-14,8	40,1-41.9	const. 15,3	MgO	4,10-3,10	0,218-0,195
					SiO_2	2,55-2,32	0,271-0,255
IV	16,1-18,1	const. 16,0	40,1-41,9	12,2-16,5	Fe_{total}	3,66-2,65	0,255-0,209
					CaO	2,75-2,35	0,295-0,226
					SiO_2	2,55-2,30	0,300-0,272
V	const.	12,8-14,8	40,1-41,9	12,2-16,5	Fe_{total}	3,45-2,48	0,237-0,219
					SiO_2	2.35-1,94	0,295-0,217
					PLANT SLAG	3,40-3,10	0,238-0,217

Figure II-49 VARIATION OF VISCOSITY AND ELECTRICAL CONDUCTIVITY WITH THE CHANGE OF COMPOSITION IN FLAT GLASS.

Temperature: 1400°C

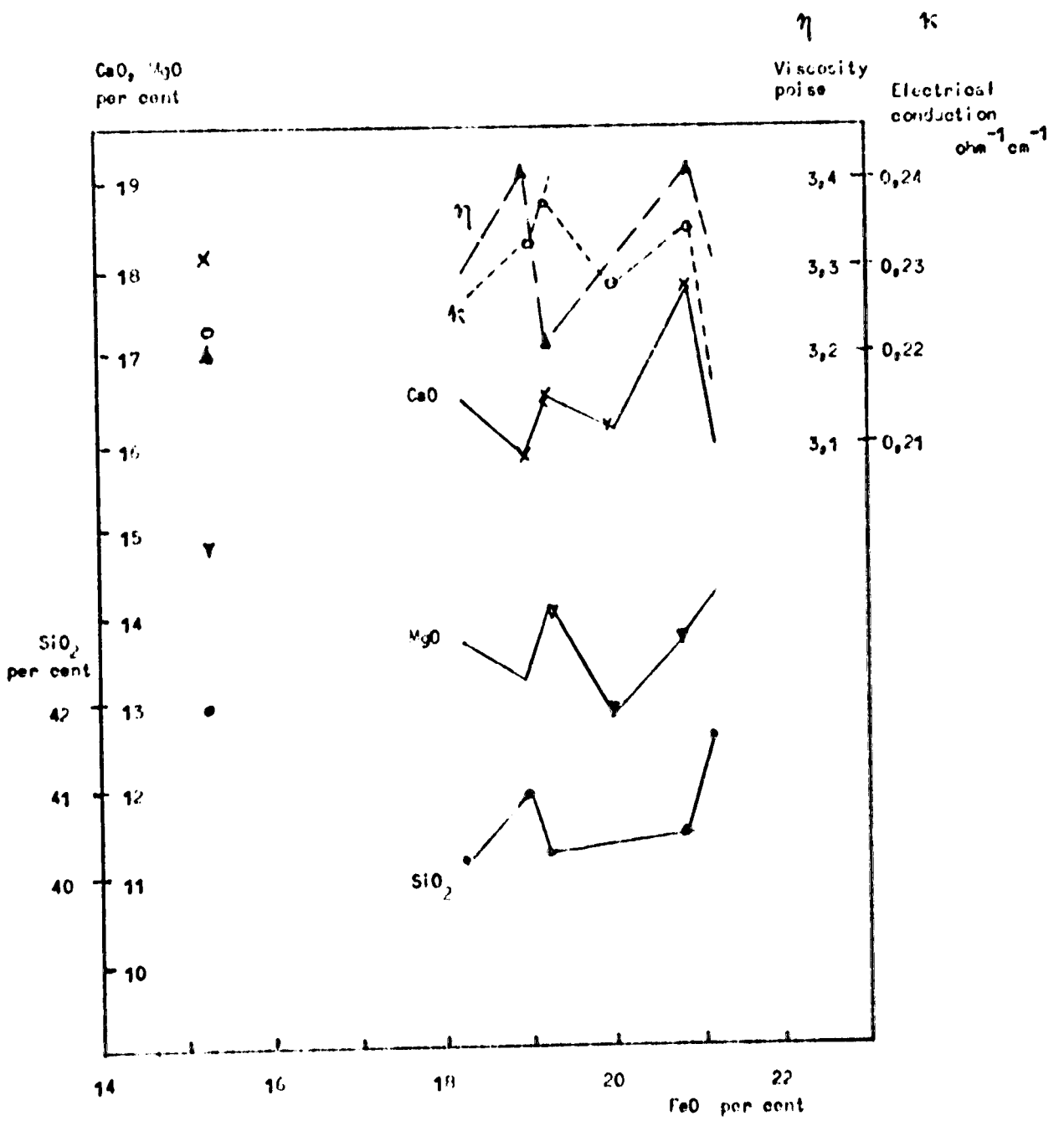

of slag composition on viscosity and conductivity can be compared with the relationship of the same parameters in plant slags. The main difficulty encountered with this kind of comparison arises from the difference in the range of the various constituents of the two types of slags, in other words, in the selection of the appropriate constituents as a reference point for the comparison. This is illustrated in Table II-11 in which the synthetic slags are represented by groups II, IV and V. The table shows the percentage variation of the constituents in the seven plant slags investigated and the range of viscosities and electrical conductivities. (last row in the table.) The variation of these parameters in the same range of composition of the synthetic slags for various reference constituents within each group upon which the comparison between the two types of slag is based are given in columns 7 and 8 of the table.

It is obvious from the data that the values of k and η will largely depend on which constituent in the slag is taken as the reference for comparison. Whereas in synthetic slags the relation of the percentage of components to eachother within each group is a result of careful pre-selection and along definite trends, in plant slags the same components exhibit a completely random variation and follow no set pattern. For the further illustration of this aspect figure 49. was constructed from analysis data of the plant slags. The mode of indicating slag composition on the x and y axes was not intended to construe that CaO, MgO and SiO_2 are by any means functions of the FeO content. Rather, it was meant to show clearly the random pattern in which the constituents vary in plant slags as opposed to those in synthetic slags. In this context the indication according to the figure is that the effect of the change of constituents (when taken separately) upon viscosity and conductivity does not follow the trend that could be expected from laboratory tests. In fact it does not follow any trend apart from fluctuating within a certain upper and lower limit.

From the comparison it becomes evident that, as mentioned already, great caution will have to be exercised in projecting the results of laboratory investigations with regard to the effect of the various slag-forming constituents onto their possible effect in actual working slags. From the data shown the large variation in conductivity and viscosity with the change of slag composition are considerably reduced in plant slags of similar compositions due to the previously noted random variation of the slag-forming constituents. This fact has also an important bearing in assessing the effect of slag composition upon the electrical characteristics of the furnace. It would indicate that the response of current and power

input rates/...

input rates and electrode movements following changes in slag composition might be far less pronounced than could be predicted on the basis of laboratory measurements on viscosities and comductivities.

However, the importance and usefulness of laboratory data becomes apparent when the question, say, of whether to increase or decrease one or more of the slag constituents will have to be answered. That is in case of considering the change in flux composition, the quantity of flux charged, the amount of converter slag returned, etc. The alteration of any of these variables might introduce a sudden change into the slag composition and through that into the operating characteristics of the furnace. By doing so the even, day-to-day operation will be disturbed but the response of the unit might become predictable from the determined physical characteristics of the produced slags.

References.

1./ Riebling W.E.-Lorel P.C.: Dipping electrode electrical conductance instrument for use at 1700°C. Rev. Sci. Instr. 34. 4, 1965, 475-478

2./ Attwood S. S.: Electric and Magnetic Fields. Wiley, N.Y. 1949, pp 88

3./ Engell H.J. - Wygen F.: Ionen und Elektronenleitung in $CaO-FeO-Fe_2O_3-SiO_2$ Schmelzen. Z. Elektrochem. (Ber. Bunsen Gesellaschaft) 72, 1, 1968, 5-12.

4./ Pasthukov et al. - O. Esin : Elektrodniye processi v rasplavlennikh shlakah (Electrode processes in molten slags) in "Fizicheskaya Khimiya Rasplavlennikh Shlakov". Ed: Yu. Delimarskii. Akad. nauch Ukranskoy SSR, Kiev, 1970

5./ Kaiser M.E. (Editor) : Phase Diagrams for Ceramists. Amer. Ceram. Soc. McGraw-Hill, 1964, 78

6./ Fellecht K.: Metallurgie und Giessereitechnik, 5, 3, 1955, 85-89

7./ Cooper C.E. - Kitchener J.A.: Foaming of molten silicates. J.I.S.I. Sept. 1959, 49-55

(References continued)

8./ Bonfil P.A.: A study of the physical properties of slags belonging to the system FeO-CaO-MgO-Al_2O_3-SiO_2. Summarising Report, Sept, 1972. University of the Witwatersrand, Johannesburg.

9./ Higgins R. - Jones T.J.B.: Viscosity characteristics of Rhodesian copper smelting slags. Trans. I.M.M. (London), 72, 1962-63. 826-64.

10./ Jones T.J.B.: Viscosities and settling characteristics of Rhodesian copper smelting slags. 8-th Commonwealth Met. Congr. London, 1965, Paper No-121, 1247-66.

11./ Bills P.M.: Viscosities in silicate slag systems. J.I.S.I. Feb, 1963. p 132 - 140

12./ Ishkanov T.K. - Pushkov K.V.: Viscosity, electrical conductivity and liquidus temperature in the system SiO_2 -Al_2O_3 -FeO -CaO. Nauch. Trudi Kazakh. Politekn. Inst. 1971, 446-455

13./ Bockris J. 'O.M.◆ Kitchener J.A.-Ignatovicz S.- Tomlinson J.W.: The electrical conductivity in silicate melts: Systems containing Ca, Mn. and Al. Disc. Farad. Soc. 4, 1948, 265-280

14./ Rasch E. - Hinrichsen F.V.: Z. Elektrochem. 14, 1908, 41-46.

SECTION III.

PRACTICAL SIGNIFICANCE OF SLAG RESISTIVITY IN FURNACE OPERATION: FURNACE RESISTANCE, HEAT GENERATION AND ELECTRODE MOVEMENT.

1./ Formulation of expressions for furnace resistance and cell constant.

From a furnace design point of view it is important to determine the voltage-current relations that influence electrode size and spacing, as well as furnace dimensions. In order to determine these parameters, first the resistance of the furnace will have to be evaluated. In this context the resistivity of the slag will be regarded as primarily ohmic in character in which case

$$R_{sl} = \varsigma_s k \qquad 1./$$

here R_{sl} is the slag resistance ohm, ς_s the slag resistivity in ohm.cm and k a constant for the electrode geometry in cm^{-1} (called also cell constant, denoted by ? in the previous experimental part). The values of the specific resistivity were determined as presented in Section II, thus the knowledge of the cell constant will enable the estimation of furnace resistance. Several attempts have been maie to correlate resistivity with various parameters of furnace geometry, one of these parameters and probably the most often used one being the size of the electrode. The results of investigations and suggestions of researchers pertinent to this aspect will be delineated briefly in the following.

Back in the 1920's Andreae (1) introduced the electrode periphery resistance concept which in its wide acceptance can be regarded as the basis of all subsequent furnace design considerations. According to this concept

$$k = \frac{E}{I}\Pi D_e = R\Pi D_e \qquad 2./$$

where E = electrode to ground voltage, I = current per electrode, D_e = diameter of electrode. That is the resistance between hearth and electrode times the electrode circumference is constant and k depends upon the character of the raw materials and products of electric furnace processing. Later, as will be discussed in an other section of this study, Andreae carried further this idea and equated the heat generated by current flow in an electrode with the heat conducted from the exposed surface of the electrode and combined this relationship with the concept of electrode periphery resistance.

A simple formulation/...

A simple formulation of furnace resistance based on the action of a cylindrical electrode of length L and diameter D_e was given by Schwarz von Bergkampf (2) as

$$R_f = \frac{\varrho_s L}{\pi D_e^2/4} \qquad 3./$$

Using more or less the same relationship but with particular application to Thysland-Hole furnaces Kjølseth (3) introduced an additional parameter according to which

$$R = k(H - p)$$

H being the distance from the surface of the charge to the matte or metal bath, p the depth of the immersion of the electrode into the charge and proposed the following formula for the evaluation of furnace resistance:

$$R_f = \frac{\varrho}{2\pi p}\left(1 - \frac{\frac{D_e}{4H}}{(1 - \frac{D_e}{4H})(2H - p)}\right) \qquad 1./$$

In other words, the resistivity is inversely proportional to the depth of electrode immersion as

$$RD_e = \frac{k}{p/D_e} \qquad 4a./$$

Nilsen (4) developed further Kjøiseth's formula on the basis of model tests from which it was found that R_f is proportional to $D_e^{-0,79}$, while the furnace capacity defined as $P_w = 3E_r I$ is then proportional to $D_e^{2,79}$. In his final expression

$$RD_e = 0,527 \frac{(H - p)^{0,24}}{(\frac{p}{D_e} - k)^{0,45}} \qquad 5./$$

All these models assume negligible inter-electrode conduction. To account for this type of conduction Bowning and Urban (5) formulated an expressio. which incorporates the capacitance effect between two electrical conductors as was proposed originally by Attwood and referred to already in connection with the cell constant (see Section II). In Attwood's original formulation in case of equally charged parallel cylindrical infinite wires of radius r, length l, being distance S apart and charged opposite with ϱ_l coulombs the capacitance of such condenser is given by

$$C_l = \frac{\varrho_l \cdot l}{\frac{\varrho_l}{\pi\epsilon} \ln\left[\frac{S}{2r} + \sqrt{(\frac{S}{2r})^2 - 1}\right]} = \frac{\pi\epsilon l}{\ln\left[\frac{S}{2r} + \sqrt{(\frac{S}{2r})^2 - 1}\right]} \qquad 6./$$

in farads, where ϵ is the dielectric constant of the medium. Pertaining to the capacitance of/...

the capacitance of the whole system a further point of interest was the capacitance in the region of the electrode tips. Kjølseth took considerable pains to develop an expression for the capacitance of what he considered hemispherical electrode tips, approximating it by the formula for two equal spheres

$$C_2 \approx 2\pi\epsilon r\left[1 + \frac{r}{S} + \left(\frac{r}{S}\right)^2 + \ldots\right] \qquad 7./$$

Assuming symmetrical field about a plane through the centre

$$C_2/2 = \pi\epsilon r\left[1 + \frac{r}{S} + \left(\frac{r}{S}\right)^2 + \ldots\right] \qquad 8./$$

In this way the total capacitance of the system is $C = C_1 + C_2/2$. Equations 7./ and 8./ respectively were also incorporated in the formula proposed by Downing and Urban, thus their final equation for furnace resistance took the form

$$R_f = \frac{\rho}{\pi}\left[\frac{1}{\frac{p}{\ln\left[\frac{S}{D_e} + \sqrt{\left(\frac{S}{D_e}\right)^2 - 1}\right]} + r\left[1 + \frac{r}{S} + \left(\frac{r}{S}\right)^2 + \ldots\right]}\right] \qquad 9./$$

assuming uniform conduction. For easier recapitulation, the figure below summarises the symbols used in the previous expressions:

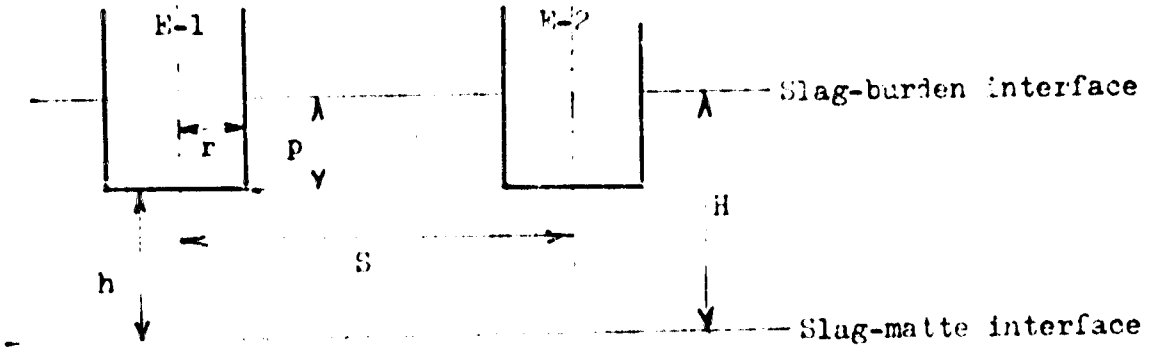

More recently Persson's investigations (6) lead to an expression relating to an electrode-to-hearth parameter to the k factor as follows:

$$\frac{E_h}{D_e^{\frac{1}{2}}} = \left[k - \frac{P_d}{4}\right]^{\frac{1}{2}}$$

in which E_h = in-phase component of the electrode-to-hearth voltage
P_d = power density
D_e = electrode diameter

These design expressions were used initially in the present study to estimate the resistance of a working unit. The reference furnaces are operated at full capacity at an average 18,5 MW power input and currents of 17,5 to 18,5 kA (7).

By instrument readings/...

Figure III - 1 FURNACE RESISTANCE AS A FUNCTION OF SLAG COMPOSITION;

Estimated with the use of formulas proposed by various researchers

Notations: K : Kjølseth
N : Nilsen
B : von Bergkampf
D-U : Downing and Urban

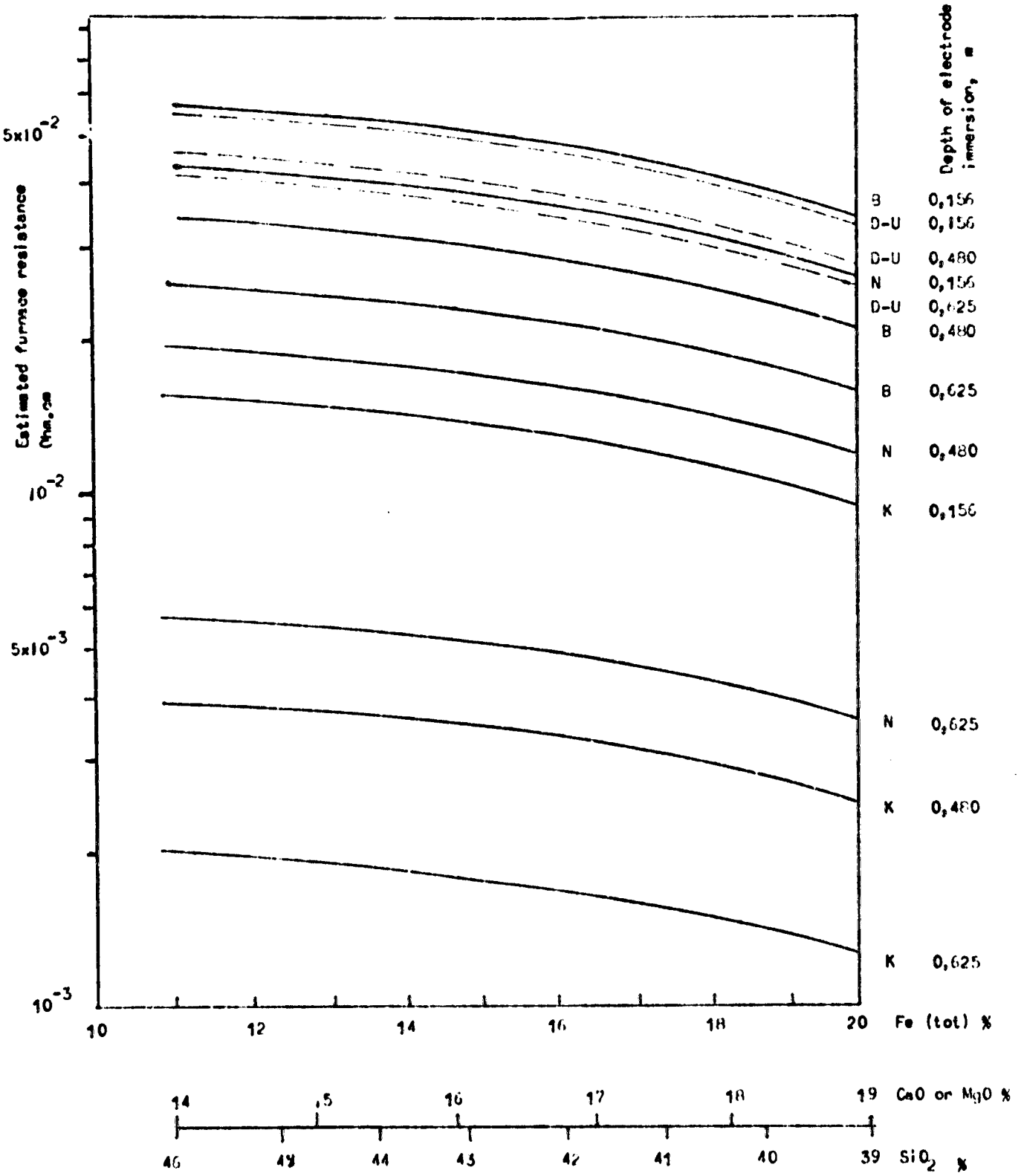

By instrument readings the $\cos\varphi$ was 0,98. Then at a maximum 18,5 kA the furnace resistance would be

$$3\,RI^2 = P_w$$

$$3\,R = 1{,}85\times10^{7}/3{,}42\times10^{8} = 5{,}42\times10^{-2}\ \text{ohm}$$

that is $(5{,}42\times10^{-2})/3 = 1{,}84\times10^{-2}$ ohm per phase

The portion of the current passing between electrode and electrode was given as two-third or three-quarter of the total by Barth (8) and was also confirmed by the model tests of Urquhart (9). As for a first approximation the interelectrode conduction was neglected and the resistivity value given above was divided between two electrodes due to the double path through the slag. Only half of the path will be considered here initially which represents the actual resistivity of the slag layer as measured between electrode and matte giving thus in the above range of current 10,1 to 9,0 milliohms per electrode, i.e. 20,2 to 18,0 milliohms per phase.

Now with the aid of the outlined expressions the furnace resistance is calculated as follows: using for a reference the laboratory conductivity data obtained e.g. with slag Group V the resistivities are evaluated over the composition range of the slag investigated, that is 11 to 20 per cent $Fe_{tot.}$, 39 to 46 per cent SiO_2, 13 to 19 per cent MgO with 16 per cent CaO as constant value. This calculation is performed for depth of electrode immersions of $D_e/2$, $D_e/2{,}6$ and $D_e/8$, expressed in terms of electrode diameter. The result of these calculations is given in figure III-1. The resistivity values of the graph were compared with those estimated from actual furnace operation. With a reference depth of electrode immersion of approximately $D_e/3$ the relationship suggested by Downing and Urban gave the lowest electrode movement i.e. variations in depth of electrode immersion. With Fjøleth's equation and to a lesser degree with Nilsen's close to an order of magnitude increase in resistivities occurred when the depth of electrode immersion decreased from $D_e/2$ to $D_e/8$.

The cell constant of the electric furnaces by the expression of Downing and Urban (equ,9.) will be

$$k = \frac{p\pi}{\ln\left[\frac{S}{D_e} + \left(\frac{S}{D_e}\right)^2 - 1\right] + r\left[1 + \frac{r}{S} + \left(\frac{r}{S}\right)^2 + \ldots\right]} \qquad 11./$$

or simply, if denoting the reciprocal expression in 9./ by N

$$R_f = \frac{\varrho}{\pi} N \qquad \text{or} \qquad k = \pi N \qquad 11a./$$

From equ.5./ of Nilsen/...

From equation 5./ of Nilson

$$k = \frac{0,3034}{D_e} \frac{[(H - p)/D_e]^{0,45}}{(p/D_e)^{0,24}} \qquad 12./$$

A comparison of k values obtained with the different expressions is given in the following table:

Table III-1. Calculated k values obtained with the suggested expressions as functions of the depth of electrode immersion in the slag.

Depth of immersion in D_e	in meter	Value of k as per electrode, x 10^{-3} cm^{-1} Nilson equ. 12	Downing and Urban equ. 11a.	Von Bergkampf equ.3.	Persson and Treilhard equ.15
$D_e/2$	0,625	1,60	2,76	1,66	1,15
$D_e/2,6$	0,480	1,80	2,90	2,22	1,18
$D_e/5$	0,250	2,30	3,40	2,84	1,24
$D_e/8$	0,156	2,92	3,68	3,10	1,27

Here the original equation of von Bergkampf was used in a slightly modified form to suit conditions created by the material processed in matte smelting furnaces. According to this

$$R_f = \rho \frac{1,3(H - p)}{\pi D_e^2} \qquad 13./$$

Formulation of an alternative expression to estimate furnace resistance.

The equations discussed above were primarily proposed for ferroalloy producing submerged arc furnaces having three electrodes arranged in the corners of an equilateral triangle. For the type of slag produced in slag - resistance heated matte smelting furnaces having 6-in-line electrode arrangement a more specific expression was necessary to describe the operation of the furnace. Although the equation developed by Downing and Urban accounts for inter-electrode action, in its derivation a uniform conduction was assumed between isothermal homogeneous conductors. Furthermore, the conducting medium was considered to have infinite length or extension in vertical direction. Because of the three-dimensional convergence of current the expression is

valid for conditions/...

valid for conditions of "sufficient bed depth" as this was noted by Persson and Treilhard (10). For higher power furnaces a greater slag depth is required than for smaller furnaces. Second, the inclusion of the capacitance term as applied specially for hemispherical electrode tips (equs. 7 and 8.) can hardly be justified. While the concept may be of some value with completely new electrodes if their tip happened to be formed as a hemisphere, from practical experience its value will be rather tenuous in considering the incredible shapes assumed at times by battle-scarred working ends of Söderberg electrodes. These conditions, particularly with regard to the effect of electrode movement give rise to certain restrictions in the general applicability of the formula.

Persson and Treilhard (10) have suggested recently a modification to the Downing - Urban formula to measure the resistance between two flat - tipped electrodes as

$$R_f = \varsigma / \left[\frac{p\pi}{\ln\left[\frac{S}{D_e} + \sqrt{\left(\frac{S}{D_e}\right)^2 - 1}\right] + D_e\left[1 + \frac{r}{S} + \left(\frac{r}{S}\right)^2 + \ldots\right]} \right] \qquad 14./$$

The logarithmic portion of the equation drops out at high electrode position i.e. when the electrodes merely touch the surface of the bath. From equ.14 the cell constant is expressed as

$$k = \frac{1}{\frac{p\pi}{\ln\left[\frac{S}{D_e} + \sqrt{\left(\frac{S}{D_e}\right)^2 - 1}\right]} + \pi D_e\left[1 + \frac{r}{S} + \left(\frac{r}{S}\right)^2 + \ldots\right]} \qquad 15./$$

The expression of furnace resistance representing more specifically the operation of matte smelting furnaces was obtained empirically. The resistance of the working units was calculated for optimum operating conditions pertinent to power input and current. In the knowledge of the resistance values the constant of the suggested formula was determined by successive approximation until the expression yielded identical results with the optimum practical data. Consequently, the equation obtained in this way is fully representative of the character of material processed and the operation of the units treating this material:

$$R_f = \frac{1}{k}\,\frac{K(H - p)}{\pi}\,\frac{1}{4}\left[\ln\left(\frac{S}{D_e} + \sqrt{\left(\frac{S}{D_e}\right)^2 - 1}\right) + C_t\right]^{-0,5} \qquad 16./$$

involving four main parameters viz. the total depth of slag bed (H), depth of electrode penetration, p, electrode diameter D_e and electrode spacing, S. The logarithmic term after Attwood, represents the capacitance between

electrodes as/...

Figure III - 2. VARIATION OF CELL CONSTANT WITH ELECTRODE POSITION

Average cell constant values based on 17,5 to 18,5 kA operating current and 18,5 MW power input represerting optimum range of furnace operation.

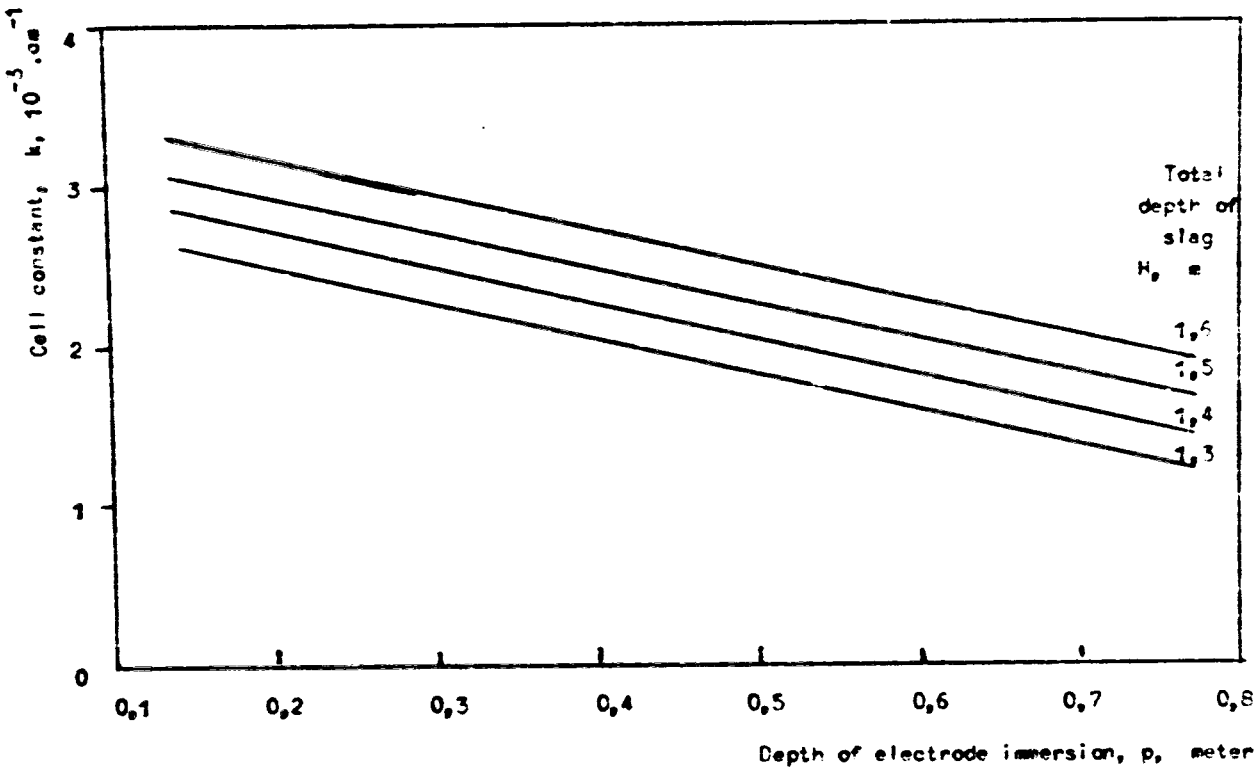

Figure III - 3.

a. FURNACE RESISTANCE, POWER AND OPERATING CURRENT RELATIONSHIP FROM A WORKING FURNACE

Average resistivity of plant slag : 4,85 ohm.cm
Temperature : 1400°C

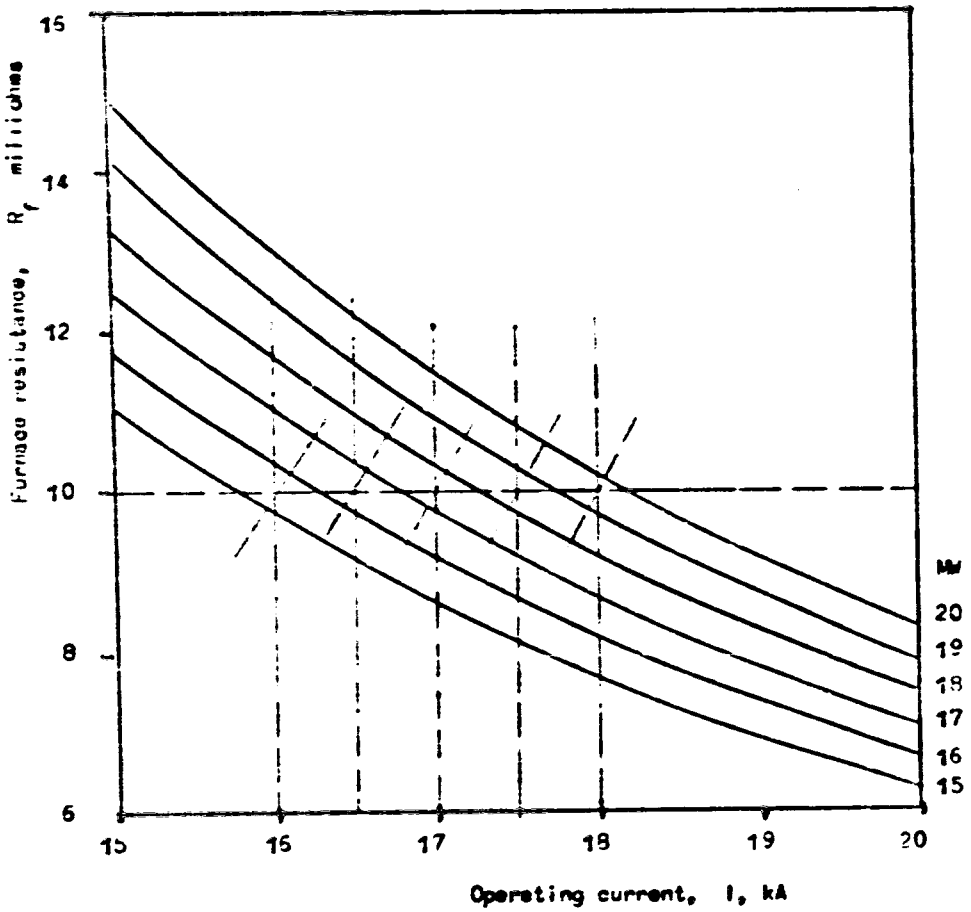

b./ FURNACE LOAD AND OPERATING CURRENT RELATIONSHIP FROM A WORKING FURNACE

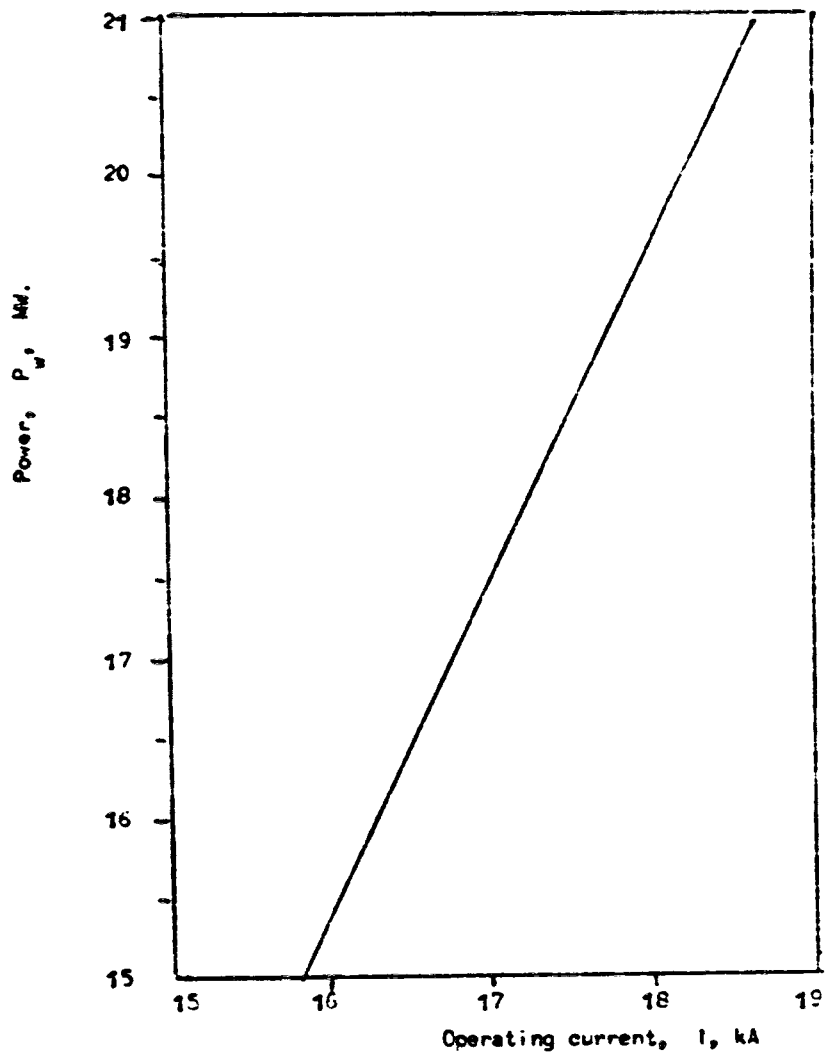

electrodes as parallel conductors, while the second capacitance term, C_t) accounts for the capacitance between flat electrode tips as suggested by Persson and Treilhard

$$C_t = D_e \left[1 + \frac{r}{3} + \left(\frac{r}{3}\right)^2 + \left(\frac{r}{3}\right)^3 + \ldots \right]$$

For the particular symmetry relationships of the reference furnaces equ.16. can be written as

$$R_f = \frac{1}{K} \frac{K(H - p)}{n} \frac{1}{4} \left[\ln\left(2{,}72 + \sqrt{(2{,}72)^2 - 1}\right) + 1{,}226\ D_e \right]^{-0{,}5} \qquad 17./$$

Figure III-2 shows the variation of the estimated cell constant with the change of the depth of electrode penetration into the slag. On this basis the value of the constant K which depends on the character of the material treated or slag produced, was estimated as 3,19 when the average temperature of the molten slag bed is 1400°C. As for a test of this equation, for various loads and operating currents the resistance of the operating furnace can be calculated by the relationship $R_f = (P_w/I^2)/6$. This is shown in graph III-3/A.

Now, as for an example, using a slag resistivity value of 4,85 ohm .cm determined in the laboratory, the furnace resistance is calculated with equation 17./ by which R_f = 10,05 mohm. Using this figure in the $P_w = 6\ RI^2$ formula, for various operating currents the furnace power will be obtained as shown by plot B in fig III-3. Then the intersection of the horizontal line representing R_f = 10,0 mohm with the vertical dotted lines of the operating currents in graph 3A should give the same load values as the plot of 3B which evidently appears to be the case. The agreement between the two sets of values is very good.

For the comparison of furnace resistances calculated by the formulas of a.) Downing and Urban, b.) Persson and Treilhard and c.) the present study let the conditions be as follows:

average slag resistivity : 4,85 ohm.cm at 1400°C

depth of electrode immersion, p : 0,48 m

then with the various formulas we get

a./ Downing and Urban

$$R_f = \frac{4{,}85}{3{,}14 \left[\frac{0{,}48}{\ln\left(\frac{3{,}40}{1{,}25} + \sqrt{\left(\frac{3{,}40}{1{,}25}\right)^2 - 1}\right)} \right] + 0{,}625 \left[1 + \frac{0{,}625}{3{,}4} + \left(\frac{0{,}625}{3{,}4}\right)^2 \right]}$$

$$= \frac{4{,}85}{1{,}02} = 4{,}62 \text{ mohm}$$

b./ Persson- Treilhard / ...

b./ Persson- Treilhard

$$R_f = 4,85/\frac{3,14\times0,48}{\ln\left[\frac{3,40}{1,25}+\sqrt{\left(\frac{3,40}{1,25}\right)^2-1}\right]+1,25\left[1+\frac{0,625}{3,4}+\left(\frac{0,625}{3,4}\right)^2\right]}$$

$$= \frac{4,85}{(3,14\times0,48)/3,70} = 10,3 \text{ mohm}$$

c./ Present study $R_f = (4,85\ \frac{3,15 \times 0,92}{3,14/4})\Big/\sqrt{1,66 + 1,528}$

$= 4,35 \times 2,07 = 10,05$ mohm

From this comparison the results obtained by the Persson-Treilhard formula and that of the present study show very good agreement while the Downing-Urban expression falls short in giving less than half resistance values approximately in the form $R_{f(act)} = 2,23 R_{f(D-U)}$.

The proposed equation for furnace resistance takes into account besides the depth of electrode penetration into the slag also the total depth of the slag layer. The matter is important from the point of view of cell geometry and cell constant, since the latter will depend, by virtue of H-p = h on both variables. This fact is realized in the formulas of Kjølseth and Nilser while in both the Downing and Urban and Persson-Treilhard equations it is left out of consideration. The shape of current flow or current distribution around and below an electrode is determined primarily by h, i.e. the distance between electrode tip and matte surface. At a constant value of h it is largely immaterial in this respect whatever the total depth of the molten bed happens to be. On the other hand by defining p only, the value of h will change with the variations of the depth of the slag layer and conditions may become ill-defined in case of varying both H and p. Thus from the standpoint of h it is more adequate to eliminate simultaneously these parameters. In this way the cell constant of the reference furnace from equ.17./ will be expressed as

$$k = \left[(H - p)\ \frac{K}{\pi/4}\right]\Big/\sqrt{3,19} = 2,25(H - p) \qquad 18./$$

The variation of cell constant with the depth of electrode penetration into the slag is shown in figure III-2.

In an alternative way the cell constant can be expressed in terms of the following parameters : maximum operating power ($P_{w(m)}$), internal furnace area A or alternately hearth area as related to the slag bed $A_{h(sl)}$, electrode diameter D_e, total depth of slag bed H, and depth of electrode immersion p. With these parameters the formula suggested for k in the present study/...

b./ Persson- Treilhard

$$R_f = 4,85/\frac{3,14\times0,48}{\ln\left[\frac{3,48}{1,25}+\sqrt{\left(\frac{3,48}{1,25}\right)^2-1}\right]+1,25\left[1+\frac{0,625}{3,4}+\left(\frac{0,625}{3,4}\right)^2\right]}$$

$$= \frac{4,85}{(3,14\times0,48)/3,70} = 10,3 \text{ mohm}$$

c./ Present study $R_f = (4,85\ \frac{3,15 \times 0,92}{3,14/4}) \Big/ \sqrt{1,66 + 1,528}$

$= 4,95 \times 2,07 = 10,05$ mohm

From this comparison the results obtained by the Persson-Treilhard formula and that of the present study show very good agreement while the Downing-Urban expression falls short in giving less than half resistance values approximately in the form $R_{f(act)} = 2,23_{f(D-U)}$.

The proposed equation for furnace resistance takes into account besides the depth of electrode penetration into the slag also the total depth of the slag layer. The matter is important from the point of view of cell geometry and cell constant, since the latter will depend, by virtue of H-p = h on both variables. This fact is realized in the formulas of Kjølseth and Nilsen while in both the Downing and Urban and Persson-Treilhard equations it is left out of consideration. The shape of current flow or current distribution around and below an electrode is determined primarily by h, i.e. the distance between electrode tip and matte surface. At a constant value of h it is largely immaterial in this respect whatever the total depth of the molten bed happens to be. On the other hand by defining p only, the value of h will change with the variations of the depth of the slag layer and conditions may become ill-defined in case of varying both H and p. Thus from the standpoint of h it is more adequate to delineate simultaneously these parameters. In this way the cell constant of the reference furnace from equ.17./ will be expressed as

$$k = \left[(H - p)\ \frac{E}{H/4}\right] \Big/ \sqrt{3,19} = 2,25(H - p) \qquad 18./$$

The variation of cell constant with the depth of electrode penetration into the slag is shown in figure III-2.

In an alternative way the cell constant can be expressed in terms of the following parameters : maximum operating power ($P_{w(m)}$), internal furnace area A or alternately hearth area as related to the slag bed $A_{h(sl)}$, electrode diameter D_e, total depth of slag bed H, and depth of electrode immersion p. With these parameters the formula suggested for k in the

present study/...

present study will be as follows:

$$k = K_k \left[\left(\frac{P_{w(m)}/A}{4} \right) (D_e^{\frac{1}{2}})^{-1} \right] (H - p) \qquad 19./$$

With the reference furnaces the maximum operating power is in the range of 19 MW and the internal area $A = 26 \times 7 = 182\ m^2$. The value of the constant is close to unity, here $K_k = 0,96$. Expressing all lengths in meters and the area in square meters, equation 19./ for the working units would yield

$$k = K_k \frac{P_{w(m)}/A}{4\sqrt{D_e}} (H - p) = 0,96 \frac{(1,96 \times 10^4)/(1,82 \times 10^2)}{4 \times \sqrt{125}} (H - p) \times 10^{-2}.m^{-1}$$

or

$$k = 2,25(H - p)$$

If, instead of the internal area, the hearth area covered by the slag is taken into consideration, according to established best operating practice at an average depth of the slag bed the realtionship between internal area and hearth area related to the slag bed $A_{h(sl)}$ is $A \sim 2/3\ A_{h(sl)}$, therefore the cell constant is

$$k = K_k \left[\frac{P_{w(m)}}{2/3\ A_{h(sl)}} (4\ D_e^{\frac{1}{2}})^{-1} \right] (H - p) \times 10^{-2}.m^{-1} \qquad 20./$$

Obviously, the fraction P_w/A represents the power density under any particular condition of furnace operation, and with the symmetry terms D_e, H and p the value of k is defined for any given furnace size by the above expressions when the character of the feed is similar to that processed in the reference furnaces. The broader applicability of the formula is ensured by the constant K_k the value of which, as noted, will depend on the character of the feed material used.

Then, in general, to estimate the effect of change in slag composition upon load the resistance is calculated from equ.18./ as

$$R_f = 2,25(H - p)$$

with the use of the specific slag resistivity data obtained in laboratory measurements which are given in Section II. Then

$$\text{for current} \quad I = P_w(MW)/6\ R_{sl}$$

$$\text{for power} \quad P_w(MW) = 6R \times I^2$$

As for an example Table III-2 gives an outline of the mode of calculation while the complete set of results pertinent to the effect of slag composition

upon the power/...

Figure III - 4. EFFECT OF SLAG COMPOSITION UPON VARIOUS CHARACTERISTICS OF FURNACE OPERATION.

SLAG GROUP II. Total depth of slag bed : 1,4 m
Temperature of slag : 1400°C

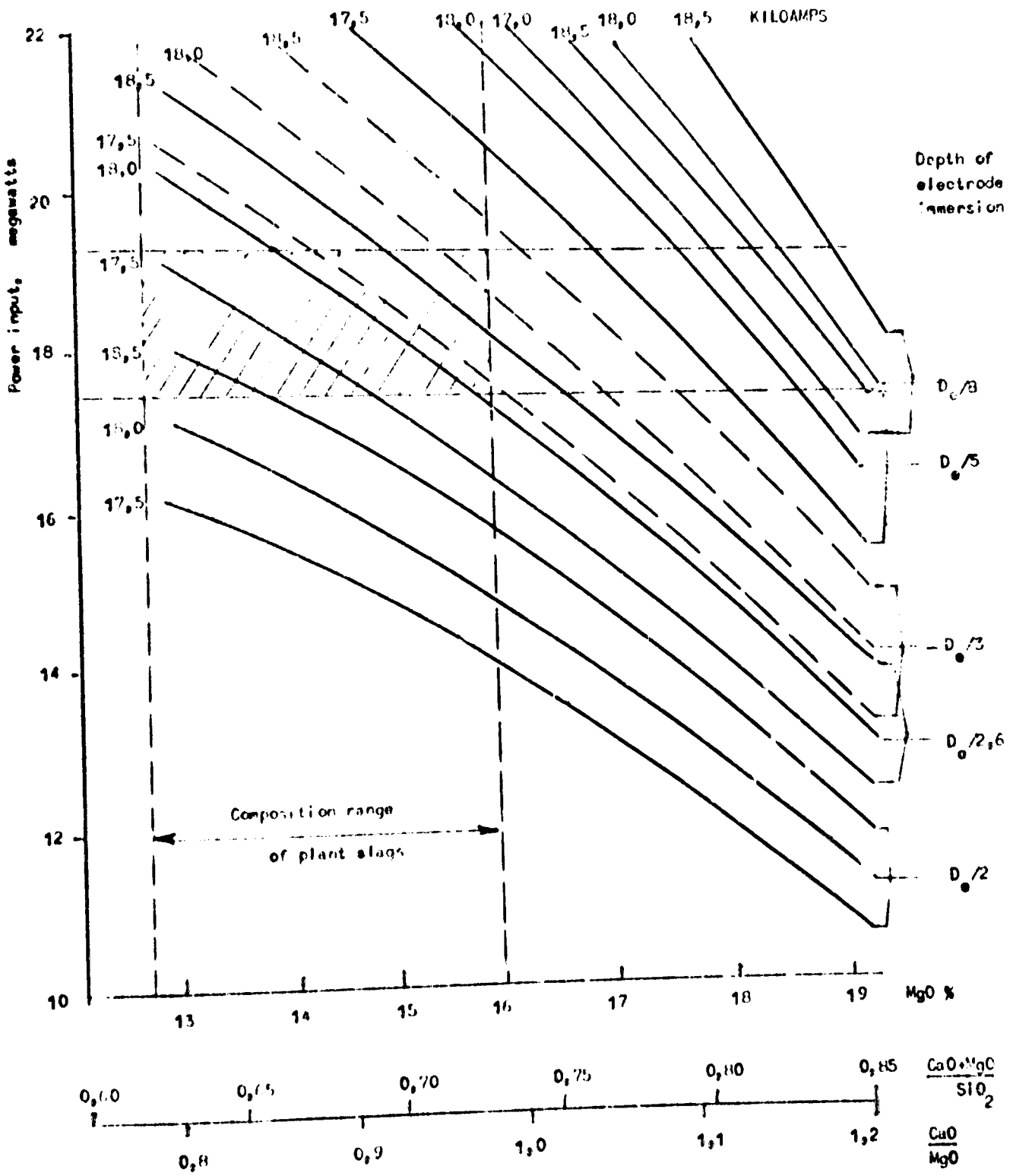

Figure III - 5. EFFECT OF SLAG COMPOSITION UPON VARIOUS CHARACTERISTICS OF FURNACE OPERATION.

SLAG GROUP V. Total depth of slag bed : 1,4 m
Avg. temperature of slag : 1400 °C

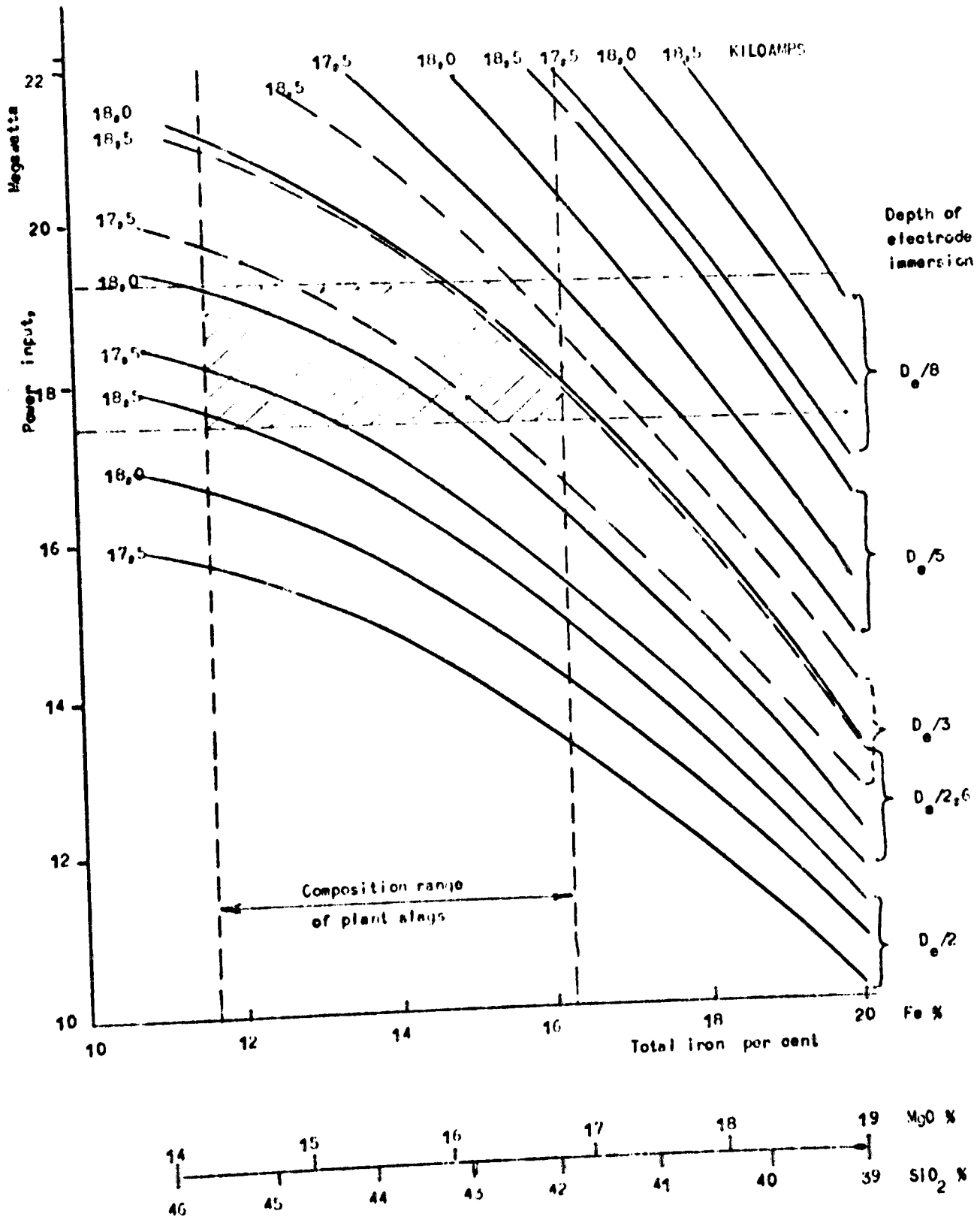

Figure III-6. EFFECT OF THE COMPOSITION AND TEMPERATURE OF THE SLAG ON FURNACE OPERATION CHARACTERISTICS.

Slag Group V.

Solid lines 1420°C

Dotted lines 1450°C

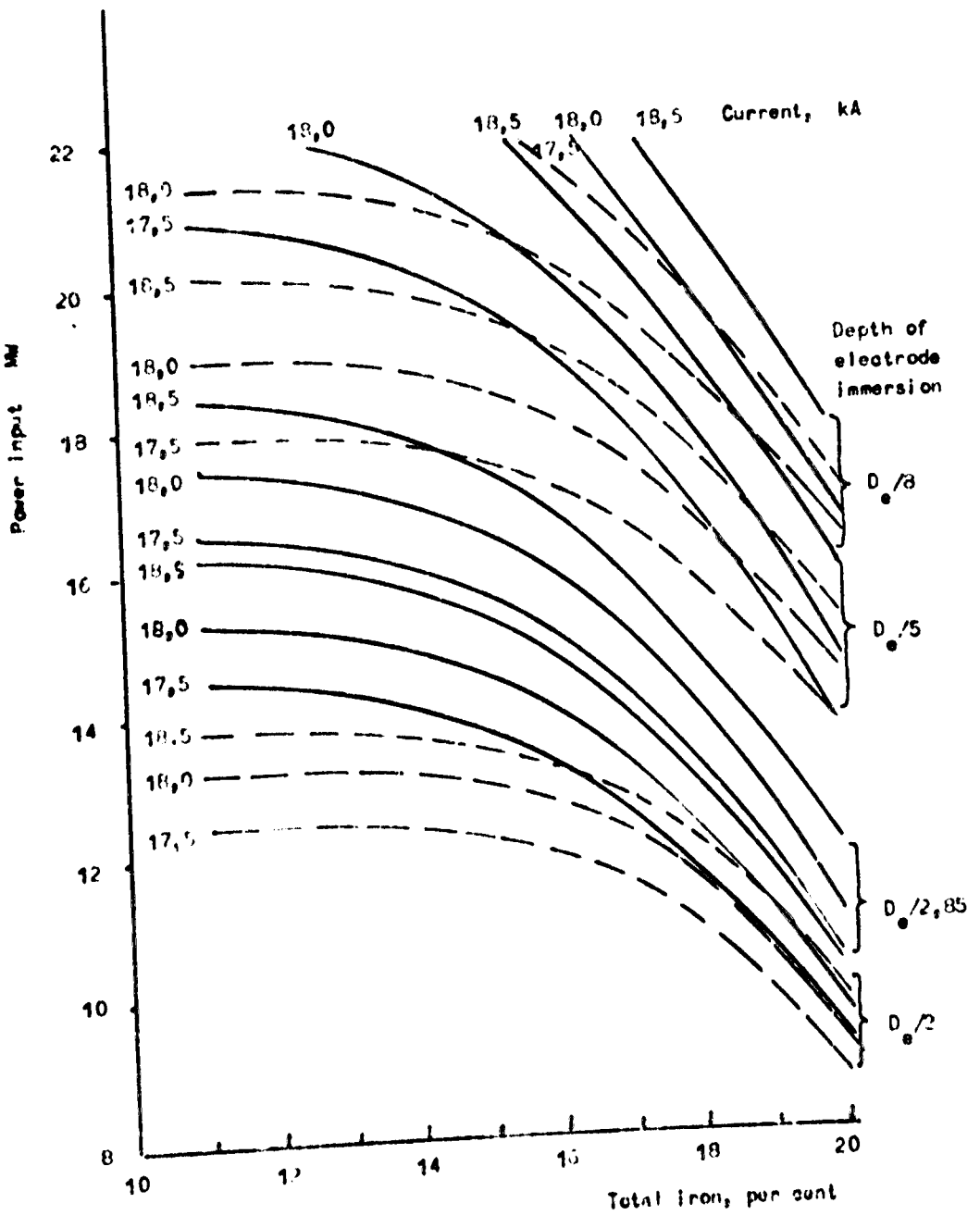

Figure III -7. RELATION BETWEEN POWER INPUT AND DEPTH OF ELECTRODE IMMERSION AT THE TEMPERATURE OF SLAG AS A PARAMETER.

Conditions : Operating current 18 kA
Fe (total) in slag 15,5 per cent
Slag Group V

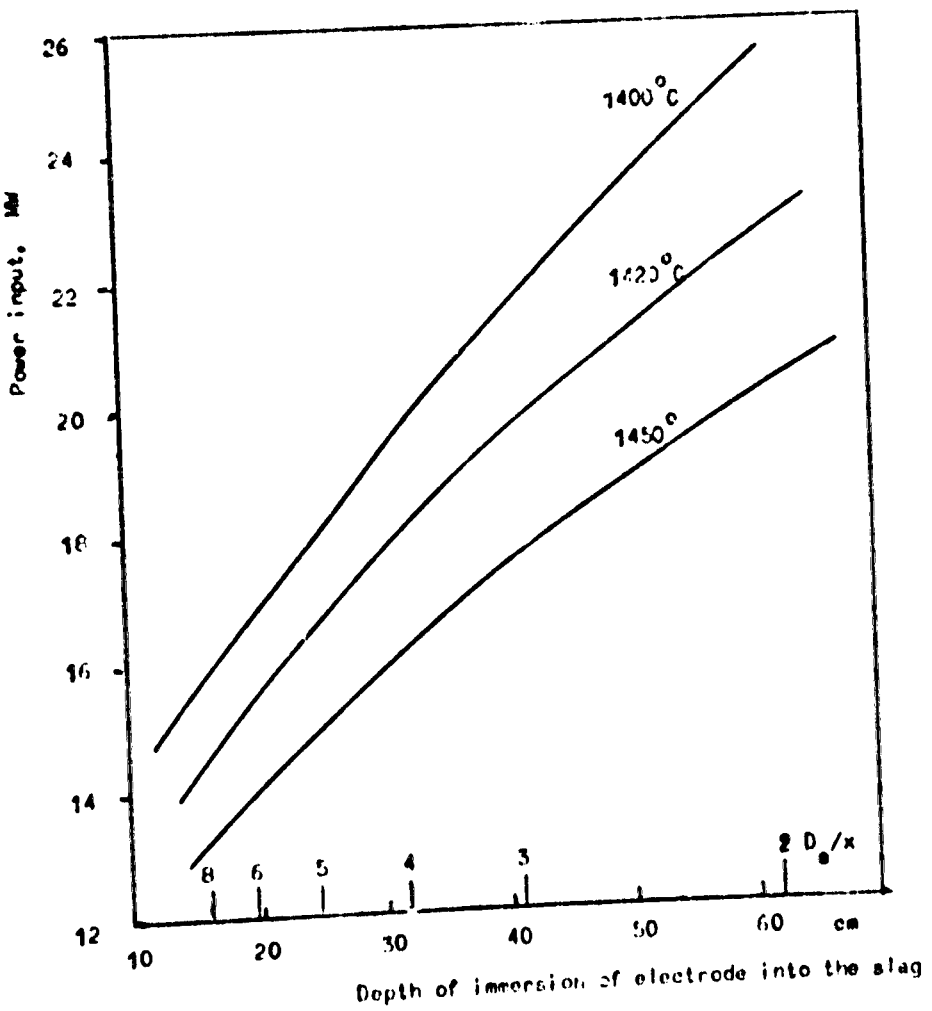

upon the power input to the furnace with 17,5, 18,0 and 18,5 kA current is depicted in figures III-4 and III-5 as referred to slag groups II and V.

Table III-2. Effect of slag composition on power input to the furnace.

Mode of estimation.

Slag group V. Average slag temperature 1400°C

$p = D_e/2,6 = 0,48$ m

Reference slag constituent % Fe	Resistivity ohm.cm ς	R_f (mohm) $2,25(H-p)\varsigma$	$P_w = 6 R \times I^2$ (MW) at operating currents of		
			17,5 kA	18,0 kA	18,5 kA
11	4,88	10,10	18,4	19,7	20,8
12	4,81	9,95	18,2	19,4	20,5
13	4,69	9,70	17,8	19,0	19,9
14	4,55	9,41	17,3	18,3	19,3
15	4,35	9,00	16,5	17,5	18,5
16	4,13	9,55	15,8	16,7	17,6
17	3,86	7,98	14,7	15,6	16,4
18	3,61	7,35	13,6	14,3	15,1
19	3,33	6,90	12,7	13,4	14,2
20	3,12	6,46	11,9	12,5	13,3

Effect of temperature on resistance.

The change of slag temperature has a marked effect on both operating current and power input rates as well as on electrode position in the molten slag as shown in figure III-6./ and becomes even more clear in figure III-7./, plotted as regards to furnace load at a fixed operating current and slag composition. Therefore, as an important factor, the effect of temperature will also have to be taken into account in performing calculations with equations 16 or 17. The temperature effect was demonstrated earlier by the straight line relationship between $\log \kappa$ and $1/T$, the slope of the line being dependent on the chemical composition of the slag. As it was shown the slope gives the temperature coefficient of electrical conduction represented by the change of conductivity upon the change of temperature as

$$\lambda = \frac{\kappa_1 - \kappa_2}{(T_1 - T_2)\kappa_{avg}}$$

The log vs $1/T$ /...

Figure III - 8. VISCOSITY AND RESISTIVITY RANGE OF PLANT SLAGS AS A FUNCTION OF TEMPERATURE

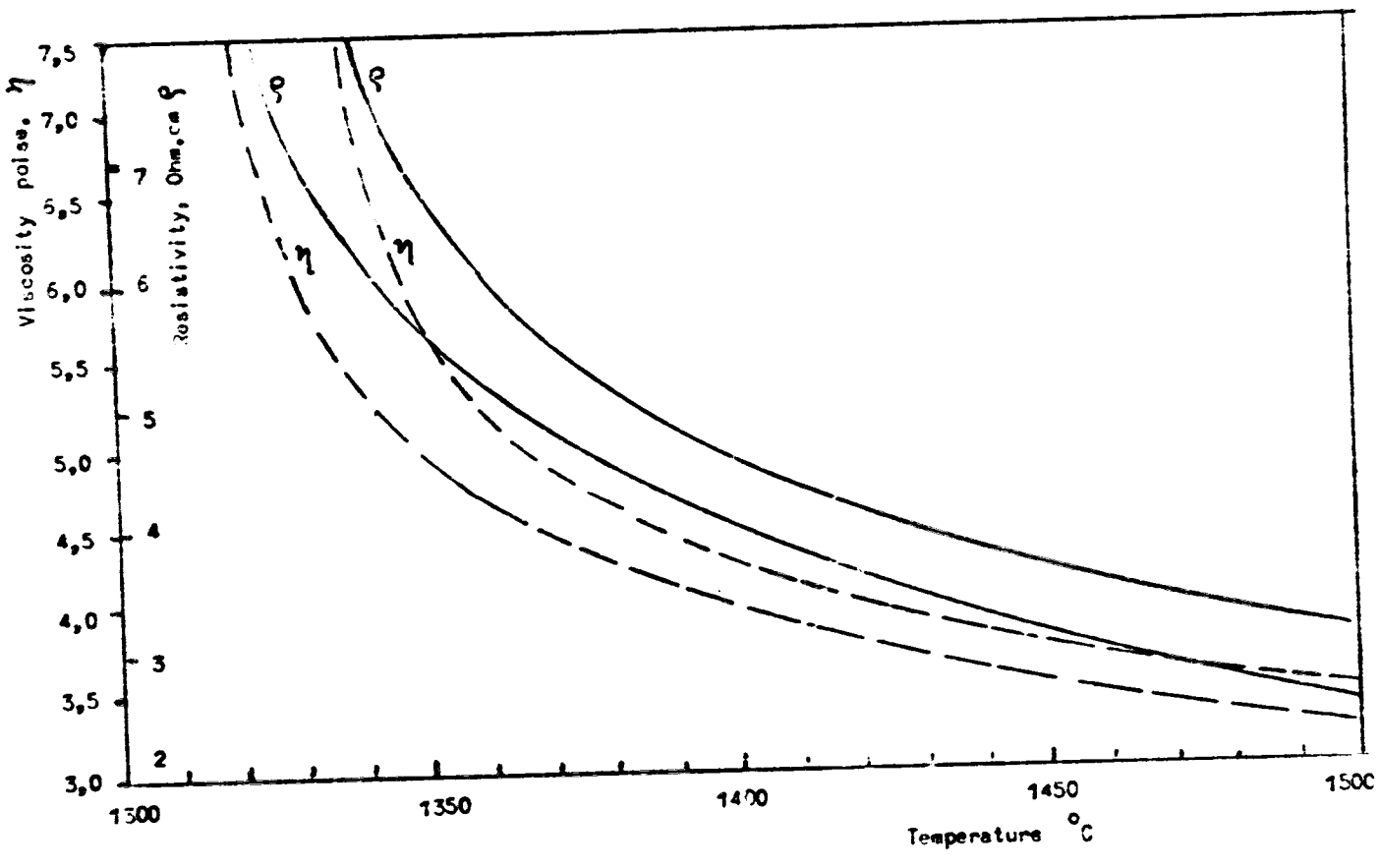

The log κ vs. 1/T relationship can be expressed by

$$\log \kappa = a - \frac{b}{T} \qquad 21./$$

or

$$\kappa = A(\exp -B/T) \qquad 22./$$

where the constants a, b, A and B respectively are determined from the appropriate plots. Then the value of R_f at any desired temperature is obtained by using the estimated values of κ in equ. 17.

Instead of equ.22./ the temperature effect may be calculated conveniently by a polynomial expression using a computer for curve fitting calculations. Thus for example the data represented in the plots of figure 8. obtained from measurements on plant slags, the change of slag resistivity for the higher and lower extreme values were computed as

$$R_{sl-1} = 5{,}94\text{x}10^{2} - 1{,}17\ T + 7{,}83\text{x}10^{-4}T^{4} - 1{,}76\text{x}10^{-7}T^{3} \qquad 23./$$

$$R_{sl-2} = 5{,}04\text{x}10^{2} - 1{,}62\ T + 1{,}10\text{x}10^{-3}T^{2} - 2{,}51\text{x}10^{-7}T^{3} \qquad 24./$$

* * *

Equations 16 and 17 describe conditions somewhat more accurately than the ones used previously in connection with the operation of the model furnaces. The expressions are by no means of general validity and apply only to a particular furnace type processing a particular material under carefully specified conditions. However, as it is suggested by the literature, an expression of general validity for electric smelting furnaces is simply non-existent. Probably the only exception is Andreae's genuine formula upon which all subsequent relationships were based. These relationships may be regarded purely as adequate approximations (at the best) to conditions prevailing in actual operating units.

The basic shortcomings of the proposed equations for cell constant and the basic concept of cell constant proper is attributable to the high current densities inherent in the operation of a large-scale working unit. Theoretical predictions are hampered by both thermal and electrical effects, in the former case by convection and change of specific resistivity of the slag with temperature, and in the latter case by skin effects and slag ionisation potentials. This makes the direct translation of results obtained on specific resistivities in laboratory tests into usable figures for plant-scale operation and furnace design somewhat difficult.

2./ The movement of the electrode: its effect upon the shape of current flow under the electrode and on the heating conditions of slag and matte.

Several attempts have been made in the past decades to determine the geometric shape of current path under the electrode with a view to

facilitate thereby furnace dimensioning. The earliest of these (at the end of the 1930's) is attributable to Ya. F. Sibakin (11, 12) who investigated the current distribution in both single-phase and three-phase iron melting furnaces. Using coke beds made up of 1 and 5 mm particles respectively, he determined the current distribution by measuring out equipotential contoures between the electrode and the bottom in a model furnace. Supported by a very comprehensive theoretical analysis from the measurements up to that time little-known relationships like electrode position vs. furnace resistance and operating current, operating current and resistance vs. furnace diameter, then heat distribution and furnace cross-section vs. electrode distance from the furnace bottom could be established with good accuracy for three-electrode iron melting furnaces of circular cross-section. The shape of current flow found by Sibakin was that of a paraboloid passing through the perimeter of the electrode tip and across the electrode above the tip.

Morkramer (13) was the first to suggest a relationship between the dimensions of the system and the specific resistivity of the charge in the form

$$R_f = \varrho \pi D_e \qquad 25,/$$

based on Andreae's electrode periphery concept. By this equation he assumed a geometrical shape of the current flowing between the electrode and the hearth, the volume of which is equal to that of a truncated cone.

On the basis of model experiments Nilsen (4) attempted to correlate electrical conduction with the shape of current flow between electrode tip and metal surface (or furnace hearth). Potassium chloride of two different concentrations were used in the tests. Three models were considered for the geometrical shape of current flow, viz. truncated cone, cylinder with superimposed paraboloid and paraboloid passing through the perimeter of the electrode tip. In the simplified analytical solution Nilsen assumed that all resistance is between electrode tip and furnace bottom. Further he made no account for the rounding-off of the electrode tips which, from practical standpoint, is of considerable importance and eliminates the source of good deal of misinterpretation and confusion.

Undoubtedly the most impressive and sophisticated technique applied to the investigation of this problem was used recently by Rabey at Cape Town University (14) in conjunction with furnaces having 6-in-line electrode arrangement. He also, like Nilsen, used a salt solution in his model to represent the slag bath of a working furnace with the inherent disadvantage of small current production which is out of proportion to the real size of current in an operating unit when the size of the model and the

working furnace/....

Figure III - 9 ELECTRIC FIELD BETWEEN TWO ELECTRODES OF A PHASE IN THE ELECTRIC FURNACE.

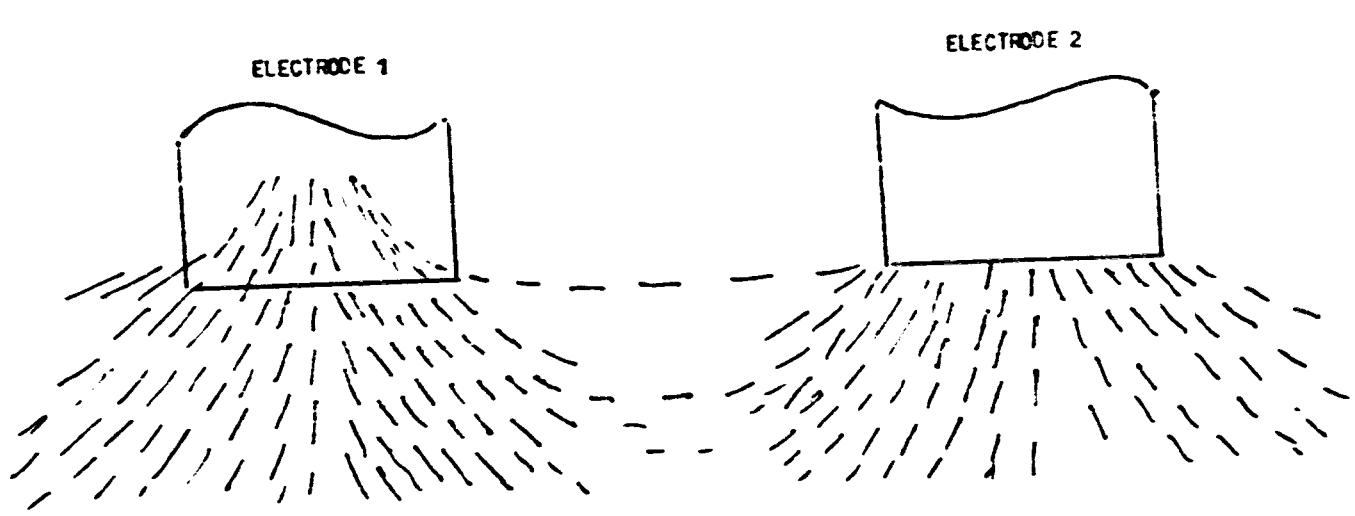

Figure III - 10 ILLUSTRATION OF THE CONCEPT OF HEAT GENERATION IN THE GEOMETRY OF CURRENT FLOW UNDER AN ELECTRODE.

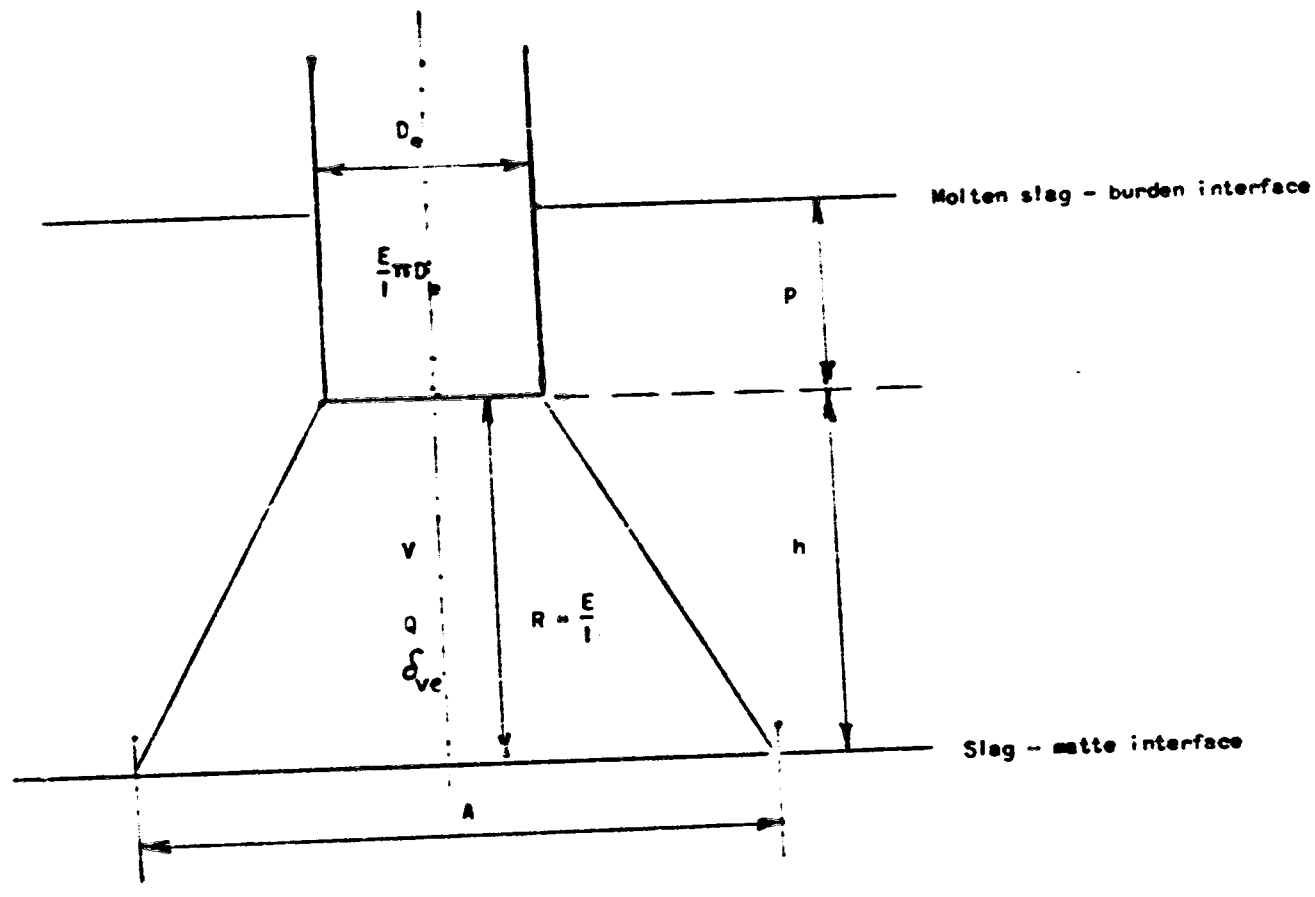

working furnace is compared, on an equal scale. This modifies the effect due to magnetic fields. Likewise, skin effects which might be significant on large electrodes are completely lost in the case of a model. So is the considerable reactance always present in an arc furnace circuit and also the inductance, present in the busbars of a large-scale unit. However, an attempt was made involving theoretical considerations to account for these shortcomings, thus the results can be regarded as being representative of conditions prevailing in industrial-size furnaces. The basic principle of measuring equipotential fields was similar to that applied by some 40 years ago by Sibakin, but the sophistication of the experimental technique permitted the accumulation of vast amounts of data with the use of a mini - computer hooked directly to the model for the purpose of both giving instructions to, and receiving data from the model furnace.

From the results obtained by Rabey it would appear that the geometric shape of current flow under the electrodes could not be described fully by a paraboloid as it was suggested earlier by the models of Sibakin and Nilsen. The shape was closer to that of a hyperboloid or at least could be fitted between a hyperboloid and a truncated cone. (see figure 9.). Applying these two configurations for the geometric shape of current flow, two models are proposed in this study to determine the volumetric energy density, as expressed in watt/cm^3 slag volume, and the current distribution in the reference furnaces. The basic thinking behind the following analysis is that the amount of heat is represented by the volume of the geometric body of current flow which is shaped between electrode tip and matte surface. Thus obviously, at a constant rate of heat generation by the electrodes the amount of heat contained in the geometric body is inversely proportional to its size or else, to the distance between tip and matte surface on account of the decrease of the volume with the decrease of the distance. This is understandable because the energy contained in the body, irrespective of its shape or size, at a constant rate of heat generation will be the same. Hence the energy level in an elementary body placed in the path of current flow will be inversely proportional to the depth of electrode penetration. With the aid of figure 10. let the point be illustrated as follows:

For a given size of electrode by Andreae's formula $(E/I)\pi D_e$ = const, that is the principle of the electrode control system is based on the resistivity of the slag. When the resistivity is assumed to remain constant, then from E = IR = const. relationship if we

a./ decrease the/...

Figure III - 11 TRUNCATED CONE MODEL FOR THE SHAPE OF CURRENT FLOW BETWEEN ELECTRODE AND MATTE.

a./ Truncated cone model

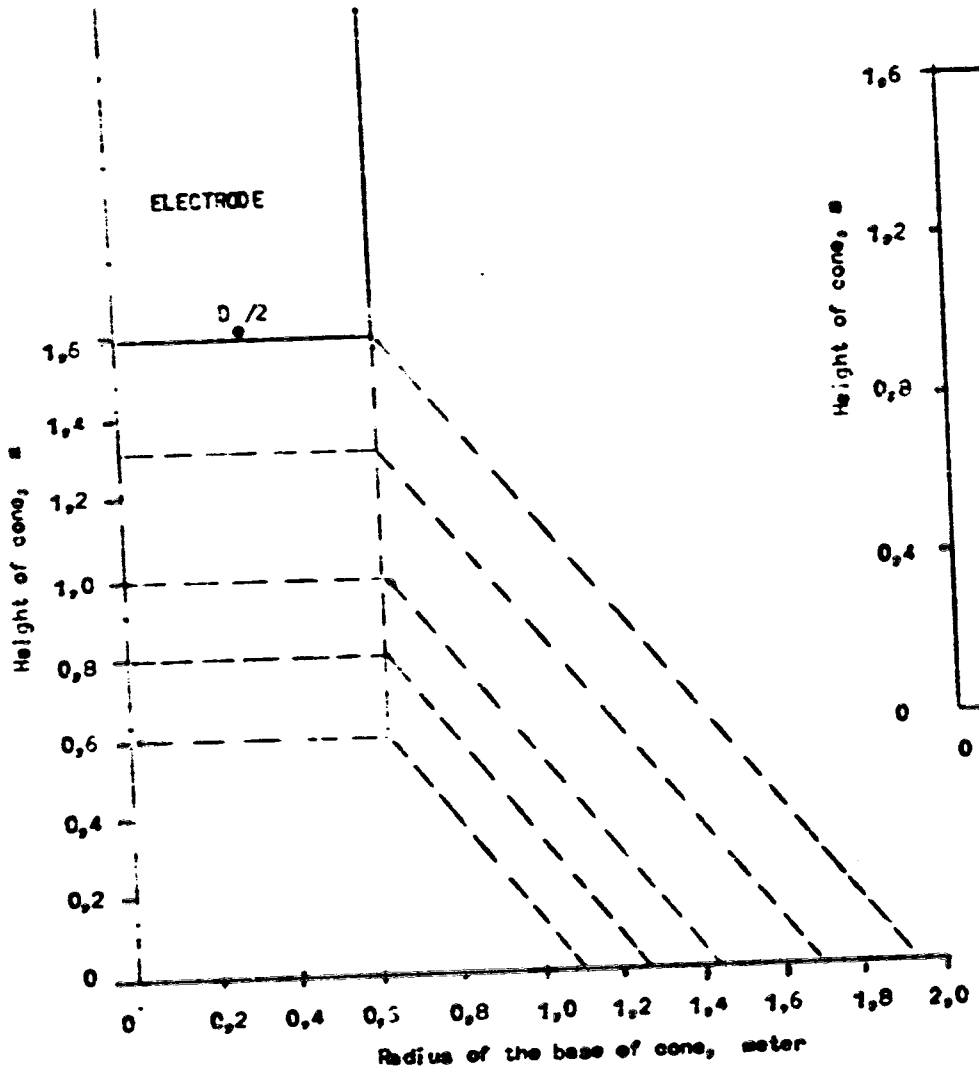

b./ Relationship between the base and height of the cone

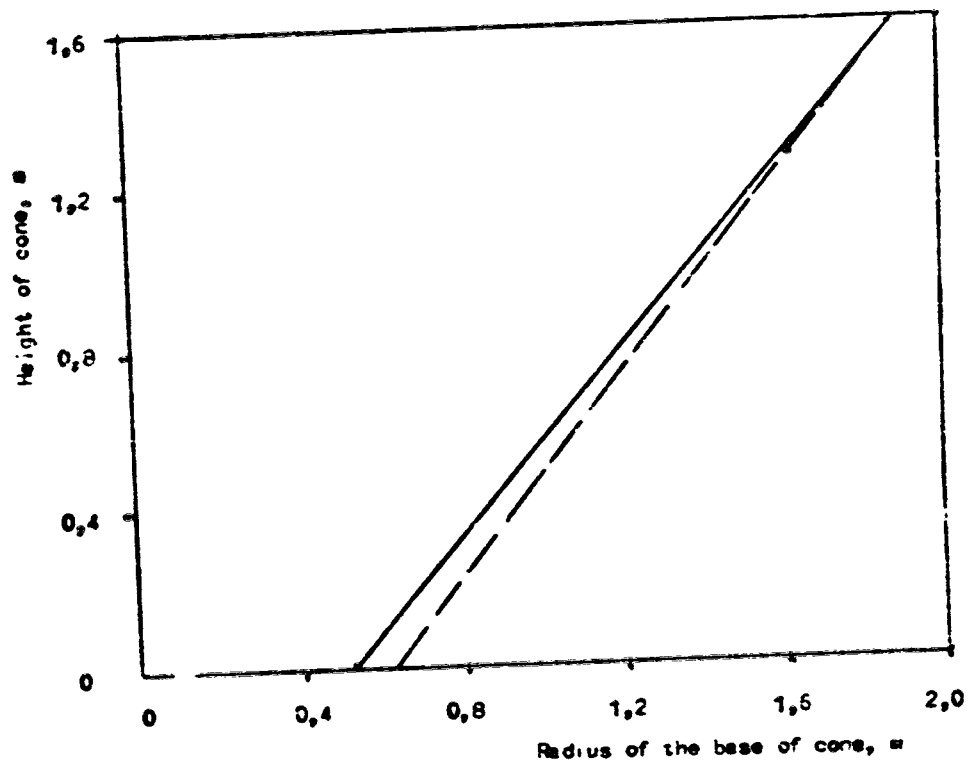

Figure III - 12. HYPERBOLOID MODEL FOR THE SHAPE OF CURRENT FLOW.

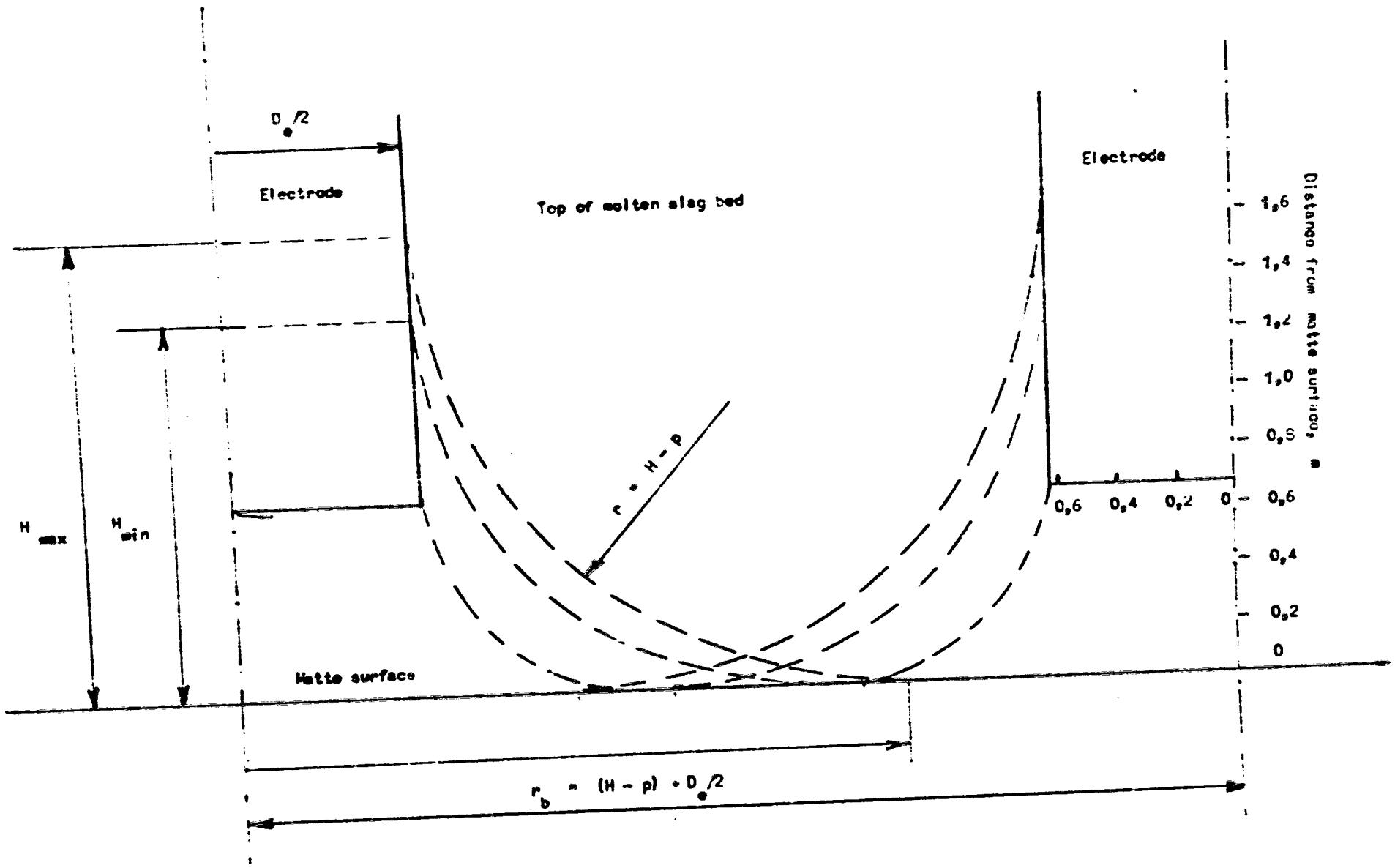

Figure III - 13. RELATIONSHIP BETWEEN VOLUMETRIC ENERGY DENSITY AND THE DISTANCE OF ELECTRODE TIP FROM THE MATTE SURFACE.

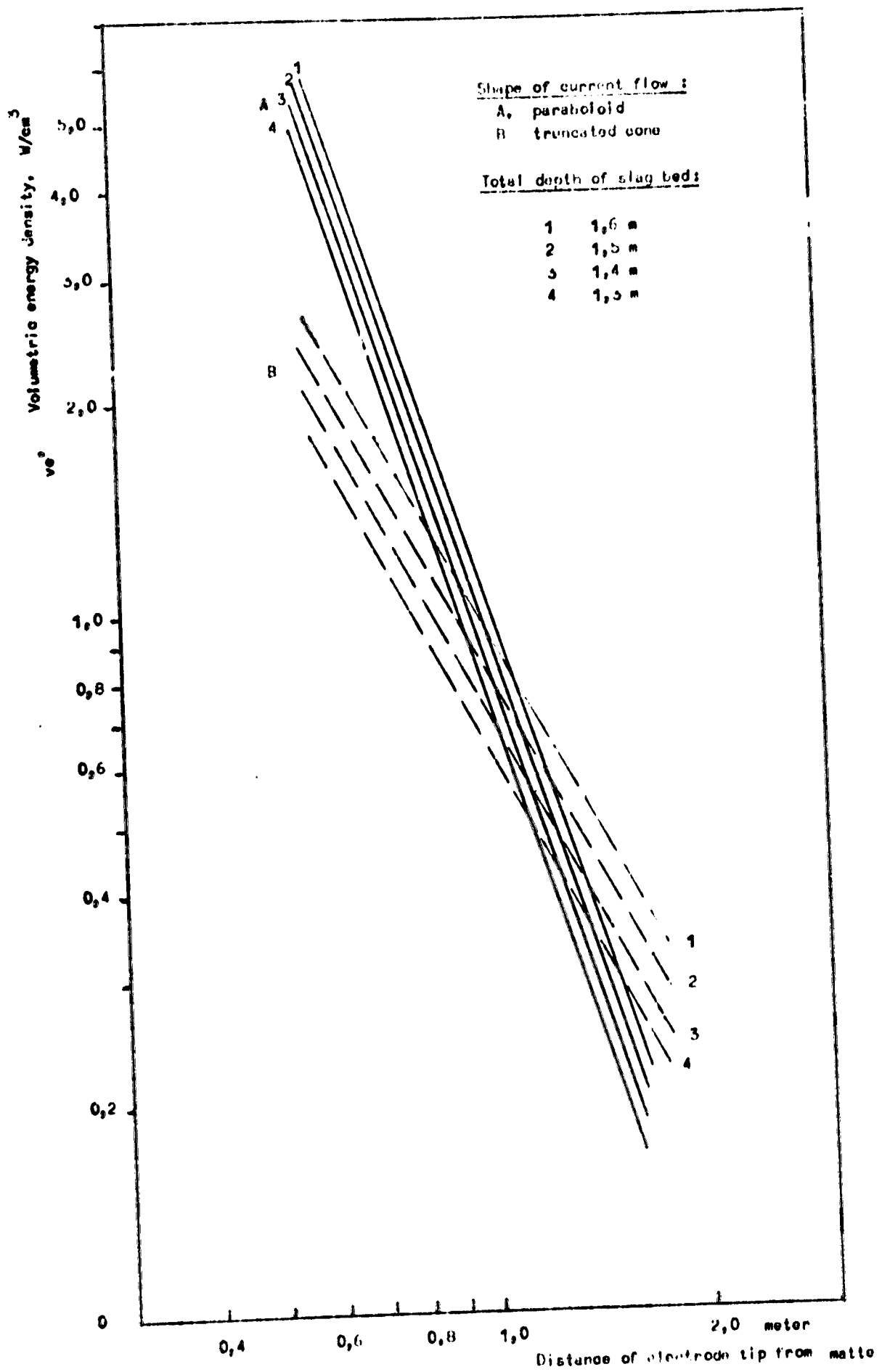

a./ decrease the output voltage of the transformer (E decreased) , then by symbolic representation the result will be

$$E\downarrow \rightarrow (I\uparrow R\downarrow);\ h\downarrow,\ p\uparrow.\ V\downarrow,\ q/v\uparrow.\ \delta_{ve}\uparrow.\ A\downarrow.$$

since $I^2R = Q = \text{const.}$

That is with the increase of the current R will have to decrease, the distance h betweenelectrode tip and matte surface decreases, the depth of electrode immersion p increases, the volume V of the geometrical body decreases, thus, since $I^2R = Q$(total heat input) is constant, the heat contained per unit volume (q/v), that is the volumetric energy density (δ_{ve}) will increase, while the area A projected unto the surface of the matte, i.e. the area of current flow will decrease.

b./ Increase the output voltage of the transformer (E increased) with increased tapchanger position, the reverse of the above-described case will result. That is

$$E\uparrow \rightarrow (I\downarrow R\uparrow);\quad h\uparrow.\ p\downarrow,\ V\uparrow.\ q/v\downarrow.\ \delta_{ev}\downarrow,\quad A\uparrow,$$

Consequently, if the slag resistivity varies, say increases then, in order to restore equilibrium, the current I will drop. Then this decreases E and the sequence of procedure a./ will set in.

The proposed models of current shapeare snown in figures III-11 and 12. From figure III-11 the height of the truncated cone in relationship to its base is given as

$$H - p = 1{,}25\ r_b - 0{,}78$$

(r_b= radius of base) and with this the volume is expressed

$$V_c = \pi \left(\frac{1{,}25\ r_b - 0{,}78}{3} \right) (r_b^2 + r_t r_b + r_t^2) \qquad 26./$$

where r_t = radius of top and r_b = radius of base of the cone.
The volume of the rectangular hyperboloid in terms of electrode diameter

$$V_h = \int_{D_e/2}^{h+D_e/2} \pi (H - p)^2 dh \qquad 27./$$

With the volume thus known the change of the volumetric energy density δ_{ve}, as a function of the distance between electrode tip and matte surface, h. is plotted for four different rates of power input, viz 14, 16, 18 and 20 MW in figure III-13, expressing δ_{ve} in watts/cm^3 slag volume. In this way the volumetric energy density as a function of the depth of electrode

immersion can be/...

immersion can be approximated by the following formulas :

truncated cone : $\delta_{ve} = 0{,}045\ P_w(H-p)^{-1,7}$ W/cm^3 28./

hyperboloid $\delta_{ve} = 0{,}050\ P_w(H-p)^{-3,0}$ W/cm^3 29./

The equation of the truncated cone was obtained by averging out the slight curvature of the log-log plots so as to obtain a stright line on this scale. In a true sense then equation 28. represents a hyperboloid with very slightly curved surface.

The difference between the energy densities obtained by the two models is very sizeable, but in both cases the indication is that the movement of the electrode is associated with very substantial variations in energy dissipation. A change of about 0,4 m in electrode position which may easily occur in working units, would bring about a more than twofold change in energy density per unit volume of slag within the geometric body and would point to the necessity of correct electrode positioning and as little as possible electrode movement in order to secure the best efficiency for the operation.

Interelectrode conduction.

Although the capacitance terms of the equation developed for furnace resistance make allowance for interaction between electrodes, they give no information as to the degree of interelectrode conduction. This has also been neglected in the formulas of Kjølseth, Nilsen and von Bergkampf.

Pertinent to electric smelting furnaces with 6-in-line electrode geometries Urquhart (9) carried out laboratory model tests using a salt solution to represent the slag layer and mercury to represent the highly conductive matte layer. The relative roles played by the electrode tips and sides were determined by insulating either the side or the tips. The cell constant was then estimated from the relationship $R = \rho_{sl} k$ (ρ_{sl} = specific resistivity of slag) with the dimensionless parameter kD_e for the purpose of scaling the furnace. The equation for cell constant was developed from the model proposed by Nilsen (4) for a paraboloid passing through the perimeter of the electrode tips and enables the estimation of cell constant for the size of the reference furnaces in question in the following form (9)

$$k = 0{,}00148 \ln \frac{(H-p) + 24{,}3}{24{,}3} \qquad 30./$$

Equation 30. when combined with the Attwood formula (Section II) gives cell

constant values/...

Figure III - 14. CURRENT FLOW LINES IN VERTICAL DIRECTION IN THE ELECTROLYTE OF LABORATORY-SCALE MODEL
(After Rabey, ref. 14)

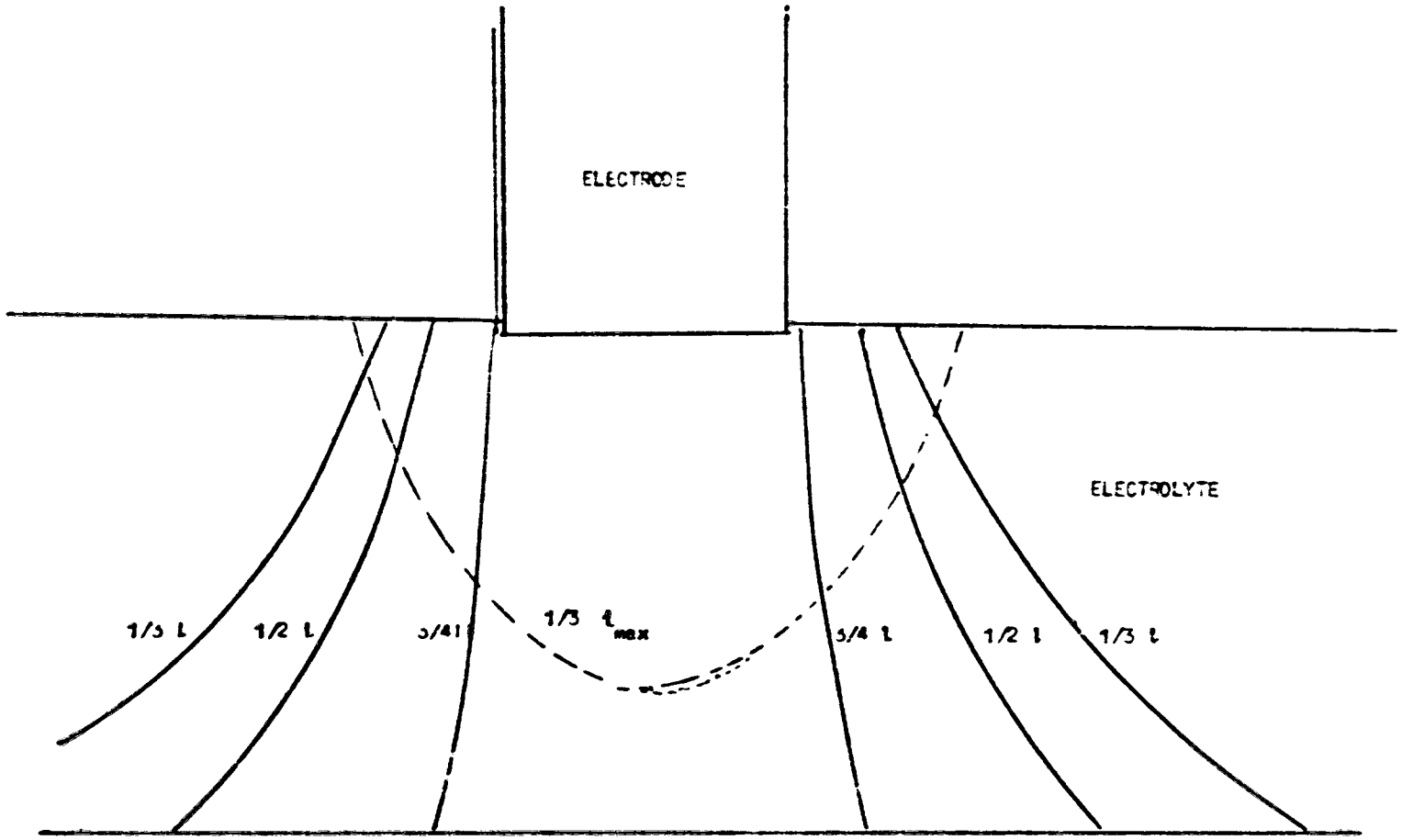

constant values similar to those obtained with expression III-17 of this study.

In the analysis of the results obtained by Urquhart on inter - electrode conduction, denoting the fraction of current between electrode and matte as $I_{e/m}$, electrode and electrode $I_{e/e}$ and the total operating current by I_{tot}, the equation of current partition of the experimental data as it was found by the writer of this study, can be expressed by the following approximating formulas

$$100\,\frac{I_{tot} - I_{e/m}}{I_{tot}} = I_{e/e}\,; \quad \text{here } I_{e/e} = \% \text{ of } I_{tot}$$

or

$$1 - I_{e/m} = I_{e/e} \qquad 31./$$

$$1 - I_{e/m} = 0{,}18(H-p)^{0{,}85} = 0{,}18\,h^{0{,}85} \qquad 32./$$

that is with increasing distance between electrode tip and matte surface the inter-electrode conduction increases. These equations give the relationship between depth of electrode immersion, total depth of molten slag bed and current flowing from electrode to electrode and from electrode to matte. From these data with the depth of electrode penetration encountered in practical operation with 3-electrodes-in-line furnaces, about 75-80 per cent of the current flows via electrode-matte-electrode and 20-25 per cent can be attributed to inter-electrode conduction. These results have been confirmed by the mentioned investigations of Kaboy (14) who further found that the power dissipation is concentrated in a small area around the electrode tips. Thus for example in a distance of about one electrode diameter from the tip the voltage drops to 1/3 of its original value and, due to further sharp drops the power dissipation is such that very little extends beyond this area. The current flow lines obtained are shown in figure III-14 in which the dotted line indicates the boundary where the field strength drops to 1/3 of its maximal value. The other lines have been drawn through points at which the magnitude of current has decreased to a certain fraction of the maximum value in the plane. The sharp voltage drop from the tip of the electrode was already observed by Kjølseth and the potential gradient along the distance between the electrode and hearth was also similar to that proposed by the same researcher.

The temperature and energy gradients developed in the geometric body in vertical and horizontal directions represent sizeable deviation from the idealised case of even energy distribution, for which the volumetric energy densities were estimated. The values given in figure III - 13

III-13 and by/...

Figure III - 15. TWO - DIMENSIONAL ANALOGUES OF BIFILAR ELECTRODE IN THE ESR PROCESS.

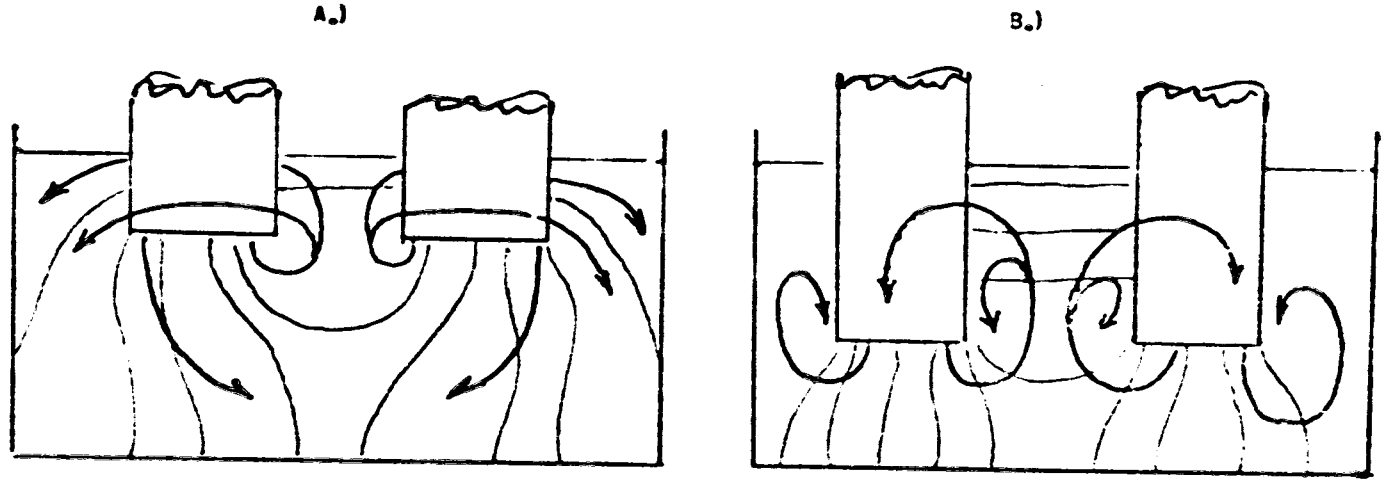

Figure III - 16. CONDUCTION BETWEEN ELECTRODES IN AN ELECTRIC FURNACE
A./ INFINITE BATH
B./ SHALLOW BATH

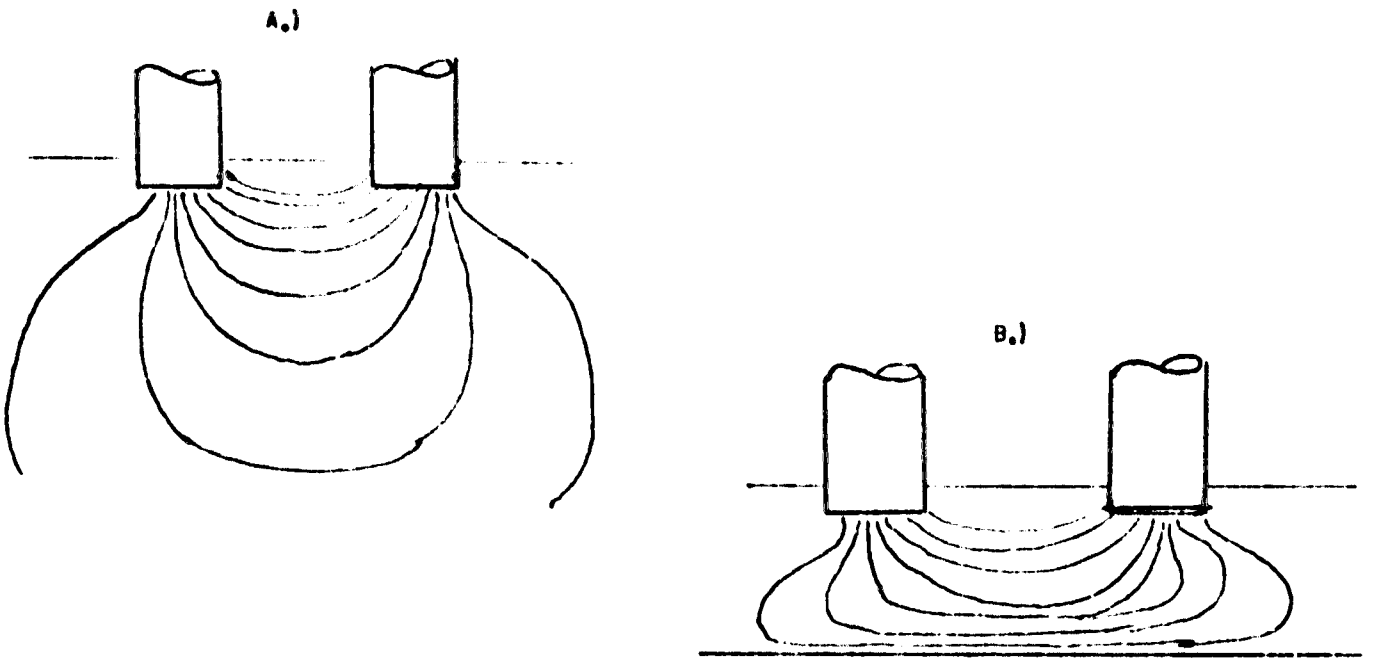

Figure III - 17. EFFECT OF BIFILAR ELECTRODE IMBALANCE (ESR PROCESS)

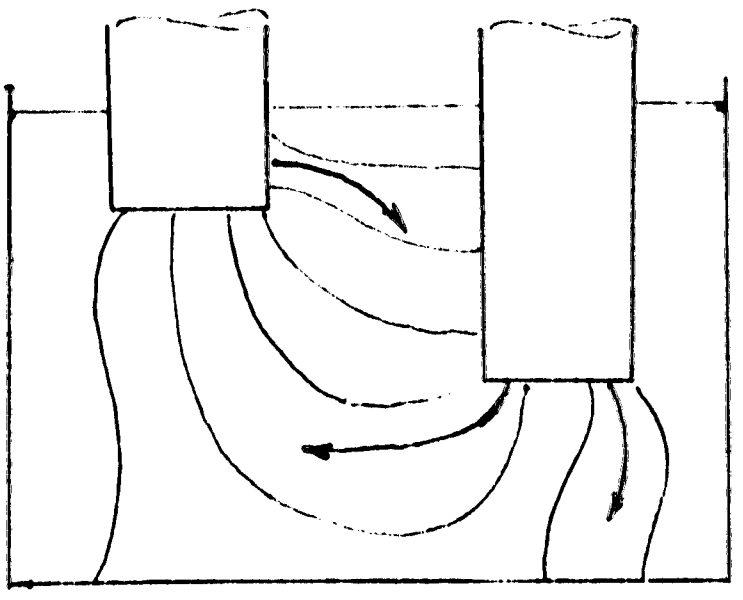

III-13 and by equations 25 and 26 are averages for a given volume of the geometric body in question.

The flow pattern becomes more complicated when the electrodes of a phase are in different position which is very often the case in practical furnace operation. For this condition Rabey showed that very little energy escaped through the side walls of the submerged electrode and the same amount of power was dissipated around each electrode irrespective of its submergion provided it was not too close to the matte.

It may be of interest to compare these findings with the results obtained in electro slag remelting (ESR) model tests which have been carried out extensively in recent years by various researchers. (15, 16, 17). The flow in the bifilar electrode process may be regarded as that most comparable with the matte smelting furnaces having two electrodes per phase of current. Figures III-15a and 15b based on the results of these model tests give an indication of what the flow pattern of slag might be at higher (a) and lower (b) electrode position. When the current is dissipated from one electrode to an other identical electrode each with identical immersion, the slag heating seems to be essentially in the upper part of the pool and generally in its central region. At higher electrode position the slag circulates past each electrode while with a shallower bath or deeper electrode penetration there is a much stronger tendency for descending slag column below each electrode. In the context of electric furnaces this aspect is illustrated in figure III-16. in which a./ represents conditions in an infinite bath as e.g. referred to in the formula of Downing and Urban (equ.9.) while b./ shows the pattern of conduction between electrodes in a shallow bath. - With two electrodes in different position, figure III-17, after Rawson et al. (16) demonstrates the effect of an inbalance of electrode immersion in the bifilar ESR process. Here the lower electrode produces a distorted, strong toroidal flow. A portion of the current passes directly between the electrodes in the upper part of the bath creating a slag flow toward the lower electrode. The pressure gradient between the electrode and the metal pool is steeper in the case of the lower electrode and the flow there, as a consequence, more vigorous.

Let us consider now the case when <u>differently sized furnaces working on the same raw materials form geometrically and electrically similar systems.</u> The ohmic voltage drop within the geometric body of current flow may be evaluated by integrating along the current path :

$$E = \int \varsigma \Lambda_{ii} \, dl \qquad 33./$$

where Λ_{ii}/...

where Δ_{il} is the current density at a distance l from the electrode tip. Likewise, the electrode current may be found by integrating over an equi - potential surface :

$$I = \int \Delta_{il} dA \qquad 34./$$

dA being here the surface increment to which Δ_{il} belongs. Then the ohmic resistance in the geometric body will be

$$R = \frac{\int \rho \Delta_{jl} dl}{\int \Delta_{il} dA} \qquad 35./$$

Since the numerator contains a linear parameter (distance) while the denominator involves the area which is quadratic so, obviously, the increase of the size of the system while the resistance is kept constant will imply that E increases with the first power and I with the second power. In this way R is inversely proportional to linear dimensions which is the basic criterion in Andreae's electrode periphery concept.

The practical importance of the problem will be apparent in scale-up considerations pertinent to furnace symmetries. When the systems to be compared are geometrically similar, i.e. corresponding points will have equal resistivities, the aspect of the shape of current path and, also, the variation of resistivity within the geometric body of this current path becomes a matter of secondary importance, even may be left out completely from further consideration.

3./ Practical features of the effect of the change of slag composition on electrode movement with particular reference to the operating furnaces.

With due regard to the implications outlined above pertaining to the flow pattern of current and the movement of slag associated with it, the difficulty of making generally valid predictions as regards their effect on furnace operation becomes obvious. On the other hand with some caution it may be possible to draw some practical conclusions in respect of certain features of the operation. Some considerations in connection with the reference furnaces which, however, are thought to be applicable also to other units of the same type are outlined below.

Graphs III-4 and 5 show the response of various parameters, such as current and power input rates as well as electrode movement upon the

change in slag/...

change in slag composition as evaluated from equ. 17. The relationships are based on synthetic slags but, as was referred to previously, in case of plant slags the effect is much less pronounced due in all probabilities mainly to the random variation in the percentage of the various slag-forming constituents as against the carefully controlled composition change of the synthetic slags. However, the basic principle governing the com - position effect should be the same in both cases, therefore the findings outlined are of general validity for these types of slags.

The two most influential slag components in the change of the electrical parameters of furnace operation were found to be the FeO and MgO. As will be apparent from figures III-4 and 5, their effect in the com - position range of the plant slags is by and large the same. Since, fortunately from the evaluation point of view, the percentage variation of these con - stituents is also similar, (11,5 to 16,5% $Fe_{tot.}$ as against 12,5 to 16,0% MgO), the following discussion will relate to the effect of both components.

The shaded area in the figures denotes the actual operating range with regard to current and power in the context of the composition variation of the plant slags. It is clear that in order to remain in the desired range of optimum 17,5 to 19 MW power input, the depth of electrode immersion will have to vary from $D_e/2$ (at 18,5 kA as a maximum) up to $D_e/5$ (at 17,5 kA as a maximum) when the average slag temperature is taken as 1400°C and the height of the slag layer 1,4 m. This would mean an electrode movement of 62,5 - 25 = 42,5 cm. Increasing now either the FeO or MgO content of the slag the shaded area will extend toward the right on account of the increased conductivity, i.e. decreased resistivity of the slag. To compensate for the loss of resistivity and in order to keep the range of power input unchanged, the automatic control rises the electrode, thus increasing R and lowering I.

If one decided to increase the transformer capacity with a view of increasing the power input and thereby the throughput rate in the furnace, according to graphs III-4 and 5 an upward shift in power input would in - variably cause the electrodes to "ride higher" at unchanged currents, i.e. between 17,5 and 18,5 kA. However, with the higher current from the trans- former, say 20 to 22 kA, the current plots associated with lower electrode positions would be shifted more and more to the right of the graph. Calculations indicated that in this case the electrode could be kept at its conventional $D_e/2,5$ to $D_e/3$ depth of immersion even if the MgO content increased to more than 19% and the FeO above 26%. Thus with slags of high

FeO and MgO contents/...

Figure III – 18. CHANGE IN ELECTRODE – TO – BATH RESISTANCE WITH THE MOVEMENT OF THE ELECTRODE.

1. Pellets falling into cavity
2. Pellets falling into cavity plus arcing
3. Clear slag pool

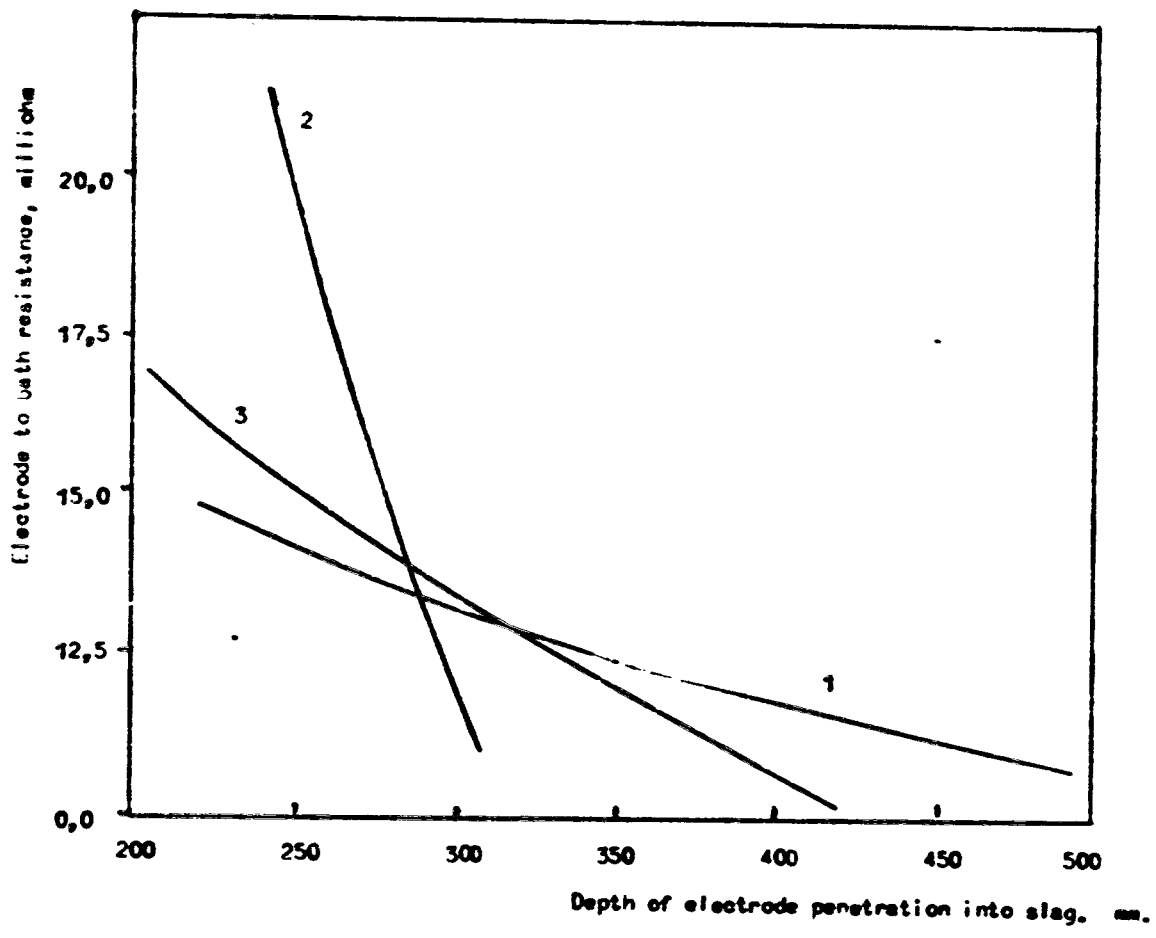

FeO and MgO contents provisions should be made for increased heating power, that is for increased transformer capacity. - If, on the other hand, the rate of power input were decided to be decreased to say 16 MW, the conditions would be such that even at an extreme value of 26% FeO in the slag the electrode would comfortably operate at a maximum of 18 kA current and electrode positions not higher than $D_e/3$.

As may be judged from the plots of figure III-13, the average rate of heat generation, depending on the assumed shape of current flow, would increase or decrease by about 27 to 40 per cent if the electrodes were lowered or raised by about 15 cm. On account of the regulating system taking care of any change in resistivity by virtue of the E/I = constant relationship, the part played by moderate electrode movement might be diminished and, as a result, a more even heating of the slag ensured. The extent of this "moderate" electrode movement can be judged again from graph 13. Say a $\pm$ 5 per cent change in heating power would indicate a change in electrode position between $D_e/2{,}4$ and $D_e/2{,}8$ that is about 8 cm. This is a rather small movement and points to the necessity of close control on electrode positioning. It must be emphasized again here that these suggestions are based on results of electrical conductivity measurements obtained in the laboratory on synthetic slags. In plant slag relations the influence of the change of slag composition i.e. the resulting change in electrode positioning on heating power will be considerably less pronounced.

Furthermore, all calculations of furnace resistance based on any of the suggested expressions will necessarily reflect ide nditions, since in an operating furnace the actual electr sistance will vary from time to time in a random pattern acco. ne flux of feed material to the electrodes. Measurements carried out on the resistance of one phase with the movement of one electrode of that phase in a working unit (18) resulted in findings summarised in figure 18. The effect of the con - dition of charge around the electrode (solid or semi-solid molten pellets, or fluid slag) is apparent from the graph indicating considerable variations in electrode movement with the change of the physical character of the feed material.

4./ Further notes on the effect/...

Figure III-19. VOLTAGE, ELECTRODE CURRENT, POWER FACTOR AND SLAG COMPOSITION RELATIONSHIP AT VARIOUS TRANSFORMER TAPS OF THE REFERENCE FURNACES.

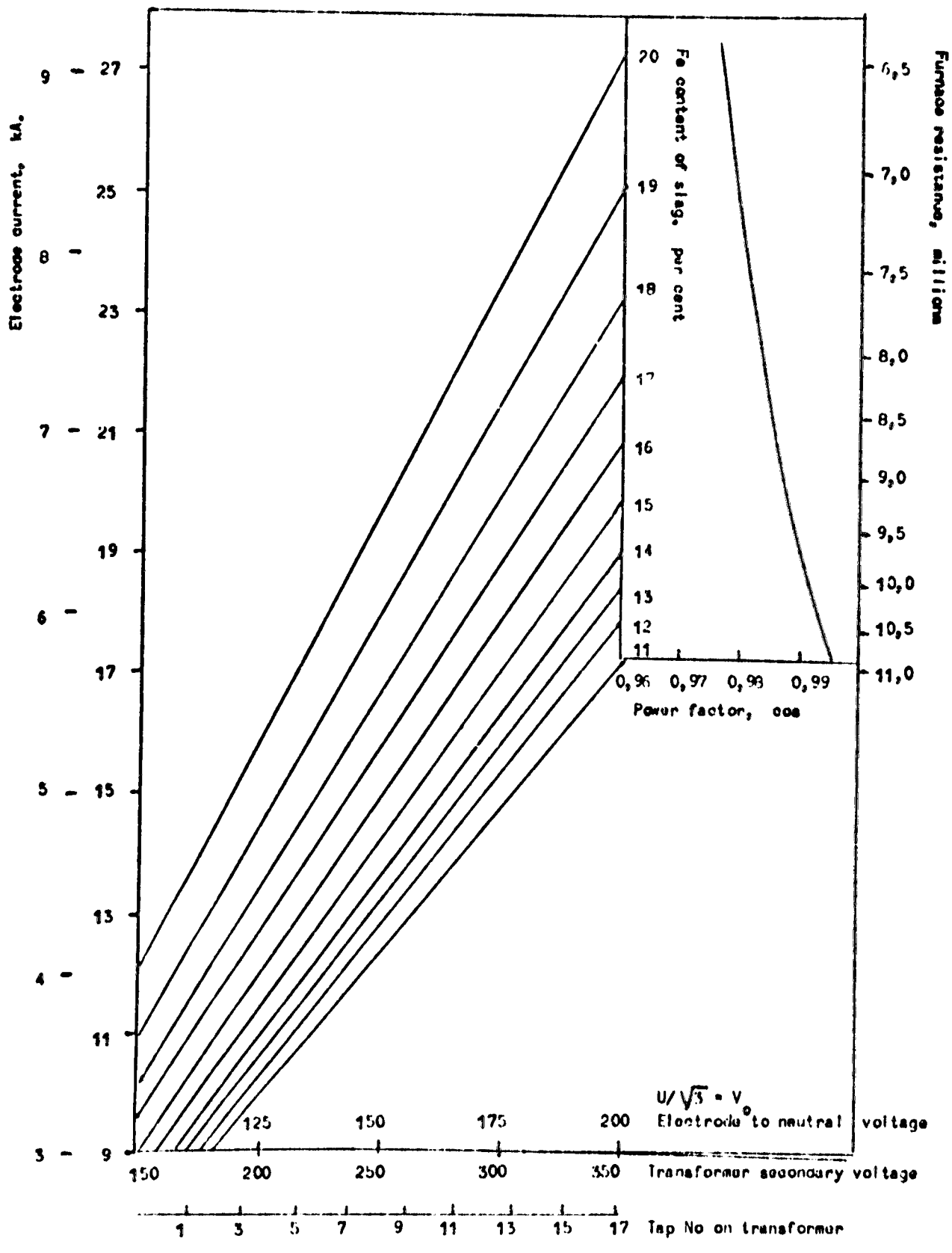

4./ Further notes on the effect of slag composition on furnace operating parameters with particular reference to submerged arc-slag resistance furnace relationship.

Figures III-4 and 5 assess the effect of slag composition upon power, current and electrode position relations. Further to some of the furnace operating characteristics the following general considerations may be of interest.

a./ Current and power.

The magnitude of electrode current in case of submerged electrode, slag resistance heated furnaces is given by Ohm's law. In ohmic resistance the voltage is in phase with the current, therefore $V = IR$, while in case of inductive resistance the current is 90^{o} behind the voltage, and $V_i = IL$ or IX_c, X_c being the circuit reactance. To this comes the resistance of the leads, transformer, etc. denoted as R_c. Now with the total resistance of the system the electrode current is given as

$$I_e = \frac{1}{\sqrt{3}} \frac{U}{\sqrt{(R_f + R_c)^2 + X_c^2}} \qquad 37./$$

For a phase of the six electrode furnace and with two electrodes per phase one can write

$$I_e = \frac{V_{ph}}{\sqrt{(R_f + R_c)^2 + X_c^2}} \qquad 37a./$$

here $V_{ph} = U/\sqrt{3}$

In determining the electrode current equ. 37a reletes to one single electrode position and slag bed depth. The importance of these factors in calculating furnace resistance has been discussed in the foregoings and various formulas for the evaluation of cell constant were suggested. Therefore the furnace resistance is calculated by using one of the outlined equations for the cell constant k, with $k = K(H - p)$, where constant K in the case of the reference furnaces is 2,25 giving thus R_f in milliohms. Then expression 37a becomes

$$I_e = \frac{V_{ph}}{\sqrt{\left[\rho\, 2(2{,}25(H - p)) + R_c\right]^2 + X_c^2}} \qquad 38./$$

With the use of equ.38 figure III-19 was constructed based on conditions prevailing in the reference furnaces with an average slag bed depth of 140 cm and depth of electrode immersion 48 to 50 cm ($= D_e/2{,}4$ to $D_e/2{,}6$). Slag Group V was taken as an example with the iron oxide content varying from 4,98 to 3,09 ohm.c,. This gives a variation of furnace resistance of 10,6 to 6,4/...

Figure III-20. RELATIONSHIP BETWEEN HEARTH VOLTAGE AND ELECTRODE CURRENT

Estimated by Workmanship formula

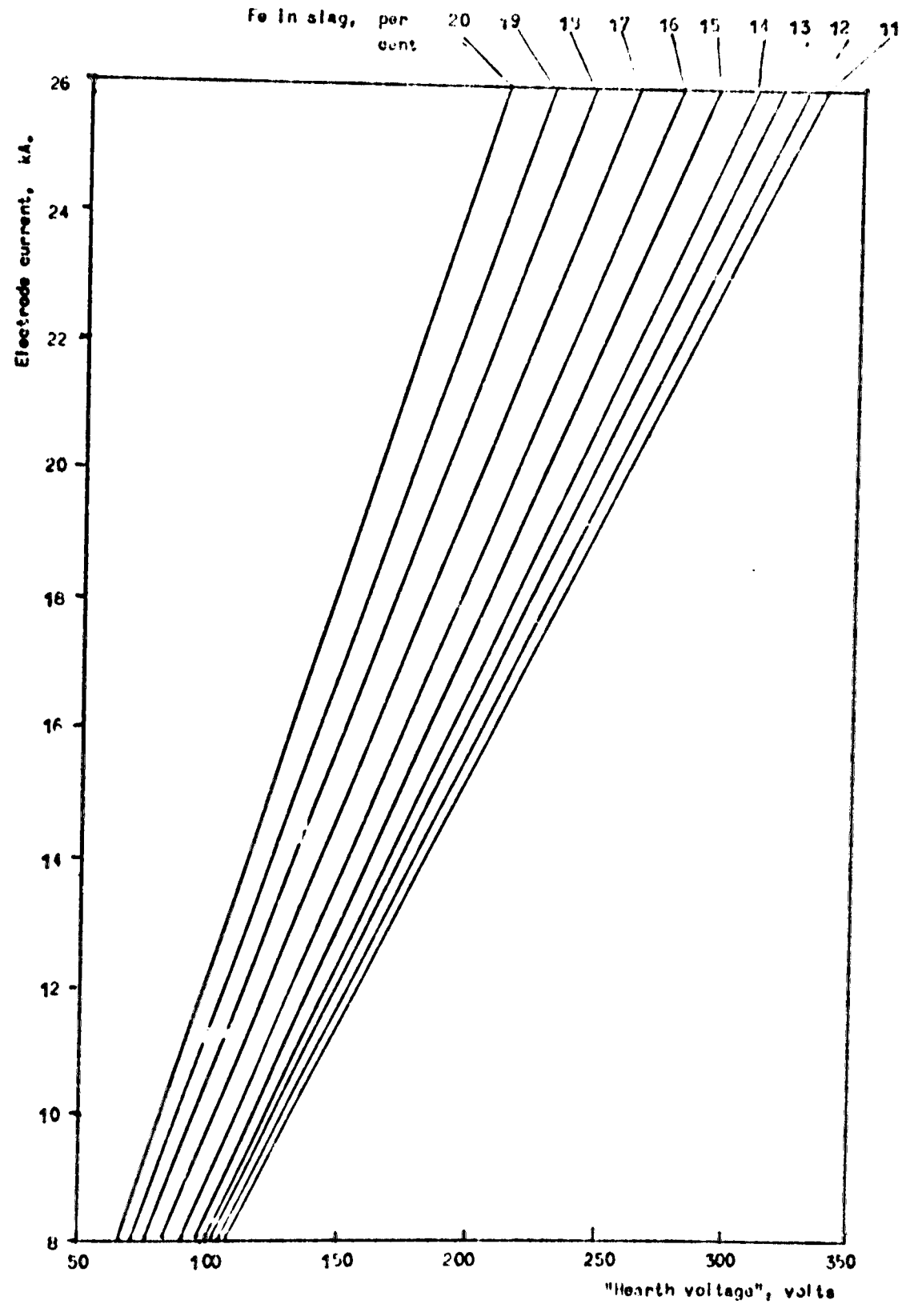

to 6,4 milliohm at an average slag temperature of 1400°C. The graph incorporates also the effect of slag composition upon the power factor when $\cos\varphi$ is calculated as

$$\cos\varphi = \frac{R_f + R_c}{\sqrt{(R_f + R_c)^2 + X_c^2}} \qquad 39./$$

As will be seen in the graph the change in slag composition has only a very limited effect on the power factor.

By the suggestion of Morkramer(13) the "hearth voltage" V_H (which is equivalent to the electrode-to-neutral voltage) can be calculated with the following formula

$$V_H = I\varsigma_H \frac{1}{\pi D_e} \qquad 40./$$

With the incorporation of the electrode diameter as a variable, equation 40 involves also furnace symmetry aspects. The current-voltage-slag composition relationship estimated with this equation is depicted in figure III-20. At lower slag resistivities the agreement between the values of figures III-19 and III-20 is excellent. As the resistivity increases, the "heart voltage" calculated by Morkramer's formula becomes somewhat higher and, correspondingly, the electrode current lower than indicated in figure III-19.

The circuit resistance R_c of the system is constant. As to the other memebers of the resistance group the inductive resistance X_c depends, apart from the short circuit reactance of the furnace, on the geometric outline and measure of the high current leads between furnace and transformer. The electrode position has only little effect on the value of X_c. The active, or furnace resistance R_f, on the other hand, changes greatly with the position of the electrodes at constant feed rate and composition of the burden. Figures III-4 and 5 give a good indication of the effect of electrode position on the variation of power input to the furnace at any specific slag composition, so this aspect needs no further discussion in this place.

For a comparison let us assume now that an arc furnace is operating with a slag the resistivity of which is similar to that produced in the reference slag resistance-heated furnaces. The transformer tapping gives a voltage range of 170 to 350 volt on the high current side. With the highest tap (=17) the voltage is 350V and the voltage-current relation will be thus represented by the second highest line in figure III-19. Then the power input P_w can be calculated by the following considerations:

$$P_w = 3 V_o I_e \cos\varphi$$

that is/...

Figure III-21. LOAD CURVES OF A SUBMERGED ARC FURNACE RELATING TO A PARTICULAR VOLTAGE (U = 350 V)

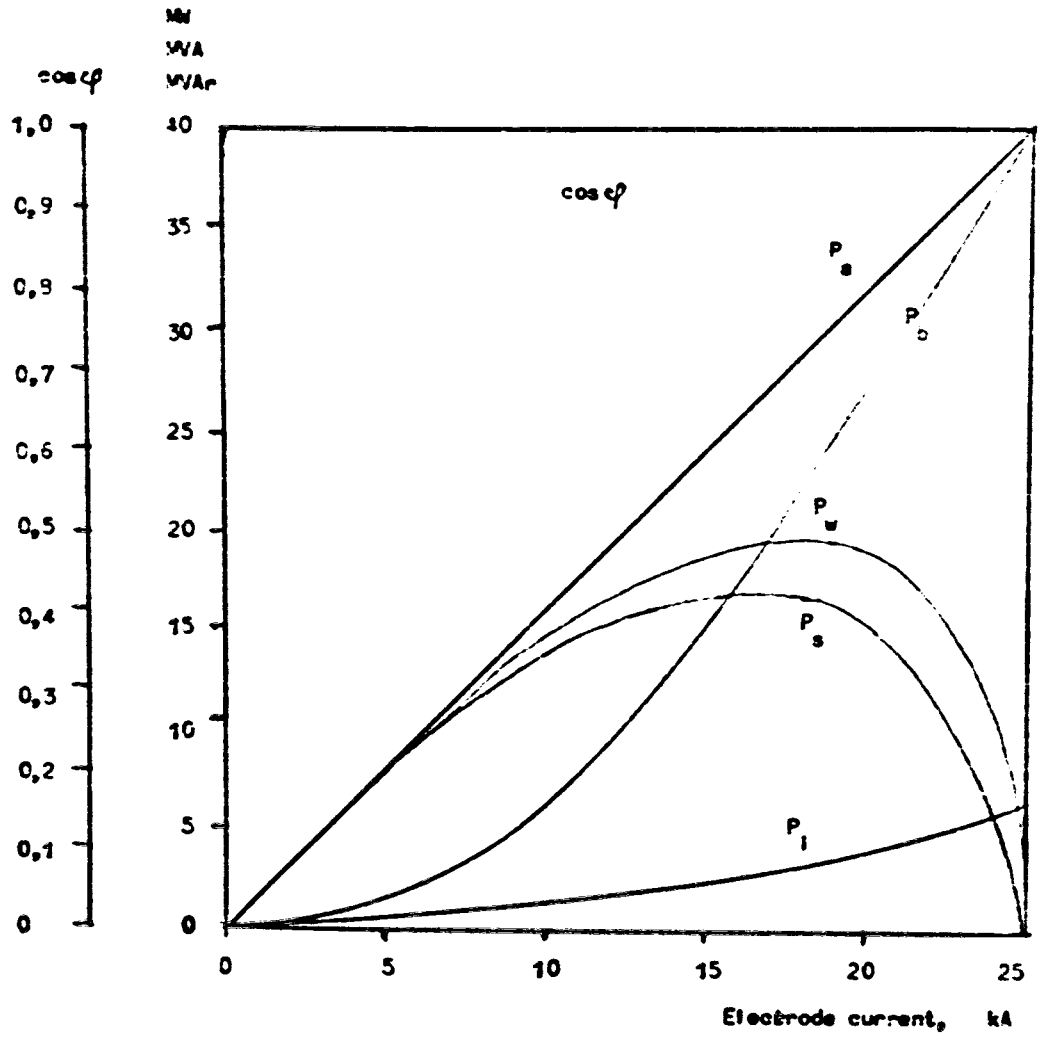

Figure III-22.

A./ ARC FURNACE LOAD CURVES AT VARIOUS FURNACE RESISTANCES

1. 10,5 milliohm
2. 9,95 "
3. 9,15 "
4. 8,17 ohm
5. 7,05 "

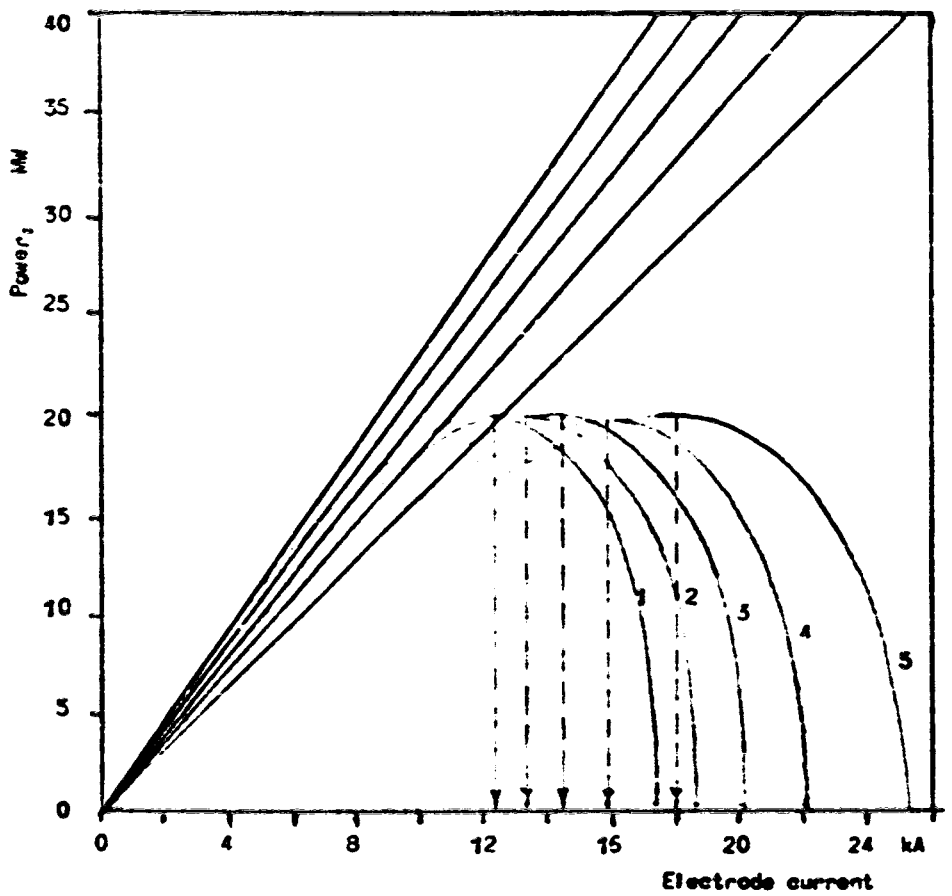

B./ CIRCLE DIAGRAM SHOWING FURNACE REACTANCE AND RESISTANCE (WATTLESS POWER AND EFFECTIVE POWER) RELATIONSHIP IN A SUBMERGED ARC FURNACE.

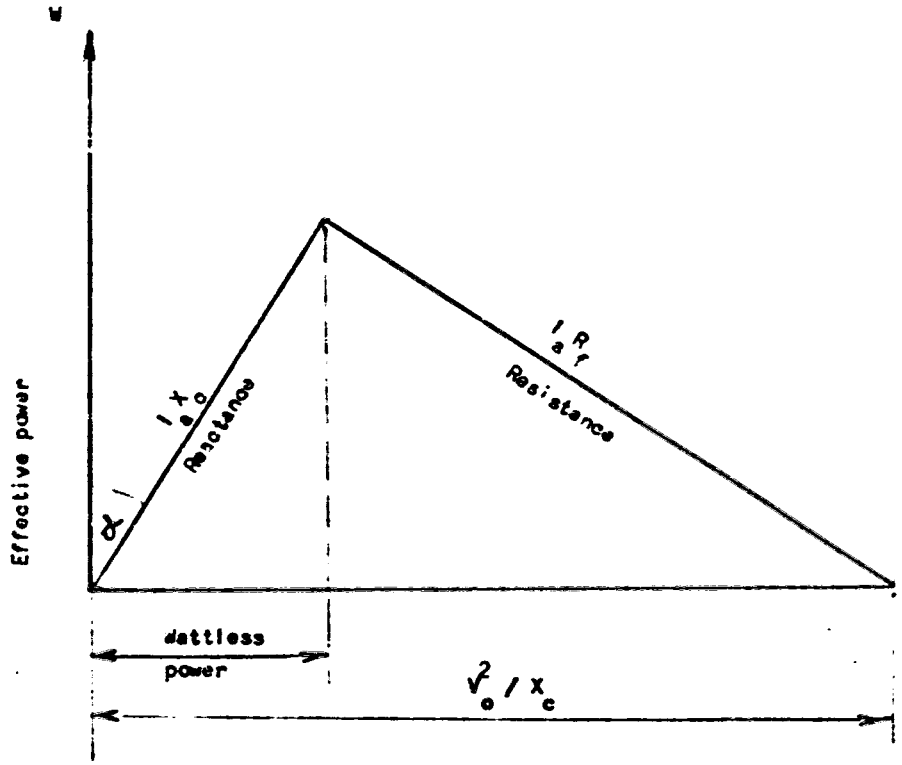

that is per phase $$P_{ph} = V_o I_e \cos\varphi \qquad 41./$$

Since $$V_o = I_e R_f + I_e X_c$$

and by figure III-22b $$I_e X_c = V_o \sin\varphi$$

therefore $$I_e = \frac{V_o \sin\varphi}{X_c} \qquad 42./$$

Putting 42 into 41 gives then the applied reactive power as

$$P_w = \frac{V_o^2}{X_c} \sin\varphi \cos\varphi \qquad 43./$$

The wattless power $$P_b = \frac{V_o^2}{X_c} \sin^2\varphi \qquad 44./$$

and the total apparent power (circuit input power or Mw)

$$P_a = \frac{V_o^2}{X_c} \sin\varphi \qquad 45./$$

while the loss of power $$P_l = 3 I^2 R_c \qquad 46./$$

from which the effective melting power is given as

$$P_e = P_w - P_l$$
$$= 3 I^2 R_f = \left(\frac{V_o^2}{X_c} \sin\varphi \cos\varphi\right) - 3 I^2 R_c \qquad 47./$$

Using the quoted data and the above equation figure III-21 is obtained giving a graphical display of the conditions for the particular arc furnace, the maximum power coinciding with $\cos\varphi = 45^\circ$, that is $\varphi = 0{,}707$ or $1/\sqrt{2}$. In this way the optimum operating range is restricted to $\cos\varphi = 40^\circ$ to 50° or, as regards maximum effective smelting power, to 45° to 55°. A decrease to 30° or increase beyond 60° of the phase angle brings about an abrupt de - terioration in smelting efficiency.

The change in furnace resistance from 7,05 to 10,6 milliohms (corresponding to a variation in the iron content of the slag from 19 to 11 %) would result in the shift of the optimum operating current as oulined in graph III-22, for five different slag resistivities.

As against these operating characteristics of a submerged arc furnace, the slag resistance-heated submerged electrode furnaces exhibit a vastly different behaviour. The main difference in the operation of the two furnace

types is reflected/...

Figure III-23. CIRCLE DIAGRAM OF ARC FURNACE.

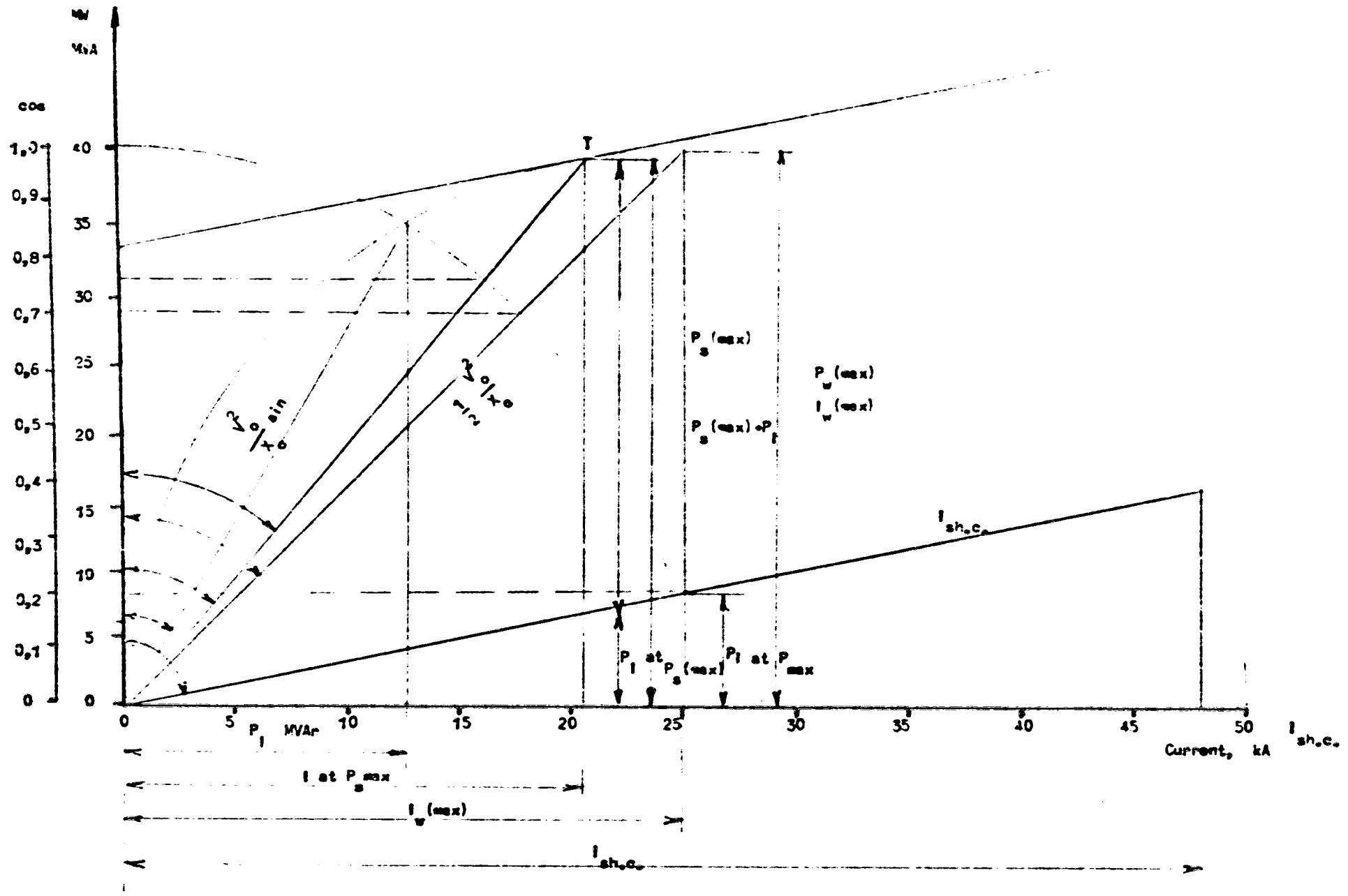

types is reflected primarily in the considerable inequality between the ohmic and inductive resistance of a charge resistance furnace as compared to that obtaining in a submerged arc furnace. Owing to this fact the familiar load curves related to the latter furnace type cannot be constructed within the range of operating current characteristic to slag resistance-heated units. This becomes immediately obvious from the very slight response of the power factor to changes in slag composition, i.e. resistivity. Consequently, these furnaces operate without any particular effort (in case of appropriate slag composition) way on the left of the power (or voltage) circle diagram shown in figure III-24b with high resistance and low reactance voltages.

For a comparison figure III-23 represents the full circle diagram of the imaginary arc furnace (the load curves of which were drawn in figure III-21) based on the following data: transformer secondary voltage 350V, slag resistivity 3,4 ohm.cm, furnace resistance 7,05 mohm, maximum electrode current at 350V = 25,5 kA, furnace reactance 1 mohm. With these characteristic values of R_f and X_c the arc furnace is imaginary in contrast to the true arc furnace for which R_f and X_c in balanced and efficient operation are equal or by and large of the same magnitude. The gravity of this assumed condition, by which the operation of the arc furnace would be thrown into a great degree of inbalance is fully appreciated even if it is set for comparison purposes only.

The various parameters indicated by the arrows in figure III-23 are expressed as (19)

$$P_w(max) = \frac{1}{\sqrt{2}} \frac{V_o^2}{X_c} \qquad 48./$$

$$I(max) = \frac{1}{\sqrt{2}} \frac{V_o}{X_c} \qquad 49./$$

$$P_s(max) = \frac{1}{2} \frac{V_o^2}{\sqrt{R_f^2 + R_c^2} + R_c} \qquad 50./$$

The current used at the maximum smelting power

$$I_s \text{ (at } P_s(max)) = \frac{V_o}{X_c} \sqrt{\frac{1}{2}} \left(1 - \frac{R_c}{\sqrt{X_c^2 + R_c^2}}\right) \qquad 51./$$

The tangent parallel to the short circuit current ($I_{sh.c}$) vector contacts the half circle at point A by which the apparent current I_a at $P_s(max)$ is defined, that is the current coupled with the maximum smelting power. The short circuit current is expressed with the circuit voltage U and

reactance as/...

Figure III-24. RELATIONSHIP BETWEEN CURRENT AND POWER IN A SLAG RESISTANCE-HEATED FURNACE AT THREE DIFFERENT VOLTAGES OF THE TRANSFORMER SECONDARY.

Dotted lines refer to V_φ = 200 V and the projections on the current and power axis denote respectively maximum current and power obtainable at this particular voltage at 1,0, 1,5 and 2,0 milliohm reactance values.

Small dotted square represents the actual operating range of the reference furnaces under study.

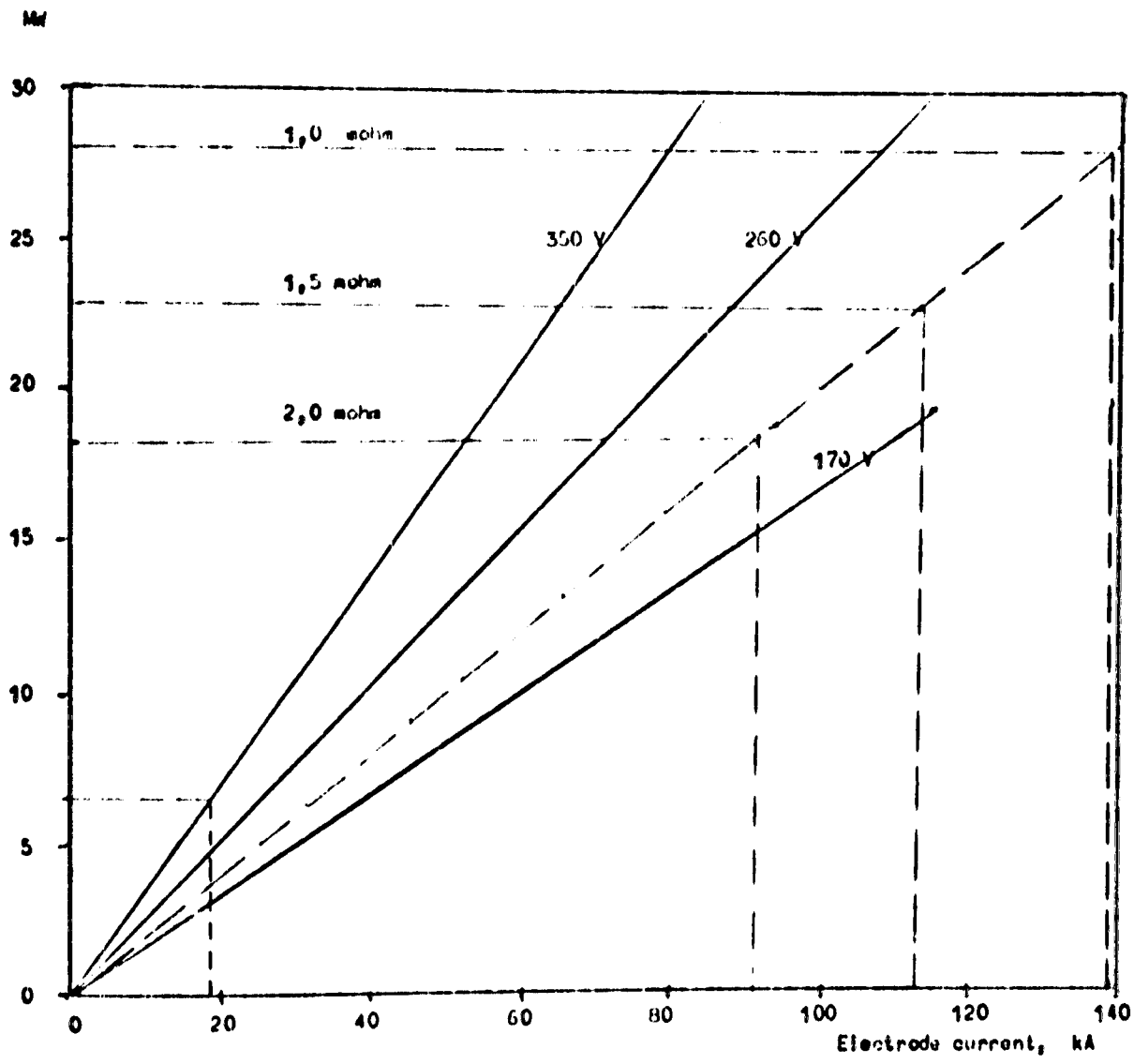

Figure III-25. OPERATING DATA FROM A SLAG RESISTANCE-HEATED FURNACE

A./ OPERATING CURRENT, VOLTAGE, REACTIVE POWER AND TOTAL POWER RELATIONSHIP IN THE REFERENCE FURNACE.

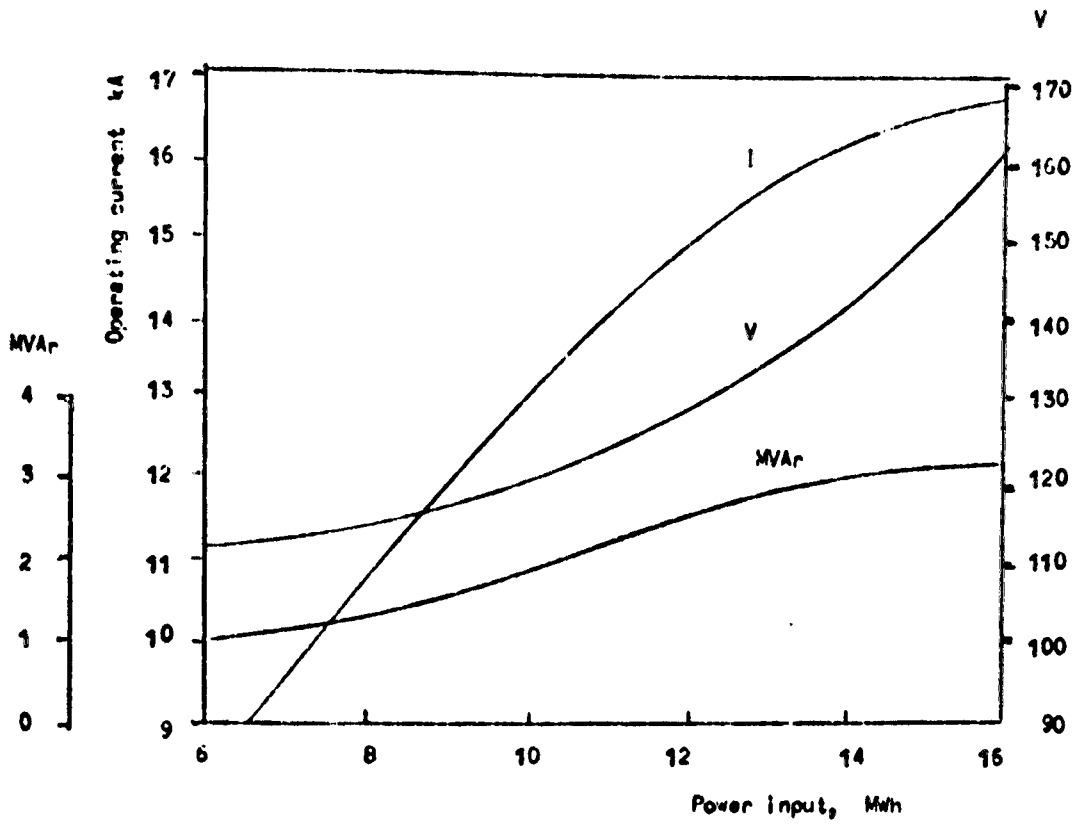

B./ RANGE OF VARIATION IN SMELTING POWER WITH THE CHANGE OF TOTAL POWER

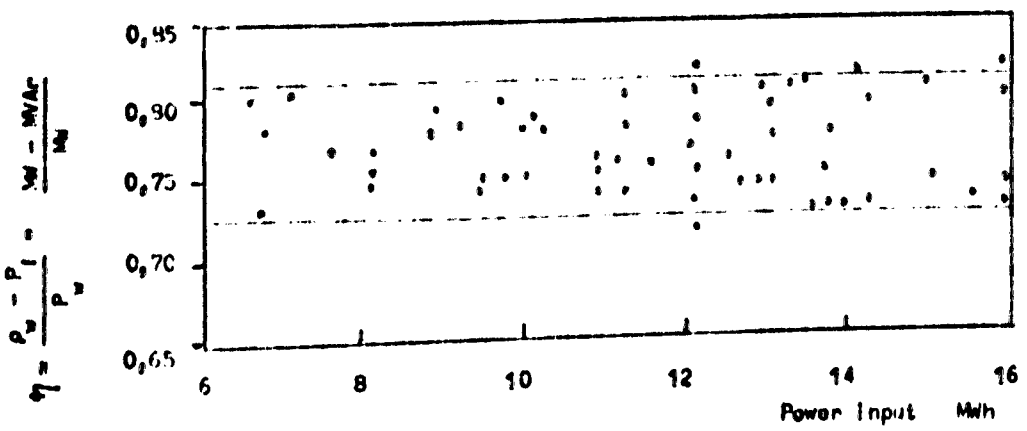

reactance as $$I_{sh.c.i} = \frac{U}{X_c} \qquad 52./$$

and the electrode current as before

$$I_e = \frac{V_o}{\sqrt{R_c^2 + X_c^2}}$$

Actually by equ. III-52 the "ideal" short circuit current is given which is equal to the diameter of the current half circle. The actual short circuit current $I_{sh.c.}$ is smaller than $I_{sh.c.i.}$ since the furnace cannot be ideally short-circuited due to the circuit resistance R_c, i.e. the resistance of leads which is always present in the system.

Figure III-24 shows the current-voltage-power relationship calculated with the aid of equations 37 and 37a for furnace resistances varying from 10 to 1 mohm. The operating range of the reference furnaces is indicated by the dotted square corresponding to a maximum 6,5 MW power per phase and an optimum operating current of 18 to 18,5 kA at a furnace res - istance of about 9,8 to 10,3 mohm. Apparently there is no curving-down of the plot which continues as a straight line far beyond the boundary of the operating range. The phase angle is in the range of 10 to 25 degrees giving $\cos\varphi$ values in excess of 0,9. Consequently, the conditions characteristic to arc furnaces by which the maximum power input occurs when $X_c = R_f + R_c$, leading to maximum operating current at

$$I_{max} = \frac{1}{\sqrt{2}} \frac{V_o}{X_c}$$

with equ.39 becoming $$\cos\varphi = \frac{1}{\sqrt{2}} = 0{,}707$$

will also alter in case of slag resistance furnaces due to the mentioned great difference in the active and inductive resistances. The high ohmic resistance coupled with the low reactances permit the units to be run with phase angle values considerably below those termed as optimum for arc furnaces. In this instance it is desirable to operate at the possible highest voltage the transformer secondary can yield. This is self-explanatory from figure III-24 showing power-current plots of the reference furnaces for tap numbers 1, 9, and 17 corresponding respectively to 170, 260 and 350 volts.

As for a practical example to these points figure III-25 based on actual plant operating data indicates the reactive power (MVAr), operating current, voltage and power input relations. The figure is based on data loggings carried out during "running-in" a newly built furnace close to the end of the start-up period. As will be obvious from the graph, the reactive

power increased by/...

power increased by some factorial expression upon the increase of the load up to about 13 MW. From then on the increase of the MVAr became insignificant. At lower power input (6 to 9 MW) higher voltages and lower currents were used, then between 9 and 14 MW the current was considerably raised. Finally above 14 MW power the current decreased while the voltage increased further. A characteristic feature of the operation of this period was a relatively constant relationship between the total applied power and the useful smelting power, restricted to a band indicated in figure III-25B. The efficiency here is expressed as

$$\eta_e = \frac{MW - MVAr}{MW} \qquad 53./$$

b./ Comparison between submerged arc and slag-resistance heated furnaces.

Finally, in rounding up this section, in connection with the above consideretions it may be of interest to attempt a brief, general comparison between submerged arc and slag resistance heated furnaces; in American terminology often called "special arc" and "charge resistance" units. In a broad outline they are similar in that a./ the process voltages are low, in the order of few hundred volts only, b./ current is high, tens of thousands of amperes, c./ voltage has to be adjusted with the variation of process conditions.

The electrical resistance of most charge materials is relatively constant, that is it does not change rapidly with time. The basic difference is caused by the fact that the electrical resistance of an arc can be termed as unstable, its value fluctuates rapidly during much of the process cycle causing thereby fluctuations in both MW and MVA. These fluctuations, especially that of MVA, can have an adverse effect on the power system and may require expensive corrective measures. The arc characteristics may introduce harmonic voltages or currents, sometimes both, into the power supply system. (20). Owing to the rapid variations in resistivity, faster response from the electrode positioning system is desirable. Also, arc furnace processes tend to be batch type rather than continuous.

The role of reactance in the two cases is particularly interesting. Charge resistance, as mentioned already, tends to be relatively stable varying only slowly with time as the temperature, or eventually the composition of the charge material varies. Arc resistance, on the other hand, can undergo substantial changes in a fraction of a second. Pertaining to stable and unstable resistances, figure III-26 may serve as an illustration based on

the various topics/...

Figure III-26. THE EFFECT OF REACTANCE ON THE VOLTAGE-CURRENT RELATIONSHIP IN ARC FURNACES AND SLAG RESISTANCE-HEATED FURNACES.

A./ Arc furnace

1. Combined impedance
2. Arc impedance (resistance)
3. Circuit impedance (reactance)

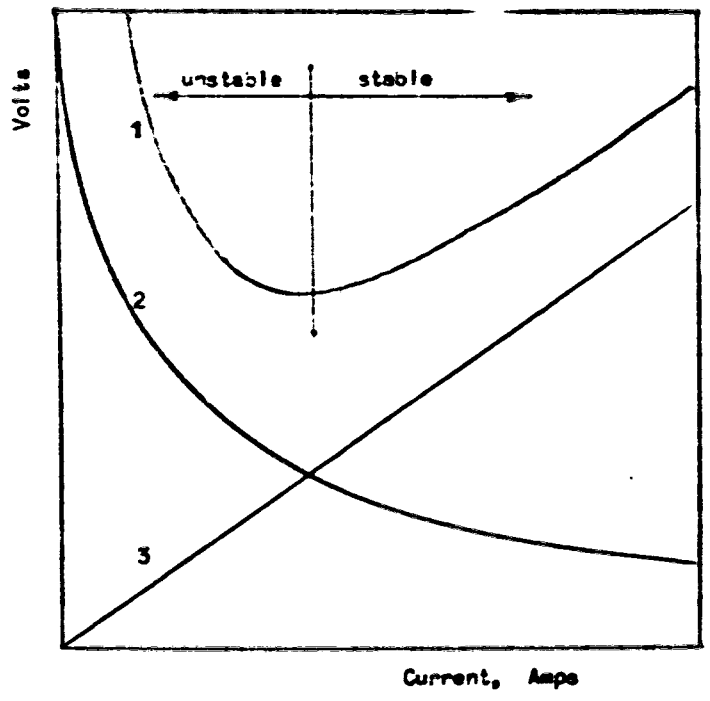

B./ Slag resistance-heated furnace

1. Combined impedance
2. Charge (slag) resistance (impedance)
3. Circuit impedance (reactance)

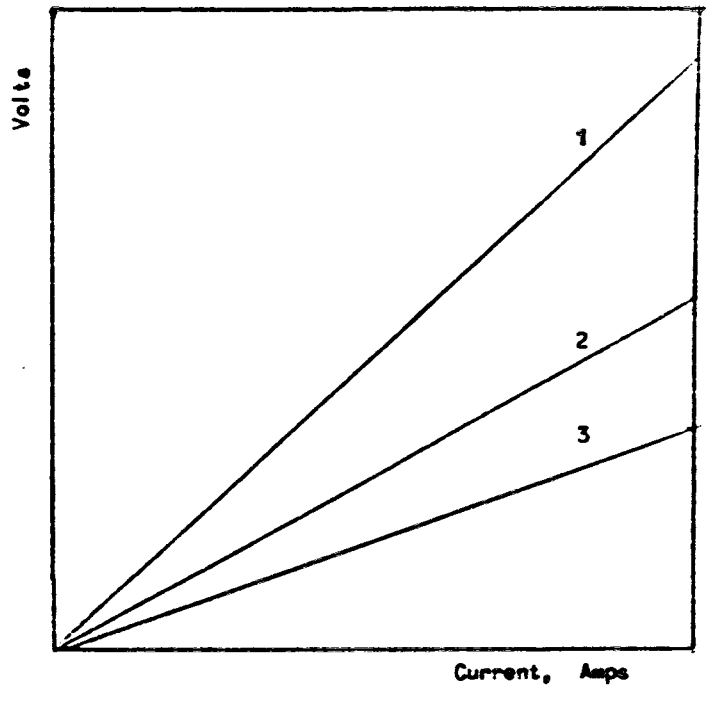

Figure III-2: RELATIONSHIP BETWEEN CIRCUIT REACTANCE, POWER, CURRENT AND VOLTAGE IN AN ARC FURNACE.

1. 350 V, X_c = 1,0 mohm
2. 494 V, X_c = 2,0 "
3. 350 V, X_c = 2,0 "

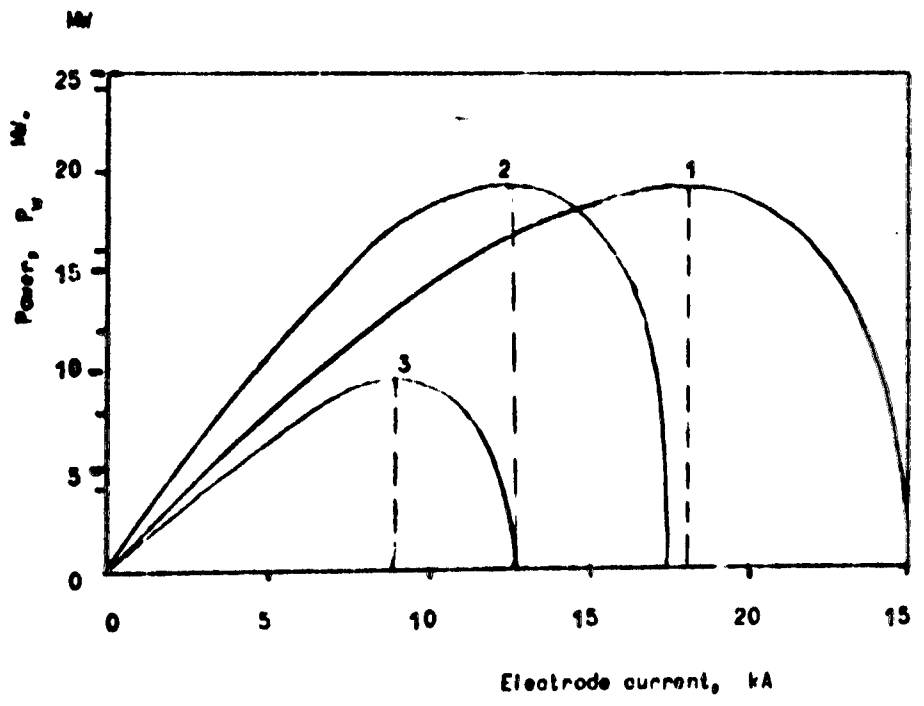

the various topics discussed previously in this section, showing the character of resistance or impedance in voltage-current relationship as regards arc furnace and slag resistance (or charge resistance furnaces. The combined impedance shown in the graph is made up as arc impedance (resistance) + circuit impedance (reactance) respectively for the two types of furnaces. In case of arc furnaces the arc resistance (impedance) is unstable and, as a result, its combination with the circuit impedance will also be unstable below a certain operating current value. Above this critical current the circuit impedance will exert a stabilising effect so that the combined impedance will also become stable. In this way the arc furnace circuit reactance can be regarded, within certain limits, as a useful electrical parameter.

With slag resistance heated furnaces the case is different in that the charge or slag impedance, replacing the arc impedance in a virtually arc-free system is also stable and helps to fulfill the general requirement for a convenient current control by which the volt-amper characteristics must slope upwards to the right in the chosen coordinate system. Since this requirement is "a priori" satisfied, the circuit reactance does not serve any useful purpose and therefore, will have to be minimised for example by the most appropriate arrangement of conductors between the transformer and the electrode.

However, even with arc furnaces when the reactance becomes excessive, it tends to affect adversely the control of current. Let us take again the example given in figure III-21 showing load curves that would result in an arc furnace having slags of similar resistivities as those produced in the reference furnaces. On doubling the circuit reactance, the maximum possible power for the circuit will be halved, as shown in figure III-27. Obviously, the voltage applied to the circuit can be increased which will restore the power at the peak of the power curve to the same value as that of the original curve. But this will also increase the arc voltage in straight proportion to the rise effected to the circuit voltage leading to changes in arc characteristics thereby affecting smelting and, also, general heat distribution conditions which may lead to excessive refractory wear. - The reactance requirement depends also on the size of the furnace and with larger units it may become excessive and will have to be reduced as much as possible.

For a given reactance, referred to the secondary side of the transformer, when keeping a pre-determined active power (P_w) and apparent power

(P_a), the secondary/...

Figure III-29. RELATIONSHIP BETWEEN POWER, VOLTAGE, REACTANCE AND CURRENT IN AN ARC FURNACE.

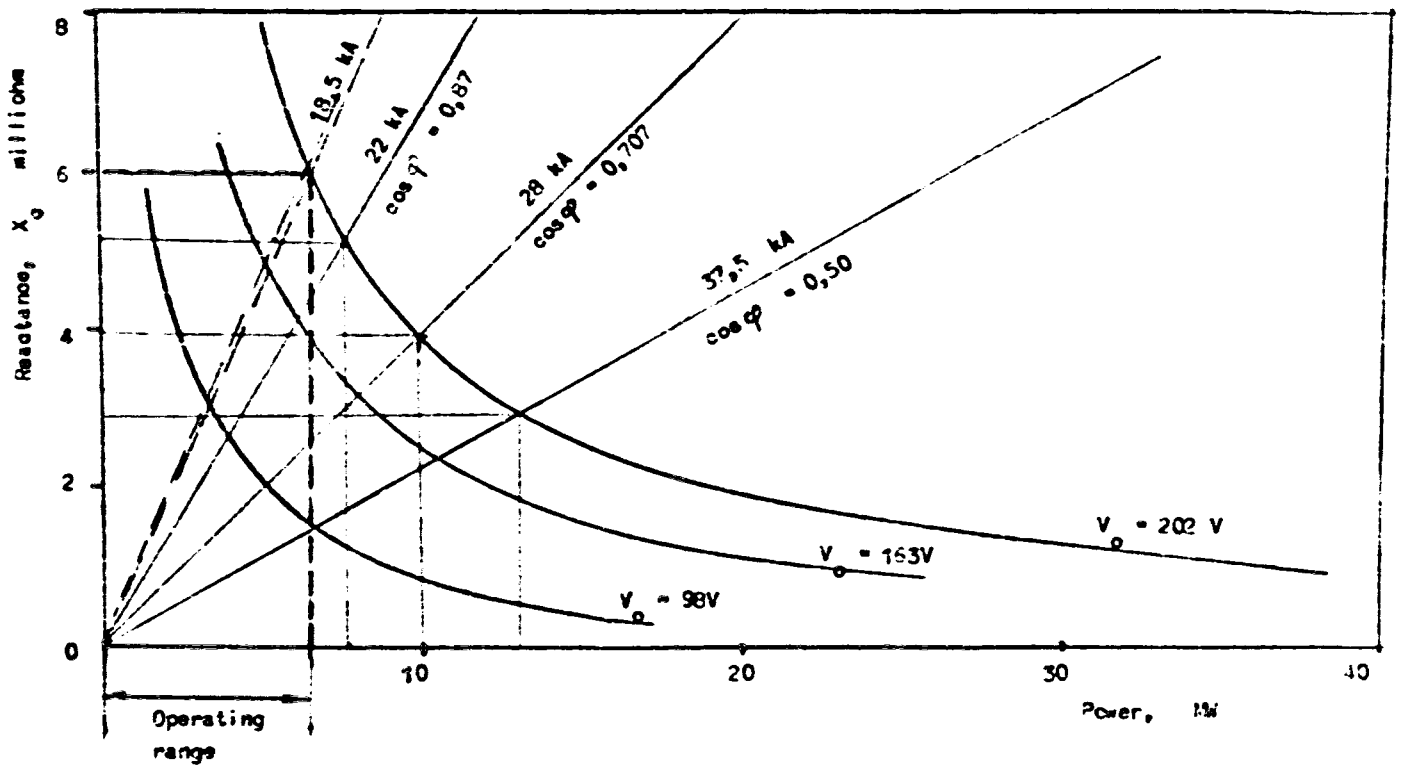

(P_a), the secondary current and voltage can be defined by the equations (21)

$$U = \sqrt{\frac{2 P_w X_c}{\sin 2\varphi}} = \sqrt{\frac{P_a X_c}{\sin \varphi}} \qquad 54./$$

and

$$I = \sqrt{\frac{P_w \tan \varphi}{3 X_c}} = \sqrt{\frac{P_a \sin \varphi}{3 X_c}} \qquad 55./$$

Thereby any point on the previously discussed graphs in terms of U and I is characterised as

$$U, I = f(P_w, X_c, \varphi) = f(P_a, X_c, \varphi) \qquad 56./$$

By virtue of equ. 54 (straight relationship of U and X_c) maximum reactance is coupled with maximum secondary voltage and by equ. 55 the smallest reactance determines the maximum secondary current. From equations 54 and 55 a change in X_c to X'_c at constant active or apparent power and with unaltered impedance angle φ will bring about the following conditions:

$$\frac{U'}{U} = \sqrt{\frac{X'_c}{X_c}} \quad \text{and} \quad \frac{I'}{I} = \sqrt{\frac{X_c}{X'_c}} \qquad 57./$$

Further to the power, voltage, reactance and current relationships in arc furnaces the reactance from equ. 54 is obtained as

$$X_c = \frac{V_o^2 \sin 2\varphi}{2 P} \qquad 58./$$

and from equ. 55.

$$X_c = \frac{P \tan \varphi}{3 I^2} \qquad 59./$$

For an illustrative example of arc furnace operation let the conditions be similar again to those of the reference slag resistance heated furnaces, i.e. maximum voltage on the transformer secondary V = 350, current I = 18 kA, then $P = U.I.\sqrt{3} = (350 \times 18 \times 10^4)\sqrt{3} = 10{,}9$ MW. $3 I^2 = 3 \times (3{,}24 \times 10^8) = 9{,}72 \times 10^8$ from which $X_c = 11{,}2$ mohm. Now using equ. 59 with $\tan \varphi = 0$ to 45° the value of X_c will be given. With transformer taps of 3, 9, and 17, V_o will be respectively 202 V, 163 V and 98 V, and from $P_w = V_o^2/X_c$ the power can be calculated. Figure III-28 shows the relationship between the various electrical parameters for three different voltages. The graph clearly indicates the trends represented by equ. 57, that is maximum reactance is associated with maximum secondary voltage and with the decrease of the reactance the secondary current increases considerably.

More detailed discussion on the reactance problem concerning arc furnaces like the mode and the extent of corrective measures necessary to reduce the reactance e.g. with the application of reactors would be out of the scope of this study.

References:

1./ Andreae F.V.: Design and control of ferroalloy furnaces. Trans AIEE, vol. 59, 1950, 557-562

2./ E Schwarz von Bergkampf : Modellbetrachtung des Lichtbogenofens. in "Metallurgie der Ferrolegierungen". Ed: Volkert G - Frank D. II Aufl. Springer,Berlin, 1972

3./ Kjølseth O.: Electrochemical conditions of the Thysland-Hole furnace. Kjemi Bergv. Metallurgi, 21, No-2, 1961, 27 - 33.

4./ Nilsen P.H.: Determination of the electrical resistance in idealised resistance furnaces from model experiments. Ibid. 24, 11, 1964, 203-208.

5./ Downing J.H.- Urban L.: Electrical conditions in submerged arc furnaces. J. Metals, 1966, 337-344.

6./ Persson J.A.: The significance of electrode-to-hearth voltage in electric smelting furnaces. Electric Furnace Proc, 28, 1970, 168-9.

7./ Mostert J.C. - Roberts P.N : Electric smelting at Rustenburg Platinum Mines Ltd. of nickel-copper concentrates containing platinum group metals. J. South Afr. Inst. Min. Met. Apr, 1973, 290 - 299

8./ Barth O.: Electric smelting of copper ores. in "Extractive Metallurgy of Copper and Nickel". Ed: Queneau P. Interscience, New York, 1961. p 241 ff.

9./ Urquhart R.C. - Rennie M.S.: The smelting of copper-nickel concentrates in an electric furnace. NIM Technical Memorandum, Aug. 1973, Johannesburg.

10./ Persson J.A.- Treilhard D.G.: Electrothermic smelting of copper and nickel sulphides and other metal-bearing constituents. J. Metals, Jan. 1973, 34 - 39.

11./ Sibakin Ya.F.: Raspredeleniye toka v odnofaznii ferrosplavnikh petshakh. Teoriya i Praktika Matallurgii., No-1, 1938, 39-51. USSR.

12./ " " Raspredeleniye toka v trekhfaznikh ferrosplavnikh petshakh. Ibid. No-7, 1939, 18-24.

13./ Morkramer M : Dimensionierungsgrundlagen von Elektroreduktionsöfen. 4-th Internat. Congr. on Electroheat, 1959, 4-811. see also: Elektrowärme, 19, 1961, 110 - 116.

References continued.

14./ Rabey C.C. : Computerised Evaluation of Furnace Fields. M.Sc. Thesis, University of Cape Town, Sept. 1974.

15./ Campbell J.:: Fluid flow and droplet formation in electroslag re - melting, (ESR) process. J. Metlas, July, 1970, 23-35.

16./ Rawson J.D.W.- Dawson I.D.- Kirkham V.: Slag and metal flow in electroslag remelting. ESR Symposium 73, Tokyo, 1973, 55-68.

17./ Latash Yu,N.- Medovar B.I.: Electroslag Melting. Iz-dvo Metallurgiya, Moscow, 1970.

18./ R. de Kock - Forbes A.W.: The smelting of copper-nickel concentrates in an electric furnace. NIM Technical Memorandum, Jan. 1974, Johannesburg.

19./ Driller A.: Die elektrische Seite der Ferrolegierungsöfen. in "Mettalurgie der Ferrolegierungen" Ed. Volkert G-Frank K.D. Chapter 2.

20./ Webs A.- Kaufhold W.- Kulicke B.: Rückwirkungen von Drehstrom Lichtbogenöfen in elektrischen Versorgungsnetzen. Elektrizitätswirtschaft, 71, 1972, 222-228.

21./ Markworth E.: Zur elektrischen Auslegung von Lichtbogenofen-Anlagen. Elektrowärme International, 31, 1973, B-5, 218-221.

SECTION IV.

I. ON SOME ASPECTS OF THE FLOW OF HEAT IN THE ELECTRIC FURNACE.

Thermal conditions in an electric furnace are extremely complex so that a quantitative treatment of the system is not possible except with a great number of simplifying assumptions. This fact alone might considerably limit the usefulness of the results. The methods applied have to be necessarily complicated because of the need to treat complex boundary conditions. A further difficulty is encountered in the proper selection of these conditions in a system which is never in a true steady state. The changes involved in its operation are very substantial and might come about within short time intervals.

In addition, model tests are also difficult to design so that they would yield meaningful and representative results which could be used for simulation and scale-up purposes.

In the following survey it will be attempted to investigate certain aspects of the flow of heat that may prevail in various areas of the molten slag bed in rectangular submerged electrode resistance heated furnaces having 6 electrodes-in-line arrangement. Because of the intermittent character of the matte tapping and, as a consequence, a more uniform temperature distribution in the molten matte the investigations will be restricted to the slag bed only and carried out with the main purpose to facilitate the selection or design of proper furnace geometry. In this instance, for example, the mode of heat distribution around the electrode in vertical direction through the slag layer determines the melting area, i.e. the depth of the molten slag bed while the horizontal heat distribution defines the working area, thereby also the spacing of the electrode and the width of the furnace.

The two main simplifying assumptions involved in the analysis are:

a./ steady state in which the heat is transferred primarily by conduction in a rigid, rather than a deformable medium. The serious limitations of this assumption are fully appreciated since obviously, the diffusion of heat in a rigid medium differs from that in a deformable medium, as the latter includes the diffusion of momentum. Thus form the viewpoint of solution, the technique applicable to a deformable body should involve non-linear equations which govern the diffusion of momentum as compared with the application of the much simpler linear equations involved in a rigid medium on which the present analysis is based.

b./ Heat transfer/...

b./ Heat transfer occurs equally in all directions, x, y, and z in the system. (complete isotropy).

Two main areas in the molten slag will be investigated:

1./ in vertical direction between the top of the molten bed and the level of the electrode tip, then between the level of the electrode tip and the slag-matte interface,

2./ In horizontal direction from the electrode to the furnace wall, representing the active, or working area of the electrode in this direction.

1./ Flow of heat in vertical direction in the molten bed of slag.

Temperature profile between a./ the top of the slag bed and the level of the electrode tip and b./ level of electrode tip and slag-matte interface obtained by applying the thermal conductivity of two-phase mixtures.

Practical temperature measurements carried out on the slag bath of a working unit indicated the existence of an extensive layer in vertical direction in which the temperature variations were rather limited (42.). On approaching the boundary, i.e. the top of the melt below the solid crust of burden, the temperature then starts decreasing very rapidly.

The temperature gradient in vertical direction is characterised by the combined heat flux of the molten slag bath and the matte prills descending through the media. The top of the melt in close vicinity to the solid crust of burden is already in the molten state though as an inhomogeneous mixture of high viscosity. By the heat flow model applied to this problem the top of the molten slag layer above the solidified crust of slag is insulated by the solid burden through which the conduction of heat is not being considered in this study. Thus we have two fixed boundary temperatures, viz. on the top of the slag just below the crust which, from simulated laboratory tests carried out in connection with liquidus temperature determinations in the present work, wasmeasured as 1280°C, and at the level of the electrode tip approximately 1450-1460°C.

The molten slag layer with the settling matte particles in it can be regarded as a two-phase mixture, the thermal conductivity of which is given by the Maxwell-Eucken equation. Let the thermal conductivities be denoted as follows:

k_{mix} = two-phase mixture

k_c = condensed phase (slag)

k_d = dispersed phase (matte)

and V_d = volume fraction of dispersed phase

then by the/...

then by the mentioned equation

$$k_{mix} = k_c \left[\frac{1 + V_d\left(\frac{1 - (k_c/k_d)}{2\,k_c/k_d + 1}\right)}{1 - V_d\left(\frac{1 - (k_c/k_d)}{k_c/k_d + 1}\right)} \right] \qquad 1./$$

On applying the special conditions obtaining in the reference furnaces with regard to the thermal conductivities and flow volumes of slag and matte respectively: (subscripts c = condensed phase, d = dispersed(matte) phase).

k_c = 4,9 kcal/hr.m^2.^{o}Cm^{-1} (3); an approximate value extrapolated for the present quinnary system

$c_{p(c)}$ = 300 cal/kg at 1100^{o}C (4); each further 20^{o}C rise in temperature corresponds to 10 cal. increase; then at an average slag temperature of 1400^{o}C $c_{p(c)}$ = 450 cal/kg

γ_c = 2,77 g/cm^3 at 1400^{o}C

$\kappa'_c = k_c/\gamma_c c_{p(c)} = 4,9/(2,77 \times 0,45) = 3,92$ m^{2}hr^{-1}

k_d = 49,0 kcal/hr.m^2^{o}C/m ; approximate value in which the termal conductivity of matte was regarded as being very similar to that of the metal (by analogy of electrical conductivity)

$c_{p(d)}$ = 217 cal/kg at 1200^{o}C (4); each further 20^{o}C rise in temperature corresponds to about 5 cal increase of the c_p value,

γ_d = 3,8 g/cm^3 at 1400^{o}C

$\kappa'_d = k_d/\gamma_d c_{p(d)} = 49,0/(0,247 \times 3,8) = 52$ m^{2}hr^{-1}

Total weight of slag produced	21	tons/hr
+ converter return	4	"
Furnace matte produced	4,5	"
Volume of slag 25/2,77	8,95	m^3
volume of matte 4,5/3,8	1,185	m^3

V_d = 1,185/8,95 = 0,133

and

$$k_{mix} = 4,9\left[\frac{1 + 0,133\left(\frac{1 - (4,9/49)}{2(4,9/49) + 1}\right)}{1 - 0,133\left(\frac{1 - (4,9/49)}{(4,9/49) + 1}\right)}\right] = 4,9\,\frac{1,098}{0,892}$$

k_{mix} = 6,0 kcal/hr.m^2.^{o}C/m

Let us consider now the conduction of heat as being analogous to that in a semi-infinite solid with initial temperature t_o and the surface kept at a constant ϕt. (5). If the boundary at x=0 is kept at a constant temperature then in the direction of temperature decrease

$$\Delta t = t_o\left(1 - \mathrm{erf}\frac{x}{2\sqrt{\kappa'_{mix}\theta}}\right) = t_o \,\mathrm{erf}\, c\,\frac{x}{2\sqrt{\kappa'_{mix}\theta}} \qquad 2./$$

and in the/...

Figure IV - 1. CONDITIONS FOR THE ESTIMATION OF VERTICAL TEMPERATURE GRADIENT IN THE MOLTEN SLAG BATH. APPLICATION OF THE THERMAL CONDUCTIVITY OF TWO-PHASE MIXTURES.

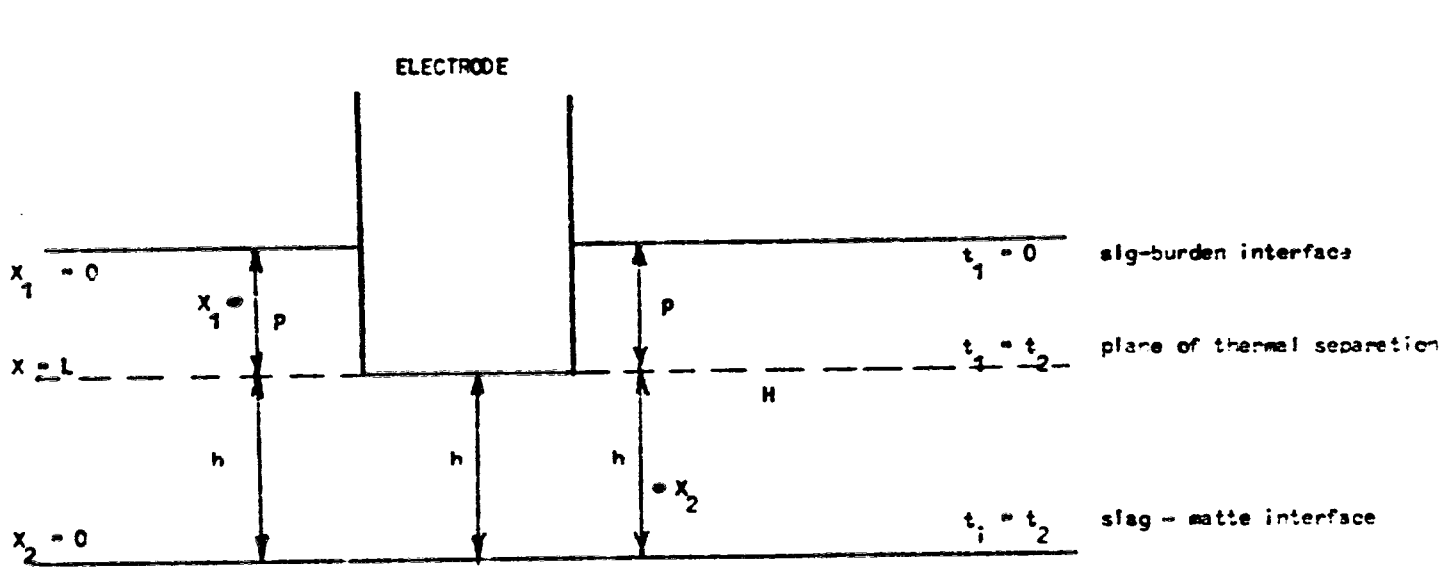

Figure IV - 2. COMPARISON OF MEASURED AND PREDICTED VERTICAL TEMPERATURE GRADIENTS.

Legend Crosses : measured values

circles : by thermal conductivity of two-phase mixtures
triangles: by the first order Ritz profile

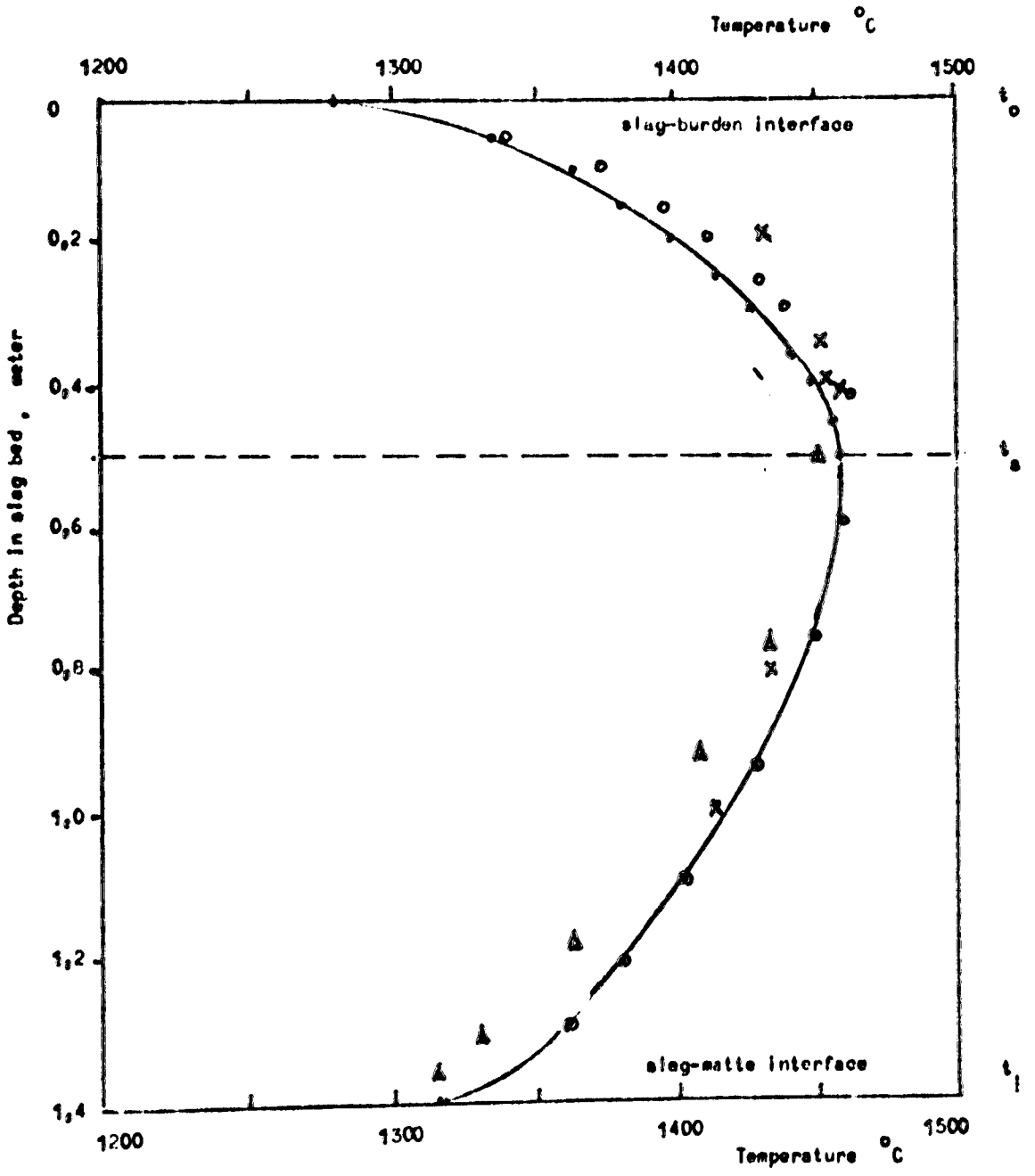

and in the direction of temperature increase

$$\Delta t = t_o\left(1 + \operatorname{erf}\frac{x}{2\sqrt{\kappa'_{mix}\Theta}}\right) \qquad 3./$$

here κ'_{mix} = thermal diffusivity of the mixed phase and Θ = time. How to calculate κ'_{mix}

$$\kappa'_{mix} = \frac{k_{mix}}{\gamma_{mix} c_{p(mix)}} \qquad 4./$$

$$\gamma_{mix} = \left[(8,95x2,8)+(1,84x3,8)\right]/(8,95+1,84) = 3,0\ g/cm^3$$

and $c_{p(mix)} = \left[(450x25)+(267x7)\right]/32 = 408\ cal/kg$

therefore $$\kappa'_{mix} = \frac{6,0}{3,0x0,408} = 4,9\ m^2hr^{-1}$$

The level of the electrode tip may be regarded as a plane of heat separation in the slag bed between two temperature regions, the upper one as discussed previously, extending upward to the solid burden - slag interface, while the lower one reaching downward to the slag-matte interface. The conditions are shown in graph 1.) and may be expressed as follows:

in region 1. (upper region) $0 < x_1 < L$

$t_o < t_x < t_s$

in region 2. (lower region) $L > x_2 > 0$

$t_s > t_x > t_i$

furthermore, with normalized conditions

region 1.	at	$x = 0$,	$\Theta = 0$,	$t_x = t_o$
		$x = 0,5$	$\Theta = 0,5$	$t_x = t_s$
region 2.		$x = 1 = L$	$\Theta = 1,0$	$t_x = t_s$
		$x = 0$	$\Theta = 0$	$t_x = t_i$

Then the vertical profile in both regions between temperature faces t_o and t_i can be estimated. Say at $(\Theta,x) = 0,5$ equation 3. will yield

$$\Delta t = 1280\left(1-\operatorname{erf}\frac{0,05}{2\sqrt{4,9x0,05}}\right) = 117^oC$$

and $$t_x = t_o + \Delta t = 1280+117 = 1397^oC$$

The values estimated in this way are indicated by circles in graph 2.), while the experimentally measured data (1,2) are denoted by crosses. There appears a reasonable agreement between the measured values and those predicted by the foregoing considerations on heat conduction. This is especially noteworthy in the trend of the vertical temperature gradient across the slag bath. A comparable temperature gradient was found by Mitchell and Joshi (6) from experimental temperature measurement across the slag bath of the ESR (Electro Slag Remelting) process.

1.1/ Significance of/...

and in the direction of temperature increase

$$\Delta t = t_o\left(1 + \operatorname{erf}\frac{x}{2\sqrt{\kappa'_{mix}\,\Theta}}\right) \qquad 3./$$

here κ'_{mix} = thermal diffusivity of the mixed phase and Θ = time. Now to calculate κ'_{mix}

$$\kappa'_{mix} = \frac{k_{mix}}{\gamma_{mix}\, c_{p(mix)}} \qquad 4./$$

$$\gamma_{mix} = \left[(8{,}95\text{x}2{,}8)+(1{,}84\text{x}3{,}8)\right]/(8{,}95+1{,}84) = 3{,}0\ g/cm^3$$

and $$c_{p(mix)} = \left[(450\text{x}25)+(267\text{x}7)\right]/32 = 408\ cal/kg$$

therefore $$\kappa'_{mix} = \frac{6{,}0}{3{,}0\text{x}0{,}408} = 4{,}9\ m^2hr^{-1}$$

The level of the electrode tip may be regarded as a plane of heat separation in the slag bed between two temperature regions, the upper one as discussed previously, extending upward to the solid burden - slag interface, while the lower one reaching downward to the slag-matte interface. The conditions are shown in graph 1.) and may be expressed as follows:

in region 1. (upper region) $0 < x_1 < L$

$t_o < t_x < t_s$

in region 2. (lower region) $L > x_2 > 0$

$t_s > t_x > t_i$

furthermore, with normalized conditions

region 1.	at	$x = 0$,	$\Theta = 0$,	$t_x = t_o$
		$x = 0{,}5$	$\Theta = 0{,}5$	$t_x = t_s$
region 2.		$x = 1 = L$	$\Theta = 1{,}0$	$t_x = t_s$
		$x = 0$	$\Theta = 0$	$t_x = t_i$

Then the vertical profile in both regions between temperature faces t_o and t_i can be estimated. Say at $(\Theta,x) = 0{,}5$ equation 3. will yield

$$\Delta t = 1280\left(1-\operatorname{erf}\frac{0{,}05}{2\sqrt{4{,}9\text{x}0{,}05}}\right) = 117^oC$$

and $$t_x = t_o + \Delta t = 1280+117 = 1397^oC$$

The values estimated in this way are indicated by circles in graph 2.), while the experimentally measured data (1,2) are denoted by crosses. There appears a reasonable agreement between the measured values and those predicted by the foregoing considerations on heat conduction. This is especially noteworthy in the trend of the vertical temperature gradient across the slag bath. A comparable temperature gradient was found by Mitchell and Joshi (6) from experimental temperature measurement across the slag bath of the ESR (Electro Slag Remelting) process.

1.1/ Significance of/...

Figure IV - 5. EFFECT OF ELECTRODE POSITION ON THE VERTICAL TEMPERATURE GRADIENT.

Depth of electrode immersion
into the slag

1 $D_e/4,2$
2 $D_e/2,5$
3 $D_e/1,8$

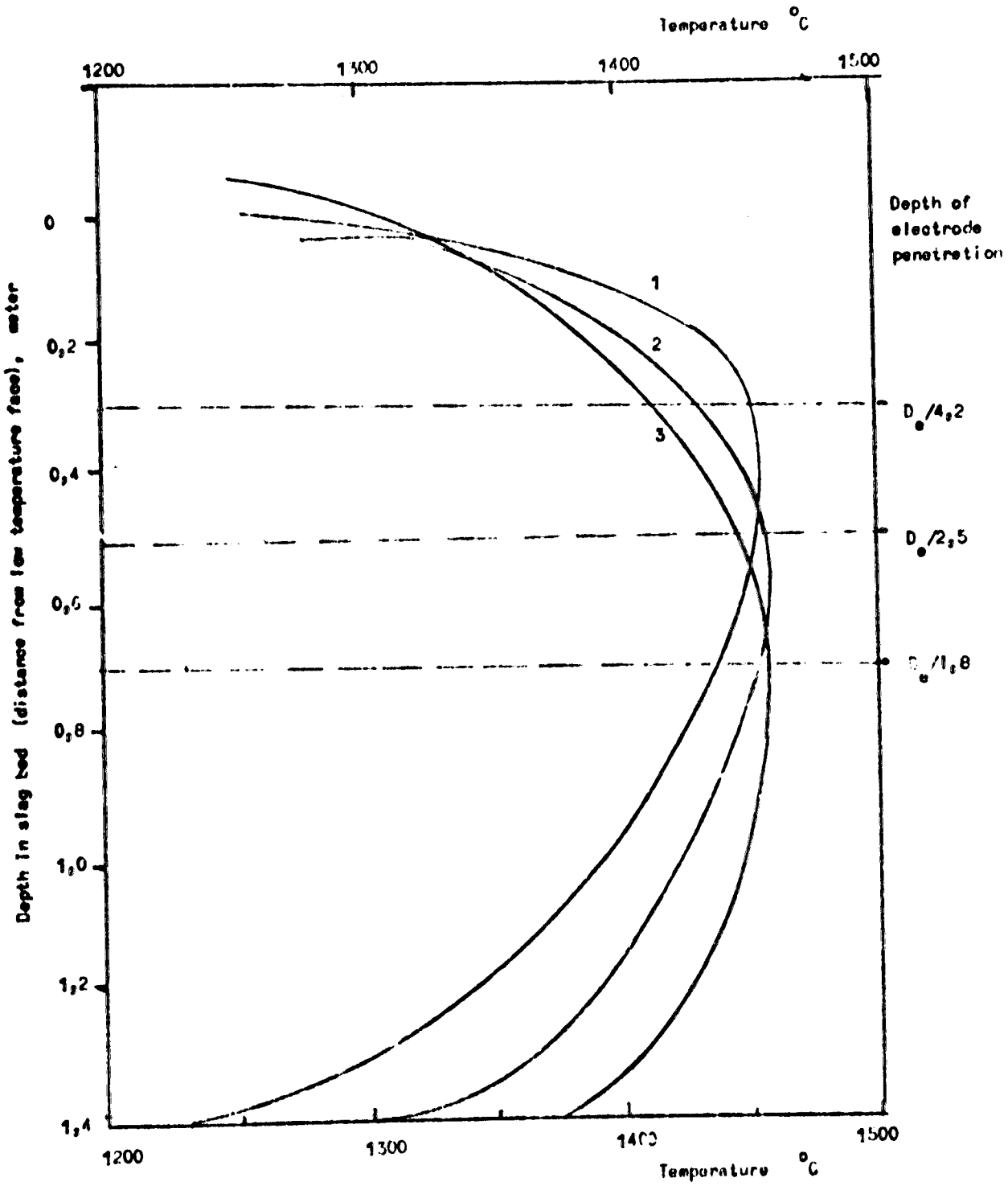

1.1. Significance of the vertical temperature profile.

The vertical temperature profile reflects the depth of the molten slag bath and, also, the tapping temperature of the matte. The profile shown in figure 2.) relates to average operating conditions of the reference furnaces having electrodes of 1,25m dia. immersed at 45 - 50 cm into the melt at 18,0 - 18,5 MW power input. Obviously, the depth of electrode immersion, this being a function of slag resistivity and also of the rate of power input, has a strong influence on the vertical temperature gradient.

With regard to the effect of electrode movement let us consider the case when, due to a sudden change in slag resistivity in the close vicinity of the electrode, for example by collapse of crust in the upper layer or increased feed rate of burden, will make the electrode to occupy a new position. If the effect is such that the electrode has to move upward, then the keeping of the furnace load unchanged (power input) will result in an increased heat dissipation in the upper region of the melt because of the upward shift of the hypothetical plane of temperature separation at the level of the electrode tip. On the basis of the model of the shape of current flow under the electrodes this would mean, as has been discussed earlier, a decrease in heat generation per unit volume of slag in the path of the current. Though the hot spot will now be closer to the top of the slag bath, the position of the cold face boundary would remain by and large the same. In fact the rate of upward heat dissipation, as calculations indicated, may even decrease mainly because of the cooling down of the slag in the region below the level of the electrode tip. Furthermore, the temperature of the slag-matte interface would considerably decrease even to the extent of slag crystallisation on the surface of the matte layer and would result in a cold matte tap.

Naturally the opposite trend may set in if the depth of electrode penetration increased. In this case the increased heat generation per unit volume of melt in the path of the current will increase the interface temperature and, in the meantime, although the high temperature zone of the electrode tip moved now away from the cold face, will facilitate heat dissipation toward the upper region of the slag bath. With decreasing rates of power input these effects become more noticeable.

The conditions obtaining at three different depths of electrode penetration are shown in figure 3.).

2./ Flow of heat in horizontal direction in the molten bed of slag: estimation of radial heat distribution around an electrode.

The knowledge of the extent of this zone is important in that it determines the/...

Figure IV-4 CONCEPT OF RADIAL HEAT FLOW FROM THE HOT ZONE BELOW THE ELECTRODE.

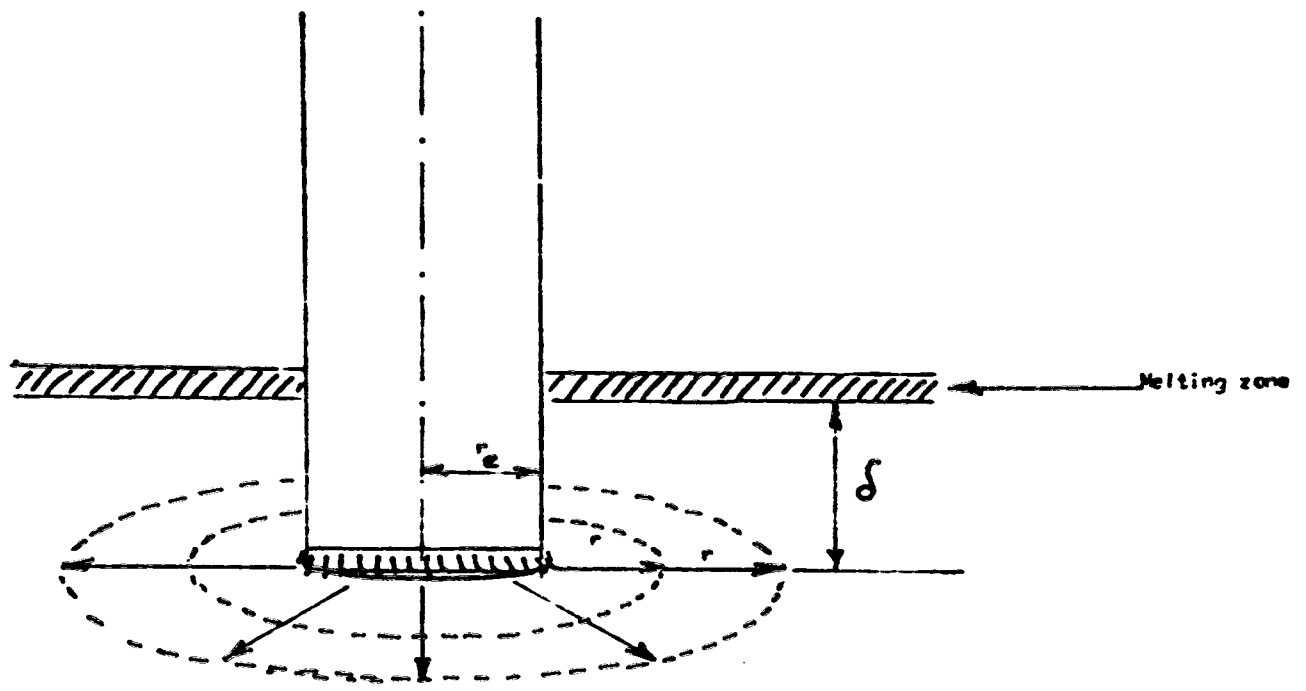

Figure IV-5. Model of radial heat conduction in the slag around an electrode.

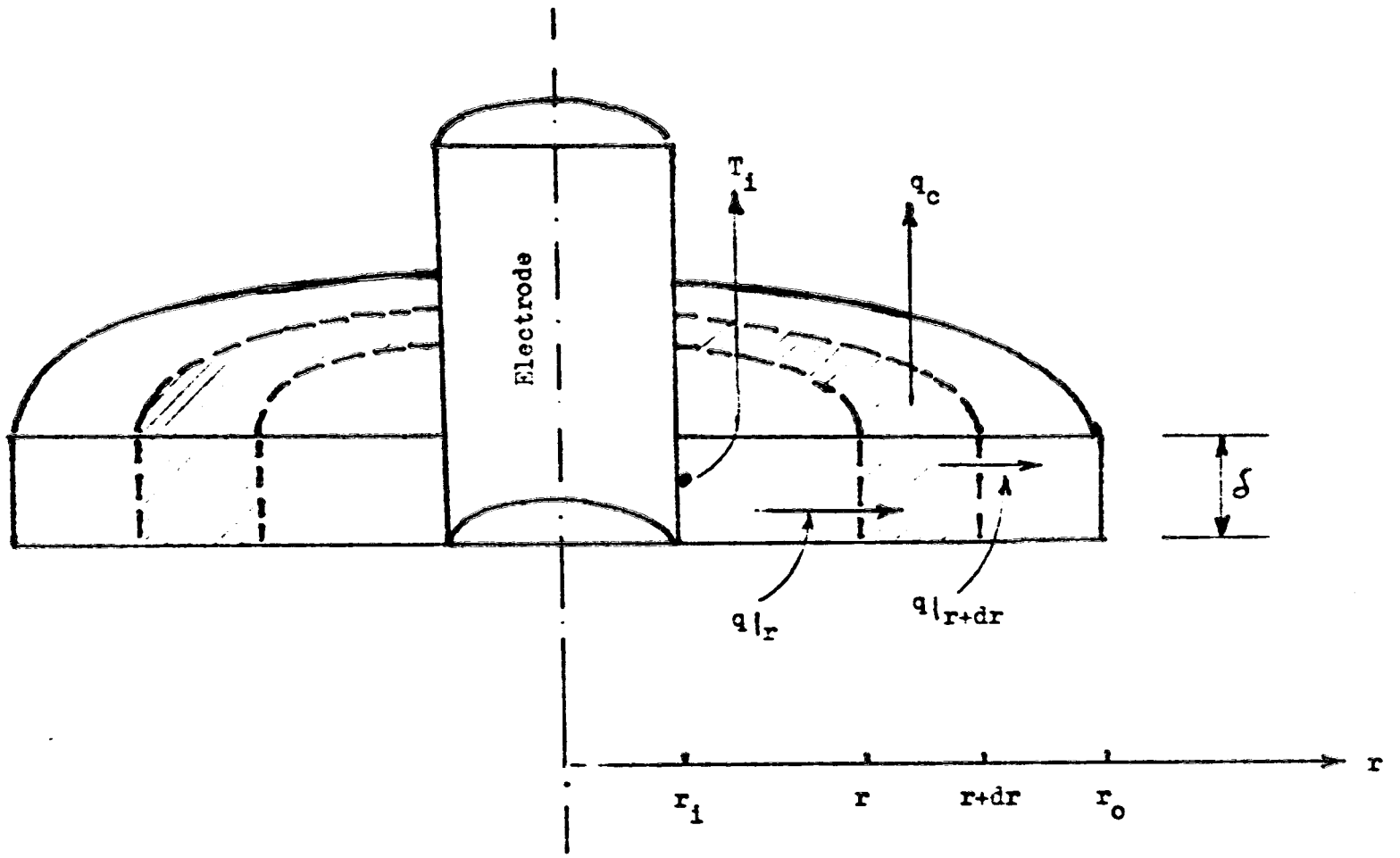

determines the spacing of the electrodes and thereby the general furnace geometry. - In order to simplify the analysis, in a similar way to the foregoing, steady state conditions with a minimum of turbulence in the slag bath will be assumed.

In a working unit the hottest spot in the slag is located just under the electrod tip confined to a relatively narrow layer. Due to obvious difficulties in measuring techniques, the exact temperature and the extent of this layer is not known. For the purpose of the present analysis, as a conservative estimate based on measurements carried out close to the periphery of the electrode tip, a temperature of 1500°C will be assigned to this slag layer regarded here as a disc in continuation or extension to the electrode.

It has been discussed previously that practical temperature measurements conducted on operating furnaces indicated a region extending upwards from the level of the electrode tip in the molten slag, in which the temperature gradient is relatively small (25 - 40°C). Based on this finding the system can be visualised as the heat being distributed in a thick plate from a cylindrical heat source embedded into this plate. Since we are interested here only in the radial flow of heat, the temperature drop along the lower surface of the plate will be investigated. Figures IV-4 and IV-5 give a general outline of the model. As will be seen in graph IV-5 heat is flowing out from the high temperature zone radially with r re - presenting the radius of the disc and dr the increment distance from the surface of the hot area expressed in terms of radius of a circle concentric to the disc. The differential heat balance on an anular surface element with the rate of heat output q at radius r is given by

$$q = k\delta 2r\pi \frac{dT}{dr} \qquad 5./$$

at r + dr the rate of heat output is

$$q+dq = -k\delta 2r\pi \frac{dT}{dr} + \frac{d}{dr}(-k\delta 2r\pi \frac{dT}{dr})dr + h(T-T_a)2r\pi dr \qquad 6./$$

Our analysis is restricted to close to steady state in which the accumulation is zero. Thus at constant thermal conductivity, k, and slag thickness of relatively constant temperature, δ, equation 6 transforms into the following expression (derivation see in Appendix I) :

$$\frac{d^2T}{dT^2} + \frac{1}{r}\frac{dT}{dr} - \frac{h(T - T_a)}{k\delta} = 0 \qquad 7./$$

Now, if $(T - T_a) = y$ and $h/k\delta = \sigma$, equation 7. becomes

$$r^2 \frac{d^2y}{dr^2} + r \frac{dy}{dr} - r^2 y = 0 \qquad 8./$$

which is a form of the familiar modified Bessel function. The function in the form

$$zw'' + w' - zw = 0 \qquad 9./$$

has the general solution $w = AI_o(x) + BK_o(x)$ 10./

In a more general form equ. 9 can be written as

$$zw'' + w' - m^2 zw = 0 \qquad 11./$$

having the general solution $w = AI_o(mx) + BK_o(mx)$ 12./

The solution of equ. 12 by standard texts (7) is given as

$$y = C_1 I_o(r\sqrt{\sigma}) + C_2 K_o(r\sqrt{\sigma}) \qquad 13./$$

It is possible to eliminate the first term from equ. 13 since it increases with positive values of r (that is I_o increases with increasing variable), while the temperature should decrease assymptotically with increasing distance from the hot zone. Thus the result will be

$$T - T_a = C_2 K_o(r\sqrt{\sigma}) \qquad 14./$$

Now in the expression of $h/k\delta$ let

δ : thickness of the slag layer at relatively uniform temperature = 0,4m

k : average thermal conductivity of slag : 4,9 kcal/m^2hr.^oC/m

h : surface coefficient of heat transfer, in this context an empirical constant the value of which may vary between 0,9 and 1,1.

With these data σ will be calculated

$$\sigma = \frac{1,0}{4,9 \times 0,4} = 0,515$$

The diameter of the disc-like hot zone under the electrode can be regarded as being identical with that of the electrode, then r = 0,625 m, (D_e=1,25m).

For the purpose of the present calculations C_2 in equ. 14 will be defined by ΔT as a constant temperature difference between the two boundary temperatures, viz. an assumed maximum under the electrode close to, or at the periphery of the electrode tip T', and the lower boundary about 25-30^oC below the liquidus temperature of the slag, T_a, at which the average plant slag exhibits already a high viscosity for practical flow considerations, beyond which, however, it becomes rapidly too viscous and no slag flow would occur. From laboratory measurements carried out on plant slags this condition appeared to set in at an average temperature of 1300^oC.

The use of two different values for the boundary temperature of the cold face on top of the molten slag, viz. 1280^oC for the estimation of the vertical temperature gradient and 1300^o for the horizontal one was made in accord with/...

Figure IV - 6. X vs $K_o(x)$ IN MODIFIED BESSEL FUNCTIONS OF THE SECOND KIND.

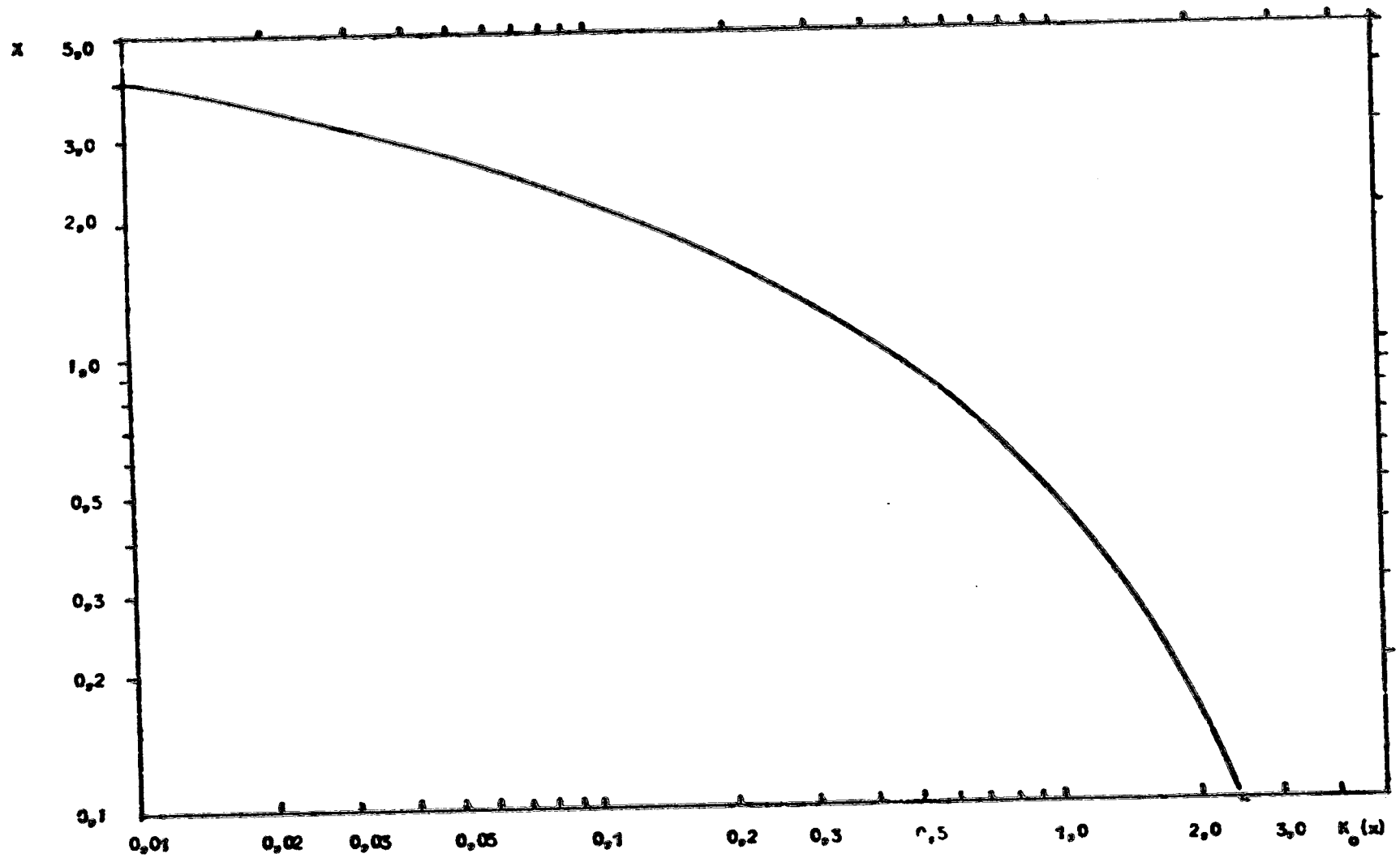

Figure IV - 6. X vs. $K_0(x)$ IN MODIFIED BESSEL FUNCTIONS OF THE SECOND KIND.

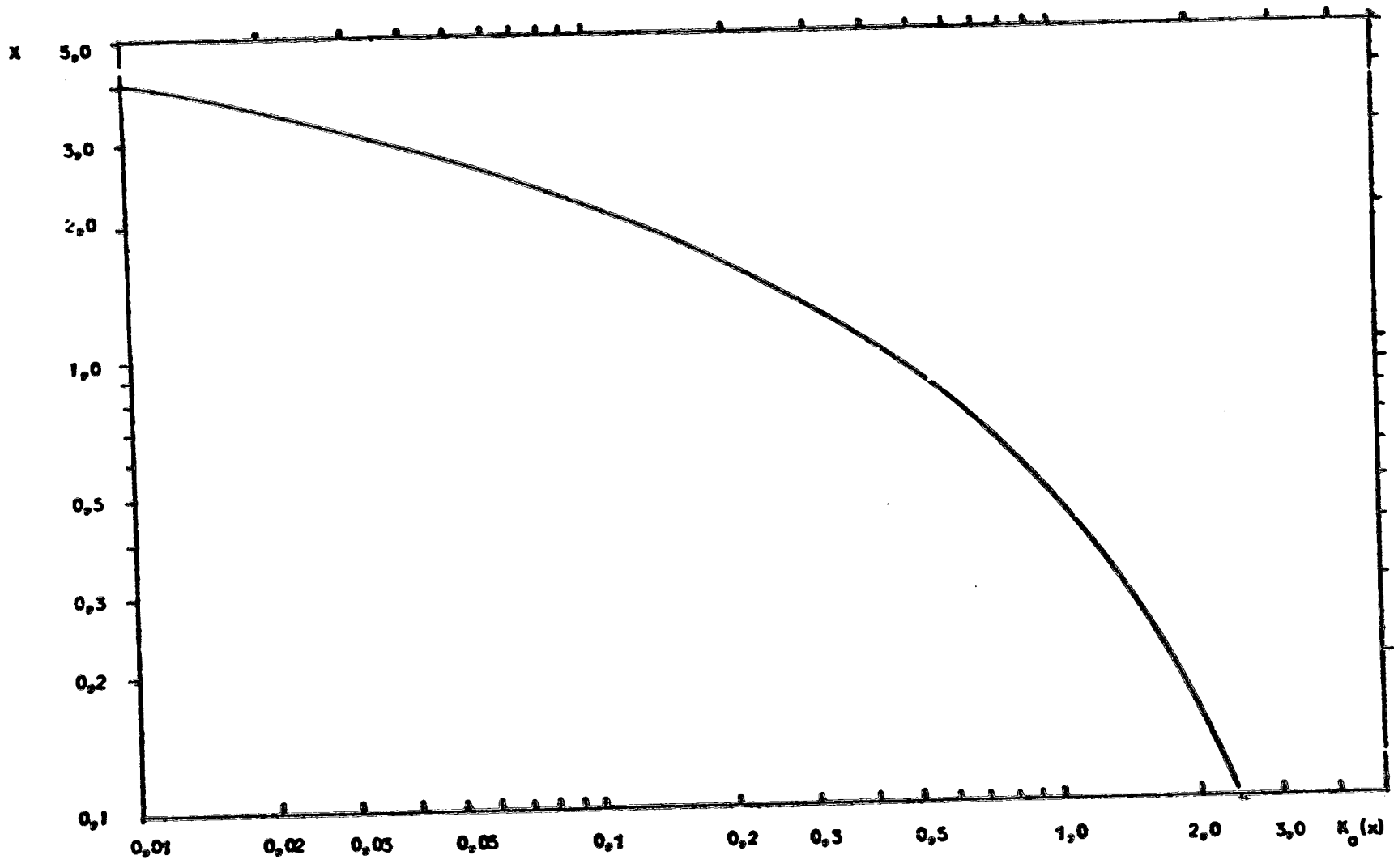

Table IV - 1. Calculation of radial temperature distribution with the outlined heat flow model using the Bessel function method.

dr (meter)	$\frac{x}{r}$	$K_o(x)$	$T K_o(x)$ (T' ^oC)	$T'+T_a$ $(T_x)^oC$
0,625	-	1,00	200	1500
1,0	0,72	0,64	128	1428
1,5	1,08	0,40	80	1380
2,0	1,44	0,27	54	1354
2,5	1,80	0,16	33	1333
3,0	2,16	0,10	20	1320
3,5	2,52	0,06	6	1306

accord with the different purposes the calculations are envisaged to serve. In the former case the point of slag solidification was chosen for physical boundary condition, whereas in the latter case the aim was to set the boundary according to the reaction zone of the electrode. This involves the viscosity parameter that is the flow of slag, since the reaction zone will be defined as an area of active mixing surrounding an electrode. Thus the choice for 1300°C reflects the results of viscosity measurements supported by reasons mentioned above.

In support of the selection of these temperature limits one has to recall further the results of electrical conductivity measurements obtained with an average plant slag as shown in graph II-16 of Section II. A sharp rise in the resistivity can be noticed at 1280°C in the graph indicating the start of complete solidification. Obviously, the heating action of the electrode extends beyond this limit, but the main concern of these investigations is the distribution of heat in the liquid phase of the system, i.e. in the molten slag, therefore the conduction of heat in the solid phase was excluded from the study.

1300°C appears to be the lowest limit for any flow considerations with the slags produced in the plant and for practical purposes a temperature probably about 10°C above this could be regarded as an acceptable value.

On taking 1500°C for T', the temperature gradient will be given by

$$T = T_a + \Delta T\, K_o(r\sqrt{\sigma}) \qquad 16./$$

that is

$$T = T_a + \Delta T\, K_o(x) \qquad 17./$$

and

$$T'_x = T\, K_o(x) \qquad 18./$$

T'_x giving the temperature at a distance x from the surface of the electrode. Then with $r_e = 0{,}625$m; $\sqrt{\sigma} = \sqrt{0{,}515} = 0{,}72$; $T = 1500-1300 = 200$°C and by taking various values (expressed in meters) along the distance between the electrode surface and the furnace wall, the expression $x = r\sqrt{0{,}515}$ will be obtained. The corresponding values of $K_o(x)$ are taken from tables for modified Bessel functions of zero order and zero kind (8) or read from graph IV-6 drawn after the values given in reference 8., then the data compiled in Table IV-1 will result.

3./ Viscosity and electrical conductivity profiles in the slag layer based on measured viscosity and conductivity data and estimated temperature profiles.

With the estimated vertical and horizontal temperature profiles and the measured values of electrical conductivities and viscosities at various temperatures, the conductivity and viscosity profiles in the slag bed can be determined/...

Figure IV - 7. VERTICAL GRADIENT OF VISCOSITY AND SPECIFIC RESISTIVITY IN THE SLAG BED BETWEEN THE LEVEL OF THE ELECTRODE TIP AND THE MOLTEN SLAG LAYER.

1. Specific resistivity
2. viscosity

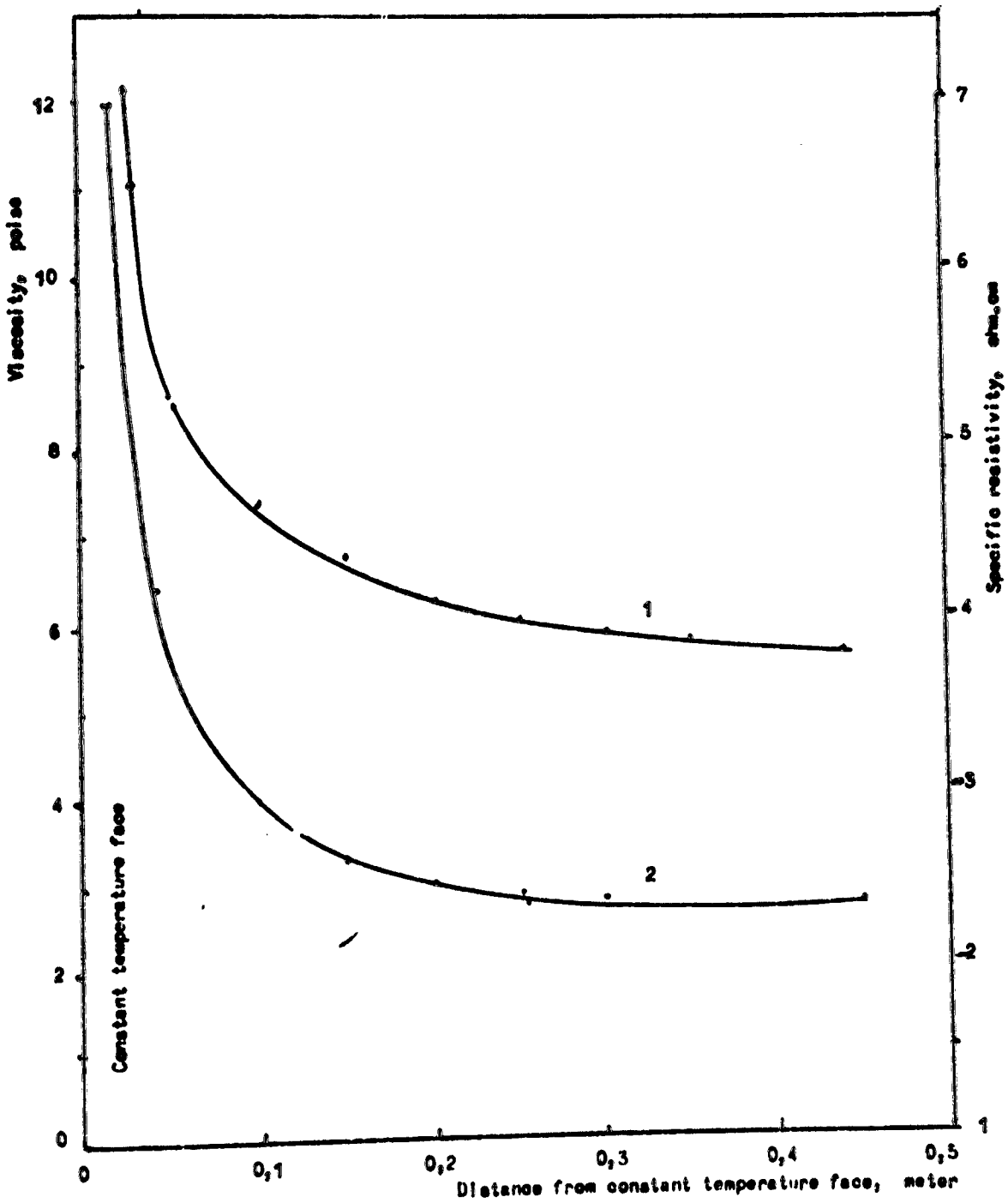

Fig. IV - 8. HORIZONTAL GRADIENT OF VISCOSITY AND SPECIFIC RESISTIVITY IN THE SLAG BED BETWEEN THE ELECTRODE SURFACE AND THE FURNACE WALL.

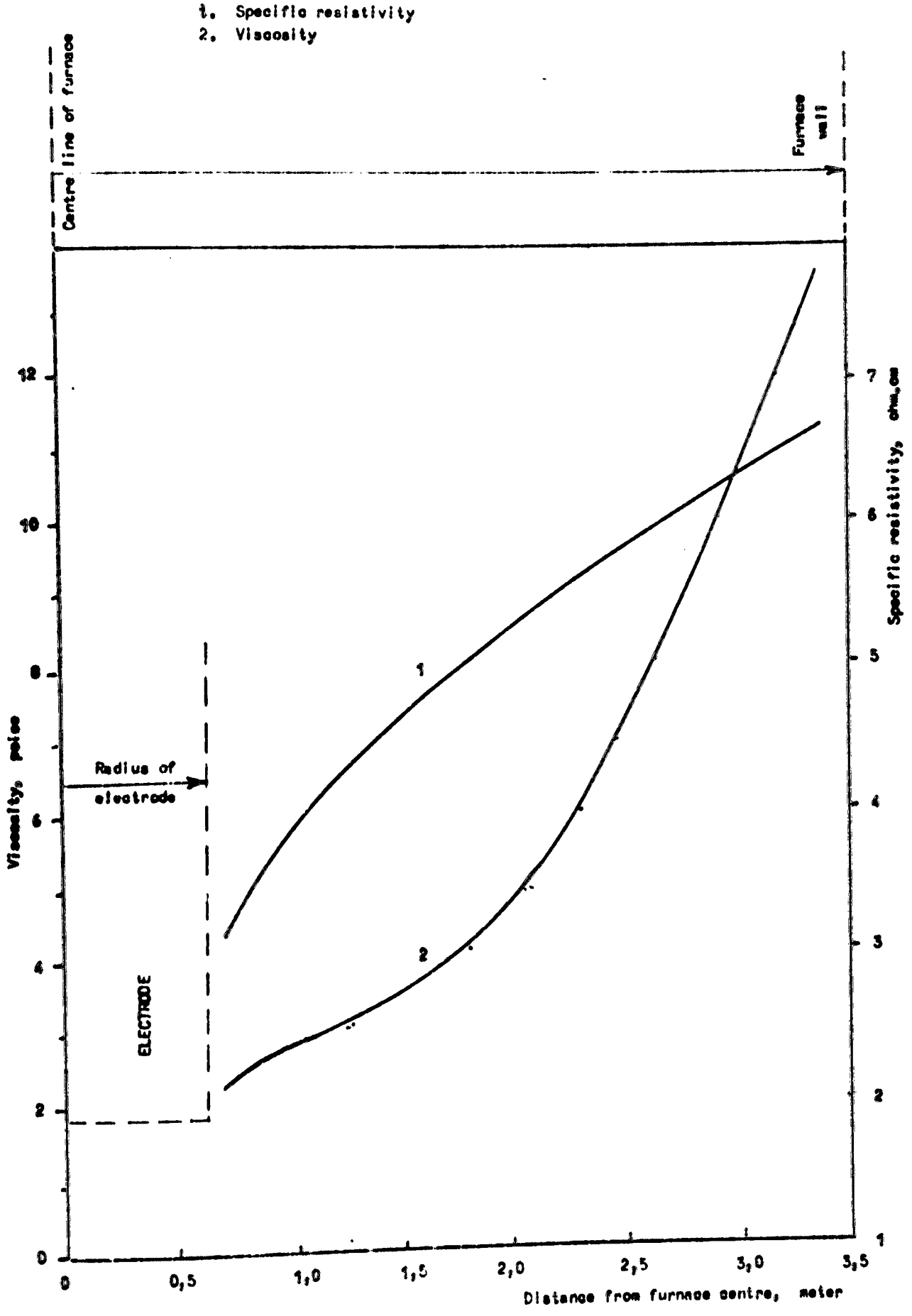

Figure IV -. 9. HORIZONTAL RESISTIVITY CONTOURES AROUND A PAIR OF ELECTRODES IN PHASE.

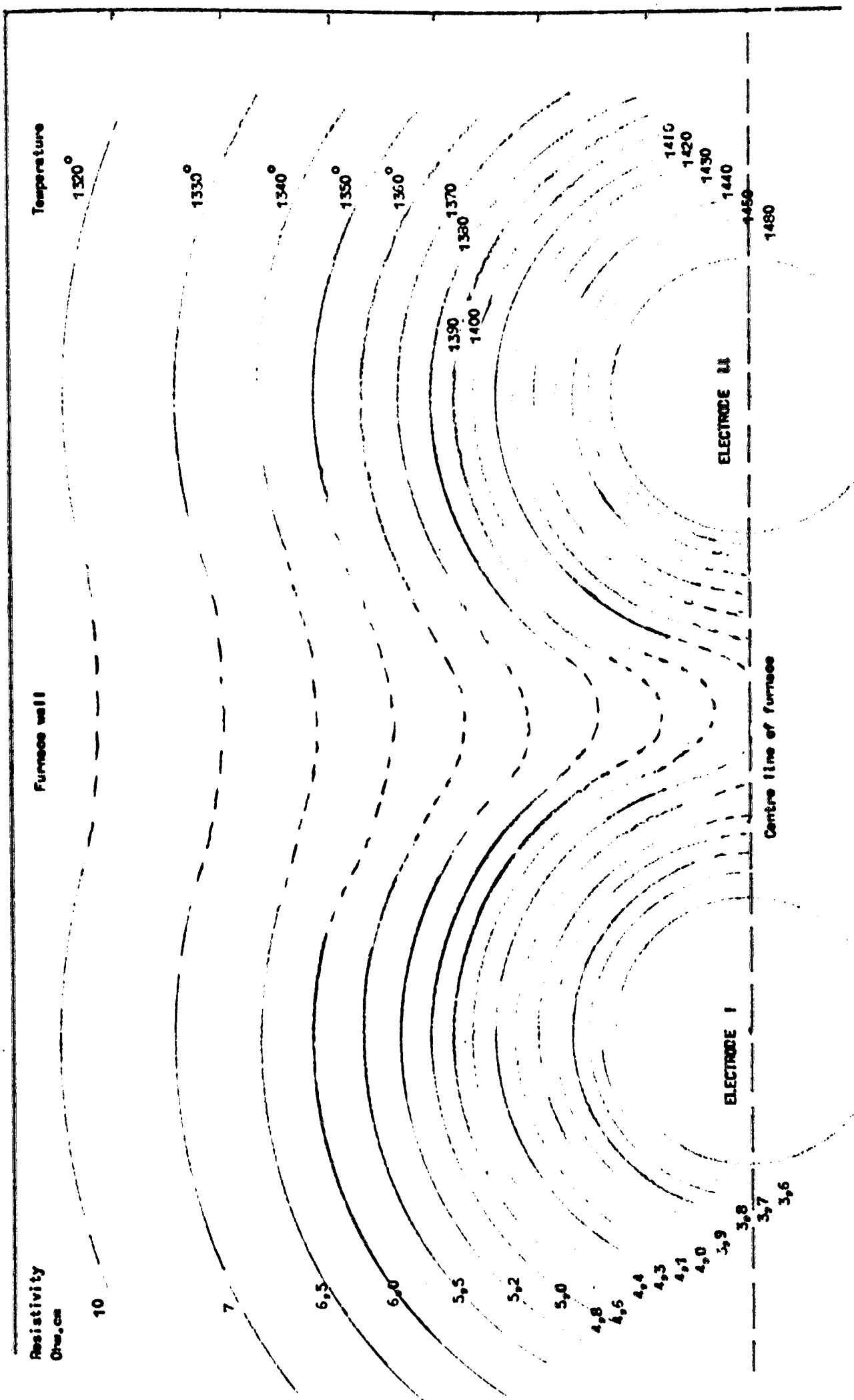

Figure IV - 10 HORIZONTAL VISCOSITY CONTOURES AROUND A PAIR OF ELECTRODES IN PHASE.

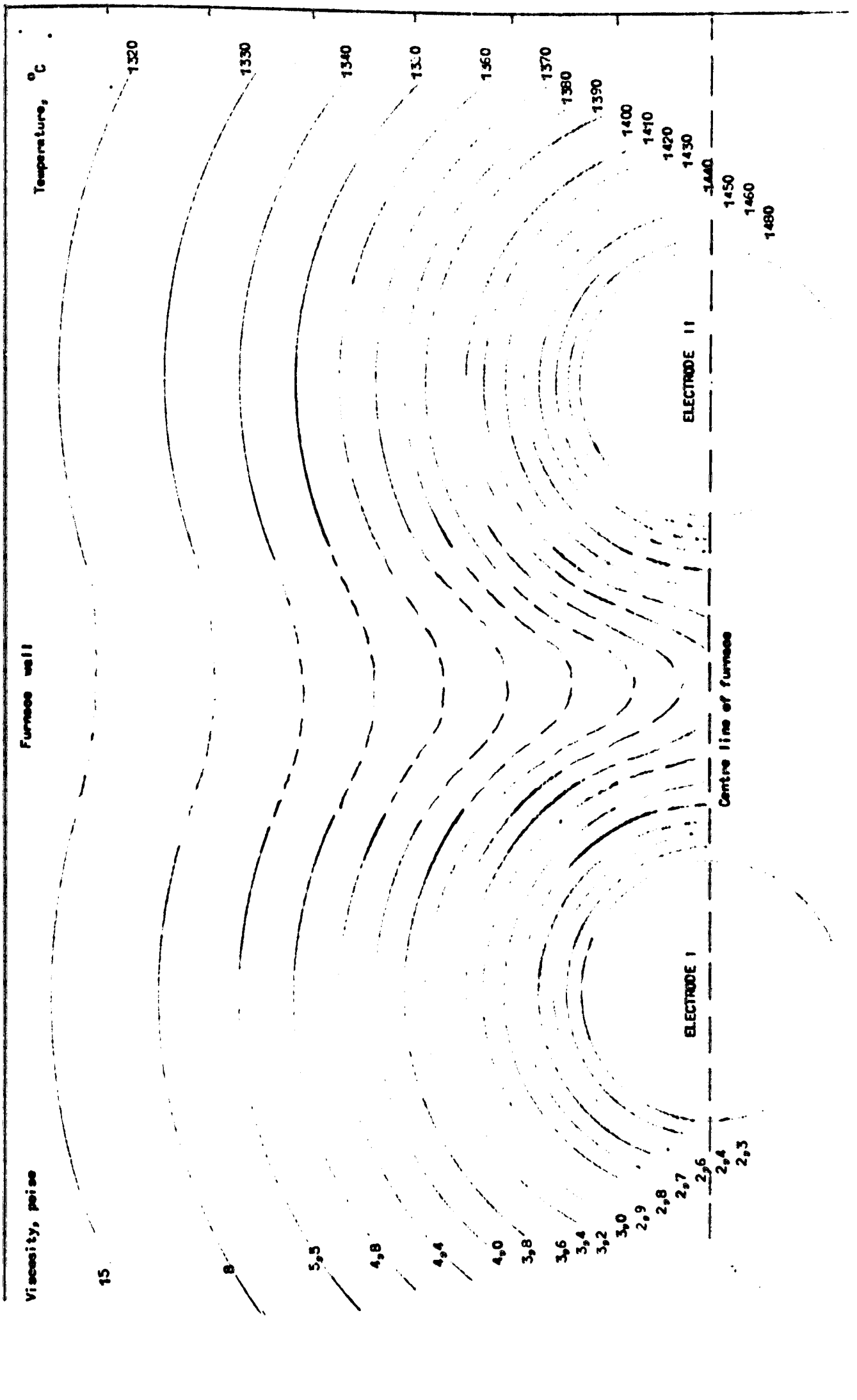

determined. Again, the basic assumption is that the heat transfer from the electrode occurs in a steady state and the flow of heat is effected primarily by conduction through the melt.

3.1./ Vertical viscosity and and conductivity profiles in the slag bath.

Figure IV-7 constructed on the basis of graphs III-8 and IV-2 re - presents the vertical conductivity and viscosity profiles obtaining with an average slag composition in the working furnace. As will be apparent, the values of both slag properties start increasing rapidly as a distance of about 10 cm from the semi-fluid, viscous boundary layer is reached. If the thickness of the burden were uniform above the molten slag securing thereby a uniform heat insulation to the bath, then by the indication of the graph in about 7 to 10 per cent of the total bed volume the settling of the matte would be very limited.

A probable temperature gradient between the level of the electrode tip and matte surface was given in graph IV-2. Unfortunately, the exact temperature of the slag-matte interface is hard to establish but, as it was mentioned before, it cannot be much lower than the average liquidus. Due to the substantial temperature difference between the level of the electrode tip and the interface and, the ensuing increase in slag viscosity, the settling velocity of the matte particles will considerably decrease. Therefore the approach of assigning constant settling velocities to,particles of a given size across the entire depth of the slag bed will not reflect actual settling conditions.

3.2./ Horizontal conductivity and viscosity profiles.

These were estimated with the aid of graph III-8 and Table IV-1. The results are presented in figure IV-8, which indicates the gradients of the two two slag properties between the electrode surface and the furnace wall. Along the entire width of the furnace the viscosity appears to follow a parabolic distribution.

The distribution of conductivity and viscosity concentric to the electrode (based again on the values of graph III-8) is shown in figures IV-9 and IV-10 assuming idealised conditions, i.e. very limited slag movement beyond the laminar flow and identical position of the electrodes, that is depth of immersion into the molten slag. Obviously, disruptive effects created by buoyancy forces and amplified further by electromagnetic action might modify the pattern of distribution outlined in the figures, the extent of these forces is going to be inventigated in a subsequent

paragraph/...

Figure IV - 111 CHANGE OF VOLUMETRIC ENERGY DENSITY IN THE SLAG BATH OF A FURNACE SMELTING TITANIUM -BEARING ORES.
Depth of electrode penetration as a parameter.
(After Denisov and co-workers)

Depth of electrode penetration

1. 0,3 meter
2. 0,5 "
3. 0,9 "

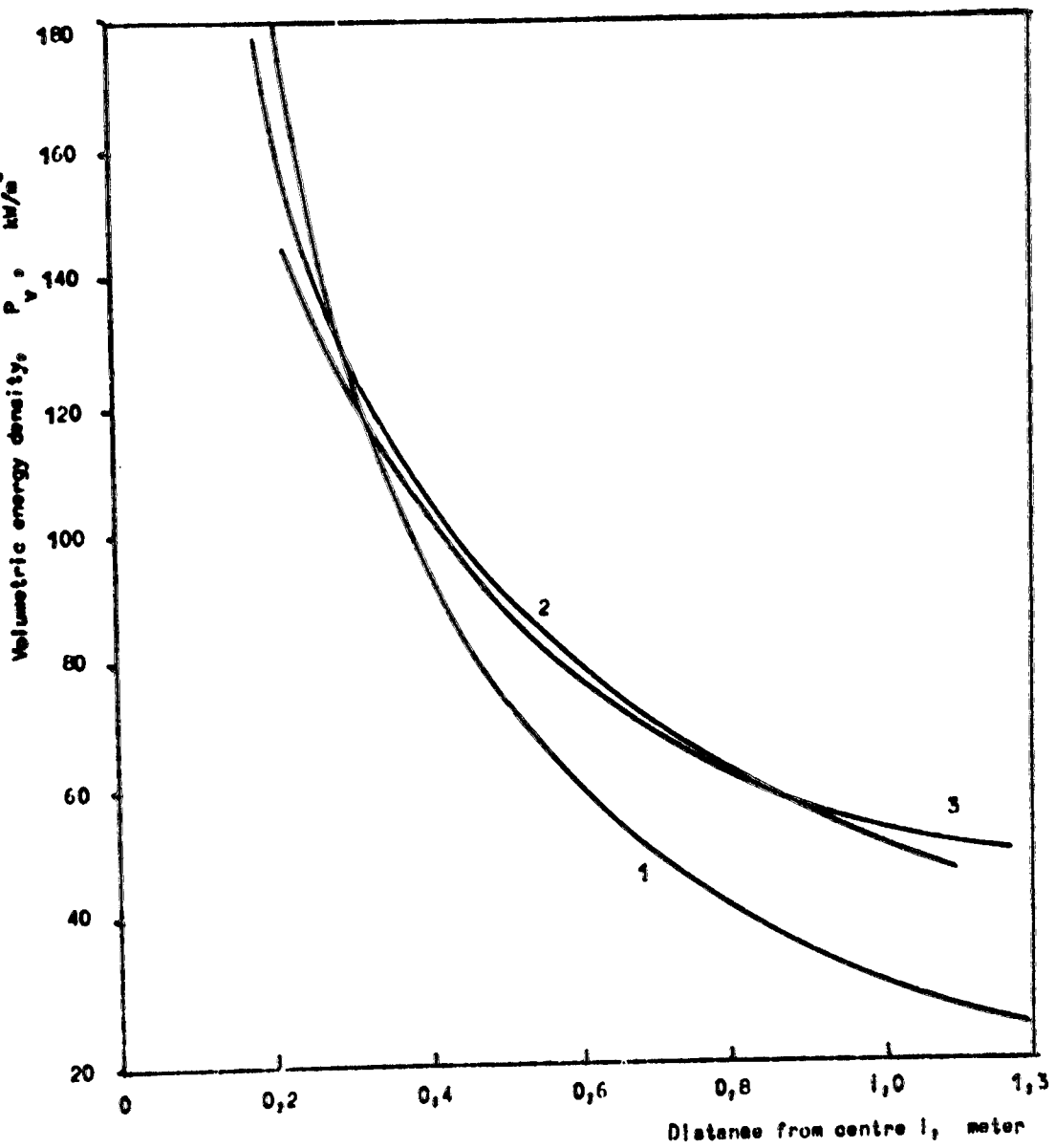

paragraph. Nevertheless the tendency is that with the increase of temperature the gradients of both viscosity and conductivity will become stesteeper around the electrode and will give rise to increased buoyancy effects. FrcFrom the point of view of the settling of matte particles this means that the strongly decreased slag viscosities would promote settling and would tend to create pockets favourable for the settling of prills around the surface of the electrodes. On the other hand the counteracting buoyancy forces will tend to prevent the formation of such pockets and disperse the particles into farther regions of the slag bath rendering thereby the pattern of of settling much less, if at all, predictable.

3.3/ Heat flow and energy distribution.

In the previous section the energy distribution in the slag bath as a function of the geometric shape of current flow and the position (depth of immersion) of the electrode in the melt has been investigated. Extending this further to the effect of the flow of heat, the outlined mode of heat distribution would suggest increasing power densities with the decrease of the distance from the electrode surface. To some degree this has been dealt with in the mentioned theoretical considerations of Sibakin and Kjølseth and confirmed by the practical work of Rabey. The findings of Russian researchers (9, 10), especially those of Denisov et al. pertinent to the variation of current distribution in working units seem to substantiate further the outlined trend. The energy distribution (P_v) per unit volume of slag was expressed as

$$P_v = \Delta_i \frac{\Delta V}{l} \qquad 19.)$$

where Δ_i is the specific current density A/cm^2, P_v the volumetric energy density kW/m^3 melt, ΔV the the potential difference at a given point in the bath and l the distance in meters from the lateral surface of the electrode. The variation of the volumetric energy density with l at various depths of electrode immersion based on ref.9. is shown in graph IV-11.). In comparing the trends of the plots with graph IV-8.) it has to be remembered that the latter indicates the variation of resistivity with the distance whereas the volumetric energy density varies roughly as the square of the current.

In the context of this study the approach of describing the change of volumetric energy density may be similar to that applied to the distribution of heat in radial direction by the method of Bessel functions. The problem is fully analogous since, disregarding heat losses caused by radiation from the furnace walls, the temperature gradient may represent as a first approximation the energy gradient as well in the same direction.

Thus in the sense/...

Figure IV - 12. OUTLINE OF THE TWO-DIMENSIONAL HEAT FLOW MODEL IN THE CROSS SECTION OF THE MOLTEN BED OF SLAG.

A.)

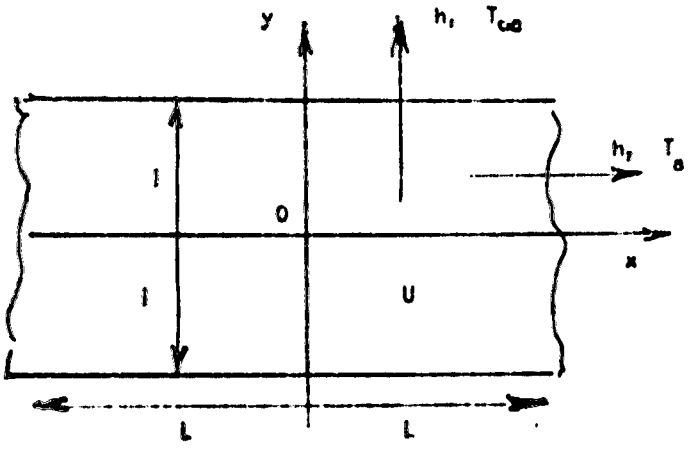

B.)

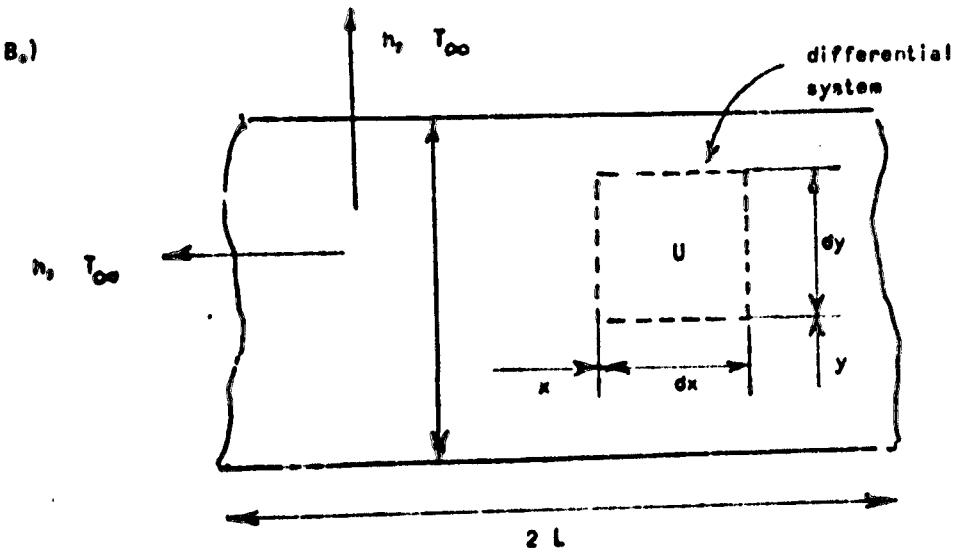

C.) C.)

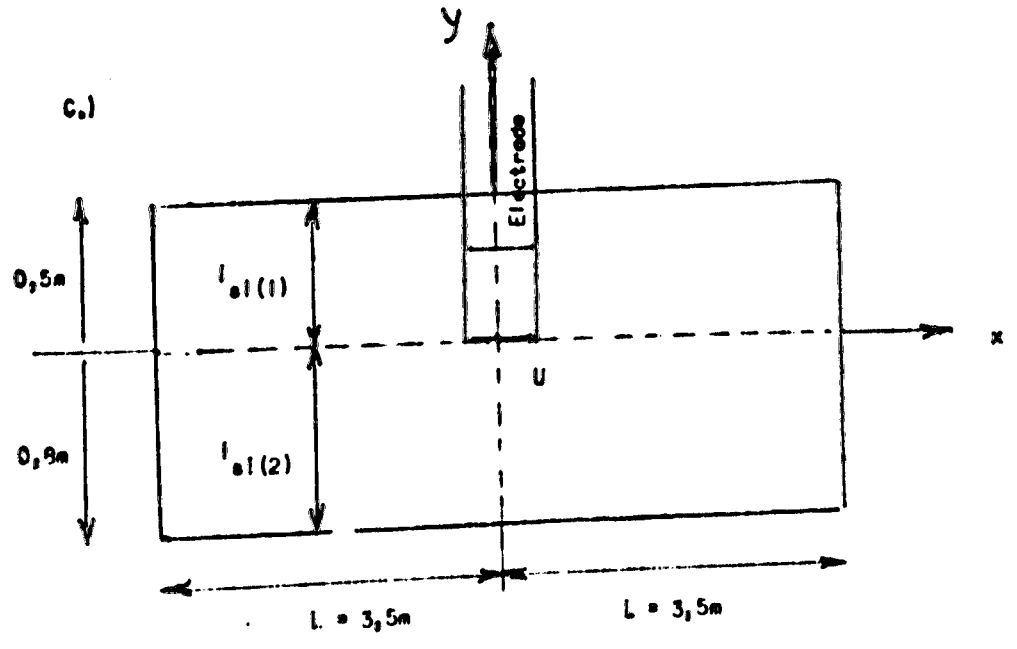

Thus in the sense of equations 16, 17 and 18 we can write

$$P_v = P_{v(a)} + \Delta P_v K_o(r\sqrt{\sigma}) \qquad 20./$$

that is $$P_v = P_{v(a)} + \Delta P_v K_o(x) \qquad 21./$$

and $$P_{v(x)} = \Delta P_v K_o(x) \qquad 22./$$

Here ΔP_v stands for the volumetric energy difference between the electrode surface and the lowest energy face at the perimeter of the active area (or reaction zone) of the electrode.

4./ Two-dimensional heat flow model. Temperature distribution in the cross section of the rectangular furnace: Ritz and Kantorovich profiles.

As a supplement to the foregoing considerations pertinent to linear heat flow in one direction, either in the x or y plane of the coordinate system, the possibility of extending the simple one-dimensional heat flow concept into a two-dimensional model will be discussed in the following. In the analysis the electric furnace is regarded as a rectangular duct of unit length with constant energy generation in the slag. The cross sectional area is in the vertical plane cutting through the centre line of an electrode. Figure IV-12a gives the basic outline of the two-dimensional heat flow model. (This "lumped system" can be regarded in terms of a differential system as shown in figure IV-12b.). On applying the first law of thermodynamics to the differential system

$$-\frac{\partial q_x}{\partial x} + \frac{\partial q_z}{\partial y} + U = 0 \qquad 23./$$

where U stands for constant energy generation. By Fourier's law for isotropic media

$$q_x = -k\frac{\partial T}{\partial x}; \qquad q_y = -k\frac{\partial T}{\partial y} \qquad 24./$$

Substituting these into equation 23 and noting that k is a constant we obtain

$$\frac{\partial^2 T}{\partial x^2} + \frac{\partial^2 T}{\partial y^2} + \frac{U}{k} = 0 \qquad 25./$$

Arpaci (11) integrated equ. 25 over the cross section of the rectangular duct as

$$\int_0^L \int_0^1 \left(\frac{\partial^2 T}{\partial x^2} + \frac{\partial^2 T}{\partial y^2} + \frac{U}{k}\right) dx\, dy = 0 \qquad 26./$$

and obtained after a lengthy and complicated manipulation the desired temperature distribution in the form of the first order Ritz profile:

Figure :V - 13 VERTICAL TEMPERATURE GRADIENT IN THE SLAG, CALCULATED BY THE RITZ AND KANTOROVICH EQUATIONS.

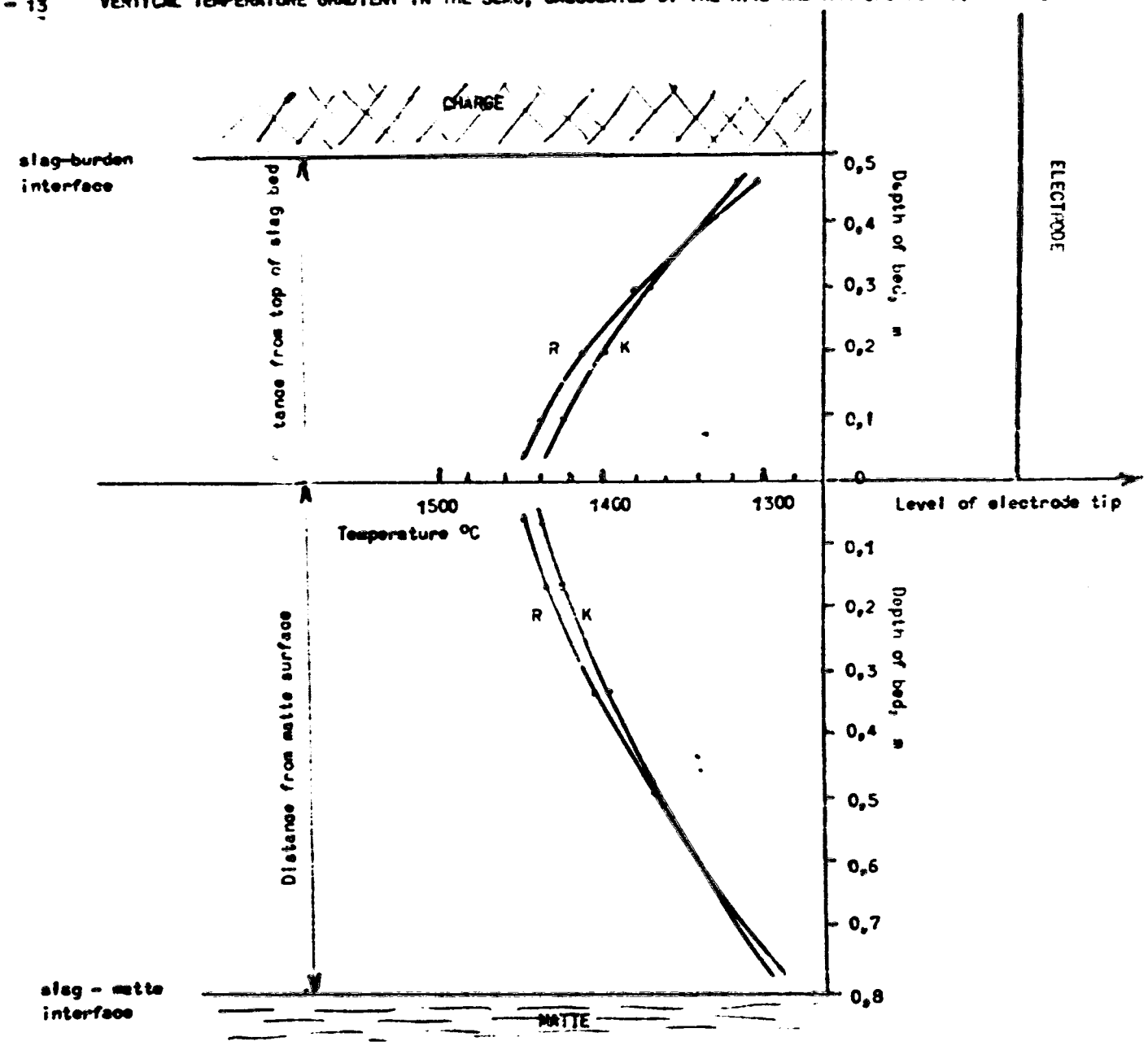

Figure IV - 14. FIRST ORDER RITZ PROFILE OF TWO-DIMENSIONAL HEAT DISTRIBUTION IN THE MOLTEN SLAG BED.

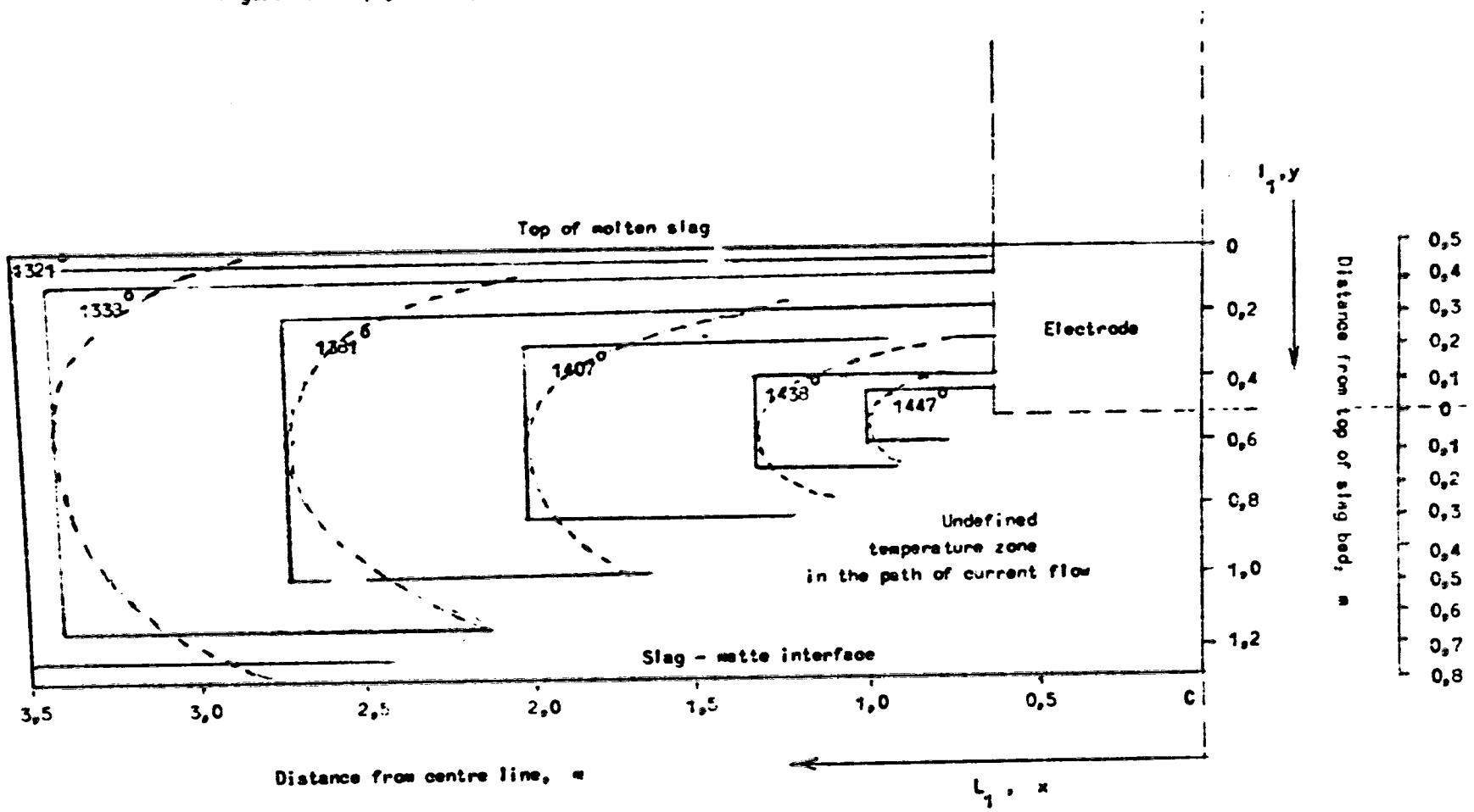

$$\frac{T(x,y) - T_{\infty}}{U\,l^2/k} = \frac{3}{4}\,\frac{\left[1 - (x/L)^2\right]\left[1 - (y/L)^2\right]}{1 + (1/L)^2} \qquad 27./$$

The first order polynomial Kantorovich profile for the temperature distribution in the system under investigation can be likewise written as

$$\frac{T(x,y) - T_{\infty}}{U\,l^2/k} = \frac{1}{2}\left[1 - \left(\frac{y}{l}\right)^2\right]\left[1 - \frac{\cosh(\sqrt{3}/l)x}{\cosh(\sqrt{3}/l)y}\right] \qquad 28./$$

At an assumed 50 cm depth of electrode immersion ($= D_e/2{,}5$) approximately equivalent to that in the reference furnaces in operation) and a total 130 cm dept of slag bed the results of calculations showing the vertical thermal profile based on both the Ritz and Kantorovich formulae is depicted in figure IV-13. The two-dimensional temperature distribution in the half - width of the furnace, based on the first order Ritz profile equation (equ. 27) is indicated in figure IV-14.). For the calculation in the direction of L (horizontal profile x) and l (vertical profile y) the conditions for the hali-width of the furnace are given as (when L = 0 at the face of the electrode):

x (m)	0,35	0,7	1,4	2,1	2,8	3,15
y (m)	0,05	0,1	0,2	0,3	0,4	0,45

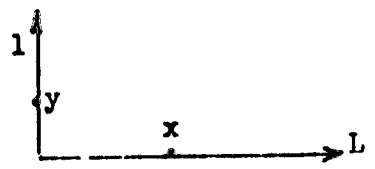

here l in vertical direction representing the distance between the top cold face of the slag bath and the plane of temperature separation at the level of the electrode tip, when the depth of immersion is 0,5 m. Thus actually l = p by earlier notation.

The squares drawn with solid lines in graph IV-14 represent the boundaries determined with the aid of equ.27 from the L-x and l-y re - lationships with x and y as chosen lengths within the horizontal L and vertical l dimensions of the furnace. Dotted lines beyond the boundaries of the squares indicate approximate temperature boundaries when the true parabolic profiles become distorted in a deformable medium by the movement of the slag as a result of buoyancy forces and electromagnetic effects. The plots are based on temperature readings obtained in operating units at a given distance from the electrode at various elevations in the slag bed (1,2).

Apparently there is a noticeable difference between the vertical temperature gradients estimated by the two methods and those obtained with formulas relating to simple linear, one-dimensional heat flow models. Numerically the estimated average slag temperature by the two-dimensional profile would be about 15°C below that found by the linear heat flow model.

Results of/...

Results of practical temperature measurements would lend support to the latter ones in relation to the particular problem investigated.

5./ The extent and character of disrupting effects acting upon the suggested temperature profile.

Because in a later section of this study the temperature profiles are intended to be used for furnace dimensioning and also as scale -up factors in furnace design, it is important to know the character and extent of effects which may be instrumental in modifying the outlined patterns of thermal distribution in the slag layer. The hydrodynamic motion of the bath is influenced by various factors from which the two most important ones, viz. the buoyancy forces caused by temperature and specific gravity differences in various parts of the bath, and the electromagnetic effects will be discussed in this paragraph.

5.1./ Estimation of natural convective currents with the use of dimensionless numbers.

The difference in temperature between the top and the bottom of the molten slag layer and, also, the horizontal and vertical temperature gradients create buoyancy forces leading to natural convection currents in the bath. This can be expressed by the Grashof number (N_{Gr}) which is the dimensionless expression of the buoyancy, inertia, and viscous forces:

$$N_{Gr} = \frac{g_c L^3 \gamma^2 \Delta T \alpha}{\eta^2} = g_c L^3 \frac{\gamma^2}{\eta^2} (T_c - T_w) \alpha \qquad 29./$$

where the subscripts denote conditions at the centre and at the walls of the furnace, and α is the expansion coefficient, in case of liquids expressed as

$$\alpha = \frac{\Delta v / \Delta T}{\bar{v}} \qquad 30./$$

$\bar{v}$ denoting average specific volume kg/m^3 or g/cm^3; γ = density, g/cm^3 ; L = characteristic length, usually unit length in meter ; g_c = gravity due to acceleration and η = viscosity. In the scope of a more detailed discussion in the next section it will be shown that the value of α for the average plant slag composition was found as $\alpha = 3{,}2 \times 10^{-4}$ causing an expansion of 14,1 per cent when the temperature of the slag increased from $20^{\circ}C$ to an average of $1400^{\circ}C$. For calculation purposes the temperature difference between electrode tip and the surface of the molten slag layer still in a fluid but highly viscous state will be $1500\text{-}1300^{\circ}C = 200^{\circ}C$. Further data to be used are: $\gamma_{1300^{\circ}} = 2{,}80\ g/cm^3$, $\gamma_{1500^{\circ}} = 2{,}72\ g/cm^3$,

η_w = 15poise η_c = 2,4 p ; $C_{psl(w)}$ = 0,3 kcal/kg; $C_{psl(c)}$ = 0,4 kcal/kg.
Then for a characteristic length of 1 meter N_{Gr} is written as

$$N_{Gr} = g_c L^3 \left(\frac{\gamma_c^2 T_c}{\eta_c} - \frac{\gamma_w^2 T_w}{\eta_w}\right) = 9,81x1x\left(\frac{2,72^2 x1500}{2,42^2} - \frac{2,8^2 x1300}{15^2}\right).3,2x10^{-4}$$

$$N_{Gr} = 61 \qquad (10^2 \text{poise} = 1\text{Nm})$$

The other important dimensionless number correlating viscosity, specific gravity and heat transfer coefficient is the Prandtl number

$$N_{Pr} = \frac{\eta C_p}{k} = \frac{\text{molecular diffusivity of momentum}}{\text{molecular diffusivity of heat}} \qquad 31./$$

for a characteristic distance of 1 meter and with C_p expressed as cal/kg mole when the mole weight of the average plant slag is calculated as 57,3 and $C_{p(1500^o)}$ = 0,4 kcal/kg, $C_{p(1300^o)}$ = 0,3 kcal/kg, then in the temperature range of 1300 to 1500°C we write

$$N_{Pr} = \frac{\left[(\eta_w C_{p(w)}) - (\eta_c C_{p(c)})\right] M_w}{k_{sl}} = \frac{\left[(15^2 x0,3)-(2,4^2 x0,4)\right] x57,3}{4,9}$$

$$N_{Pr} = 7,6x10^2$$

Jacob (12) using the Grashof and Prandtl numbers as velocity components of natural convection, defined laminar and turbulent flow regions as

$$\text{laminar} \quad 2x10^3 < N_{Gr}.N_{Pr} < 150x10^3$$

$$\text{turbulent} \quad 300x10^3 < N_{Gr}.N_{Pr} < 3x10^7$$

From the data above $N_{Gr}.N_{Pr} = 61 \times (7,6x10^2) = 4,6x10^4$

Thus the estimated value of the product of the two characteristic numbers would indicate natural convection with avg. laminar flow conditions with the type of slag produced in the electric furnaces investigated and operating conditions applied. In practice the actual distance between walls and furnace centre (say 3 m) should be taken instead of the characteristic length of 1m, accounting thus for both transverse and longitudinal currents which must be present because the sides of the bath are at the same tem - perature limit as the top. Even under these conditions the product would be $N_{Pr}.N_{Gr} = (1,23x10^3)(1,86x10^2) = 2,3x10^5$, that is the system as a whole just around the starting stage of turbulence.

Circumstances in practice, however, may differ considerably from those predicted by dimensionless relationships. For example when, due to disturbances in feeding and smelting rates, the molten slag surface instead of being covered with burden became clearly visible, a rather noticeable slag movement could be recorded in the reference furnaces. At the matte

tapping end/...

tapping end the molten slag appeared to move away radially from the electrode surface and the velocity of this movement was measured as 15 to 20 cm.sec^{-1}. With this measured velocity value the Peclet number (N_{Pe}) can be determined and thereby the ratio between convective and conductive heat transfer obtained:

$$N_{Pe} = \frac{C_p \, u \, L}{k_{sl}} = \frac{\text{heat transf. by convection}}{\text{heat transf. by conduction}} \qquad 32./$$

Using again 3m for the distance between the high and low temperature faces and expressing C_p in cal/kg mole, N_{Pe} will be calculated as

$$N_{Pe} = \frac{(0,4-0,3)57,3x2,7x0,2x3,0}{4,9} = \frac{9,5}{4,9} = 1,94$$

The computed value of N_{Pe} would indicate that the amount of heat transferred by convection is approximately twice of that moved by conduction. The result is somewhat conflicting to that obtained with the application of the Grashof and Prandtl numbers.

Apparently there is some uncertainty involved in the use of dimensionless numbers with the purpose of characterising the conditions of slag flow and too great exactness could not be expected from the results obtained. The uncertainty is caused primarily by the very great difference in the viscosities of the flow media between the temperature limits of interest, that is by the inherent physical characteristics of the slag systems.

5.2./ Bath mixing due to electromagnetic forces.

In a greatly simplified assessment of the complex nature of electromagnetic forces in bath mixing, the following model suggested by Geiger and Poirier (13) may be used to obtain an approximative estimate on the stirring action of the electrodes. For this purpose let us imagine that a flat steel plate is inserted into the slag between the electrode and the matte surface, i.e. under the electrode in the path of the current. The fluid motion exerts a drag force on both sides of the plate of steel the magnitude of which is given as

$$F_k = 2 \, f(LV)\left(\tfrac{1}{2}\gamma u_{sl}^2\right) = fLV\gamma\left(\frac{\eta^2}{L^2\gamma^2} N_{Re(sl)}^2\right) \qquad 33./$$

Here L= characteristic length in meter; V the volume of flow media involved; γ its density; $N_{Re(sl)}$ Reynolds number of slag flow, the velocity of which u_{sl} is expressed as

$$u_{sl} = \frac{\eta}{L\gamma} N_{Re(sl)}^2 \qquad 34./$$

f is the friction factor or drag coefficient

$$f = \frac{F_k}{A.e_k} \qquad 35./$$

Figure IV – 15. FRICTION FACTOR FOR FLOW PARALLEL TO FLAT PLATES.

After Vennard

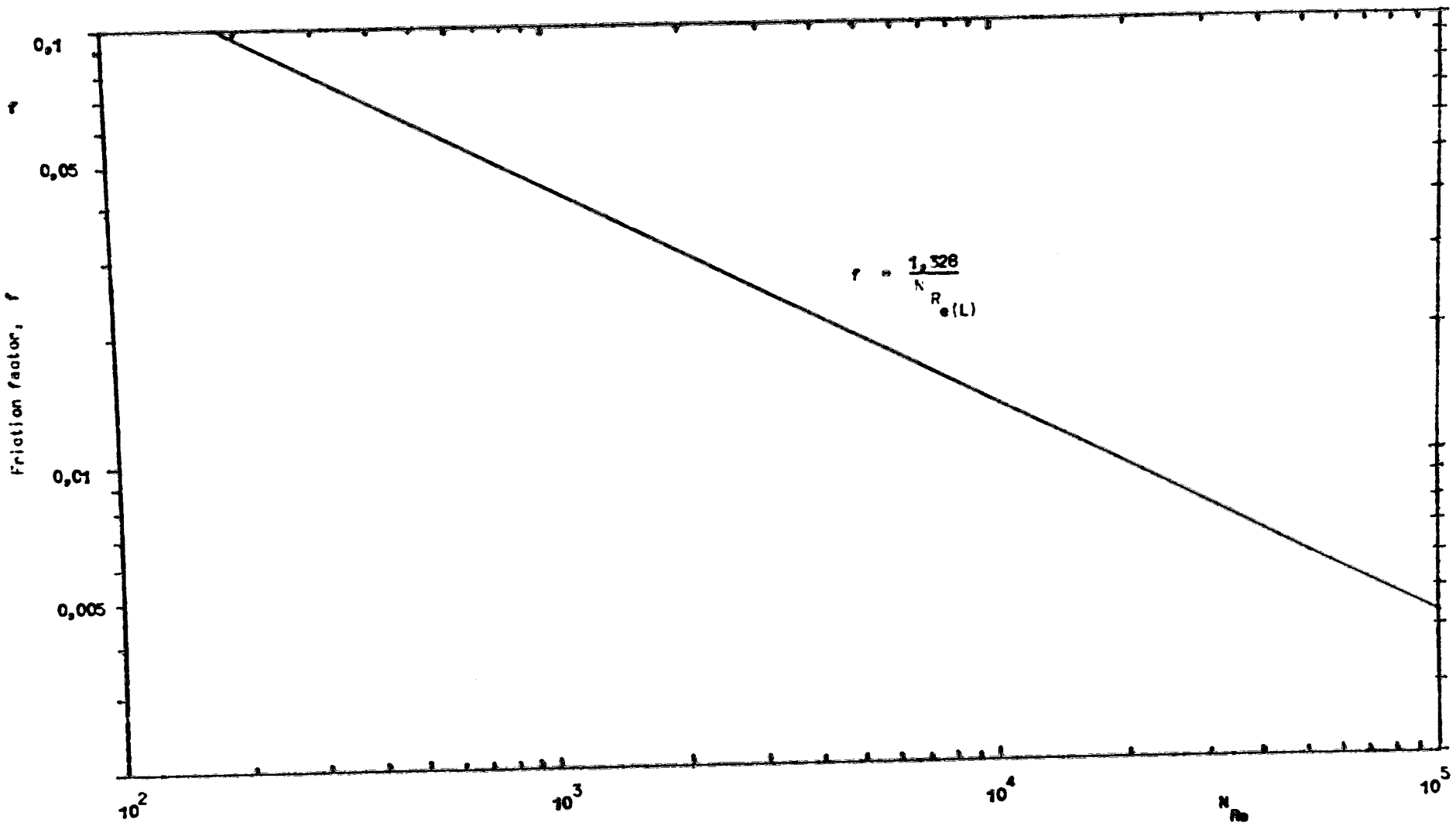

with A = characteristic area; A=V, and the characteristic kinetic energy e_k expressed

$$e_k = \tfrac{1}{2}\rho u_{sl}^2 \qquad 36./$$

The friction factor in laminar flow in terms of the Reynolds number, for a flat plate was expressed by Vennar (14) as

$$f = 1{,}328\, N_{Re}^{-\frac{1}{2}} \qquad 37./$$

The corresponding relationship between friction factor and N_{Re} is shown in graph IV-15.) indicating that the laminar region may extend up to about $N_{Re} = 10^6$.

The velocity of slag is calculated with the aid of equ. 34 by taking various N_{Re} values for the flow system in the vicinity of the electrode and in the path of the current. Let a temperature of 1400°C be chosen for the illustration of the mode of calculation. $N_{Re} = 10^3$ and the characteristic length 1 meter, then

$$u_{sl} = \frac{\eta}{L\rho} N_{Re} = \frac{3{,}4}{1x2{,}8} x10^3 = 1215\ m.hr^{-1} = 0{,}337\ cm.sec^{-1}$$

To calculate now F_k from equ.33 : the value of the friction factor at $N_{Re}=10^3$ from figure IV-15 is given as f = 0,44; in noting that V = $1m^3$ = 1000 dm^3 (since ρ is given in kg/dm^3)

$$F_k = fLV\rho\left(\frac{\eta^2}{L^2\rho^2} N_{Re(sl)}^2\right) = 0{,}044x1x(1x10^3)x2{,}8\,\frac{3{,}4^2}{1x2{,}8^2} x\,(10^3)^2 =$$

$$= 1{,}83x10^8\ kg.m.hr^{-1} = 5{,}07x10^4\ kg.m.sec^{-1}$$

Since 1 HP = 75 $m.kg.sec^{-1}$ therefore F_k = 67,6 HP = 50,7 kW/m^2 surface. Calculated values in the range of $N_{Re} = 5x10^2$ and $5x10^3$ are compiled in the table below

N_{Re}	f	u_{sl} $m.sec^{-1}$	F_k $kg.m.sec^{-1}$	HP per m^2 slag surface per electrode	kW
$5x10^2$	0,088	0,168	$2{,}54x10^4$	34	25,4
10^3	0,044	0,337	$5{,}07x10^4$	68	51

Mention was made earlier of the movement of slag observed on the surface of the bath in radial direction from the electrode, the velocity of which was measured as 0,15 to 0,2 $m.sec^{-1}$. From the data of the table in the range of Reynolds numbers characteristic to laminar flow, the mechanical work or electrical energy involved in the slag movement is rather substantial. Under the conditions of operation of the reference furnaces the expended electrical energy may vary between 25 and 50 kW per m^2 slag surface per electrode and the mixing action associated with it is rather more significant than could

be expected/...

be attributed to buoyancy forces. It would therefore appear that the action of the electrodes manifested in the form of electromagnetic forces is one of the main factors responsible for the mixing of the slag bath and thereby also for the modification of the steady state conditions assumed for the various heat flow models.

5.3/ Main factors in bath mixing.

From a practical furnace operation point of view the part played by both buoyancy and electromagnetic forces in modifying heat and material flow patterns although significant, it may still be regarded as comparatively moderate to the role of further two factors: a./ fluctuations in the flow of feed material added to the furnace and b./ converter return slag. A sudden collapse of crust on top of the molten slag bath causing large amounts of solids to pour into the melt, or simply an abrupt increase in the availability of feed material after the action of the choke feeder - type charging system of rectangular furnaces are undoubtedly the most instrumental in altering slag resistivities, electrode positions and also in controlling heat and material flow in the molten slag and matte.

To this intermittent or periodic action comes the effect of con - verter return slag of similar intermittent nature. Large amounts of slag are poured into the furnace in a relatively short time and the sudden change in slag volume with the impact of the high velocity jet of the return slag will also alter, even if in the form of a brief step change, the flow characteristics of the slag and matte and will certainly cause periodic disturbances in the settling of matte. Depending on the angle of entry, part of the slag jet issuing from the launder flows downward and enters into the matte layer. In this instance the brief intermixing of converter slag and matte can be considered as beneficial in diminishing copper losses due to the reducing action of the sulphides on the converter slag. The main effect however is manifested in that the jet cone which is not impeded by the matte layer may travel a considerable distance in a short time. Themelis and Spira (15) estimated that a portion of the converter slag jet of initial velocity of 1m per second may traverse one half of the furnace length (reverberatory furnaces) in about 3 minutes.

6./ Possibilities of refining the mode of estimation of heat flow in the molten slag.

Following the simplifying assumption applied in the previous arguments that the flow of heat is effected primarily by conduction through the slag, some consideration was given to the possible extension of the mode of calculation in order to a./ increase the accuracy of the estimation and b./

b./ make it/...

Figure IV - 16. PRINCIPLES OF THE FINITE ELEMENT METHOD IN HEAT TRANSFER FOR A ONE-DIMENSIONAL TRANSIENT PROBLEM.

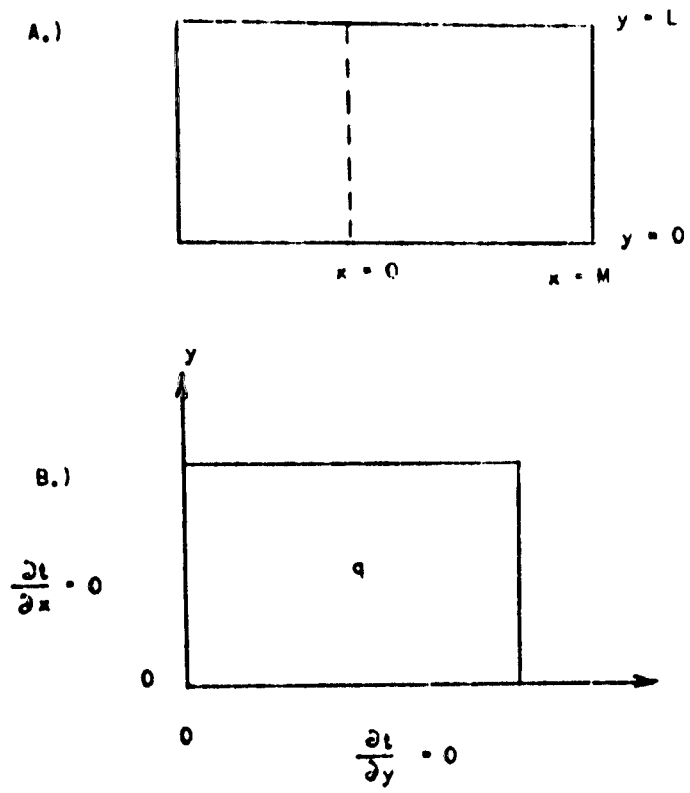

b./ make it amenable to computer processing with the use of the available computing techniques.

Such a more refined and well-known method, though still a greatly simplified one for the complex system under investigation, involves the application of either finite differences or finite elements; (16); that is 1./ subdivision of the region under investigation into a finite number of small sections (nodal system) see figure IV-16.

2./ minimisation of a function over the space coordinate, say in a one dimensional transient problem a single integral of the form

$$I = \int_{x=0}^{L} F(x, \Theta, u, u_x, u_\Theta)dx \qquad 38./$$

The integral is minimised at every point in time to obtain relationship between the nodal temperatures and the time-derivatives leading to a system of ordinary differential equations,

3./ simultaneous solution of the equations in matrix representation, the input data to the computer consisting of nodal coordinate information pertaining to slag characteristics e.g. as $/i,/x_i/(e)/i,j/k\,\rho\,C_p/$, where (e) denotes the element.

The numerical application of this method in a more likely unsteady state system of electric furnace slags did not bring about any improvement or offered any advantage whatsoever above the simple methods discussed, mainly because a./ the demarcation of the nodal points is fortuitious and could represent actual positions only for extremely short time intervals in the melt continuously in motion, b./ the computational technique is time - consuming and does not warrant on account of the uncertainties inherent in the present instance in the structure of the nodal system, the expenses involved in computer application.

The ESR (Electro Slag Refining) system lends itself more readily to the game of modelling than the considerably less stable operation of the electric furnaces and, concerning the former one, a number of excellent studies appeared more recently in the literature on this topics. Since the ultimate test of any mathematical model is its ability to predict the behaviour of actual systems, it is felt that any further effort of ex - tending the calculations into the suggested, or even toward a more com - plicated line like for example that suggested by Maulvault and Elliot (Electric Furnace Proceedings, 28, 1970, 13-29) would serve no useful purpose in the present context and as such, would only be a futile theoretical exercise.

7./ Thermal stability of the slag bath

Finally, in connection with the thermal characteristics of slags

used in the smelting of copper-nickel concentrates a brief discussion of an important parameter in the control of the smelting operation, i.e. the thermal stability of the slag bath will offer further insight into, and facilitate the evaluation of the slags produced.

The temperature of the slag, in addition to the resistivity, is governed by the current density across the slag bath. Therefore a non-uniform distribution of current will result in hotter and cooler regions in the slag. It is therefore of interest to have some mode of estimation of the probable changes in temperature with the change of current. For this purpose let us consider in accord with the suggestion of Kazemensky and co-workers (17) a parallelepiped microvolume of the slag bath being embedded into the flow line of the electric current. At steady state conditions, that is in the close vicinity of the geometric body, all the heat generated by the current-flow in a period of $d\Theta$ is equal to the heat losses from the micro-volume. Now suppose that the instantaneous current intensity changes by ΔI. If the heat loss from the micro-volume under steady state conditions is

$$Q_{loss} = 0,24\ I^2 R d\Theta \qquad 39./$$

and the change of current will bring about a change in the temperature of the micro-volume

$$dQ = Q_{mv} - Q_{loss} = m\ C_{p(sl)} dt^o \qquad 40./$$

where Q_{mw} is the heat contained in the micro-body and $C_{p(sl)}$ is the specific heat of slag, then

$$0,24(I + \Delta I)^2 R d\Theta = 0,24 I^2 R d\Theta = m C_{p(sl)} dt^o \qquad 41./$$

and

$$\frac{dt^o}{d\Theta} = 0,24\ I(\Delta I \pm 2I)\ \frac{R}{m C_{p(sl)}} \qquad 42./$$

where Θ = time. Let d_{cp} be the average diameter of the current path of finite length l, ρ = the specific resistivity in ohm.cm and γ the density of slag in g/cm^3, then since

$$R = \rho \frac{l}{d_{cp}} \quad \text{and} \quad m = l\ d_{cp} \gamma \qquad 43./$$

therefore

$$\frac{dt^o}{d\Theta} = \frac{0,24\rho}{\gamma C_{p(sl)}} \cdot \Delta i(\Delta i \pm 2i) \qquad 44./$$

here i = current density amp/cm^2 at steady state conditions and Δi is the changed current density. Now with the conditions obtaining in the reference furnaces with γ = 2,8 g/cm^3, ρ = 4,2-4,7 ohm.cm, $C_{p(sl)}$ = 0,35 kgcal/kg at $\bar{t}$ = 1400°C

$$\frac{dt}{d\Theta} = \frac{0,24 \times 4,45}{2,8 \times 0,35} = 1,10 \Delta i(\Delta i + 2i)$$

At the operating current of 18,5 kA, electrode diameter of 1,25m and in close proximity to the electrode tip where the cross-sectional area of current path

can be/...

can be assumed to be equal to that of the electrode, i.e. 1,23 m^2, the current density in the path of electrical conduction will be 18500/12300 = =i = 1,5 A/cm^2. On assuming a 5% variation inoperating current that is ΔI = 925 amp and Δi = 925/18500x1,5 = $7,5x10^{-2}$ amp/cm^2, then for $dt^o/d\Theta$ we get

$$\frac{dt^o}{d\Theta} = 1,10x0,075(0,075 + 2x1,5) = 2,6x10^{-1}\,{}^oC.sec^{-1}$$

This would indicate that fluctuations up to 5% in the current for a short duration of seconds only, do not affect the prosess of smelting. These changes could not be regarded as infrequent in practical operation of some plants due to excessive fluctuations in supply voltage on the furnace transformer primaries. Even cycles lasting for 1 minute with 5% variations in current, the change in slag temperature would not amount to more than about 16°C which, in any case, would be absorbed by the large mass of slag. Consequently, the physico-chemical characteristics appear to provide a good thermal stability to the slag produced in the process of smelting copper-nickel concentrates in the reference furnaces.

The thermal stability of the slag secures uniform snd balanced operation to the furnace, therefore it is an important factor among the control parameters of the unit. Thermal conditions within the furnace are governed basically by the properties of the slag, that is by its specific resistivity, specific heat and density and all these, in turn, depend on composition. Further calculations indicated that an anticipated increase of the FeO content to 28 per cent and of the MgO to about 22 per cent would not affect significantly the thermal stability of the slag.

* * *

Table IV - 2.

Densities of synthetic slags, plant slags and electric furnace matte

Slag number	Density at room temperature	Density at 1400°C extrapolated $\gamma_{20°C}-(0,141x\,\gamma_{20°C})$
Synthetic slags		
1	3,124	2,684
2	3,141	2,698
3	3,245	2,788
4	3,171	2,724
5	3,180	2,732
6	3,254	2,795
7	3,106	2,668
8	3,085	2,650
9	3,073	2,640
10	3,342	2,871
11	3,068	2,635
12	3,473	2,983
13	3,331	2,861
14	3,169	2,722
Plant slags		
	3,15 - .	2,760
Matte		
	4,68 - 4,73	3,770

II. ON CERTAIN ASPECTS OF THE FLOW OF MATERIAL IN THE ELECTRIC FURNACE

The knowledge of the flow characteristics of slag and matte in the electric furnace is of great importance because the molten slag bed acts as a./ a heating medium for the matte and b./ as a carrier, that is the settling medium of the molten matte droplets released from the concentrate. In this way it plays a decisive role in the whole economy of the furnace.

From the previous discussion of heat distribution in the slag bed it will be obvious that the pattern of material flow as a function of the flow of heat is rather complicated. In the following part of this section certain aspects of the movement of the molten media will be considered in conjunction with results obtained in laboratory investigations. The main parameters affecting the correct dimensioning of the furnace, apart from the distribution of heat, are the settling rate and the size of the matte particles. The function of these will be handled in the first part of this section regarding the flow of the carrying medium, in order to simplify the problem, as truly laminar. In the second part the flow of the slag will be discussed in the light of the heat and viscosity distribution in the molten bed, as a continuation of the line of thought that has been followed in the previous scetion. The discussion of the problem will be focussed only on the movement of slag since the flow of matte, due to intermittent matte tapping with considerable stagnancy and its periodic contribution to the general flow pattern of the slag could not be regarded as too significant.

1./ The settling of matte particles through the slag.

The settling velocity of the molten matte particles was estimated by Stokes' law expressed as

$$u_m = \frac{2\, r^2 g_c (\gamma_m - \gamma_{sl})}{9\eta} \text{ cm.sec}^{-1} \qquad 45./$$

where r = radius of matte prills, g_c = acceleration due to gravity and γ_m and γ_{sl} = specific gravities of matte and slag respectively in g/cm^3, η = viscosity of slag in poise. The settling velocity is thus higher the greater the value of r and $\Delta\gamma$ and the smaller the value of η. Obviously, in the expression r, as a quadratic term has the strongest influence.

To enable an estimate of the settling velocities to be made, the densities of both synthetic and electric furnace slags as well as matte samples were determined using the conventional picnometric method. The results are compiled in Table IV-2. The actual densities obtaining at the operating temperature of the furnace (taken as an average of 1400°C) were

estimated/ ...

Figure IV - 17. DENSITY OF MELTS IN THE SYSTEM $CaO-FeO-Fe_2O_3-SiO_2$ at 1600 °C.
(after H.G. Schubert)

Legend Weight per cent SiO_2: 1 34%
2 39
3 44

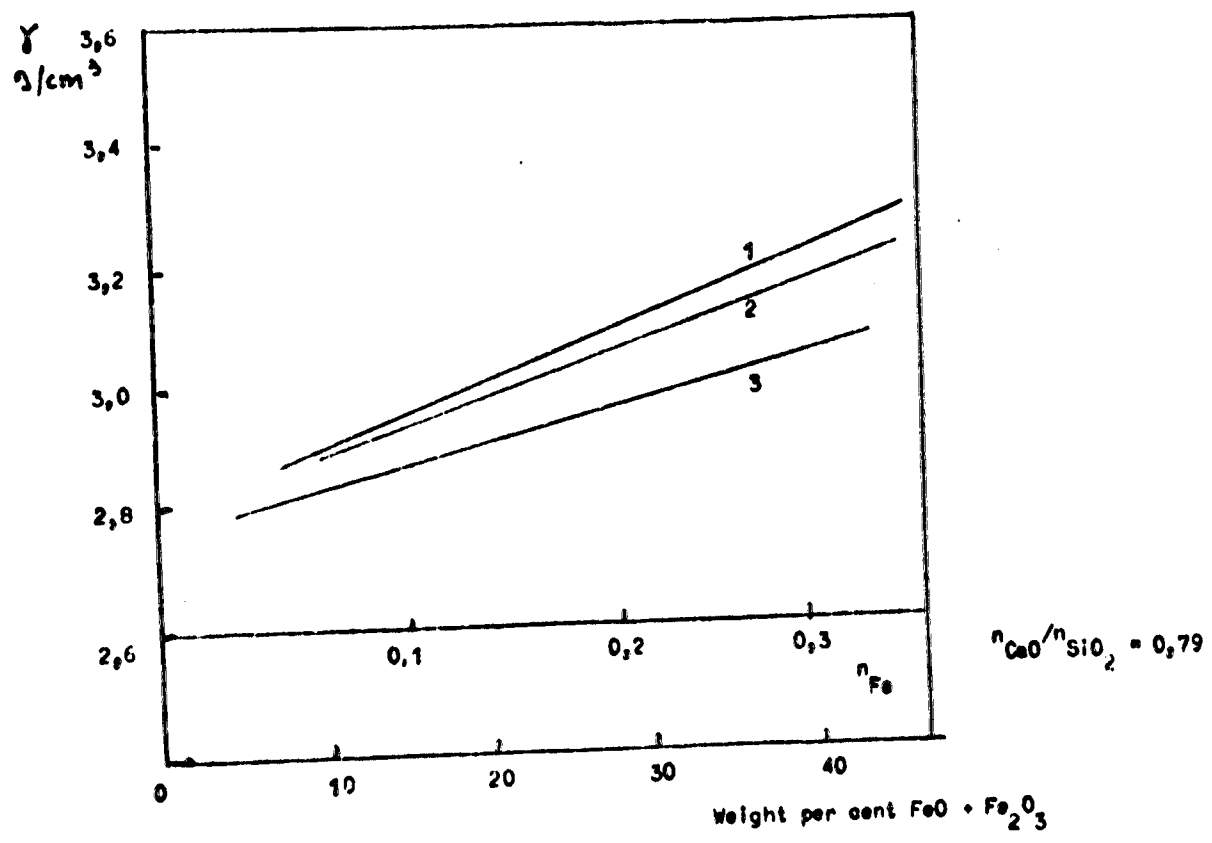

Figure IV - 18. SPECIFIC GRAVITY OF MATTE AS A FUNCTION OF COPPER CONTENT AND TEMPERATURE.

(after Johannsen and Wiese)

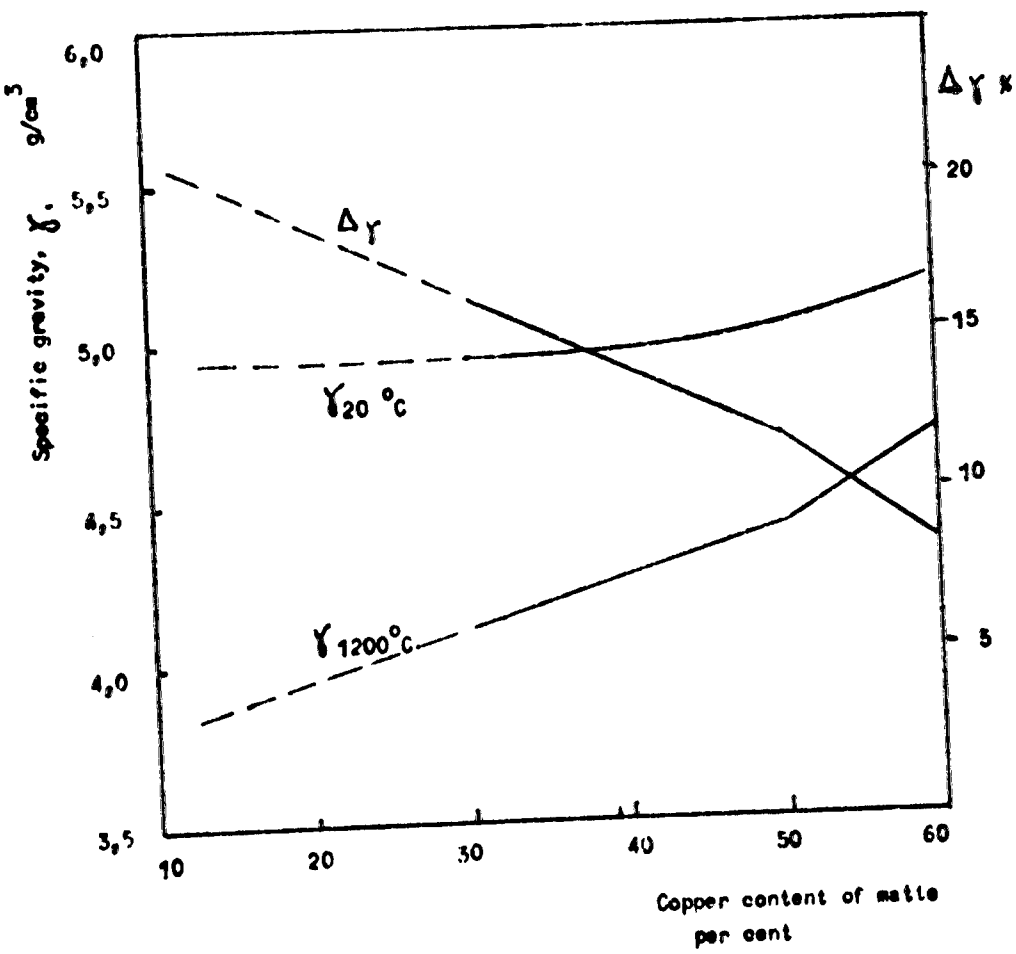

estimated from the basic values using data available in the literature relating to measurements carried out on molten slags of similar composition, or at least, of comparable behaviour. Unfortunately, data of these types of investigations are rather scarce and, pertinent to the quinnary system of this study, simply non-existent. The best sources found were based on the systems $CaO-FeO-SiO_2$, (18), $CaO-Al_2O_3-SiO_2$ (19), $Al_2O_3-MgO-SiO_2$ (20), then for comparison purposes certain binary and ternary silicates (21). In the knowledge of the expansion coefficient of the material the density can be calculated at any temperature between ambient and the temperature of operation f om the corresponding expansion

$$\alpha = \frac{1}{v}\left(\frac{\partial v}{\partial T}\right)_p \qquad 46./$$

thus the volume at temperature will be

$$v_t = v_o\left[1 + \alpha(t - t_o)\right] \qquad 47./$$

and the density

$$\gamma_t = \gamma_o\left[1 + \alpha(t - t_o)\right] \qquad 48./$$

The difference between the expansion coefficients calculated for the various systems was very great varying between $0,5x10^{-4}$ and $4,5x10^{-4}$ $cm^3/°C$. By careful interpolation of all literature data a value of $\alpha = 3,2x10^{-4}/°C$ was found to represent best the quinnary system under study from which the expansion from 20°C to 1400°C in case of plant slags with their average density of 3,20 g/cm^3 at ambient will be

$$\gamma_{1400^o} = 3,20-(1400-20)x3,2x10^4 = 2,76\ g/cm^3$$

that is about 14,1 per cent. Lime-silica melts containing iron oxide were studied by Schubert (22). His findings are partly reproduced for comparison in figure IV-17.) for $FeO-Fe_2O_3-CaO-SiO_2$ systems. As will be seen from the graph in the range of iron oxide contained in the quinnary system of this study $CaO-MgO-FeO_x-SiO_2-Al_2O_3$, the specific gravity of slags varied between 2,8 and 3,0 g/cm^3 at the temperature of concern to the present work.

The specific gravity of matte as a function of copper content was examined by Johannsen and Wiese (18). Their values are extrapolated for lower metallic contents and plotted in figure IV-18.), allowance being made here for the difference in specific gravities of copper and nickel contained in the electric furnace matte, with the total metallics taken as 28 per cent. The specific gravity at room temperature was found to vary from 4,68 to 4,73 g/cm^3 with an average value of 4,70. From figure IV-18.) at 28 per cent metallics α = 17 per cent and with extrapolation from 1200°C to 1400°C the density of matte $\gamma_{matte} = 3,77\ g/cm^3$. Thus $\Delta\gamma = (\gamma_M - \gamma_{Sl})_{1400^o} = 1,00$. (at 1250°C the specific gravity of matte would be 3,85 g/cc.). With the aid of this value/...

Figure IV - 19. MATTE DRILL SIZE - SETTLING VELOCITY - VISCOSITY RELATIONSHIP BASED ON STOKES' LAW.

$(\Delta\gamma = 1)$

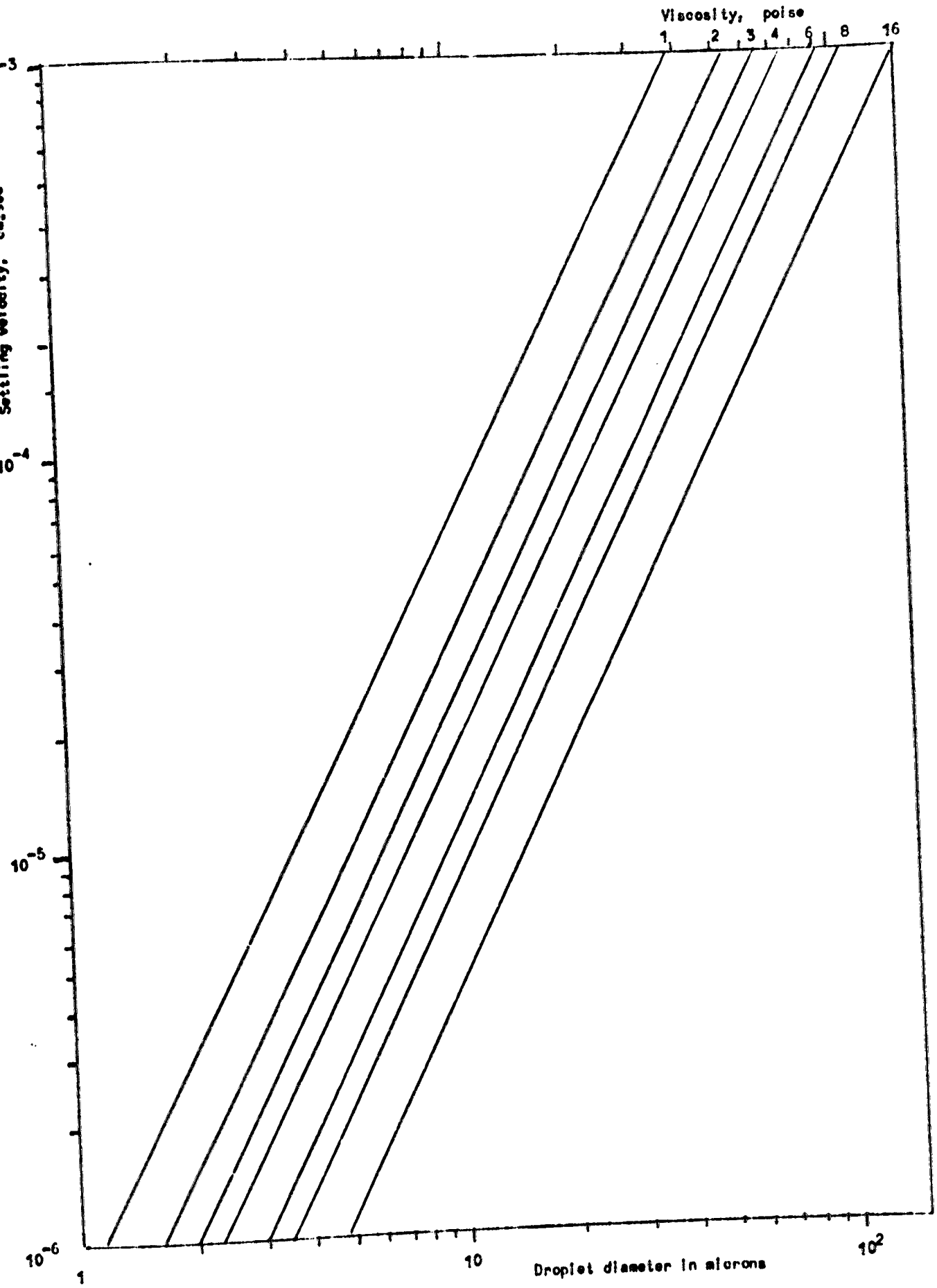

Figure IV - 19a MATTE PRILL SIZE - SETTLING VELOCITY - VISCOSITY RELATIONSHIP BASED ON STOKES' LAW.

$(\Delta\gamma = 1)$

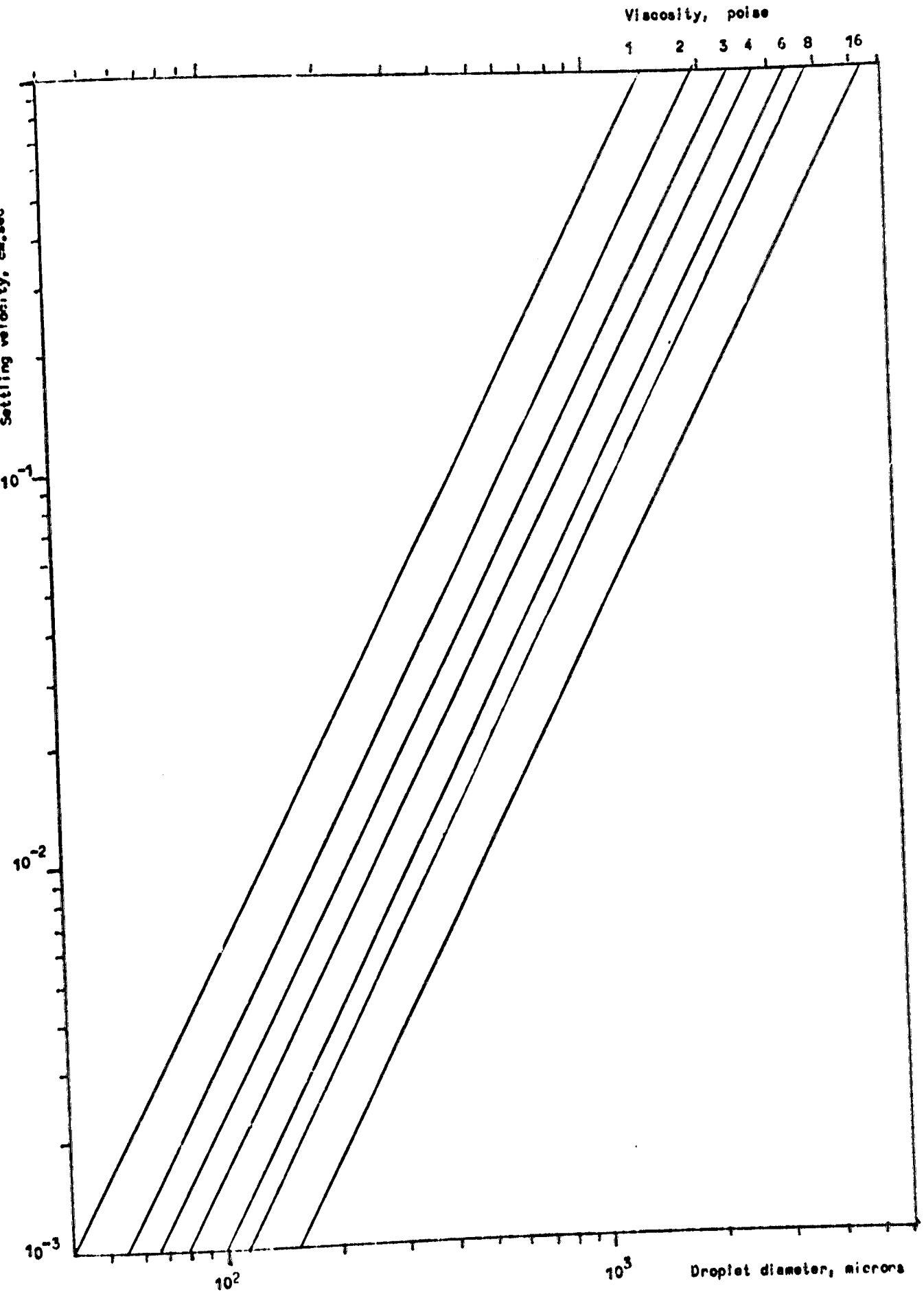

Figure V-30

A./ Arrangement of reactors.

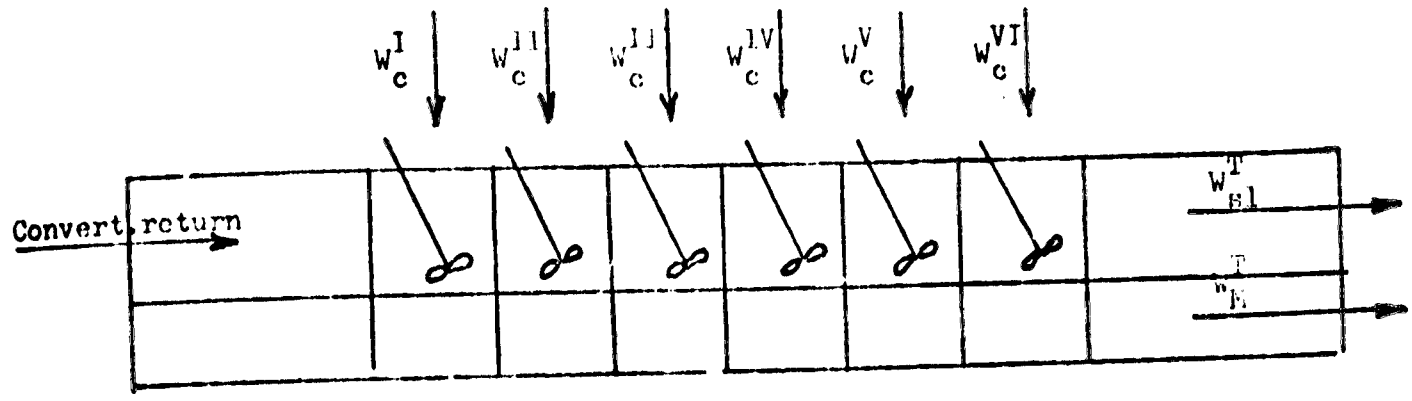

B./ Conditions for dimensioning of settler.

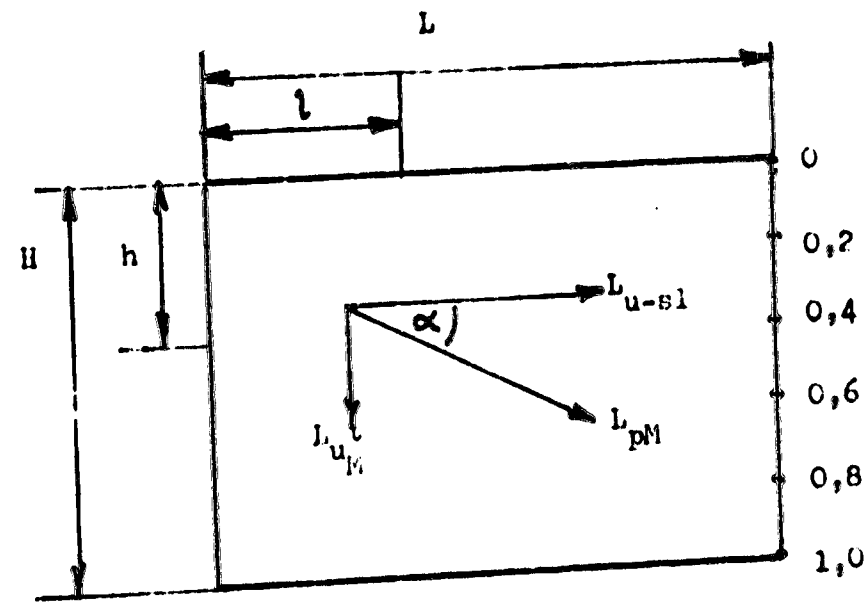

of this value the settling velocity of the matte particles was calculated using Stokes' equation for droplet diameters of 1 to 10^6 microns in the viscosity range of 1 to 16 poise. The results are given in figures IV-19 and 19a.). From the graphs it will be apparent that a matte droplet of 1 mm diameter at a slag viscosity of 2 poise has a settling velocity of approximately 0,25 $cm.sec^{-1}$, whereas a particle of 0,1 mm diameter will settle only at a velocity of 0,0025 $cm.sec^{-1}$. On the other hand a 1 mm dia. droplet at a slag viscosity of 1 poise settles at 0,6 $cm.sec^{-1}$ velocity but at 8 poise the settling velocity is 0,07 $cm.sec^{-1}$.

By virtue of hydrodynamics the effect of the liquid upon a settling particle is such that it tends to reduce the acceleration due to gravity by a certain factor. A sphere falling under gravity will have forces acting on it mg downward and m'g upward and a resistance $\frac{1}{2}$ m'(du/dΘ) upwards; here m=mass of sphere, m'=mass of liquid displaced by sphere and Θ time. The equation of motion of sphere is (23)

$$mg - m'g - \tfrac{1}{2}\, m'(du/d\Theta) = m(du/d\Theta) \qquad 49./$$

therefore the acceleration is

$$\text{if } \gamma_M > \gamma_{sl} \qquad \frac{du}{d\Theta} = \frac{m - m'}{m + \frac{1}{2}m'} g_c = \frac{\gamma_M - \gamma_{sl}}{\gamma_M + \frac{1}{2}\gamma_{sl}} g_c \qquad 50./$$

Then with the physical characteristics of slag and matte investigated, at an average operating temperature of 1400°C

$$\frac{du}{d\Theta} = \frac{3,8-2,8}{3,8+\frac{1}{2}(2,8)}\, 9,81 = 1,89\ kg.m.sec^{-1} = 1,89\times10^{-5}\ g.cm,sec^{-1}$$

2./ Settler dimension and matte particle carry-over with the slag.

In the knowledge of the settling velocity of matte particles estimated from Stokes' law an attempt is made now to formulate a quantitative re - lationship between matte settling rate, particle size and location of tap - holes which eventually will enable the estimation of the approximate di - mensions required for a settler to separate effectively matte prills from slags of given character under specified conditions. In order to achieve this we will consider the furnace as consisting of six reactors of the back- mix type arranged in series with regard to material flow but operating in parallel by receiving equal weights of concentrate feed and producing equal weights of slag and matte. An unstirred settling compartment is attached to the end of the series as shown in figure IV-20A.

Since theoretically/...

Since, theoretically (!) each reactor receives the same amount of concentrate + flux, the weight of the feed (W_c) from reactor to reactor

$$W_c^I = W_c^{II} = \ldots = W_c^{IV} = W_c^{VI} \qquad 51./$$

Under optimum conditions there is no slag loss in the system as a whole, that is the total amount of slag represented by the concentrate (W_{sl}^c) will be discharged (W_{sl}^{disch})

$$W_{sl}^c = W_{sl}^{disch.} \qquad 52./$$

The slag is withdrawn continuously, that is Input = Output, while the matte intermittently, i.e. Input - Accumulation = Output in tap-to-tap cycles.

Let u_{sl} denote the velocity of slag moving in the bed and u_M^t the free-falling (terminal) velocity of matte particles. Then the length of path travelled by the matte prills (L_{pM}) is represented by the relation of these two velocities as

$$\frac{u_M^t}{u_{sl}} = \left(\frac{dL}{d\theta}\right)_M^t \Big/ \left(\frac{dL}{d\theta}\right)_{sl} = \frac{L_{u-M}^t}{L_{u-sl}} \qquad 53./$$

and

$$L_{pM} = L_{u-sl}/\cos\alpha$$

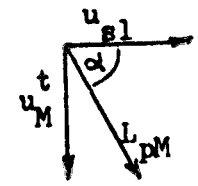

Because the velocity of slag flow u_{sl} is constant and because for a given particle diameter its terminal velocity, u_M^t is const t, α will be also constant for these conditions. Consequently, L_{pM} changes in the proportion L_{u-M}^t/L_{u-sl} that is the distance stipulated by the velocity of slag flow and the terminal velocity of the free-falling matte particles. Further to the role of α we can write

$$\alpha < 45^o \quad \text{then} \quad u_{sl} > u_M^t$$
$$\alpha = 45^o \qquad u_{sl} = u_M^t$$
$$\alpha > 45^o \qquad u_{sl} < u_M^t$$

From these considerations the effect of the dimensions of the settling unit becomes immediately obvious. Let figure IV-20B illustrate the dimensional relationships. As will be seen in the graph, the matte particle released from the concentrate in the course of smelting at any length (ℓ) in the total length of L will travel a distance set by α in terms of $L - \ell/L$, or in case of unit length of settler $1 - \ell$. Thus there is a terminal value below which all the particles will enter the second reactor. This terminal value at a constant α is fixed by the proportion of H/h, i.e. the distance between the taphole and slag level and the total depth of slag. It is also clear that the carry-over factor is maximum when $\ell = L$ in which case all the particles

released at/...

Figure IV- 21. RATE OF MATTE SETTLING AS A FUNCTION OF TAPHOLE LOCATION — — — AND MATTE PARTICLE SIZE.

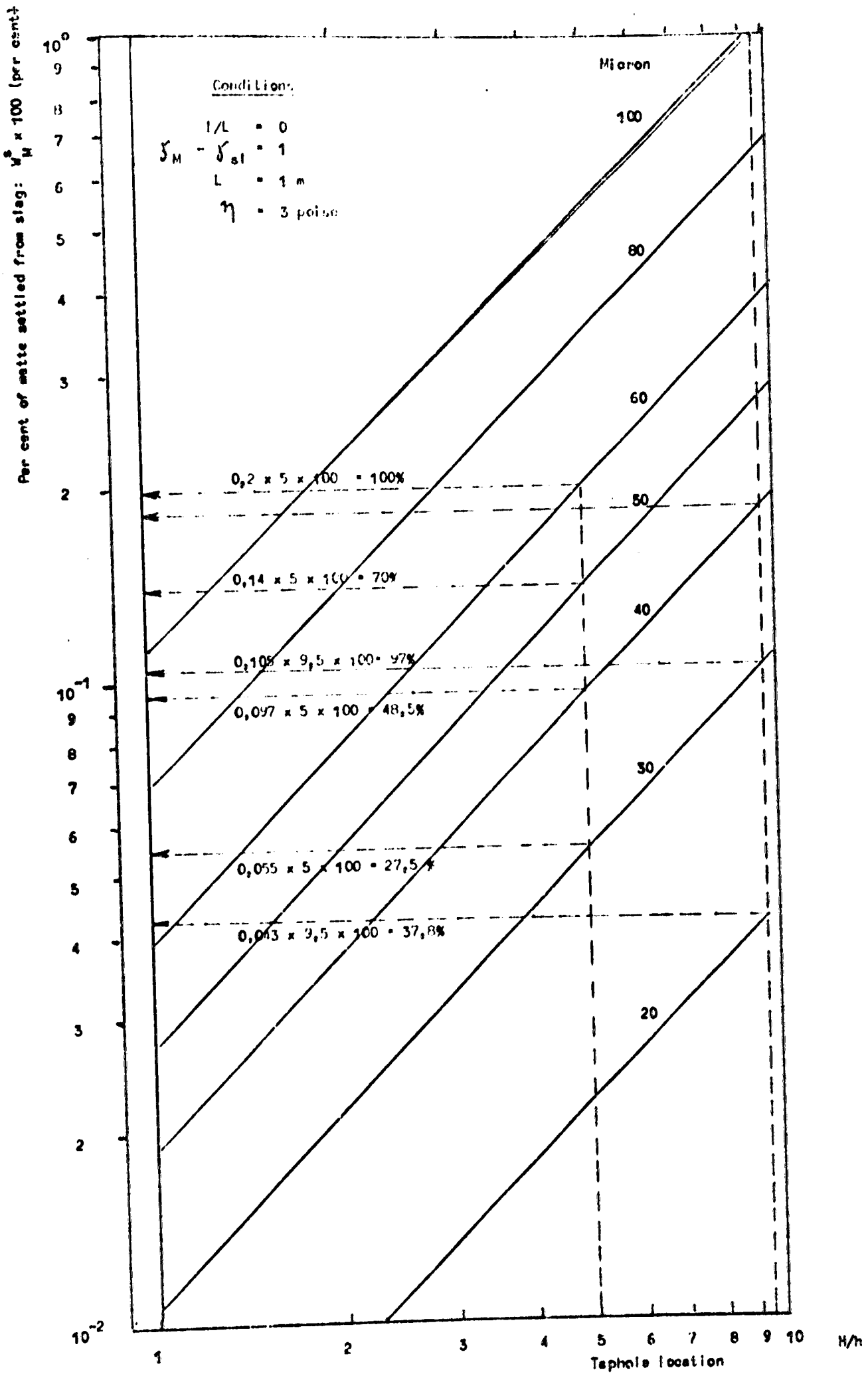

Table IV-3

A./ Terminal velocity of matte particles

Particle size in microns	10	20	30	40	50	60	80	100	150
Viscosity poise	TERMINAL velocity. $cm.sec^{-1}$								
2	$3,5x10^{-5}$	$1,4x10^{-4}$	$3,1x10^{-4}$	$5,5x10^{-4}$	$8,3x10^{-4}$	$1,2x10^{-3}$	$2,1x10^{-3}$	$3,2x10^{-3}$	$7,1x10^{-3}$
3	2,4	$9,0x10^{-5}$	2,1	3,8	5,7	$8,1x10^{-4}$	1,4	2,2	4,8
4	1,8	6,8	1,6	2,5	4,4	6,1	1,05	1,6	3,6
5	1,4	5,5	1,25	2,25	3,5	4,8	$8,6x10^{-4}$	1,3	2,9

B./ Calculated values of u_{Mi}^{t} / u_{sl} $\bar{u}_{sl} = 2x10^{-2}$ $cm.sec^{-1}$

2	$1,7x10^{-3}$	$7,0x10^{-3}$	$1,6x10^{-2}$	$2,2x10^{-2}$	$4,2x10^{-2}$	$6,0x10^{-2}$	$1,0x10^{-1}$	$1.6x10^{-1}$	$3,5x10^{-1}$
3	1,2	4,	1,1	1,9	2,8	4,0	$7,0x10^{-2}$	1,1	2,4
4	$9,1x10^{-4}$	3,4	$8,0x10^{-3}$	1,47	2,2	3,0	5,2	$8,7x10^{-2}$	1,8
5	7,5	2,7	6,1	1,13	1,75	2,4	4,3	6,5	1,45

Table IV-4. Weight of matte settled in unit length (1m) of the settler, as a fonction of particle size and taphole position. (W_M^s x 100 = per cent of total weight).

Average slag viscosity = 3 poise

H/h Taphole position	Particle size in microns	10	20	30	40	50	60	80	100	150
		Per cent of tctal matte weight settled, W_M^s x100 = per cent								
9,45		$1,13x10^{-2}$	$4,25x10^{-2}$	$1,01x10^{-1}$	$1,8x10^{-1}$	$2,64x10^{-1}$	$3,8x10^{-1}$	$6,6x10^{-1}$	1,04	2,26
3,88		$4,65x10^{-3}$	1,75	$4,04x10^{-2}$	$7,4x10^{-2}$	1,09	1,55	2,56	$4,04x10^{-1}$	$8,8x10^{-1}$
2,48		2,98	1,26	2,66	4,7	$6,95x10^{-2}$	$9,9x10^{-2}$	1,73	2,73	5,95
1,00		1,2	$4,5x10^{-3}$	1,07	1,9	2,8	4,0	$7,0x10^{-2}$	1,1	2,4

released at this point will be carried over to the next settling unit. In this way for the weight of settled matte we can write

$$W_M^s = \frac{u_M^t}{u_{sl}} (L - \ell/L) \frac{H}{h} \sum W_M \qquad 55./$$

where W_M^s is the settled, and $\sum W_m$ is the total released matte weight. On the other hand the terminal velocity is a function of the particle diameter and the viscosity of the slag

$$u_M^t = f(\eta, D_p)$$

expressed by the familiar Stokes equation.

There are two further factors influencing the quantity of matte settled: the coalescence factor f_c and the recycle ratio R. These arise due to the buoyancy forces acting upon the molten slag and the stirring effect of the electrodes and both act in the direction of the increase of W_M^s. Therefore in a more exact treatment they should be included in equation 55. The coalescence factor might be expressed in terms of per cent increase in the average prill size at a certain slag depth. The recycle was found to be very limited under the conditions of operation therefore, as a reasonable first approximation, it will be omitted from this analysis.

An other aspect that will have to be taken also into account is the effect of the liquid upon a settling particle. The expression for this was given by equation 50./and the velocity decrease was found as $du/d\theta = 1{,}89$ $kg.m.sec^{-1}$, thus the acceleration due to gravity is reduced by a factor of 0,193. With the inclusion of equation 50./ the complete expression for the weight of the settled matte particles of an average diameter $\bar{D}_p$ will be

$$W_M^s = \frac{\left[f_c \bar{D}_p^2 \varepsilon_c \left[(\gamma_M - \gamma_{sl})/(\gamma_M - \tfrac{1}{2}\gamma_{sl})\right]/18\eta\right]}{u_{sl}} (1 - \frac{1}{L}) \frac{H}{h} \sum W_m \qquad 56./$$

As an example of practical application to operating units Table IV-3 based on a bulk density difference of $\Delta\gamma = 1$ between the two media at the average temperature of the reference furnace slags gives A.) the terminal velocities of the matte prills by Stokes' equation at $\eta = 2$ to 5 poise and B.) the calculated values of u_M^t/u_{sl} in the same viscosity range on taking an average value $u_{sl} = 2x10^{-2}$ cm.sec^{-1} for the flow velocity of the slag in the furnaces as calculated from material balance and bed dimensi pertinent to practical operating conditions. With the use of these data and equation 56./ the values compiled in Table IV-4 could be computed. Here the average slag viscosity was taken as 3,3 poise, the total depth of the slag bed 1,32m, the location of the tapholes below the slag surface 0,14, 0,34, 0,54 and, as a hypothetical extreme, 1,32m (slag-matte interface), giving thus for H/h 9,45, 3,88, 2,48, and 1,00. Figure IV-21.) based on the data of Table IV-4 displays the/...

displays the weight per cent of settled matte particles of various size as the function of the ratio H/h pertinent to unit length (1m) of the settler. It will be obvious from the plots that for example with the length of the settling zone of the reference furnace (5m) and all matte particles released at the front of the zone, matte prills down to 40 micron (inclusive) would settle out 100 per cent (given as 0,2x5x100 from the ordinate of the graph) if the taphole were located at H/10 = 0,132m below the slag surface. On the other hand at H/h = 5, that is at a depth of 1,32/5=0,264m, the 60, 80 and 100 micron particles will settle out 100 per cent. On following the vertical dotted line from the intersection of y = 0,2 and x = 5, the various size matte particles will settle out as follows: 50μ → 0,14x5x100=70%; 40μ → 0,097x5x100=48,5%; 30μ → 0,055x5x100-27,5%; 20μ → 0,022x5x100=11,0%. If, on the other hand, the total length of the settling zone is 2m which is close to the 2,15m length of the individual reactors, at the same H/h=0,264m taphole location only the 100 micron prills would settle 100%, the 80 micron would settle as 0,35x2x100=70%, the 60 micron at 40% and the 20 micron as 4,4% only. In case of steady state conditions it would be thus possible to determine the accurate length of the settling zone in the knowledge of the size spectrum of the matte particles necessary for the most efficient separation. The average prill size, $\bar{D}_p$, for a mixed bed of a wide spectrum of particles can be most conveniently estimated by the method of Reboux(24) as

$$\bar{D}_p = \sum X\, d_p \qquad 57./$$

where X = weight fraction of d_p. Then

$$\frac{1}{\bar{D}_p} = \sum \frac{X}{d_p} \qquad 58./$$

here $d_p = \sqrt{d_1 \cdot d_2}$, that is the square root of the product of two adjacent particle diameter. Then finally

$$\bar{D}_p = \frac{1}{\sum \frac{X}{d_p}} \qquad 59./$$

Thus the average particle size below the critical size, D_p^i (all carried over) and above the critical size, D_p^s (all settled), from equation 59./ is represented as

$$D_p^i < D_d^c < D_p^s$$

that is

$$\frac{1}{\sum_{i}^{n_i} X_i/d_{pi}} \qquad D_p^c \qquad \frac{1}{\sum_{s}^{n_s} X_s/d_{ps}}$$

and the weight of matte settled expressed in terms of particle size is then

$$\left[W\right]_{(1/\sum_{n_i}^{n_s} x_s/d_{ps}} = \sum W_M - \left[W\right]_{(1/\sum_{\sigma}^{n_i} x_i/d_{pi}} \qquad 60./$$

3./ Microscopic investigation of the size and distribution of matte particles in the slag.

In the light of the foregoing discussion of particle size - matte loss relationship it is apparent that the adequate dimensioning of the settler cannot be performed without the knowledge of the size of matte particles descending in the molten slag bath during the process of smelting. In the course of their descent the bath motion may bring about coalescence between the various size matte prills released from the concentrate. The resulting increase of size will promote settling and reduce thereby the matte losses below that could be expected from the initial or "as released" size range of the particles.

While references are available on the size distribution of matte prills produced in reverberatory smelting of copper concentrates, very little has been published on the size of particles originating from electric furnace processing. On account of the difference in bath motion and temperature distribution between the two types of units it can be anticipated that the size range of the matte particles will also differ. The following experimental work was accomplished with the aim to gain an insight into a./ the actual grain size and b./ the size distribution and possibly also the extent of coalescence, if any, of the prills during their travel through the molten slag layer.

3.1./ Experimental procedure. Various series of samples were taken from the operating furnace through the matte sounding hole with the aid of a sampling probe reaching to the bottom of the furnace. The construction of the jacketed, air-cooled probe was similar to that described by Themelis (25). After withdrawing the probe, the total length of the cooled slag crust frozen unto the surface of the rod was divided into 10 cm sections, broken off from the probe and saved. Altogether 12 samples were thus obtained from one batch each re - presenting a 10 cm section of the total depth. The 10 cm sections were further subdivided into three equal parts increasing thereby the number of samples to 36.

Each sample, having an exposed surface for investigation of about 1,5 to 2 cm^2 was cast into a plastic mould and subjected to polishing first with rough, then with fine sand paper and finally surface-finished on polishing discs with fine alumina powder suspended in water serving as a

polishing agent/...

Description of photographs

No-1. Depth of sampling : 20 cm
Smaller particles: 50 to 100 microns
Larger particles : 100 to 150 microns

No-2. Spherical particles as released from concentrate
Depth of sampling : 30 cm
Smaller particles: 15 to 70 micron
Larger particles : 130 to 200 micron.

No-3. Depth of sampling : 30 cm
Large sphere of matte, 670 micron
Smaller particles : 50 to 100 micron

No-4. Depth of sampling : $10-\frac{20}{}$ cm
Dispersed small particles, 15 to 50 micron

No-5. Depth of sampling : 110 cm
Large particle in the centre 1 mm.
Coalescence

No-6. Depth of sampling : 120 cm.
Particles up to 450 micron
Evidence of coalescence in the bottom region of the slag bed.

No-7. Depth of sampling : 130 cm
Non-spherical particles
Evidence of coalescence in the bottom region of the slag bed

No-8. Depth of sampling : 30 cm
Large particles : 300 to 400 micron
Medium size " : 150 to 200 microns
Small " : 50 to 100 microns
Evidence of coalescence in the upper region of the slag bed.

Note Depth of sampling denotes the distance from the solid crust on the top of the molten slag layer.

Magnification in all photographs is 150 x

Photograph No. 1

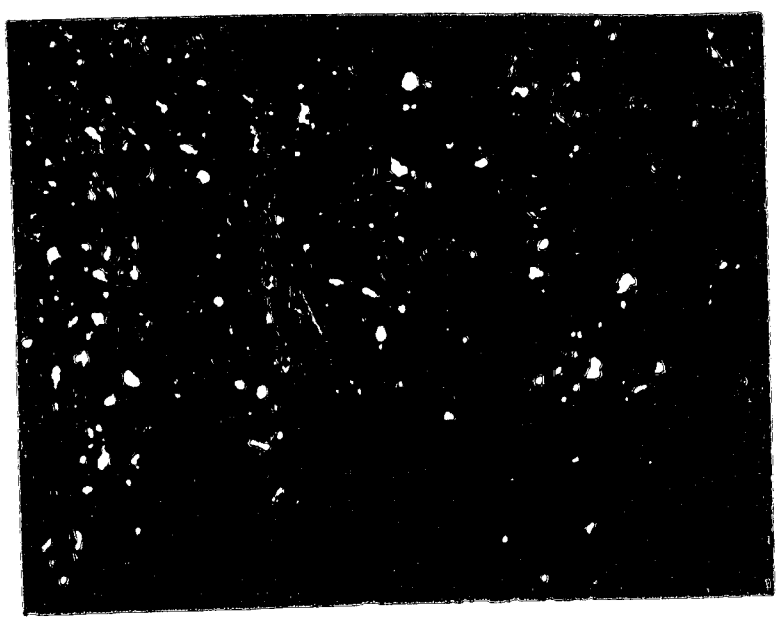

Photograph No. 2

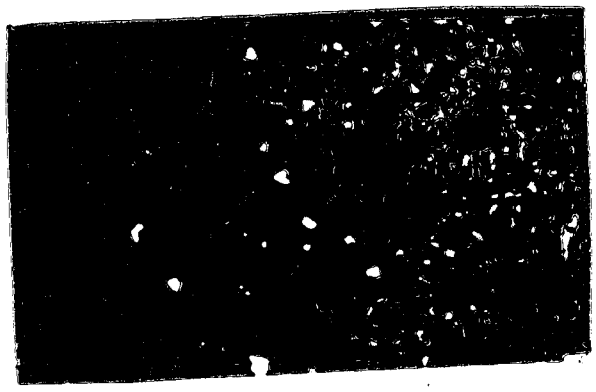

Photograph No. 3

Photograph No. 4

Photograph No. 5

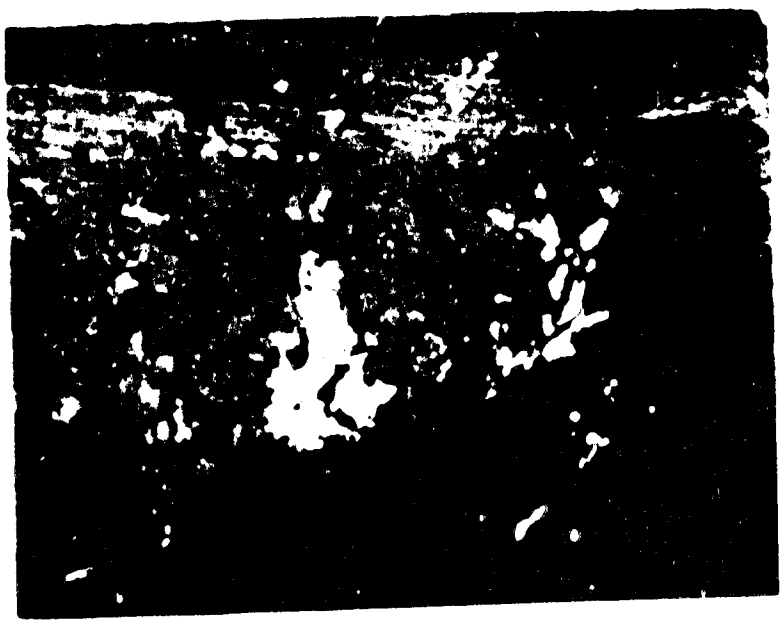

Photograph No. 6

Photograph No. 7

Photograph No. 8

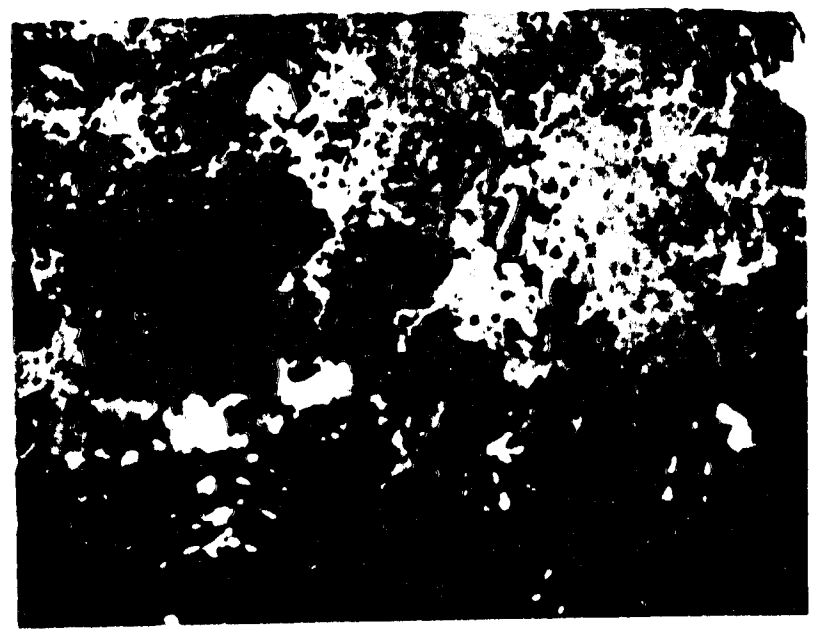

polishing agent. The polished samples were then investigated in reflected light under a Leitz metallographic microscope equipped with a polaroid camera for photographing the surfaces. The size of the grains was measured with the aid of a scale of 100 divisions etched on the surface of a glass disc which could be accommodated in one of the oculars of the microscope, 1 division representing 0,1 mm. In knowing the magnification the particle size could then be calculated.

The approximate size distribution was obtained by lengthy scanning of the surfaces and counting the number of grains of various size, that is by the familiar point count technique. Then a statistical assessment completed the procedure. A 378 times magnification was used for counting, but it proved inadequate for photography purposes due to the hazier ccntoures that resulted at this enlargement. Therefore photographs were taken with 1 lower, 150x magnification.

3.2./ Results and discussion.

a./ Particle size and size distribution. Photographs 1 to 8 taken of the samples originating from various depths of the slag bath give an indication of the dispersion of the matte prills in the slag matrix. Figure IV-22 shows the size distribution of the particles based on a given number of counts from 20 micron size upwards. The smallest size counted was 15 micron below which the information about the actual number of grains is more a result of guess-work and would be misleading in this respect to resort to the practice of extrapolation. From a practical point of view truly meaningful results can be obtained by converting the data into actual weights as represented by the various size fractions. This calculation was carried out for spherical shape, but from the photographs it is obvious that a great proportion of the particles is not necessarily spherical. This might be due to some extent to the action of the surface treatment that could have caused deformation to the friable particles. Since, however, the spherical shape appeared still predominant, this was used as a reasonable first approximation which from a statistical standpoint would not cause a too significant error. Then for example the weight of a 100 micron particle would be obtained as follows:

d_p = 0,1 mm, then volume $V=4/3\ r^3$ = $1,335 \times 3,14 \times (1,25 \times 10^{-4}) = 5,25 \times 10^{-4} mm^3$

r_p = 0,05 mm, density at 1400°C δ = $3,77\ g/cm^3$

then weight W_p = $(5,25 \times 10^{-4}) \times 3,77 = 1,97 \times 10^{-3} mg$

Number of prills counted N_p = 36

$W_p \times N_p$ = $7,1 \times 10^{-2} mg$

This calculation/...

Figure IV - 22. SIZE DISTRIBUTION OF MATTE PARTICLES IN THE SLAG DETERMINED BY POINT COUNT METHOD.

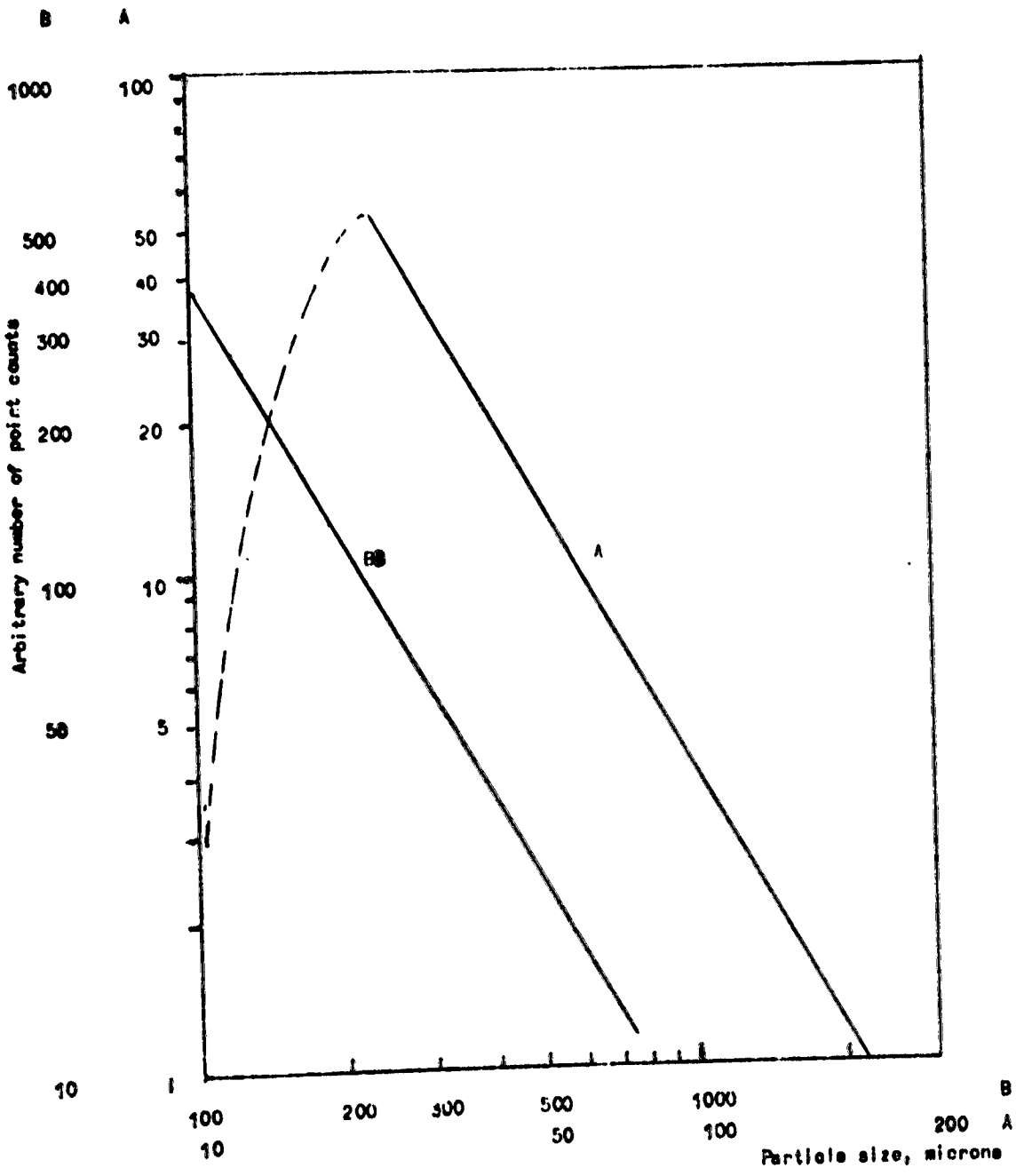

Figure IV- 23. WEIGHTS OF VARIOUS SIZE FRACTIONS AND CUMULATIVE WEIGHT INCREASE OF MATTE PARTICLES.

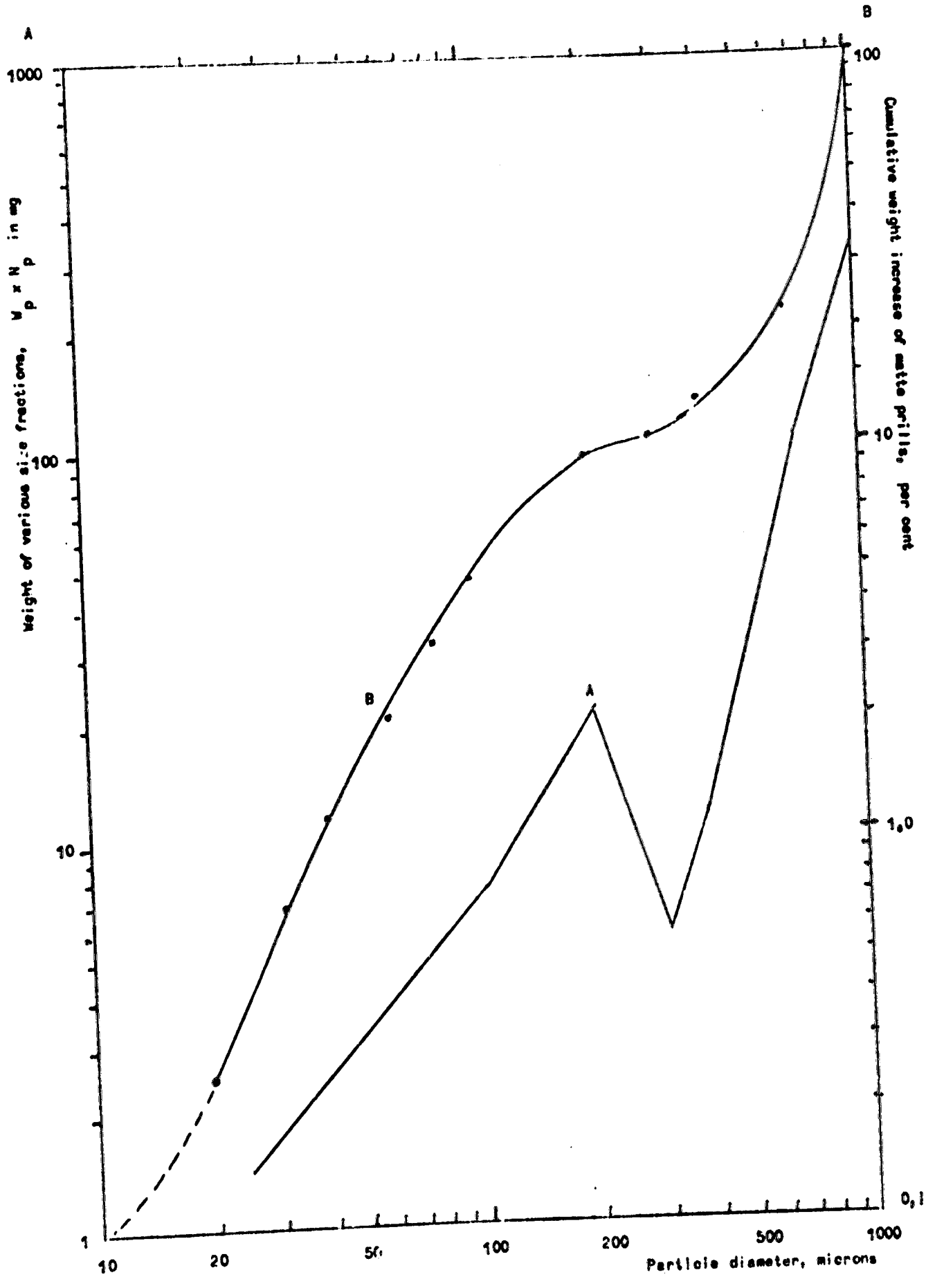

This calculation was performed on all size fractions investigated and the results, both as fractional and cumulative weight increase are illustrated in figure IV-23.).

In a brief summary it was found that

1./ No clear definition of an average matte particle size could be made in these series of investigations. The number of particles appeared to increase steadily down to about 20 micron from which size the number decreased abruptly and only a few particles could be found smaller than 10 micron. Their number between 5 and 15 micron could not be assessed with adequate certainty.

2./ The average larger size was in the range of 100 - 300 micron. Odd large size was found between 500 - 700 micron, the largest observed being 1,1 mm. If, as a rough approximation, the number of prills below 15 micron size were not included in the analysis, then the percentage size distribution from the number of counts would be as follows:

Size,	20-30	30-40	40-50	50-80	80-100	100-200	200-400	400-600	600-1000
%	40	25	17,5	14,6	4,5	2,3	0,8	0,4	0,1

3./ The weight distribution, according to figure IV-23 is inversely proportional to the number of particles and increases with increasing size range. It is interesting to note that particles up to 200 micron represent only about 10 per cent of the total matte prill weight while 90 per cent is made up of the weight of the few odd large size particles. Below 50 micron size they account for not more than 1 per cent of the total weight and only for about 0,1 per cent below the 25-30 micron size.

b./ Particle coalescence. With the photographs taken it was possible to obtain some informations as to the extent and mode of coalescence that can be expected during the travel of prills along the depth of the slag bath. Photographs 5 to 8 indicate the evidence of particle coalescence which, as will be apparent, is not confined solely to the lower regions of the molten bath but can be quite extensive already at the top of the melt. (see e.g. photograph 8.). The presence of buoyancy and electromagnetic forces due to their mixing effect may create conditions favourable for an early coalescence of the particles close to their point of release from the concentrate.

Some time ago Johannsen and Wiese (18) have already stressed the important role played by the character of the concentrate as the main

governing/...

governing factor of matte prill size "as released" from the concentrate matrix. Tus they have found that ores containing larger grains of sulphide will produce larger droplets than fine-grained flotation concentrates, half of which may contain concentrate particles smaller that 40 micron. Studies carried out in the near past on the growth of metallic copper particles in the slag drew attention to the importance of the cooling rate of slag. Thus Yazava and Kameda (26) have demonstrated that an essential factor in the precipitation process is the residence time of the slag at a temperature just below the slag liquidus when maximum growth of the precipitated particles can take place. Testwork carried out at the Noranda Research Centre (27) confirmed these results and indicated very substantial growth rate of the grains when cooling Noranda Process pilot plant slags from 1200 to 1000°C in respectively 5, 40 and 227 minutes. Cooling rates of less than 10 minutes resulted in particles of 25 micron average size while in the most slowly cooled slag the averag size was found to be 87 microns. It is therefore conceivable that the large particles observed in samples taken close to the top of the slag bed in the present study might have come about as a result of slow cooling effects. The degree of coalescence may extend to the formation of 200-300 micron size particles (photograph No-7) or large aggregates as shown for example in photos 5 and 8.

The above observations would point to the fact that the time - availability is only one aspect, though a rather important one of particle coalescence and matte settling. The role of temperature variations in the path of the prills, whether these are descending or being moved around by the agitation of the slag layer, contribute also considerably to grain growth and therefore to the settling of matte.

Ultimately however, in this process of successive heating and cooling to which the particles are subjected, the viscosity characteristics of the slag will have a decisive influence. Th steep gradients in the temperature-viscosity plots expressed by the temperature coefficient of viscosity equation with large values of λ_η in

$$\lambda_\eta = \frac{\eta_1 - \eta_2}{(T_1 - T_2)\eta_{avg}}$$

the effect of "annealing" will be less pronounced than with slags the viscosity of which is less sensitive to temperature variations. Therefore the temperature range suitable for coalescence is wider in case of the latter type of slags than with the former ones. This fact further complicates the problem of matte settling and adds to the difficulty of adequate settler dimensioning for electric furnaces producing copper or copper-nickel mattes.

The discussed/...

The discussed strong impact of slag characteristics on matte settling would suggest that in rectangular versus circular furnace symmetry with altogether different temperature distribution and mode of particle coalescence in the two types of geometry, one particular slag may be perfectly suitable as a settling medium for the matte and would facilitate excellent slag - matte separation irrespective, whether the furnace is circular or rectangular. With other slags of altogether different characteristics mainly with regards to the response of their viscosity to temperature variations, the geometry of the furnace could be a rather decisive factor and the rectangular shape with increased distance and time availability for matte settling will be preferred.

The viscosity of the matte is also an important factor in promoting coalescence. Since the viscosity is influenced significantly by tb pper and nickel content of the matte, even with similar slag composition but with varying matte grade from plant to plant the coalescence and the size of the matte prills may vary to a great extent. Schopov (28) presented the results of investigations on the size distribution of matte particles produced in smelting of copper concentrates in electric furnaces. In the case described, the percentage of the 50 micron size particles (inclusive) vas comparable to that found in the present investigations, i.e. about 88-89 per cent as against 82-83 per cent of the present study as calculated from the number of particles). The case history of the concentrate, on the other hand, differed in that it consisted of roasted sulphide ore. A high temperature centrifuge was used for the separation of the matte prills from the slag to determine the total suspended matte.
Further considerations on the aspect of matte particle coalescence are given in Appendix II.

c./ Grain size and settler dimensions. In the knowledge of the size distribution of matte prills the previous line of thought pertinent to settler dimensioning can be extended further. The following considerations like the earlier ones refer strictly to the settling zone of the furnace. The true settling compartment of a 6-electrode furnace in which conditions can be regarded as being more quiescent due to the lack of inter-electrode action, comprises the slag tapping end of the furnace extending from the face of the last electrode (no-6) to the end wall. The distance in the reference units is 5 meter. In consequence of the less perturbed flow conditions the application of Stokes' law for the calculation of particle settling velocity becomes in this region to a certain degree justifiable.
The radius of the active area of the electrode in these units, as will be seen later/...

Figure IV - 24. TWO-DIMENSIONAL PRESENTATION OF THE RELATIONSHIP BETWEEN DISTANCE AVAILABLE FOR SETTLING OF MATTE PARTICLES, TAPHOLE POSITION AND METAL LOSS DUE TO PARTICLE CARRY-OVER IN THE SLAG.

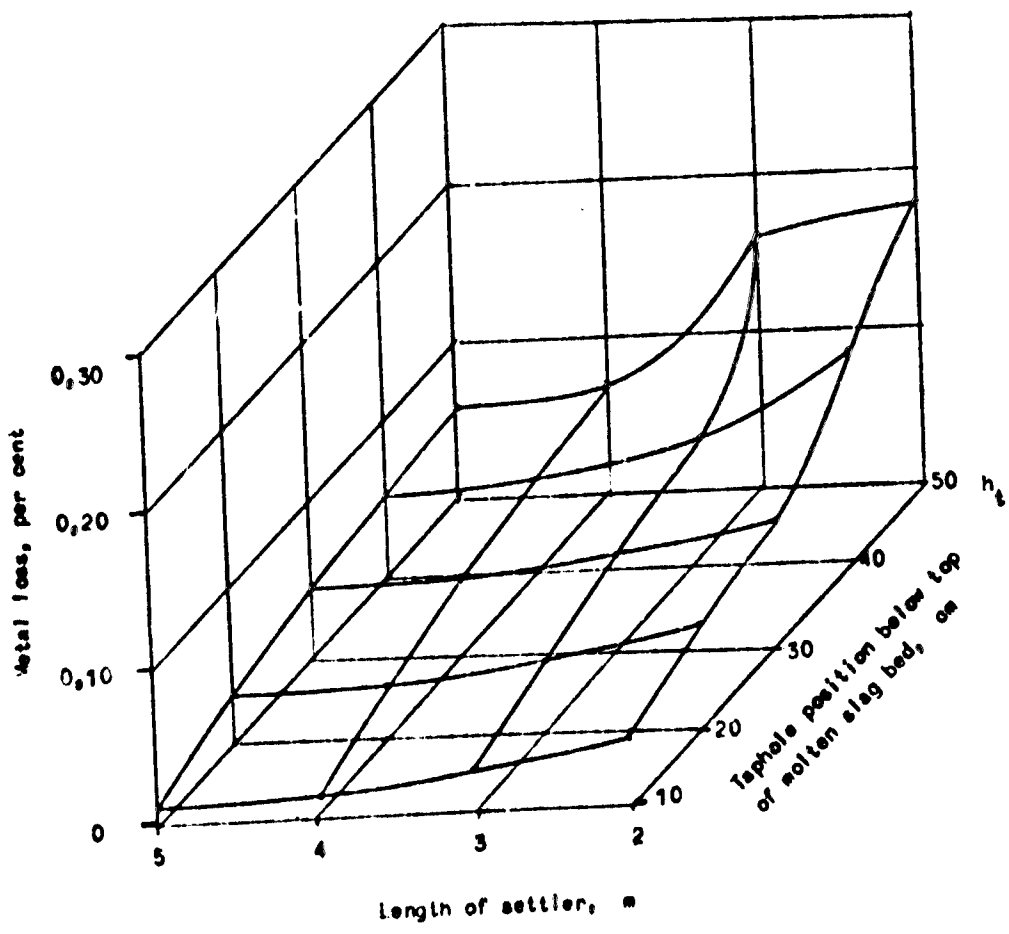

seen later, is on an average 2,5 to 2,8m thus the length of the quiescent zone could vary between 2,5 and 3,0 m. In practice, however, this may increase considerably, therefore the calculation will be performed for settler lengths of 2, 3, 4 and 5m.

As for an example from figure IV-21 at a taphole position of 0,14m below the surface of the molten slag bath about 4,6% of the 20 micron, 12,5% of the 30 micron and 19% of the 40 micron prills will settle out. On the basis of figure IV-23 the weigth fraction of the mentioned size ranges is 0,25, 0,39 and 0,54 per cent respectively, then at a length L available for settling the settled weight of matte will be $W_M^s.L$. The relattionship between the settled weight and total weight of the particular size fraction is $(W_M^s.L)W_M^{tot}$. From these the weight of matte lost to the slag in case of a particular matte prill size is then (W_M^{sl}):

$$W_M^{sl} = W_M^{tot} - (W_M^s \cdot L)\, W_M^{tot} \qquad 61./$$

and the total metallic loss for the entire size spectrum of particles will be

$$\Pi_{Me}^{sc}(\%) = \left[\sum_{d_1}^{d_i} W_M^{tot} - \sum_{d_1}^{d_i} (W_M^s \cdot L)\, W_M^{tot} \right] C_{Me(M)} \qquad 62./$$

here $\Pi_{Me}^{sc}(\%)$ is the total metallic loss as a result of the action of electrode No-6 in the settling compartment represented by matte particles in the size range d_1 to d_i carried out from the furnace in the slag, W_M^s is obtained from equation 56, i.e. figure IV-21, while $C_{Me(M)}$ is the concen - tration of metal in the furnace matte. As an illustration of the mode of calculation with the values pertinent to settled matte weight quoted above, the various steps are outlined in Table IV-5. In comparing equations 60./ to 62./ it will be obvious that

$$\sum_{d_1}^{d_i} W_M^{tot} - \sum_{d_1}^{d_i} (W_M^s \cdot L) W_M^{tot} = [W](1/\sum_{o}^{n_i} X_i/d_{pi}) \quad \text{when} \quad W_M = 1{,}00 \qquad 63./$$

The feeding of the rectangular 6-electrode furnace is effected along the length of the unit on either sides of the electrodes by which the share of each electrode in the feed is approximately 1/6-th of the total feed quantity. Hence the value of 0,167 $C_{Me(M)}$ in the Table. The calculation has been extended to include taphole levels (h) 14, 20, 30, 40 and 50 cm below the surface of the molten slag representing H/h relations of 10, 7, 4,7, 3,5 and 2,8 with H = 140 cm average. Figure IV-24 in a three-dimensional presentation shows the metal losses expressed in per cent contained in the discharged slag. Conditions pertinent to the average

thickne/...

Table IV-5. Mode of determination of metal losses in the matte discharged with the slag.

Conditions: Position of taphole below slag level, h, cm 14

Depth of slag bed, H, cm 140

H/h 10

Particle size	20	30	40	50	60	80
Total weight of matte W_M^{tot} %	0,25	0,38	0,54	0,50	0,35	0,75
Settled matte weight at L=1 W_M^s %	0,046	0,125	0,190	0,290	0,410	0,700

Distance L available for settling meter	$W_M^s \cdot L$				
5	0,230	0,615	0,950		
4	0,184	0,500	0,760		
3	0,138	0,375	0,570		
2	0,092	0,250	0,350		

	$(W_M^s \cdot L)\ W_M^{tot}$			
5	0,057	0,240	0,51	
4	0,046	0,190	0,41	
3	0,034	0,146	0,310	0,44
2	0,023	0,098	0,20[illegible]	0,38

	$W_M^l = W_M^{tot} - (W_M^s \cdot L)\ W_M^{tot}$			
5	0,19	0,15	0,03	
4	0,20	0,20	0,13	
3	0,21	0,24	0,23	0,06
2	0,23	0,29	0,33	0,12

ΣW_M^{sl}	$\Sigma W_M^{sl} \cdot C_{Me}$	x0,167
0,37	0,10	0,0167
0,53	0,14	0,0234
0,74	0,20	0,0334
1,07	0,29	0,0436

Matte grade:
Cu + Ni = 27% =0,27
C_{Me} = 0,27

thickness of the molten slag layer in the furnace, then the free settling length, i.e. the length of the quiescent zone and taphole location below the surface of the melt were the same as outlined in Table IV-5. The graph relates to losses that can be expected in the settling zone only from 1/6-th of the total feed added to the last electrode.

Considering now along the entire length of the furnace, which is assumed to consist of six reactors, each settling compartment separately, when these are fed at the same rate with concentrate it is easy to show that provided the stirring effect of the electrodes and the buoyancy forces acting on the particles is the same, the settling and carry-over of the matte particles (prills) will also be the same in each unit. In balanced operation the smelting rate at each electrode should be virtually equal (theoretically at least!) with the result of equal quantities of matte and slag produced in a unit time. The material balance with regard to the matte will be as follows: let W_M^o denote the weight of matte overflowing from one compartment into an other and R the ratio of recycle, then from reactor I to III we have

$$\text{I./} \quad W^s_{M/I} = \sum W_{M/I} R_{II} - W^o_{M/I} \qquad 64./$$

$$\text{II./} \quad W^s_{M/II} = \sum W_{WII} + (R_{III} - R_{II}) - W^o_{M/II} \qquad 65./$$

$$\text{III./} \quad W^s_{M/III} = \sum W_{M/III} + (R_{IV} - R_{III}) - W^o_{M/III} \qquad 66./$$

Between the N-th reactor and the settling zone (sz)

$$\text{N./} \quad W^s_{M/N} = \sum W_{M/N} + (R_{sz} - R_N) - W^o_{M/N} \qquad 67./$$

and in the settling zone proper

$$\text{sz./} \quad W^s_{sz} = \sum W^o_{M/N} - R_{sz} - W^t_M - W^{sl}_M \qquad 68./$$

where W^t_M = weight of matte tapped and W^{sl}_M = weight of matte lost in slags. Naturally with equal smelting rates in each reactor the value of W^o_M and R will be by and large constant. Consequently, from a matte loss point of view it is only the material balance in the settling zone that really matters. Since

$$W^o_{M/N} = W^t_M + W^{sl}_M \qquad 69./$$

the efficiency of settling in this zone is

$$\eta_{eff} = \left[1 - (W^{sl}_M / W^t_M)\right] \times 100 \qquad 70./$$

As to the metallic losses evaluated for the total feed along the entire length of the furnace using the same mode of calculation the indication is that the cumulative loss from the rest of the furnace, depending on/...

Figure IV - 25. TERMINAL VELOCITY OF MATTE PARTICLES AS A FUNCTION OF DISTANCE FROM THE TOP OF THE MOLTEN SLAG BATH.

Size of prills : 50 micron

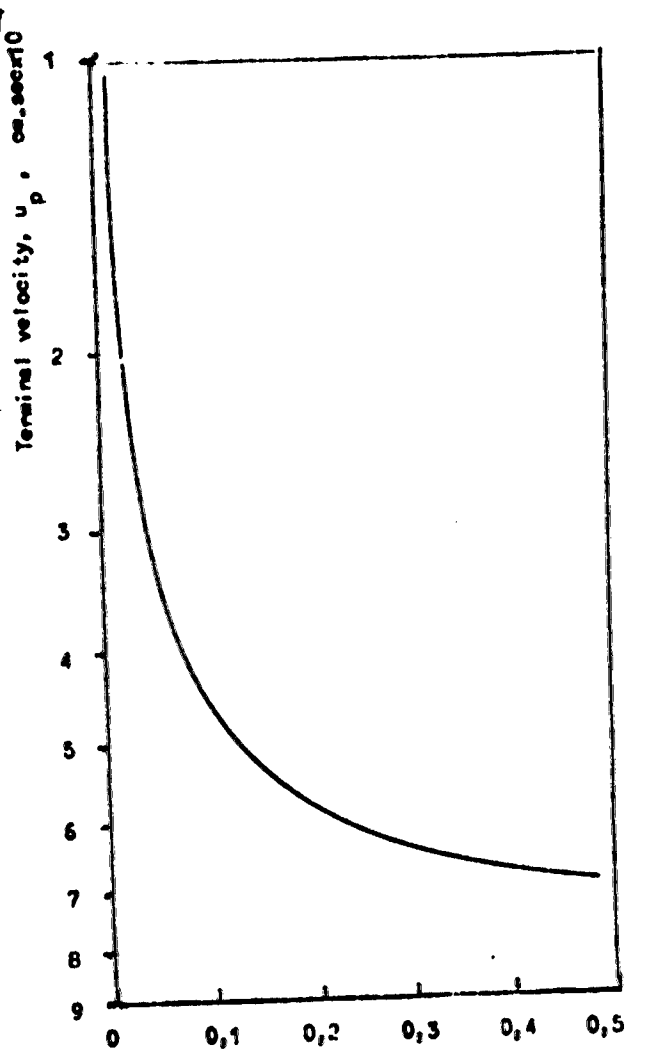

Figure IV - 26. TERMINAL VELOCITY OF MATTE PARTICLES AS A FUNCTION OF DISTANCE FROM THE CENTRE OF THE FURNACE.

Size of prills : 50 micron

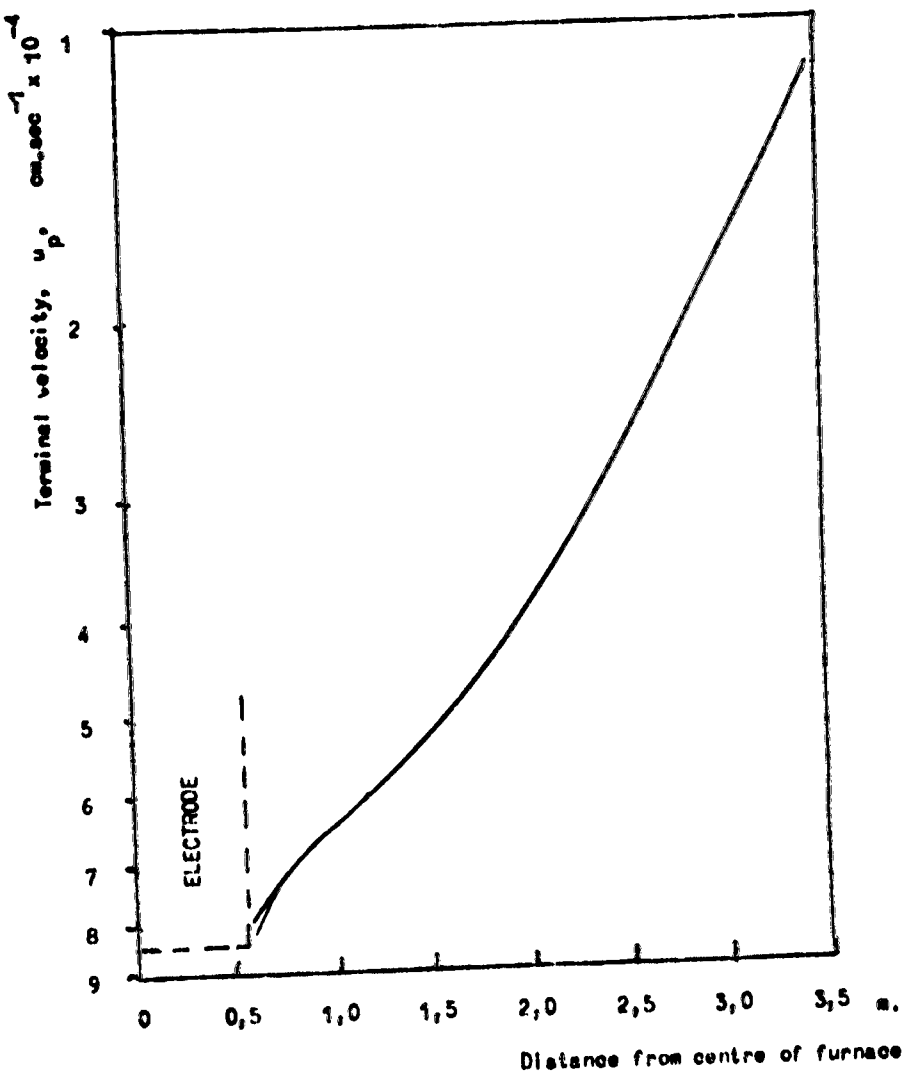

Figure IV - 27. TERMINAL VELOCITY OF MATTE PARTICLES IN VERTICAL DIRECTION BETWEEN THE TOP OF THE SLAG BED AND THE SLAG - MATTE INTERFACE

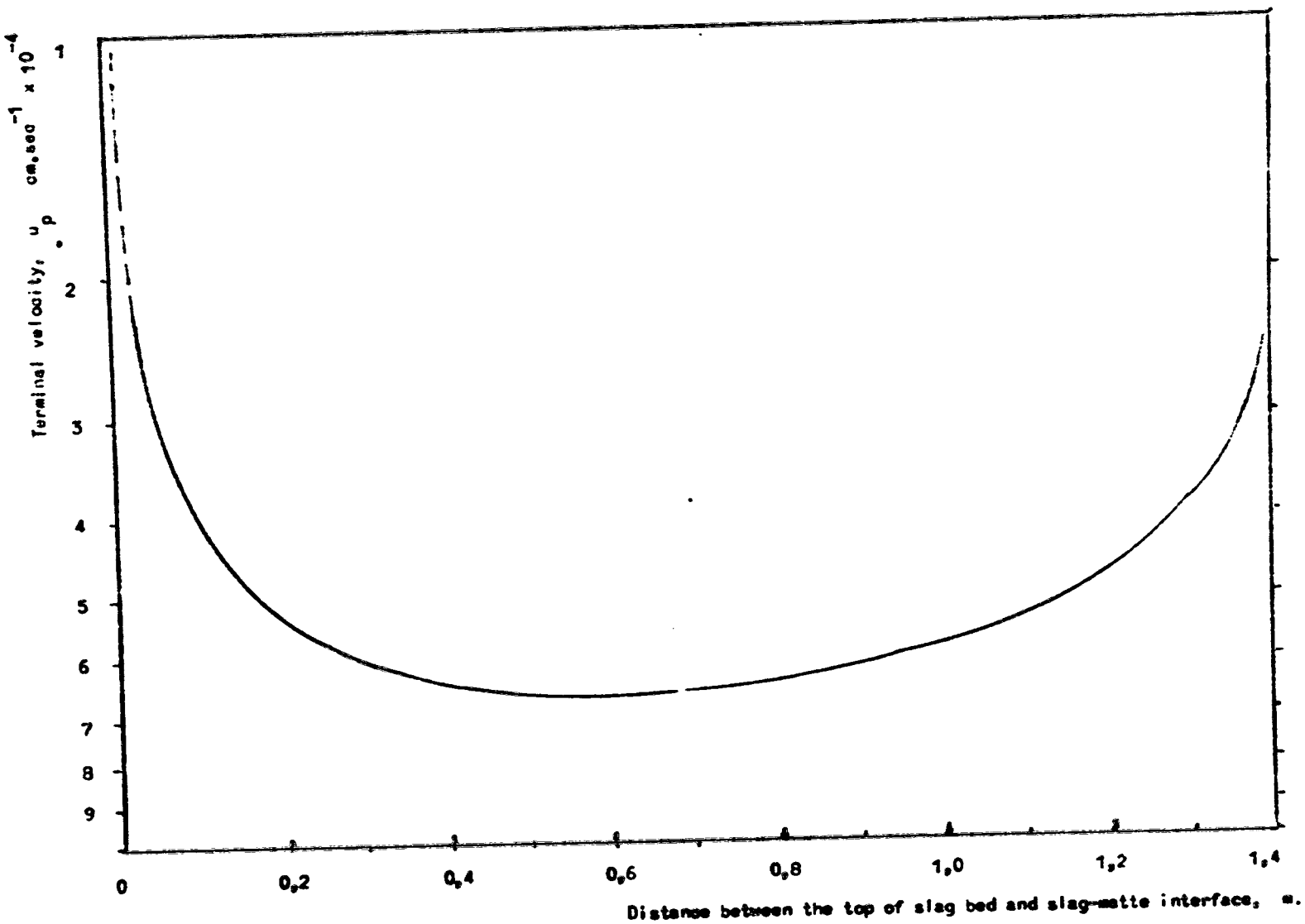

Table IV-6. Estimated temperature, viscosity and settling velocity gradient of matte prills (50 micron size) in vertical direction between the top of the molten slag bath and the slag-matte interface.

Depth in slag bath m	Temperature °C	Average viscosity of plant slag, poise	Settling velocity of matte prills $cm.sec^{-1}x10^{-4}$
0,05	1340	5,7	3,10
0,10	1365	4,2	4,00
0,20	1400	3,4	5,10
0,30	1425	3,00	5,80
0,40	1445	2,65	6,40
0,50	1460	2,60	6,60
0,60	1460	2,60	6,60
0,70	1455	2,65	6,50
0,80	1445	2,75	6,30
0,90	1435	2,87	6,05
1,00	1420	2,90	5,85
1,20	1385	3,65	4,80
1,30	1365	4,25	4,00
1,35	1350	4,75	3,25
1,40	1325	7,50	2,40

Author Hejja A A
Name of thesis Studies of factors relating to the operation and design of electric furnaces for matte smelting with particular reference to slag characteristics 1975

PUBLISHER:
University of the Witwatersrand, Johannesburg
©2013

LEGAL NOTICES:

Copyright Notice: All materials on the University of the Witwatersrand, Johannesburg Library website are protected by South African copyright law and may not be distributed, transmitted, displayed, or otherwise published in any format, without the prior written permission of the copyright owner.

Disclaimer and Terms of Use: Provided that you maintain all copyright and other notices contained therein, you may download material (one machine readable copy and one print copy per page) for your personal and/or educational non-commercial use only.

The University of the Witwatersrand, Johannesburg, is not responsible for any errors or omissions and excludes any and all liability for any errors in or omissions from the information on the Library website.